

Development of hot-melt extrusion as a novel technique for the formulation of oral solid dosage forms

By

Mohammed Maniruzzaman [B.Sc. (Hons)]

A thesis submitted to the University of Greenwich in partial fulfilment for the Degree of
Doctor of Philosophy

November 2012

School of Science

University of Greenwich, UK



UNIVERSITY
of
GREENWICH

DECLARATION

“I certify that this work has not been accepted in substance for any degree, and is not concurrently being submitted for any purpose, other than that of the PhD thesis being studied at the University of Greenwich. I also declare that this work is the result of my own investigations except where otherwise identified by references and that I have not plagiarised another’s work”.

Signed:

Mohammed Maniruzzaman (Candidate)

.....

Doctoral Supervisors

Dr. Dennis Douroumis

Dr Joshua S. Boateng

Date:

ACKNOWLEDGEMENTS

I would like to take the opportunity to extend my gratitude and appreciation to almighty 'ALLAH' who helped me numerously to make this thesis possible (Alhamdulillah). I would also like to thank my parents for their continuous support and help throughout the past years and my lovely wife and sweet sister for being with me during the three years of my research and giving me lots of inspiration and support.

I would like to express my gratitude to my supervisors, Dr. Dionysios Douroumis and Dr Joshua S. Boateng for their guidance at each step of my progress. I am particularly indebted to my first supervisor Dr. Dionysios Douroumis whose help, stimulating suggestions and encouragement helped me at all times during this research. Many thanks also to Prof Chowdhry for all his support and encouragement throughout my PhD study.

I would also like to thank the School of Science of the University of Greenwich for giving me the opportunity to undertake this doctoral research and to use department facilities.

Furthermore I would like to extend my thanks to Dr Milan Antonijevic for his kind assistance and guidance in the DSC studies, Dr Jiayun Pang for kind support in molecular modelling and Mrs Devyani Amin for her help with the HPLC experiments. I am also grateful to Dr Ian Slipper and Dr A. Mendham of the School of Science whose assistance during this project is greatly appreciated.

I would especially like to thank my parents for their moral and financial support to get me to this level of my career. I am grateful to my fellow PhD students and friends for their assistance and mental support during my project work. Finally, I want to take the opportunity to thank all the staff of the Drill Hall Library.

ABSTRACT

Hot-melt extrusion (HME) is one of the most widely used technologies in the plastic, rubber and food industries and it has also been extensively explored and used in academia and the pharmaceutical industry over the last decade. This project aims to investigate the efficiency of hydrophilic polymers to enhance the dissolution rate of poorly water-soluble APIs processed by HME. Indomethacin (INM) and famotidine (FMT) were selected as model active substances while polyvinyl caprolactam graft copolymer, Soluplus® (SOL) and vinylpyrrolidone-vinyl acetate copolymer grades Kollidon® VA64 (VA64) and Plasdone® S630 (S630) were used as hydrophilic polymeric carriers. For the purpose of the study, all drug-polymer binary blends at various ratios were processed by a Randcastle single screw extruder. The physico-chemical properties and the morphology of the extrudates were evaluated via x-ray powder diffraction (XRPD), differential scanning calorimetry (DSC) and scanning electron microscopy (SEM). INM and FMT exhibited strong plasticization effects at specific concentrations and were found to be molecularly dispersed within the polymer blends. The *in vitro* dissolution studies showed increased INM/FMT release rates for all formulations compared to that of pure APIs alone. Ibuprofen was also embedded in a methacrylate copolymer (Eudragit® EPO) matrix to produce solid dispersions by hot-melt extrusion processing. The obtained granules were incorporated into orally disintegrating tablets (ODTs). The tablets were developed by varying the ratio of superdisintegrants such as sodium croscarmellose and cross-linked polyvinylpyrrolidone while a direct compression process was used to compress the ODTs under various compaction forces to optimize tablet robustness. The properties of the compressed tablets which included porosity, hardness, and friability and dissolution profiles were further evaluated and compared with commercially available Nurofen® Meltlet ODTs. *In vitro* dissolution of the extruded ODTs showed rapid release of ibuprofen compared to that of Nurofen® Meltlets. The *in vitro* and *in vivo* evaluation of the masking efficiency of hot melt extruded paracetamol (PMOL) formulations was examined. Extruded granules containing high PMOL loadings in Eudragit EPO® (EPO) or Kollidon® VA64 (VA64) were prepared by HME. Similarly propranolol HCl (PRP), diphenhydramine HCl (DPD), cetirizine HCl (CTZ) and verapamil HCl (VRP) were used as model cationic active substances while pH sensitive anionic methacrylic acid based methyl methacrylate copolymers Eudragit® L100 (L100) and ethyl acrylate copolymer Eudragit® L100-55 (Acryl-EZE®) (L100-55) were used as polymeric carriers in order to produce taste masked extruded formulations determining drug-polymers intermolecular interactions. The

taste masking effect of the processed formulation was evaluated *in vivo* by a panel of six healthy human volunteers. In addition, *in vitro* evaluation was carried out by an Astree e-tongue (Alpha MOS) equipped with seven sensors and Taste Sensing System TS5000Z (INSENT), respectively.

The taste and sensory evaluation in human volunteers demonstrated that the formulation masked the bitter taste of the APIs and improved tablet palatability. In addition to that the taste sensing technology demonstrated taste improvement for all polymers by correlating the data obtained for the placebo polymers and the pure APIs alone. The e-tongue results were in good agreement with the *in vivo* evaluation. Molecular modelling (Gaussian 09) predicted the existence of two possible H-bonding types while Fourier Transform Infra-Red (FT-IR) and NMR studies confirmed drug-polymer interactions between the functional groups of both components (cationic drugs–anionic polymers). Furthermore, the intermolecular interactions evaluated by Flory-Huggins interaction parameters theory and X-ray photoelectron spectroscopy (XPS) showed stronger interactions between drug-polymer in L100 systems compared to that of L100-55 systems. The mechanism of the intermolecular interactions derived from this research showed the presence of H bonding between the amine group of the active substances and the carboxylic groups in the polymer.

Hydrocortisone (HCS) was also embedded and extruded with ethyl cellulose N10 (EC N10) or ethyl cellulose Premium 7 (EC P7) in order to develop sustained release tablets processed by HME. The compressed tablets were subsequently coated with an enteric coating polymer, Eudragit[®] S100 (15-20%), which showed sustained release over 12 hrs with a lag time of 2 hrs. Further analysis of the release mechanism of HCS from tablets was performed by implementing five different kinetic release models which confirmed that the release of HCS from both coated and uncoated tablets followed a first order kinetic model.

CONTENTS

<u>Contents</u>	<u>Page No</u>
TITLE PAGE.....	i
DECLARATION.....	ii
ACKNOWLEDGMENTS.....	iii
ABSTRACT.....	iv
CONTENTS.....	vi
TABLES AND FIGURES.....	xv
ABBREVIATIONS.....	xxvi
PUBLICATIONS.....	xxviii

CHAPTER 1: INTRODUCTION

1.0 Background	1
1.1 Hot-melt extrusion: Process technology.....	1
1.2 Equipment: single screw and twin screw extruder.....	3
1.3 Advantages and disadvantages of HME	6
1.4 Applications of HME	7
1.5 Formulation research and developments to date.....	8
1.6 HME in commercial products.....	12
1.7 Summary.....	12
1.8 Aims and objectives.....	13
1.9 References.....	13

CHAPTER 2: DISSOLUTION ENHANCEMENT OF POORLY WATER-SOLUBLE APIs PROCESSED BY HOT-MELT EXTRUSION (HME) USING HYDROPHILIC POLYMERS

1.0 Introduction	19
2.0 Materials and methods	20
2.1 Materials	20
2.2 Drug-polymer miscibility study by Hansen solubility parameters (δ)	20
2.3 Preparation of formulation blends	21
2.4 Hot melt extrusion process	22
2.5 Thermal analysis	22
2.6 X-ray powder diffraction (XRPD)	22
2.7 Particle size morphology and distribution	23
2.8 <i>In vitro</i> drug release study	23
2.9 HPLC analysis	24
3.0 Results and discussion	24
3.1 Miscibility studies using calculating solubility parameters (δ)	24
3.2 Particle morphology and particle size analysis	27
3.3 X-ray powder diffraction (XRPD)	28
3.4 Differential scanning calorimetry (DSC)	30
3.5 <i>In vitro</i> dissolution studies	35
4.0 Conclusions	38
5.0 References	38

**CHAPTER 3: DEVELOPMENT AND EVALUATION OF ORALLY
DISINTEGRATING TABLETS (ODTs) CONTAINING IBUPROFEN GRANULES
PREPARED BY HOT MELT EXTRUSION**

1.0 Introduction	41
2.0 Materials and methods	42
2.1 Materials	42
2.2 Hot-melt extrusion	43
2.3 Particle size distribution measurements	43
2.4 Tablet preparation	43
2.5 Flow properties and compressibility	43
2.6 Evaluation of tablets	44
2.7 <i>In vitro</i> tablet disintegration	44
2.8 <i>In vivo</i> tablet disintegration and bitterness evaluation	44
2.9 Differential scanning calorimetry (DSC)	45
2.10 X-ray powder diffraction (XRPD).....	45
2.11 <i>In vitro</i> drug release studies	45
2.12 HPLC analysis	46
3.0 Results and discussion	46
3.1 Hot-melt extrusion process	46

3.2 Powder and ODT characterization	49
3.3 <i>In vivo</i> disintegration time and taste-masking evaluation	57
3.4 <i>In vitro</i> dissolution	59
4.0 Conclusions	60
5.0 References.....	60

CHAPTER 4: TASTE MASKING OF PARACETAMOL BY HOT MELT EXTRUSION: AN *IN VITRO* AND *IN VIVO* EVALUATION

1.0 Introduction	64
2.0 Materials and Methods	65
2.1 Materials	65
2.2 Calculation of Hansen solubility parameters	65
2.3 Hot-melt extrusion (HME) process	66
2.4 Thermal analysis	66
2.5 X-ray powder diffraction (XRPD)	66
2.6 <i>In vitro</i> drug release study	67
2.7 HPLC analysis	67
2.8 <i>In vivo</i> taste masking evaluation	67
2.9 <i>In vitro</i> taste masking evaluation: Astree e-tongue.....	67
3.0 Results and discussion	68
3.1 Solubility parameters and extrusion process	68
3.2 Thermal analysis and X– ray solid state characterization studies	69
3.3 <i>In vivo</i> and <i>in vitro</i> taste masking evaluation	74
3.4 Dissolution studies	79

4.0 Conclusions	80
5.0 References	80

CHAPTER 5: *IN VIVO* AND *IN VITRO* TASTE MASKING EVALUATION OF BITTER MELT EXTRUDED APIs

1.0 Introduction	85
2.0 Materials and Methods.....	86
2.1 Materials	86
2.2 Calculation of solubility parameters	86
2.3 Preparation of formulation blends and hot-melt extrusion (HME) processing.....	87
2.4 Scanning electron microscopy (SEM)	87
2.5 Differential scanning calorimetry (DSC).....	87
2.6 X-ray powder diffraction (XRPD).....	87
2.7 <i>In vivo</i> taste masking evaluation.....	88
2.8 <i>In vitro</i> taste masking evaluation: Astree e-tongue	88
2.8.1 Sample preparation for Astee e-tongue.....	88
2.9 <i>In vitro</i> drug release studies.....	89
2.10 HPLC analysis.....	90
3.0 Results and discussion	90
3.1 Solubility parameters and extrusion process.....	90
3.2 Scanning electron microscopy (SEM).....	91
3.3 Differential scanning calorimetric (DSC)	92
3.4 X-ray powder diffraction (XRPD) analysis.....	95
3.5 <i>In vivo</i> taste masking evaluations.....	96
3.6 <i>In vitro</i> taste evaluations	97

3.7 <i>In vitro</i> drug release profiles	101
4.0 Conclusions	103
5.0 References	103

CHAPTER 6: DRUG-POLYMER INTERMOLECULAR INTERACTIONS IN HOT-MELT EXTRUDED SOLID DISPERSIONS

1.0 Introduction	106
2.0 Experimental sections	107
2.1 Materials	107
2.2 Determination of drug-polymer miscibility by Hansen solubility parameters (δ).....	107
2.3 Hot-melt extrusion process	107
2.4 Scanning electron microscopy (SEM)	108
2.5 Thermal analysis by differential scanning calorimetry (DSC).....	108
2.6 X-ray powder diffraction (XRPD).....	108
2.7 Molecular modelling.....	108
2.8 X-ray photoelectron spectroscopy (XPS) analysis.....	109
2.9 Nuclear magnetic resonance (NMR) studies	109
3.0 Results and discussion	109
3.1 Determination of drug-polymer miscibility by Hansen solubility parameters....	109
3.2 Scanning electron microscopy (SEM)	110
3.3 Differential scanning calorimetry (DSC).....	111
3.4 X-ray powder diffraction (XRPD).....	112
3.5 Intermolecular interactions of hot-melt extrudates.....	114
3.5.1 Molecular modelling.....	114

3.5.2 X-ray photoelectron spectroscopy (XPS).....	114
3.5.3 Nuclear magnetic resonance (NMR) studies	121
4.0 Conclusions	124
5.0 References	124

CHAPTER 7: EVALUATION OF THE INTER-RELATION BETWEEN INTERMOLECULAR INTERACTIONS AND TASTE MASKING EFFICIENCY IN MELT EXTRUDED SOLID DISPERSIONS

1.0 Introduction	128
2.0 Materials and Methods	129
2.1 Materials	129
2.2 Hansen solubility parameters: prediction of drug/polymer miscibility.....	129
2.3 Flory-Huggins (F-H) theory for the prediction of drug/polymer interaction	
Parameter.....	130
2.4 Differential scanning calorimetry (DSC)	130
2.5 Preparation of formulation blends and hot-melt extrusion (HME) processing....	131
2.6 Particle morphology and size distribution	131
2.7 <i>In vivo</i> taste masking evaluation	131
2.8 <i>In vitro</i> taste masking evaluation: TS-5000Z sensing system	132
2.9 Molecular modelling	132
2.10 Fourier Transform Infra-Red (FT-IR) analysis	132
2.11 X-ray photoelectron spectroscopy (XPS) analysis	133
3.0 Results and discussion.....	133
3.1 Predictions of drug/polymer miscibility: solubility parameters.....	133

3.2 Flory Huggins (F-H) theory for the prediction of drug/polymers interaction	
Parameter.....	134
3.3 SEM and particle size analysis	135
3.4 <i>In vivo</i> and <i>in vitro</i> taste masking evaluations	137
3.5 Molecular modelling	140
3.6 Fourier Transform Infra-Red (FT-IR) analysis	142
3.7 X-ray photoelectron spectroscopy (XPS) analysis	143
4.0 Conclusions	147
5.0 References.....	147

CHAPTER 8: SUSTAINED RELEASE HYDROCORTISONE TABLETS PROCESSED BY HOT-MELT EXTRUSION (HME)

1.0 Introduction	151
2.0 Materials and Methods	152
2.1 Materials	152
2.2 Calculation of solubility parameters.....	152
2.3 Preparation of formulation blends and hot-melt extrusion processing.....	153
2.4 Scanning electron microscopy (SEM) and particle size analysis.....	153
2.5 Differential scanning calorimetry (DSC).....	153
2.6 X-ray powder diffraction (XRPD)	153
2.7 Tablet preparation and characterization.....	154
2.8 <i>In vitro</i> drug release studies.....	154
2.9 HPLC analysis.....	155
2.10 Analysis of drug release mechanism.....	155
3.0 Results and discussion.....	156

3.1 Solubility parameters and extrusion process.....	156
3.2 Scanning electron microscopy (SEM).....	156
3.3 Differential scanning calorimetric (DSC).....	157
3.4 X-ray powder diffraction (XRPD) analysis.....	159
3.5 Tablet characterisation.....	160
3.6 <i>In vitro</i> dissolution studies	161
3.7 Analysis of release mechanism.....	162
4.0 Conclusions	167
5.0 References.....	168

CHAPTER 9: CONCLUSIONS AND FUTURE WORK

9.1 Overall conclusions.....	170
9.2 Future work.....	171

CHAPTER 10: SUPPLEMENTARY DATA

10.1 Supplementary figures.....	172
10.2 Supplementary calculations.....	180

LIST OF TABLES AND FIGURES

TABLES

Table N°	Title	Page N°
CHAPTER 1		
1.1	HME and other conventional processing techniques; advantages and disadvantages.	3
1.2	Different hot-melt extruded films comprising of different polymeric materials, plasticisers and active ingredients for various indications.	11
CHAPTER 2		
2.1	Drug/polymer percentages of the HME processed formulations.	21
2.2	Calculated solubility parameters of drug/polymers and compound distances in Bagley diagram.	26
2.3	DSC thermal transitions for drugs, polymers and active formulations.	32
2.4	Similarity factor (f_2) for comparing release curves with respect to drug loading of INM and FMT formulations.	37
CHAPTER 3		
3.1	Composition of ODT formulations.	50
3.2	Physical properties of powder blends and compressed tablets (n = 3).	51
3.3	Comparison of disintegration times of ODTs at various (4, 8, 10 and 12 kN) compaction forces (n = 3).	58
3.4	Taste evaluation of ODTs on healthy human volunteers (n = 10).	58

CHAPTER 4		
4.1	Calculated solubility parameters of drug/polymers.	69
4.2	Crystalline/amorphous percentage of the extruded PMOL formulations.	71
CHAPTER 5		
5.1	Sample preparation for taste masking analysis.	89
5.2	Solubility parameters calculations summery for both drugs and polymers.	91
5.3	Summary of DSC results of pure drugs, polymers and formulations.	92
5.4	Mean standard deviation (SD) and relative standard deviation (RSD) for each solution.	101
5.5	Similarity factor (f_2) for comparing release curves of CTZ and VRP formulations.	102
CHAPTER 6		
6.1	Position and percentage area of O, C, N and Cl atoms of bulk APIs, polymers and extrudates.	115
6.2	N 1s peak shifts in all extruded formulations with both drugs	120
6.3	^1H NMR assignments for drugs and polymer (samples were dissolved in CD_3OD)	122
6.4	A comparison of T_1 relaxation times for drug and drug/polymer solutions	124
CHAPTER 7		
7.1	Solubility parameters calculations summery for both drugs and	133

	polymers.	
7.2	DSC findings of all APIs and polymers as well as general information of all polymers and active substances.	135
7.3	Calculation of F–H interaction parameter of different drug–polymer extruded formulations.	135
7.4	Binding energy calculation of drug/polymer pair based on the chemical structure (Gaussian View 9).	141
7.5	Estimated N coefficient values of different formulations	146
CHAPTER 8		
8.1	Tablet contents for each of the extrudates.	154
8.2	Drug/polymer’s description; tablet characterization.	161
8.3	Dissolution rate constants and determination coefficients of HCS release from coated and uncoated tablets; n dissolution exponent.	167

FIGURES

Figure N°	Title	Page N°
CHAPTER 1		
1.1	Schematic diagram of HME process.	2
1.2	Schematic diagram of a single screw extruder.	4
1.3	Screw geometry (extrusion).	5
1.4	A twin screw extruder and screws.	6
CHAPTER 2		
2.1	Location of polymers (open symbols) and APIs (closed symbols) within the Bagley plot.	25
2.2	SEM images (magnification x 500) of extruded formulations: (a) SOL/INM 20% (b) SOL/INM 40% (c) FMT/VA64 20% and (d) FMT/S630 20%.	27
2.3	Particles size distribution of extruded formulations after milling (5 min; 400 rpm): (a) INM/SOL 20-40%, (b) FMT/SOL 20-40%, (c) INM/VA64 20-40%, and (d) INM/S630 20%, FMT/S630 20%.	28
2.4a	Diffractograms of INM formulations: pure INM (inset), (a) INM/S630 20% PM (b) INM/SC30 20% E (c) INM/ SOL 20% PM (d) INM/SOL 20% E (e) INM/SOL 40% PM (f) INM/SOL 40% E (g) INM/VA64 20% PM (h) INMO/VA64 20% E (i) INM/VA64 40% PM (j) INM/VA64 40% E (milling time 5 min at 400 rpm).	29

2.4b	Diffraction patterns of FMT formulations: pure FMT (inset), (a) FMT/S630 20% PM (b) FMT/S630 20% E (c) FMT/SOL 20% PM (d) FMT/SOL 20% E (e) FMT/SOL 40% PM (f) FMT/SOL 40% E (g) FMT/VA64 20% PM (h) FMT/VA64 20% E (milling time 5 min at 400 rpm).	30
2.5a	MTDSC thermograms of pure polymers and drugs.	31
2.5b	DSC thermograms of INM and VA64 (physical mixtures and extrudates).	33
2.5c	DSC thermograms of INM and SOL (physical mixtures and extrudates).	33
2.5d	DSC thermograms of INM and FMT with Plasdone S630 (physical mixtures and extrudates).	34
2.5e	DSC thermograms of FMT and SOL (physical mixtures and extrudates).	35
2.6a	Drug release profile of pure INM, INM/SOL 20%, INM/VA64 20%, INM/S630 20%, INM/VA64 40% and INM/SOL 40%.	36
2.6b	Drug release profile of pure FMT, FMT/VA64 20%, FMT/SOL 20% and FMT/S630 20%.	36
CHAPTER 3		
3.1	Particles size distribution of micronized IBU/EPO (40% loading) extrudates (Milling time 10 min at 6000 rpm).	47
3.2	X-ray diffraction patterns of pure IBU, physical IBU/EPO mixture and extruded IBU/EPO granules, respectively.	48
3.3	DSC thermograms of pure IBU, physical IBU/EPO mixture and extruded IBU/EPO granules, respectively.	49
3.4	Schematic diagram of ODTs disintegration times at various compaction forces with a) 2%, b) 5%, c) 10% and d) 20% superdisintegrants.	53

3.5	Schematic diagram of ODTs hardness at various compaction forces with a) 2%, b) 5%, c) 10% and d) 20% superdisintegrants.	55
3.6	Schematic diagram of ODTs friability at various compaction forces with a) 2%, b) 5%, c) 10% and d) 20% superdisintegrants.	56
3.7	Schematic diagram of ODTs disintegration times at various compaction forces with supedisintegrants at their optimal levels.	57
3.8	Release profiles of ODTs with IBU/EPO extruded granules of, ▲) 25%, (●) 40% drug loading and ■) Nurofen®.	59
CHAPTER 4		
4.1a	MTDSC thermograms of pure PMOL (inset) and Eudragit EPO, Kollidon VA64	70
4.1b	MTDSC thermograms of PMOL/EPO extrudates at different PMOL loadings.	70
4.1c	MTDSC thermograms of PMOL/VA64 extrudates at different PMOL loadings.	72
4.2a	Powder XRPD patterns of PMOL/EPO solid dispersion (SD) and physical mixtures (PM) systems: (a) PMOL (b) PMOL/EPO 60% PM (c) PMOL/EPO 60% Ext. (d) PMOL/EPO 50% PM (e) PMOL/EPO 50% Ext.50% (f) PMOL/EPO 40% PM (g) PMOL/EPO 40% Ext.	73
4.2b	Powder XRPD patterns of PMOL pure (DIF), PMOL/VA64 extruded (ext) and physical mixtures (PM) samples: (a) PMOL/VA64 50% PM (b) PMOL/VA64 50% ext (c) PMOL/VA64 40% PM (d) PMOL/VA64 40% Ext (e) PMOL/VA64 30% PM and (f) PMOL/VA64 30% Ext.	74

4.3	Schematic representation of the taste scores of pure API, bulk polymers and the extruded formulations.	75
4.4a	Electronic tongue “taste map”: Global signal comparison (PCA analysis of the electrode responses) between pure PMOL and extruded formulations with VA64 polymer after dissolution for 60s.	76
4.4b	Electronic tongue “taste map”: Global signal comparison (PCA analysis of the electrode responses) between pure and extruded formulations with EPO polymer after dissolution for 60s.	77
4.5	Distance and discrimination comparison between signal of 100% PMOL formulation and each polymer’s formulation on Astree e-tongue (after 60s).	78
4.6	Correlation of human sensory data “Reference” with Astree electronic tongue measurements “Measured”.	78
4.7a	Dissolution profiles of PMOL in PMOL/EPO extrudates (n=3).	79
4.7b	Dissolution profiles of PMOL in PMOL/VA64 extrudates (n=3).	80
CHAPTER 5		
5.1	SEM images (magnification x 500) of (i) CTZ/L100 EXT, (ii) CTZ/EZE EXT, (iii) VRP/L100 EXT and (iv) VRP/EZE EXT.	92
5.2a	DSC transitions of pure APIs and polymers.	93
5.2b	Transitions of CTZ and VRP in L100 polymers systems.	94
5.2c	Transitions of CTZ and VRP in EZE (L100-55) polymers systems.	95
5.3a	Diffraction patterns of CTZ/polymer formulations.	95
5.3b	Diffraction patterns of VRP/polymer formulations.	96
5.4	Sensory taste scores of human volunteers for all formulations and pure	97

	materials.	
5.5a	Signal comparison between active and placebo formulations with Eudragit L100 and Acryl EZE coatings on cetirizine HCl and verapamil HCl (dissolution for 60s).	98
5.5b	Distance and discrimination comparison between signal of pure cetirizine and verapamil HCl formulation and each polymer's formulation on Astree e-Tongue (after 60s dissolution).	99
5.5c	Correlation of human sensory data "Reference" with Astree electronic tongue measurements ("Measured") for both drugs.	100
5.6a	Release profiles of CTZ formulations (paddle speed 100 rpm, pH 1.2 (6.8 after 2 hr), n=3).	102
5.6b	Release profiles of VRP formulations (paddle speed 100 rpm, pH 1.2 (6.8 after 2 hr), n=3).	103
CHAPTER 6		
6.1	SEM images of (a) PRP/L100 (Magnification x 2000), (b) PRP/L100-55 (Magnification x 10K), (c) DPD/L100 (Magnification x 500) and (d) DPD/L100-55 (magnification x 10K) extruded formulations.	110
6.2a	DSC thermograms of pure drugs and pure polymers	111
6.2b	DSC thermograms of DPD/L100 (PM), DPD/L100 (EXT), DPD/L100-55 (PM) and DPD/L100-55 (EXT).	112
6.3a	Diffractiongrams of PRP formulations: PRP pure (inset), (a) PRP/L100 PM (b) PRP/ L100 extrudates (c) PRP/L100-55 extrudates, (d) PRP/L100-55 PM.	113
6.3b	Diffractiongrams of DPD formulations: DPD pure (inset), (a) DPD/L100-	113

	55 extrudates (b) DPD/L100-55 PM (c) DPD/L100 extrudates and (d) DPD/L100 PM.	
6.4	Molecular modelling of drugs/polymers (Gaussian 09).	114
6.5a	XPS BE peaks of C 1s PRP, L100 and PRP/L100 formulations	116
6.5b	C 1s BE peaks of DPD, L100 and DPD/L100 formulations	116
6.5c	O 1s peaks of DPD, L100, DPD/L100 and PRP, L100-55, PRP/L100-55 formulations.	118
6.5d	N 1s peaks of PRP and DPD formulations.	119
6.6a	Molecular structure of PRP and DPD (NMR peak assignment)	121
6.6b	¹ H NMR spectra of all PRP and DPD formulations.	123
CHAPTER 7		
7.1	SEM images (magnification x 500) of the extruded formulations (a) PRP/L100 and (b) DPD/L100-55.	136
7.2	Particle size distribution of L100 and L100-55 based formulations with both drugs (milling time 5 min, 400 rpm).	136
7.3a	Sensory scores of all formulations by panellist (n=6).	137
7.3b	Normalised DI (%) of all drug/L100 formulations in four different time scale.	138
7.3c	Normalised DI (%) of all drug/L100-55 formulations in four different time scale.	139
7.3d	Relationship between results of taste sensors and human taste scores for similar tastes. The standard deviations on the x- and y-axes are the difference between the panellists' scores and measurement error (n = 6), respectively.	140

7.4a	FTIR spectra of PRP extruded formulations.	142
7.4b	FTIR spectra of DPD extruded formulations.	143
7.5a	XPS surveys of pure PRP, DPD, L100 and L100-55.	144
7.5b	XPS surveys of extruded formulations.	144
7.5c	N 1s BE peaks of PRP and extruded formulations.	145
7.5d	N 1s BE peaks of DPD and DPD based extruded formulations.	146
CHAPTER 8		
8.1	SEM images of [(a), (b)] HCS/ EC N10 (magnification x500 and 10K, respectively) and [(c), (d)] HCS/EC P7 extruded formulations (magnification x500 and 10K, respectively).	157
8.2a	DSC transitions of pure polymers and drug.	158
8.2b	DSC transitions of HCS/EC N10 and HCS/ EC P7 physical mixtures (PM) and extruded formulations (EXT).	159
8.3	XRD diffractograms of extruded formulations and binary mixtures.	160
8.4	HCS release profiles in both coated and uncoated tablets. Each result shows the mean \pm S.D. ($n = 3$).	162
8.5a	Semi logarithmic plot of the unreleased fraction of HCS as a function of time according to a first order kinetics model. Each result shows the mean \pm S.D. ($n = 3$).	163
8.5b	A plot of the HCS released as a function of time according to the Higuchi model. Each result shows the mean \pm S.D. ($n = 3$).	164
8.5c	A plot of the cubic root of unreleased fraction of HCS from tablets as a function of time according to the Hixson–Crowell model. Each result shows the mean \pm S.D. ($n = 3$).	165

8.5d	A plot of the logarithm of HCS released as a function of the logarithm of time according to the Korsmeyer–Peppas model. Each result shows the mean \pm S.D. ($n=3$).	166
CHAPTER 10		
Supp. 1	N 1s BE peaks of DPD and DPD based extruded formulations.	172
Supp. 2	XPS O 1s peaks for PRP, L100 and PRP/L100 formulations.	173
Supp. 3	C 1s BE peaks for L100-55, PRP/L100-55 and DPD/L100-55.	174
Supp. 4	O 1s BE peaks for L100-55, DPD and DPD/L100-55 formulations.	175
Supp. 5	Part, $^1\text{H T}_1$ spectra (aromatic region) for the propanolol HCl/ Eudragit L-100 formulation.	176
Supp. 6	Part, $^1\text{H T}_1$ spectra (aromatic region) for the propanolol HCl.	177
Supp. 7	Part, $^1\text{H T}_1$ spectra for the diphenhydramine HCl/Eudragit L-100 formulation	178
Supp. 8	Part, $^1\text{H T}_1$ spectra for diphenhydramine HCl.	179

ABBREVIATIONS

<u>Abbreviation</u>	<u>Meaning</u>
API	Active pharmaceutical ingredients
CaSt	Calcium stearate
CL, CL-SF	Kollidon CL-M, Kollidon CL-BF
CTZ	Cetirizine HCl
DI	Dispersion index
DSC	Differential scanning calorimetry
DPD	Diphenhydramine HCl
EPO	Eudragit EPO
EZE	Acryl EZE polymer
E-TONGUE	Electronic tongue
FDA	Food and Drug Administration
F-H	Flory- Huggins theory
FMT	Famotidine
FT-IR	Fourier-transform infra-red
HIV	Human immunodeficiency virus
HME	Hot melt extrusion
HPLC	High performance liquid chromatography
HTS	High throughput screening
IBU	Ibuprofen
INM	Indomethacin
IVR	Intravaginal ring
L/D	Length/diameter

L100	Eudragit L100
L100-55	Eudragit L100-55
MTDSC	Modulated temperature differential scanning calorimetry
NIR	Near infra-red
NMR	Nuclear magnetic resonance
NSAID	Non-steroidal anti-inflammatory drug
ODT	Orally disintegrating tablets
PAT	Process analytical technique
PEG	Polyethylene glycol
PMOL	Paracetamol
S630	Plasdone S630
scCO ₂	Supercritical carbon dioxide
SEM	Scanning electron microscopy
SFP	Supercritical fluid processing
SOL	Soluplus
T _g	Glass transition temperature
T _m	Melting temperature
VA64	Kollidon VA64
VRP	Verapamil HCl
XL	Polyplasdone XL
XL10	Polyplasdone XL10
XPS	X-ray photoelectron spectroscopy
XRPD	X-ray powder diffraction

PUBLICATIONS

Original Research Articles

- **Maniruzzaman M**, Morgan DJ, Mendham AP, Pang J, Snowden MJ, Douroumis D. Drug-polymer intermolecular interactions in hot-melt extruded solid dispersions. *International Journal of Pharmaceutics*, 2012, accepted.
- **Maniruzzaman M**, Chowdhry BZ, Snowden MJ, Boateng JS, Douroumis D. A review of hot-melt extrusion (HME): Process technology to pharmaceutical products. *ISRN Pharmaceutics*, 2012, In press.
- **Maniruzzaman M**, Rana MM, Boateng JS, Mitchell JC, Douroumis D. Dissolution enhancement of poorly water-soluble APIs processed by hot-melt extrusion using hydrophilic polymers. *Drug Developements and Industrial Pharmacy*. 2012, **In press**.
- **Maniruzzaman M**, Bonnefille M, Aranyos A, Boateng J, Mitchell J, Douroumis D. Taste Masking of Paracetamol by Hot Melt Extrusion: an in vitro and in vivo evaluation. *European Journal of Pharmaceutics and Biopharmaceutics*. 2012, 80(2):433-42.
- Masud M, **Maniruzzaman M**, Mistry S, Douroumis D. Controlled Release of Indomethacin Polymer-lipid Extrudates. *AAPS Journal*. 2012, 14: 2094.
- **Maniruzzaman M**, Pang J, Mendham A, Morgan D, Douroumis D. Intermolecular Interactions of Solid Dispersions Processed by Hot Melt Extrusion. *AAPS Journal*. 2012, 14:5324.
- Vithani K, **Maniruzzaman M**, Mostofa S, Cuppock Y, Douroumis D. Sustained Release of Sodium Diclofenac from Compritol® 888 ATO Lipid Matrix Tablets Produced by Hot Melt Extrusion. *AAPS Journal*. 2012, 14:2095.
- **Maniruzzaman M**, Gryczke A, Schminke S, Beck J, Douroumis D. Development and evaluation of orally disintegrating tablets (ODTs) containing Ibuprofen granules prepared by hot melt extrusion. *Colloids and Surfaces*. 2011; 86(2):275-84.
- **Maniruzzaman M**, Boateng J, Douroumis D. Taste masking of bitter APIs by using hot melt extrusion (HME). *AAPS Journal*, 2011; 13 (S2): T3273-T3273. ISSN 1550-7416.
- **Maniruzzaman M**, Bonnefille M, Aranyos A, Douroumis D. Taste Masking Evaluation of Hot Melt Extruded Paracetamol using an Electronic Tongue. *AAPS Journal*. 2011; 13(S2): W5357-W5357. ISSN 1550-7416.

- **Maniruzzaman M**, Rai D, Boateng JS. Development and characterisation of sodium alginate and HPMC films for mucosal drug delivery. *International Journal of Biotechnology*. 2010; 11: (3-4) 169–181.
- Douroumis D, Onyesom I, **Maniruzzaman M** and Mitchell J. Mesoporous silica nanoparticles in nanotechnology. 2012, *Critical Reviews in Biotechnology*.
In press.

Book Chapters

- **Maniruzzaman M**, Onyesom I, Edwards M, Douroumis D. Mesoporous silica nanoparticles as a drug delivery system. In: *Silica Nanoparticles: Preparation, Properties and Uses*. 2012 (Nova Publishers).
- **Maniruzzaman M**, Douroumis D, Boateng JS and Snowden MJ. Hot-melt Extrusion (HME): From pharmaceutical process to applications. In: *Recent Advances in novel drug carrier systems (ISBN 979-953-307-1092-8)*. 2012 (InTech).

Articles under Review

- **Maniruzzaman M**, Hossain A, Joshua S. Boateng, Snowden MJ, Douroumis D. Sustained release hydrocortisone tablets processed by hot-melt extrusion (HME), *Drug Developments and Industrial Pharmacy*, 2012.
- **Maniruzzaman M**, Boateng JS, Douroumis D. A review of taste masking of bitter APIs by hot-melt extrusion (HME). *Drug Developments and Industrial Pharmacy*, 2012, Invited.
- **Maniruzzaman M**, Boateng JS, Bonnefille M, Aranyos A, Douroumis D. An *in vivo* and *in vitro* Taste Masking Evaluation of Bitter Melt Extruded APIs. *European Journal of Pharmaceutical Sciences*, 2012.
- **Maniruzzaman M**, Vithani K, Slipper I, Mostafa S, Cuppok Y, Douroumis D. Sustained release solid lipid matrices processed by hot-melt extrusion (HME). *Journal of Pharmaceutical Sciences*, 2012.

Conference Proceedings (Selected)

- **Maniruzzaman M**, Pang J, Mendham AP, Boateng JS, Douroumis D. Taste Masking of Bitter APIs through the Intermolecular Interactions Processed by Hot-

Melt Extrusion. 39th Annual meeting and Exposition of CRS 2012, Quebec, Canada.

- **Maniruzzaman M**, Rana MM, Boateng JS, Douroumis D. Dissolution Enhancement of Poorly Water-Soluble APIs Prepared by Hot-Melt Extrusion (HME) using Hydrophilic Polymers. 39th Annual meeting and Exposition of CRS 2012, Quebec, Canada.
- **Maniruzzaman M**, Vithani K, Mostafa S, Cuppok Y, Douroumis D. Compritol® 888 ATO Lipid Matrices for Sustained Release Processed by Hot-Melt Extrusion. 39th Annual meeting and Exposition of CRS 2012, Quebec, Canada.
- **Maniruzzaman M**, Hossain MA, Douroumis D. Chrono – Delivery of Hydrocortisone Tablets Processed by Hot-Melt Extrusion (HME). UKPharmSci 2012. UK
- **Maniruzzaman M**, Boateng JS, Douroumis D. (2011). Increasing the Solubility of Poorly Soluble API by Using Hot-Melt Extrusion (HME). 38th Annual meeting and Exposition of CRS 2011, USA.
- **Maniruzzaman M**, Boateng JS, Douroumis D. (2011). Taste Masking of Bitter APIs by Using Hot-Melt Extrusion (HME). 38th Annual meeting and Exposition of CRS 2011, USA.
- **Maniruzzaman M**, Boateng JS, Bonnefille M, Aranyos A, Douroumis D. (2011). Taste Masking of Paracetamol by Hot Melt Extrusion (HME): An Electronic Tongue Evaluation. 38th Annual meeting and Exposition of CRS 2011, USA.
- **Maniruzzaman M**, Boateng JS, Bonnefille M, Aranyos A, Douroumis D. (2011). Taste Masking of Hot-Melt Extruded Bitter APIs: An Astree E-Tongue Evaluation, EuPFI 2011, Strasbourg, France.
- **Maniruzzaman M**, Boateng JS, Bonnefille M, Aranyos A, Douroumis D. (2011). Taste Masking Evaluation of Hot Melt Extruded Paracetamol using an Electronic Tongue. EuPFI 2011, Strasbourg, France.
- **Maniruzzaman M**, Boateng JS, Douroumis D. (2011). Increasing the Solubility of Poorly Soluble APIs by Using Hot-Melt Extrusion (HME). PharmSci 2011, Nottingham, UK.
- **Maniruzzaman M**, Boateng JS, Bonnefille M, Aranyos A, Douroumis D. (2011). Taste Masking of Bitter APIs by Using Hot-Melt Extrusion (HME). PharmSci 2011, UK.

- **Maniruzzaman M**, Boateng JS, Bonnefille M, Aranyos A, Douroumis D. (2011). An Electronic Tongue Evaluation of Taste Masked APIs prepared by Hot Melt Extrusion (HME). PharmSci 2011, Nottingham, UK.
- **Maniruzzaman M**, Gryczke A, Schminke S, Douroumis D. (2010). Orally disintegrating tablets (odts) & taste masking of bitter APIs. PharmSci 2010, Nottingham, UK.

International Conference: Oral Presentations (invited)

- Increasing the solubility of poorly soluble API by using hot-melt extrusion (HME). **M. Maniruzzaman**, J.S. Boateng, D. Douroumis. UK-PharmSci 2011, The Science of Medicines, 31 August – 2 September, UK
- Taste masking of bitter APIs by using hot-melt extrusion (HME). **M. Maniruzzaman**, M. Bonnefille, A. Aranyos, J. Boateng, D. Douroumis. 38th Annual Meeting & Exposition of the Controlled Release Society (CRS), July 30 – August 3, 2011, National Harbor, Maryland, USA
- XPS analysis of hot-melt extruded (HME) solid dispersions. **M. Maniruzzaman**, Cardiff XPS Access Symposium, February 2012, UK
- Sustained release solid lipid matrices processed by hot-melt extrusion (HME). **M. Maniruzzaman**, K. Vithani, S. Mostafa, Y. Cuppok, D. Douroumis. 39th annual meeting and Exposition of CRS 2012, Canada.

Articles in Preparation

- **Maniruzzaman M**, Boateng JS, Teraoka M, Masaaki H, Pang J, Douroumis D. Evaluations of the interrelation between intermolecular interactions and taste masking efficiency of two anionic polymers in melt extruded solid dispersions. European Journal of Pharmaceutics and Biopharmaceutics, 2012.
- White L, **Maniruzzaman M**, Snowden MJ, Douroumis D. Progress in Pharmaceutical Development of Modified Release Oral Dosage Forms. Expert Opinion in Drug Delivery, 2012.
- **Maniruzzaman M**, Chowdhry BZ, Snowden MJ, Douroumis D. Physicochemical characterisation of amorphous melt extruded solid dispersions of ibuprofen, 2012.

- **Maniruzzaman M**, Chowdhry BZ, Snowden MJ, Douroumis D. Evaluation of the transformation of paracetamol polymorphs in the melt extruded solid dispersions, 2012.
- **Maniruzzaman M**, Boateng JS, Morgan DJ, Snowden MJ, Douroumis D. Physicochemical characterisation of hot-melt extruded solid dispersions by XPS and NMR, 2012.
- **Maniruzzaman M**, Masud SI, Chowdhry BZ, Snowden MJ, Douroumis D, Sustained release paracetamol by Hot-Melt Extrusion (HME), 2012.
- **Maniruzzaman M**, Masud SI, Chowdhry BZ, Snowden MJ, Douroumis D. Controlled release of Indomethacin polymer-lipid extrudates, 2012.

CHAPTER 1: INTRODUCTION

1.0 Background

Over the last three decades hot-melt extrusion (HME) has emerged as an influential processing technology in developing molecular dispersions of active pharmaceutical ingredients (APIs) into polymer matrices and has already been demonstrated to provide time controlled, modified, extended and targeted drug delivery resulting in improved bioavailability [1, 2, 3, 4]. HME has now provided opportunity for use of materials in order to mask the bitter taste of active substances [4]. Since the industrial application of the extrusion process back in the 1930's, HME has received considerable attention from both the pharmaceutical industries and academia in a range of applications for pharmaceutical dosage forms, such as tablets, capsules, films and implants for drug delivery via oral, transdermal and transmucosal routes [5]. This makes HME an excellent alternative to other conventionally available techniques such as solvent evaporation, freeze drying, spray drying and so on (Table 1.1). In addition to being a proven manufacturing process, HME meets the goal of the US Food and Drug Administration's (FDA) process analytical technology (PAT) scheme for designing, analyzing as well as controlling the manufacturing process via quality control measurements during active extrusion process [6]. In this chapter, the hot-melt extrusion technique is reviewed based on a holistic perspective of its various components, processing technologies as well as the materials and novel formulation design and developments in its varied applications in oral drug delivery systems.

1.1 Hot-melt extrusion (HME): Process technology

Joseph Brama first invented the extrusion process for the manufacturing of lead pipes at the end of the eighteenth century [7]. Since then, it has been used in the plastic, rubber and food manufacturing industry to produce items ranging from pipes to sheets and bags. With the advent of high throughput screening, currently more than half of all plastic products including bags, sheets, and pipes are manufactured by HME and therefore various polymers have been used to melt and form different shapes for a variety of industrial and domestic applications. The technology has proven to be a robust method of producing numerous drug delivery systems and therefore it has been found to be useful in the pharmaceutical industry as well [8]. Extrusion is the process of pumping raw materials at elevated controlled temperature and pressure through a heated barrel into a product of uniform shape and density [9]. Breitenbach first introduced the development of melt extrusion process in pharmaceutical manufacturing operations [10], however, Follonier and his co-workers first examined the hot melt technology to manufacture

sustained release polymer based pellets of various freely soluble drugs ^[11]. HME involves the compaction and conversion of blends from a powder or a granular mix into a product of uniform shape ^[9]. During this process, polymers are melted and formed into products of different shapes and sizes such as plastic bags, sheets, and pipes by forcing polymeric components and active substances including any additives or plasticisers through an orifice or die under controlled temperature, pressure, feeding rate and screw speed ^[9, 12]. However, the theoretical approach to understanding the melt extrusion process can be summarized by classifying the whole procedure of HME compaction into the following ^[13]:

- 1) feeding of the extruder through a hopper,
- 2) mixing, grinding, reducing the particle size, venting and kneading,
- 3) flow through the die, and
- 4) extrusion from the die and further down-stream processing (Fig. 1.1).

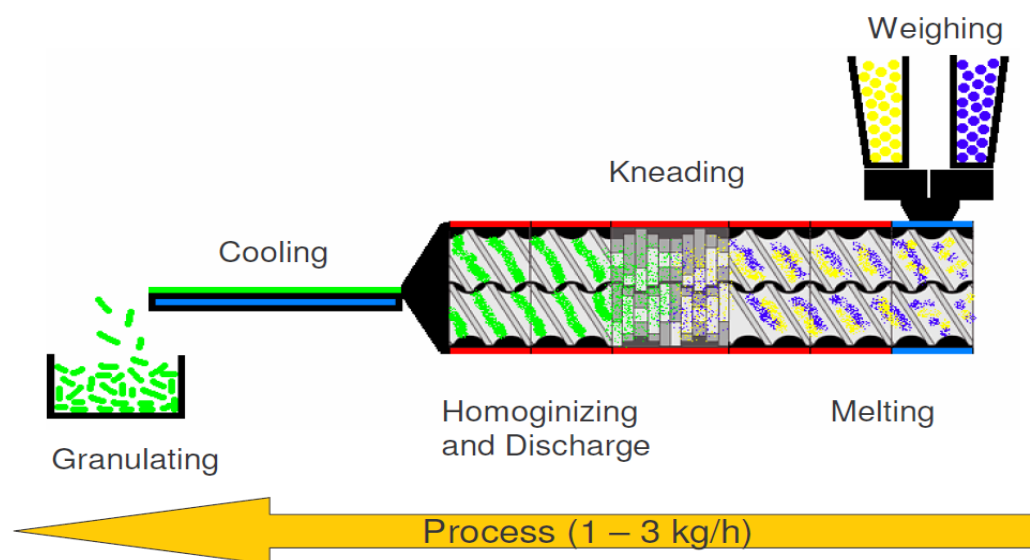


Fig. 1.1: Schematic diagram of the HME process ^[12].

The extruder generally consists of one or two rotating screws (either co-rotating or counter rotating) inside a stationary cylindrical barrel. The barrel is often manufactured in sections in order to shorten the residence time of molten materials. The sectioned parts of the barrel are then bolted or clamped together. An end-plate die is connected to the end of the barrel which is determined according to the shape of the extruded materials.

Table 1.1: HME and other conventional processing techniques; advantages and disadvantages.

Technologies	Advantages	Disadvantages
Hot-melt extrusion ^[1-6]	<ul style="list-style-type: none">- Solvent free- Fast and continuous process- Low cost- Small footprint- High recovery- In line monitoring	<ul style="list-style-type: none">- Temperature (thermolabile molecules)- Downstream processing
Spray Drying ^[5]	<ul style="list-style-type: none">- Fast process- Flexible particle sizes	<ul style="list-style-type: none">- Solvent residues (toxicity issue)- Processing parameters- Small yield- Cost
Freeze drying ^[5]	<ul style="list-style-type: none">- Mild condition- Suitable for thermolabile molecules	<ul style="list-style-type: none">- Solvent residues- Cost- Longer processing time- Cry protecting- Suitable solvent with high freezing point for sublimation process.
Supercritical fluid processing ^[5]	<ul style="list-style-type: none">- Mild conditions	<ul style="list-style-type: none">- Limited solubility of CO₂- Cost- Time- Phase separation during evaporation
Solvent evaporation ^[5]	<ul style="list-style-type: none">- Mild condition	<ul style="list-style-type: none">- Solvent residues- Cost- Time- Suitable solvent- Phase separation during evaporation

1.2 Equipment: single screw and twin screw extruder

A single screw extruder consists of one rotating screw positioned inside a stationary barrel at the most fundamental level. In the more advanced twin-screw systems, extrusion of materials is performed by either a co-rotating or counter-rotating screw configuration ^[9]. Irrespective of type and complexity of the function and process, the extruder must be capable of rotating the screw at a selected predetermined speed while compensating for the torque and shear generated from both the material being extruded and the screws being used. However, regardless of the size and type of the screw inside the stationary barrel a typical extrusion set up consists of a motor which acts as a drive unit, an extrusion barrel, a rotating screw and an extrusion die ^[13]. A central electronic control unit is connected to the extrusion unit in order to control the process

parameters such as screw speed, temperature and therefore pressure ^[14]. This electronic control unit acts as a monitoring device as well. The typical length diameter ratios (L/D) of screws positioned inside the stationary barrel are another important characteristic to consider whether the extrusion equipment is a single screw or twin screw extruder. The L/D of the screw either in a single screw extruder or a twin screw extruder typically ranges from 20 to 40:1(mm). In case of the application of pilot plant extruders the diameters of the screws significantly ranges from 18-30 mm. In pharmaceutical scale up, the production machines are much larger with diameters typically exceeding 50 - 60 mm ^[15]. In addition, the dimensions of a screw change over the length of the barrel. In the most advanced processing equipment for extrusion, the screws could be separated by clamps or be extended in proportion to the length of the barrel itself. A basic single screw extruder consists of three discrete zones: feed zone, compression and a metering zone (Fig. 1.2). Under the compression zone which is basically know as processing zone could be accompanied by few other steps such as mixing, kneading, venting etc ^[13, 15].

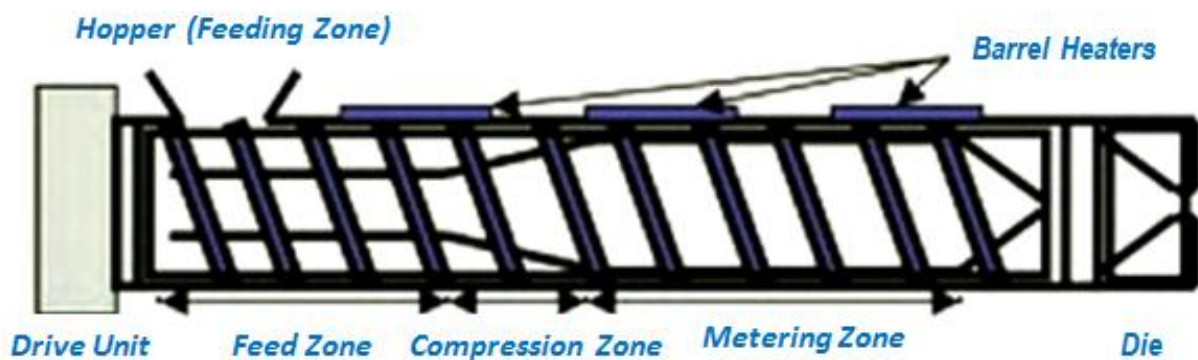


Fig. 1.2: Schematic diagram of a single screw extruder ^[10].

The depth along with the pitch of the screw flights (both perpendicular and axial) differ within each zone, generating dissimilar pressures along the screw length (Fig. 1.3). Normally the pressure within the feed zone is very low in order to allow for consistent feeding from the hopper and gentle mixing of API, polymers and other excipients and therefore the screw flight depth and pitch are kept larger than that of other zones. At this stage of the process the pressure within the extruder is very low which subsequently gets increased in the compression zone. This result in a gradual increase in pressure along the length of the compression zone effectively imparts a high degree of mixing and compression to the material by decreasing the screw pitch and/or the flight depth ^[9, 15]. Moreover the major aim of the compression zone is not only to

homogenize but also compress the extrudate to ensure the molten material reaches the final section of the barrel (metering zone) in a form appropriate for processing. Finally the final section which is known as the metering zone stabilizes the effervescent flow of the matrix and ensures the extruded product has a uniform thickness, shape and size. A constant and steady uniform screw flight depth and pitch helps maintain continuous high pressure ensuring a uniform delivery rate of extrudates through the extrusion die and hence a uniform extruded product.

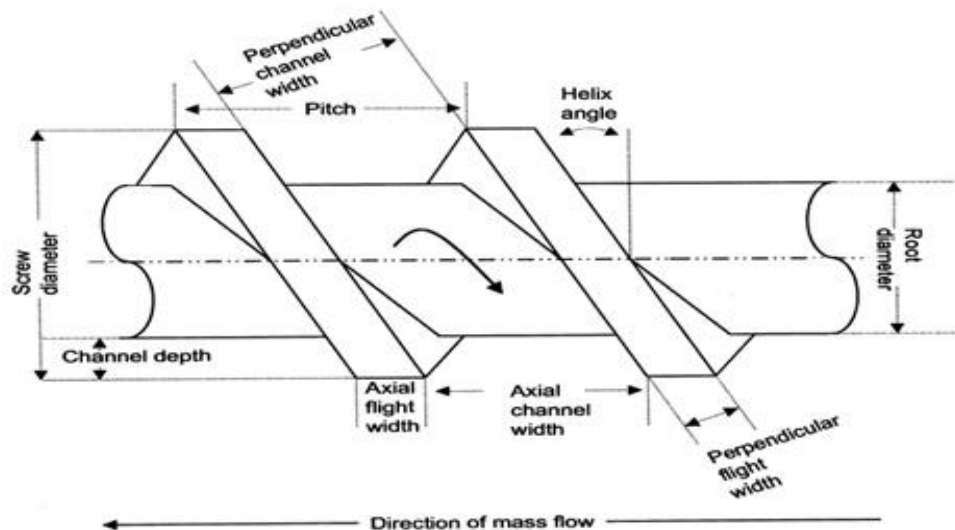


Fig. 1.3: Screw geometry (extrusion) [9].

In addition to the above mentioned systems, downstream auxiliary equipment for cooling, cutting, collecting the finished product is also typically employed. Mass flow feeders to accurately meter materials into the feed hopper, pelletizers, spheronizer, roller/calendering device in order to produce continuous films and process analytical technology such as near infra-red (NIR) and Raman, ultra sound, DSC systems are also options. Throughout the whole process, the temperature in all zones are normally controlled by electrical heating bands and monitored by thermocouples.

The single screw extrusion system is simple and offers lots of advantages but still does not acquire the mixing capability of a twin-screw machine and therefore is not the preferred approach for the production of most pharmaceutical formulations. Moreover, a twin-screw extruder offers much greater versatility (process manipulation and optimisation) in accommodating a wider range of pharmaceutical formulations making this set-up much more constructive. The rotation of the screws inside the extruder barrel may either be co-rotating

(same direction) or counter-rotating (opposite direction), both directions being equivalent from a processing perspective (Fig. 1.4). A greater degree of conveying and much shorter residence times are achievable with an intermeshing set-up. Furthermore, the use of reverse-conveying and forward-conveying elements, kneading blocks and other intricate designs as a means of improving or controlling the level of mixing required can help the configuration of the screws themselves to be varied [16].

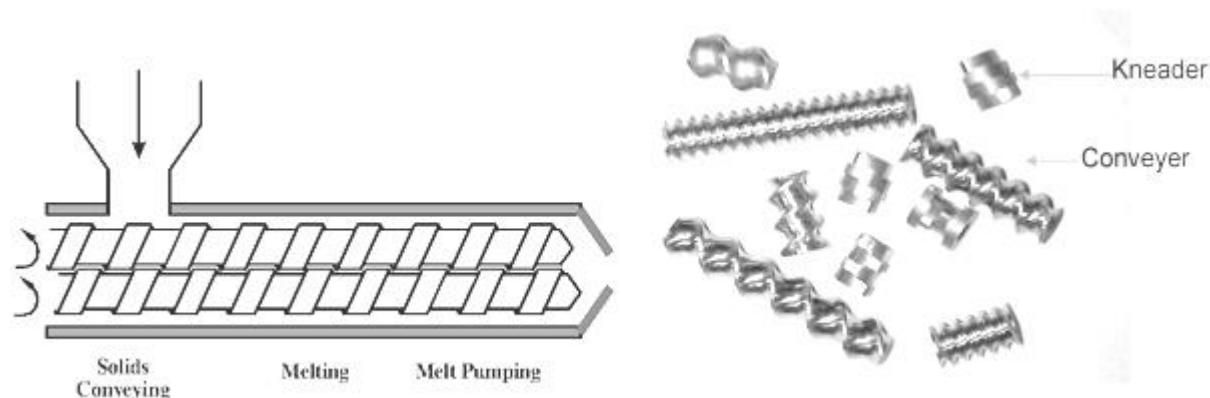


Fig. 1.4: A twin screw extruder and screws [9].

1.3 Advantages and disadvantages of HME

Advantages

HME offers several advantages over conventionally available pharmaceutical processing techniques via appropriate selections of polymeric (thermoplastic) carriers as discussed in Table 1.1, including: (a) increased solubility and bioavailability of water insoluble compounds, (b) solvent free non ambient process, (c) economical process with reduced production time, fewer processing steps, and a continuous operation, (d) capabilities of sustained, modified and targeted release, (e) better content uniformity in extrudates, (f) no requirements for the compactibility of active ingredients, (g) uniform dispersion of fine particles, (h) good stability at changing pH and moisture levels and safe application in humans, (i) reduced number of unit operations and production of a wide range of performance dosage forms, and (j) a range of screw geometries [17, 18, 19, 20, 21].

Disadvantages

However, HME has some disadvantages as well. The main drawbacks of HME include: thermal process (drug/polymer stability), use of a limited number of polymers, high flow

properties of polymers and excipients required and not suitable for relatively high heat sensitive molecules such as microbial species, proteins etc [20, 21].

1.4 Applications of HME

Extrusion technology is one of the most important fabrication processes in the plastic and rubber industries. Products made from melt extruded polymers range from pipes to hoses through to the insulated wires, cables, rubber sheeting and polystyrene tiles. Plastics that are commonly processed by HME technique include acrylics and cellulose, polyethylene, polypropylene, polystyrene and vinyl plastics [9, 22]. In the food industry, extrusion has been utilized for pasta production with a widely used multitasking technique combining cooking and extrusion in a self-styled extrusion cooker [23]. In the animal feed industry and veterinary science, extrusion is commonly applied as a means of producing pelletized feeds, implants or injection moulding [24]. HME has successfully been applied in the formulation of fast dispersing PVP melt extrudates of poorly soluble active agents as solid molecular dispersions in the crop protection field [25].

HME technology has already achieved a strong place in the pharmaceutical industry and academia due to several advantages over traditional processing methods such as roll spinning and grinding [18]. In addition to being an efficient manufacturing process, HME enhances the quality and efficacy of manufactured products and therefore over the past few years HME has emerged as a novel technique in pharmaceutical applications [15, 28]. The main use of HME is to disperse active pharmaceutical ingredients (APIs) in a matrix at the molecular level, thus forming solid dispersions [1, 26]. In the pharmaceutical industry, HME has been used for various applications, such as i) enhancing the dissolution rate and bioavailability of poorly soluble drugs by forming a solid dispersion or solid solution, ii) controlling or modifying the release of the drug, iii) taste masking of bitter APIs, and iv) formulation of various thin films [27].

The bioavailability of an active ingredient is controlled by its aqueous solubility. Therefore, increasing the solubility of water insoluble drugs is still a real challenge in the formulation development process [26]. Due to the advent of high throughput screening (HTS) in the drug discovery process, the resultant compounds are often high molecular weight and highly lipophilic and therefore exhibit poor solubility [29]. Scientists have already tried to address solubility issues by various pharmaceutical interventions. Among the many methods available to improve solubility and dissolution rate, preparation of solid dispersions and solid solutions has gained vast attention. For that reason, HME has been successfully applied to prepare solid molecular dispersion of APIs into different hydrophilic polymer matrices [26, 29].

1.5 Formulation research and developments to date

Despite the fact that initial research developments have focused on the effects of formulation and processing variables on the properties of the final dosage forms, [9, 30, 31, 34, 35] more recent investigations have focused on the use of HME as a novel manufacturing technology of solid molecular dispersions through to the development of mini-matrices, taste masked formulations and also sustained release formulations as well as paediatric formulations [26, 48]. Early work by De Brabander *et al.* (2000) described the preparation of matrix mini-tablets which was followed by further investigations into the properties of sustained release mini-matrices manufactured from ethyl cellulose, HPMC and ibuprofen [32, 33]. Extruded mini tablets showed minimised risk of dose dumping, reduced inter- and intra-subject variability. Recently, Roblegg *et al.* (2011) reported the development of retarded release pellets using vegetable calcium stearate (CaSt) as a thermoplastic excipient processed through HME, where pellets with a drug loading of 20% paracetamol released only 11.54% of the drug after 8 hours due to the significant densification of the pellets. As expected, the drug release was influenced by the pellet size and the drug loading [36]. A microbicide intravaginal ring (IVR) IVR was prepared and developed from polyether urethane (PU) elastomers for the sustained delivery of UC781 (a highly potent nonnucleoside reverse transcriptase inhibitor of HIV-1). PU IVRs containing UC781 were fabricated using a hot-melt extrusion process [37].

Moreover, a fourfold increase in the availability of propranolol in the systemic circulation was observed when the HME formulation was compared with a commercially available formulation (Inderal®). Over the last five years HME has been used largely to manufacture granules, pellets, immediate and modified release tablets, transmucosal/ transdermal films and implantable reservoir devices [3, 4, 9, 35, 38]. For instance, with respect to drug administration through the oral route, molecular solid dispersions of nifedipine [38], nimodipine [29] and itraconazole [39, 40, 41] have been successfully produced using HME technology. Amorphous indomethacin dispersions have been manufactured using pharmaceutically acceptable hydrophilic polymers by using HME technology [26, 42, 43].

Furthermore, HME research developments have driven targeted drug delivery systems including enteric matrix tablets and capsule systems over the last few years [44, 45]. Miller *et al.* (2007) have demonstrated the ability of HME to act as an efficient dispersive process for aggregated, fine engineering particles to improve dissolution rate properties by enhancing

particles' wettability ^[46]. A very interesting investigation of Verreck and co-workers (2006) ^[47] determined the use of supercritical carbon dioxide (scCO₂) as a temporary plasticiser during the manufacture of ethylcellulose through HME. A significant reduction in the processing temperature was achieved using scCO₂ without any disadvantageous effects on the extrudate. Macroscopic morphology was significantly altered due to expansion of the scCO₂ in the die. The use of scCO₂ increased the surface area, porosity and hygroscopicity of the final dosage forms. More recently Douroumis and co-workers used HME technique to effectively enhance the dissolutions of ibuprofen, indomethacin and famotidine through the effective formation of solid dispersions of active substances into the polymer matrices ^[26, 42].

The taste masking of bitter APIs is a major challenge especially for the development of orally disintegrating tablets (ODTs). HME has been reported to be an effective technique to mask the bitter tastes of various APIs by the use of taste masking polymers that create solid dispersions to prevent bitter drugs from coming in contact with the patient's taste buds. Breitkruitz *et al.* (2008) successfully applied HME in taste masking of sodium benzoate for the formulation of paediatric drugs ^[48]. More recently Gryckze *et al.* (2011) developed taste masked formulations of ibuprofen with Eudragit EPO polymer ^[42]. Basically, taste masking is achieved through intermolecular forces (e.g. hydrogen bonding) between the active substance and the polymer matrix by processing oppositely charged compounds through HME ^[42, 49, 50]. The extrusion of solid lipids using twin-screw extruders was introduced for the preparation of immediate or sustained release taste masked matrices ^[51]. In this process, occasionally called "solvent – free cold extrusion" the lipids are extruded below their melting ranges. Consequently, the lipids are not melted during extrusion and build a coherent matrix with low porosity. In these studies, the effect of lipid composition and processing parameters such as the die diameter, the size of the extruded pellets, the screw speed and the powder feeding rates on the obtained drug release patterns were thoroughly investigated. Very recently, Breitkreutz *et al.* (2012) applied solid lipid extrusion at room temperature for the taste masked formulation development of the BCS Class II drug NXP 1210. NXP 1210 is an acidic, non-steroidal anti-inflammatory drug ^[52]. The lipophilic character is described by its log P value of 3. In this study, the authors investigated powdered hard fat (Witocan® 42/44 mikrofein), glycerol distearate (Precirol® ato 5) and glycerol trimyristate (Dynasan® 114) as lipid binders. The lipid based formulations designed in this study was feasible for taste-masked granules or pellets containing poorly soluble drugs ^[52].

However, only a handful of research works have been reported in the use of hot-melt extrusion for the manufacture of films ^[53, 54]. Films can be defined as thin sheets containing one or more polymers with or without a plasticiser and may be used as a drug delivery system (device) or directly applied to facilitate a therapeutic effect as in wound dressings. Films are currently being produced mainly by solvent casting in which polymers (and excipients such as plasticisers) are dissolved in a suitable solvent until they form clear viscous solution (gel). While film preparation using the solvent-casting approach allows film uniformity, clarity, flexibility and adjustable thickness to accommodate drug loadings they are limited by decreased elongation or elasticity and increased film tensile strength when physical aging is applied ^[53]. Another, limitation associated with solvent cast films is the use of organic solvents for water insoluble polymers. The hazardous nature of most organic solvents and the residual solvents after drying affect the selection of the appropriate solvent ^[54-57] as well as complicated processing conditions and disposal of the associated waste, all of which create significant environmental concerns. As a result, alternative technologies are needed in the pharmaceutical industry to overcome some of the challenges described above. The two commonly used approaches include spray coating and hot melt extrusion with the latter becoming increasingly popular due to the many advantages it provides. Firstly, no solvents are used and fewer processing steps are required. In fact one of the key advantages of HME is the fact that extrudates can be obtained in a single processing step making it very economical. As far as films are concerned, there is no requirement for compressing of the active ingredients together with the excipients. The melting of the polymer into the molten state, coupled with the thorough initial mixing allows a more uniform dispersion of fine particles. Further, molecular dispersion of the drug helps improve its bioavailability ^[58]. Hot melt extruded films are produced through a simple process involving blending of appropriate amounts of relevant polymer, drug and plasticiser into a uniform powdered mixture prior to feeding through the hopper of the preheated extruder and transferred into the heated barrel by a rotating extruder screw. Homogeneous films are obtained with thickness generally expected to be in the range less than 1 mm. Generally three main ingredients are required for successful formulation of hot melt extruded films i.e. film forming polymer, active ingredient and plasticiser ^[59]. The latter is required to impart flexibility to the final film which ensures ease of handling and application to the site of action. Occasionally, other additives are added to affect other functionally important properties such as bioadhesive agent which ensures that the film adheres to the mucosal surface for a long enough time to allow drug absorption or action. Different polymers and drugs have been employed and reported in the literature for obtaining drug loaded hot-melt extruded films for various indications and are summarised in Table 1.2.

Table 1.2: Different hot-melt extruded films comprising of different polymeric materials, plasticisers and active ingredients for various indications.

Main polymer(s)	Plasticiser/additive	Main active ingredient(s)	Types of films
Acrylic ^[60, 61] Eudragit	- Triacetin - Triethylcitrate	Clotrimazole	Bioadhesive Control release
Hydroxypropylcellulose ^[60] Polyethylene oxide	N/A	Ketoconazole	Bioadhesive films for Onychomycosis Fast release
Hydroxypropylcellulose ^[62] Hydroxypropylmethylcellulose Polyethylene oxide	Polyethylene glycol 3350	Lidocaine	Water soluble Bioadhesive
Hydroxypropylcellulose ^[65]	Polyethylene glycol 400	Hydrocortisone Chlorpheniramine maleate	Hydrophillic Bioadhesive
Hydroxypropylcellulose ^[58] Polycarbophil	Polyethylene glycol 3350	Clotrimazole	Bioadhesive Fast release
Polyethylene oxide ^[59]	N/A	Ketoprofen	Bioadhesive Antifungal

Repka and co-workers have conducted extensive research on the use of HME for the manufacture of mucoadhesive buccal films. They successfully evaluated different matrix formers and additives for the processing of the blend prior to extrusion^[61, 62, 63, 64]. In an early investigation, it was found that even though films containing exclusively HPC could not be obtained, the addition of plasticizers, such as triethyl citrate, PEG 2000/8000, or acetyltributyl citrate, allowed for the manufacture of thin, flexible, and stable HPC films^[65]. It has also been found that increasing the molecular weight of HPC decreased the release of drugs from hot-melt extruded films which resulted in dissolution profiles exhibiting zero-order drug release. According to the models applied in the research, the drug release was solely determined by erosion of the buccal film^[66, 67, 68].

Development of films by HME may present future opportunities to develop gastro-retentive films for prolonged drug delivery and multi-layer films to modulate drug release for

oral and transdermal applications. The growing market in medical devices, including incorporating drugs into devices such as biodegradable stents and drug-loaded catheters will undoubtedly require HME manufacturing processes. These are required to be commercialised and perhaps may lead to new areas of collaboration across pharmaceutical, medical device and biotechnology research.

1.6 HME in commercial products

HME related patents which have been issued for pharmaceutical systems have steadily increased since the early 1980's ^[69]. So far, the USA and Germany hold approximately more than half (56%) of all issued patents for HME in the market. Despite this increased interest, only a handful of commercialized HME pharmaceutical products are currently marketed. Several companies have been recognized to specialize in the use of HME as a drug delivery technology, such as PharmaForm and SOLIQS (Abbott). Recently, SOLIQS has developed a proprietary formulation which is known as Meltrex® and re-developed a protease-inhibitor combination product, Kaletra®. Kaletra is mainly used for the treatment of human immunodeficiency virus (HIV) infections. The formulated, melt extruded product was shown to have a significant enhancement in the bioavailability of active substances ^[70]. Furthermore, HME Kaletra® tablets were shown to have significant advantages for patient compliance (i.e. reduced dosing frequency and improved stability) compared to the previous soft-gel capsule formulation as recognized by the FDA decision to fast-track approval. Additionally, Nurofen (Meltlets® lemon) is available in the market as a fast dissolving tablet prepared by similar technique to HME ^[42]. Ibuprofen has been used as active substance in the Meltlets® tablets. Moreover, SOLIQS has also developed a fast-onset ibuprofen system and a sustained-release formulation of verapamil (Isoptin® SR-E) through a HME related technology called 'Calendaring' that was the first directly shaped HME product in the market.

1.7 Summary

HME has proven to be a robust method of producing numerous drug delivery systems and therefore it has been found to be useful in the pharmaceutical industry enlarging the scope to include a range of polymers and APIs that can be processed with or without plasticizers. It has also been documented that HME is a solvent-free, robust, quick and economy favoured manufacturing process for the production of a large variety of pharmaceutical dosage forms.

1.8 Aims and objectives

The purpose of this research study is to develop HME as an efficient technique for the formulation of various oral solid dosage forms with the aim of increasing the dissolution rate of some poorly soluble model APIs (i.e. ibuprofen, indomethacin, famotidine) via the formation of solid dispersions. Also the evaluation of taste masking efficiency (*in vivo* and *in vitro*) of different polymeric matrices (via intermolecular hydrogen bonding) as well as characterizing all possible intermolecular interactions in the solid dispersions has been prioritised as second aim of this research.

1.9 References

1. Kalivoda A, Fischbach M, Kleinebudde P. Application of mixtures of polymeric carriers for dissolution enhancement of oxeglitazar using hot-melt extrusion. *Int J Pharm.* 2012; 439(1-2):145-56.
2. Repka MA, Shah S, Lu J, Maddineni S, Morott J, Patwardhan K, Mohammed NN. Melt extrusion: process to product. *Exp Opin Drug Deliv* 2012; 9(1):105-25.
3. Repka MA, Majumdar S, Kumar Battu S, Srirangam R, Upadhye SB. Applications of hot-melt extrusion for drug delivery. *Exp Opin Drug Deliv* 2008; 5(12):1357-76.
4. Repka MA, Battu SK, Upadhye SB, Thumma S, Crowley MM, Zhang F, Martin C, McGinity JW. Pharmaceutical applications of hot-melt extrusion: Part II. *Drug Dev Ind Pharm* 2007; (10):1043-57.
5. Kolter K, Karl M, Gryczke A. Hot-melt extrusion with BASF Pharma polymers, *Extrusion Compendium (2nd edition)*, BASF Germany. 2012.
6. Crowley MM, Thumma S, Updhye SB. Pharmaceutical applications of hot melt extrusion: part- I. *Drug Dev Ind Pharm* 2007; 33(9):909-26.
7. James S. *Encyclopedia of Pharmaceutical Technology.* 2004; 3rd Ed (3); P-20.
8. Andrews GP and Jones DS. Formulation and Characterization of Hot Melt Extruded Dosage Forms: Challenges and Opportunities. *Cheminform* 2010; 41(43).
9. Breitenbach J. Melt extrusion: from process to drug delivery technology. *Eur J Pharm Biopharm* 2002; 54:107–117.
10. Andrews GP, David S, Osama AM, Daniel NM, Mark.S. Hot Melt Extrusion: An Emerging Drug Delivery Technology. *Pharm Tech Europe* 2009; 21 (1):24-27.
11. Follonier N, Doelker E, Cole ET. Evaluation of hot-melt extrusion as a new technique for the production of polymerbased pellets for sustained release capsules containing high loadings of freely soluble drugs. *Drug Dev Ind Pharm* 1994; 20(8):1323-133.

12. Gryczke A. Melt Extrusion with EUDRAGIT® Solubility Enhancement Modified Release. Degussa. RÖHM GmbH & Co. KG, Darmstadt. 2006-06-13.
13. Chokshi R, Zia H. Hot-Melt Extrusion Technique: A Review. *I J Pharm Res* 2004; 3: 3-16.
14. Whelan T, Dunning D (Eds.). *The Dynisco Extrusion Processors Handbook* 1st ed., London School of Polymer Technology 1988, Polytechnic of North London, London.
15. Andrews GP, Margetson DN, Jones DS, McAllister SM, Diak OA. *A basic Guide: Hot-melt Extrusion*. UKICRS 2008;13.
16. White JL. *Twin Screw Extrusion: Technology and Principles*. Hanser/ Gardner Publications Inc. 1991; Cincinnati, Ohio. ISBN 1-56990-109-0.
17. <http://www.pharinfo.net/reviews/melt-granulation-techniques/reviews>.
18. McGnity JW, KOleng JJ. Preparation and Evaluation of Rapid Release Granules Using Novel Melt Extrusion Technique. *AAPS*.2004; 153-54.
19. Jones DS. Engineering Drug Delivery Using Polymer Extrusion/Injection Moulding Technologies. *Sch Pharm* 2008; 4-9: 18-27.
20. Grunhagen HH, Muller O. Melt extrusion technology. *Pharm Manu Int* 1995; 1: 167–170.
21. Singhal S, Lohar VK, Arora V. Hot-melt extrusion technique. *WebmedCentral Pharm Sci* 2011; 2(1): 001459
22. Mollan M. Historical overview, in: I. Ghebre-Sellassie, C. Martin (Eds.), *Pharmaceutical Extrusion Technology*, CRC Press 2003; 1–18.
23. Senouci A, Smith A, Richmond A. Extrusion cooking, *Chem. Eng* 1985; 417: 30–33.
24. Sebestyen E. Problems of grains preservation in storage facilities. *Flour and feed mill* 1974; 10: 24–25.
25. Wedlock DJ, Wijngaarden DV. Fast dispersing solid PVP-containing crop protection formulation and process therefore, *US Patent* 1992; 5: 665,369.
26. Litvinov VM, Guns S, Adriaensens P, Scholtens BJ, Quaedflieg MP, Carleer R, Van den Mooter G. Solid State Solubility of Miconazole in Poly[(ethylene glycol)-g-vinyl alcohol] Using Hot-Melt Extrusion. *Mol Pharm*. 2012; 9(10):2924-32.
27. Morales JO, McConville JT. Manufacture and characterization of mucoadhesive buccal films. *Eur J Pharm Biopharm* 2011; 77:187–199.
28. M. Repka, M. Munjal, M. Elsohly, S. Ross. Temperature stability and bioadhesive properties of D9-tetrahydrocannabinol incorporated hydroxypropylcellulose polymer matrix systems, *Drug Dev Ind Pharm* 2006; 32: 21–32.

29. Zheng X, Yang R, Tang X and Zheng L. Part I: Characterization of Solid Dispersions of Nimodipine Prepared by Hot-melt Extrusion. *Drug Deve Ind Pharm* 2007; 33:791–802.
30. Jana S, Miloslava R. Hot-melt extrusion, *Cesk Slov Farm* 2012; 61(3): 87-92.
31. Cilurzo F, Cupone I, Minghetti P, Selmin F, Montanari L. Fast dissolving films made of maltodextrins, *Eur J Pharm Biopharm* 2008; 70: 895-900.
32. De Brabander C, Vervaet C, Fiermans L, Remon JP. Matrix mini-tablets based on starch/microcrystalline wax mixtures. *Int J Pharm* 2000; 199: 195-203.
33. De Brabander C, Vervaet C, Remon JP. Development and evaluation of sustained release mini-matrices prepared via hot melt extrusion. *J Cont Rel* 2003; 89: 235–247.
34. Zhang F, McGinity JW. Properties of sustained-release tablets prepared by hot-melt extrusion. *Pharm Dev Tech* 1999; 4(2): 241–250.
35. Crowley MM, Zhang F, Koleng JJ, McGinity JW. Stability of polyethylene oxide in matrix tablets prepared by hot-melt extrusion. *Biomater* 2002; 23: 4241-4248.
36. Roblegg E, Jäger E, Hodzic A, Koscher G, Mohr S, Zimmer A, Khinast J. Development of sustained-release lipophilic calcium stearate pellets via hot melt extrusion. *Eur J Pharm Biopharm* 2011; 79: 635–645.
37. Clark MR, Johnson TJ, McCabe RT, Clark JT, Tuitupou A, Elgendy H, Friend DR, Kiser PF. A hot-melt extruded intravaginal ring for the sustained delivery of the antiretroviral microbicide UC781. *J Pharm Sci* 2012; 101(2):576-87.
38. Li L, AbuBaker O, Shao Z, (2006). Characterization of poly (ethylene oxide) as a drug carrier in hot-melt extrusion. *Drug Dev Ind Pharm* 2006; 32: 991–1002.
39. Rambali B, Verreck G, Baert L, Massart DL. Itraconazole formulation studies of the melt-extrusion process with mixture design. *Drug Dev Pharm* 2003; 29(6): 641–652.
40. Six K, Berghmans H, Leuner C, Dressman J, Van Werde K, Mullens J, Benoist L, Thimon M, Meublat L, Verreck G, Peeters J, Brewster M, Van den Mooter G. Characterization of solid dispersions of itraconazole and hydroxypropylmethylcellulose prepared by melt extrusion, Part II. *Pharm Res* 2003; 20(7): 1047–1054.
41. Six K, Daems T, de Hoon J, Van Hecken A, Depre M, Bouche MP, Prinsen P, Verreck G, Peeters J, Brewster ME, Van den Mooter G. Clinical study of solid dispersions of itraconazole prepared by hot-stage extrusion. *Eur J Pharm Sci* 2005; 24(2–3): 179–186.
42. Gryckze A, Schminke GS, Maniruzzaman M, Beck J, Douroumis D. Development and evaluation of orally disintegrating tablets (ODTs) containing ibuprofen granules prepared by hot melt extrusion. *Colloids Surf B Bio* 2011; 86: 275-84.

43. Chokshi RJ, Shah NHS, Sandhu KH, Malick AW, Zia H. Stabilization of Low Glass Transition Temperature Indomethacin Formulations: Impact of Polymer-Type and Its Concentration. *J Pharm Sci* 2008; 97(6):2286-98.
44. Andrews GP, Jones DS, Abu Diak O, McCoy CP, Watts AB, McGinity JW. The manufacture and characterization of hot melt extruded enteric tablets. *Eur J Pharm Biopharm* 2008; 69(1):264-73.
45. Mehuys E, Remon JP, Vervaet C. Production of enteric capsules by means of hot-melt extrusion. *Eur J Pharm Sci* 2005; 24: 207-212.
46. Miller DA, Jason TM, Yang W, Robert OW, McGinity JW. Hot-Melt Extrusion for Enhanced Delivery of Drug Particles. *J Pharm Sci* 2007; 96(2): 361-376.
47. Verreck G, Decorte A, Heymans K, Adriaensen J, Liu D, Tomasko D, Arien A, Peeters J, Van den Mooter G, Brewster ME. Hot stage extrusion of p-amino salicylic acid with EC using CO₂ as a temporary plasticizer. *Int J Pharm* 2006; 327: 45-50.
48. Breitreutz J, El-Saleh F, Kiera C, Kleinebudde P, Wiedey W. Pediatric drug formulations of sodium benzoate: II. Coated granules with a lipophilic binder. *Eur J Pharm Biopharm* 2003; 56: 255-60.
49. Douroumis D. Practical approaches of taste masking technologies in oral solid forms. *Exp Opin Drug Deliv* 2007; 4: 417–426.
50. Douroumis D. Orally disintegrating dosage forms and taste-masking technologies. *Exp Opin Drug Deliv* 2010; 8: 665-75.
51. Witzleb R, Kanikanti VR, Hamann HJ, Kleinebudde P. Solid lipid extrusion with small die diameters--electrostatic charging, taste masking and continuous production. *Eur J Pharm Biopharm* 2011; 77: 170-7.
52. Vaassena J, Bartscherb K, Breitreutz J. Taste masked lipid pellets with enhanced release of hydrophobic active Ingredient. *Int J Pharm* 2012, 429:99– 103.
53. Gutierrez-Rocca JC, McGinity JW. Influence of aging on the physical-mechanical properties of acrylic resin films cast from aqueous dispersions and organic solutions. *Drug Dev Ind Pharm* 1993; 19:315–332.
54. Steuernagel CR. Latex emulsions for controlled drug delivery. In McGinity JW. (Ed.), *Aqueous polymeric coatings for pharmaceutical dosage forms*, Marcel Dekker Inc, 1997; 79: 582.
55. Barnhart S, Thin film oral dosage forms, in Rathbone MJ, Hadgraft J, Roberts MS, Lane ME (Eds.), *Modified-release Drug Delivery Technology*, Informa Healthcare, 2008:209–216.

56. International Conference on Harmonization, ICH topic Q3C (R3) Impurities: Residual Solvents, 2009. [<http://www.emea.europa.eu/pdfs/human/ich/028395en.pdf>].
57. Palem CR, Kumar BS, Maddineni S, Gannu R, Repka MA, Yamsani MR. Oral transmucosal delivery of domperidone from immediate release films produced via hot-melt extrusion technology. *Pharm Dev Tech* 2012. In press.
58. Repka MA, McGinity JW, Zhang F, Koleng JJ. Encyclopedia of pharmaceutical technology, in Boylan J (ed.), Marcel Dekker, NewYork, 2002.
59. Tumuluri VS, Kemper MS, Lewis RI, Prodduturi S, Majumdar S, Avery BA, Repka MA. Off-line and On-line Measurements of Drug-loaded Hot-Melt Extruded Films Using Raman Spectroscopy. *Int J Pharm* 2008; 357(1-2):77-84.
60. Mididoddi PK, Repka MA. Characterization of hot-melt extruded drug delivery systems for onychomycosis. *Eur J Pharm Biopharm* 2007; 66:95–105.
61. Prodduturi S, Manek R, Kolling W, Stodghill S, Repka M. Solid-state stability and characterization of hot-melt extruded poly(ethylene oxide) films. *J Pharm Sci* 2005; 94:2232–2245.
62. Repka M, Gutta K, Prodduturi S, Munjal M, Stodghill S. Characterization of cellulosic hot-melt extruded films containing lidocaine. *Eur J Pharm Biopharm* 2005; 59:189–196.
63. Repka M, McGinity J. Bioadhesive properties of hydroxypropylcellulose topical films produced by hot-melt extrusion. *J Cont Rel* 2001; 70:341–351.
64. Thumma S, Majumdar S, ElSohly M, Gul W, Repka M. Preformulation studies of a prodrug of D9-tetrahydrocannabinol. *AAPS Pharm SciTech* 2008a; 9: 982–990.
65. Repka M, Gerding T, Repka S, McGinity J. Influence of plasticizers and drugs on the physical–mechanical properties of hydroxypropylcellulose films prepared by hot melt extrusion. *Drug Dev Ind Pharm* 1999; 25:625–633.
66. Prodduturi S, Manek R, Kolling W, Stodghill S, Repka M. Water vapour sorption of hot-melt extruded hydroxypropyl cellulose films: effect on physico-mechanical properties, release characteristics, and stability. *J Pharm Sci* 2004; 93: 3047–3056.
67. Kopcha M, Tojo KJ, Lordi NG. Evaluation of methodology for assessing release characteristics of thermosoftening vehicles. *J Pharm Pharm* 1990; 42: 745–751.
68. Thumma S, ElSohly M, Zhang S, Gul W, Repka M. Influence of plasticizers on the stability and release of a prodrug of [Delta]9-tetrahydrocannabinol incorporated in poly (ethylene oxide) matrices. *Eur J Pharm Biopharm* 2008b; 70:605–614.
69. Wilson M, Williams MA, Jones DS, Andrews GP. Hot-melt extrusion technology and pharmaceutical application,” *Thera deli* 2012; 3 (6): 787-797.

70. Klein CE, Chiu Y, Awni W, Zhu T, Heuser RS, Doan T, Breitenbach J, Morris JB, Brun SC, Hanna GJ. The tablet formulation of lopinavir/ritonavir provides similar bioavailability to the soft-gelatin capsule formulation with less pharmacokinetic variability and diminished food effect. *J Acquir Immune Defic Syndr* 2007; 44: 401-410.

CHAPTER 2: DISSOLUTION ENHANCEMENT OF POORLY WATER-SOLUBLE APIs PROCESSED BY HOT-MELT EXTRUSION (HME) USING HYDROPHILIC POLYMERS

1.0 Introduction

With the recent start of high throughput screening of potential therapeutically active ingredients, the number of poorly soluble drug candidates has increased sharply (about 25% to 40%). The availability of water insoluble APIs into systemic circulation is highly controlled and dependent on its aqueous solubility and therefore increasing the solubility/dissolution of poorly soluble substances for oral delivery is a challenging task in pharmaceutical processing and development. The manufacture of solid dispersions is considered one of the most attractive approaches to increase solubility and thus bioavailability of poorly soluble APIs ^[1]. Solid dispersions have been prepared by employing various approaches such as co-evaporation ^[2], hot spin mixing ^[3], roll-mixing or co-milling ^[4], freeze-drying ^[5], spray drying ^[6,7] and supercritical fluid processing (SFP) ^[8].

Hot-melt extrusion (HME) is considered as an effective process in pharmaceutical industry for the formation of molecular dispersions in order to improve the bioavailability of drug components which have low water solubility ^[9]. The melt extrusion process offers various advantages over conventional approaches such as it is a solvent-free process and therefore environmental friendly. Relatively low heat sensitive substances can be easily processed by HME as the exposure of the APIs is very short and processing temperatures can be lowered by selecting the appropriate drug carrier. Moreover, the melt extrusion process helps to convert crystalline active substances into the amorphous state as well as offers a chance to dissolve the drugs in the inert polymer matrix through the formation of solid solutions. Different case studies have been reported to increase solubility of various poorly soluble drugs ^[10] by HME including nifedipine, tolbutamide, lacidipine ^[11, 12], itraconazole ^[13, 14] and nitrendipine ^[15].

Famotidine (FMT) is a histamine H₂-receptor antagonist (H₂RA) mainly used for the treatment of gastric-duodenal ulcers, symptomatic gastro-oesophageal reflux disease (GERD), erosive oesophagitis, management of hypersecretory conditions ^[16, 17] for paediatric populations ^[17]. According to the Biopharmaceutical Classification System (BCS) FMT is classified as a class IV drug (low solubility, low permeability) ^[18]. Indomethacin (INM) is a non-steroidal anti-inflammatory drug (NSAID) used to treat rheumatoid arthritis, osteoarthritis, alkylosing

spondylitis, tendinitis and headaches [19, 20]. It is known as a Class II active substance which exerts high permeability and low bioavailability [19] due to the poor water solubility. The two drugs were chosen to represent the two classes and to compare the effect of HME on increasing their percent loading and dissolution properties which are important for improving their bioavailability. To the best of our knowledge, this is the first study comparing two different poorly water soluble drugs from two BCS classes for drug loading and drug dissolution properties.

Both FMT and INM have been reported to be molecularly dispersed in various polymer matrices in order to provide quick release profiles [16,19,20,21]. In the present study, solid dispersions of relatively high loadings of INM and FMT (up to 40%) embedded in hydrophilic polymers such as SOL, VA64, and S630 were prepared using hot-melt extrusion in order to achieve faster dissolution profiles. The *in vitro* dissolution properties and physico-chemical properties of the solid dispersions were investigated and compared with the physical mixtures and the pure APIs alone.

2.0 Materials and Methods

2.1 Materials

Indomethacin (INM) was purchased from Sigma Aldrich (London, UK) and Famotidine (FMT) was donated by Colorcon Ltd (Dartford, UK). Soluplus and cross-linked polyvinylpyrrolidone kollidon VA64 were kindly donated by BASF (Germany). Plasdone S630 was obtained from ISP. All HPLC solvents were of analytical grade and purchased from Fisher Chemicals (UK).

2.2 Drug-polymer miscibility study by Hansen solubility parameters (δ)

The Hansen [22] solubility parameters (δ) of both drugs as well as the polymers were calculated by considering their chemical structural orientations. In order to determine the theoretical drug/polymer miscibility, the solubility parameters were calculated by using the Hoftyzer and van Krevelen method [23] according to the following equation:

$$\delta = \sqrt{\delta_d^2 + \delta_p^2 + \delta_h^2} \quad (2.1)$$

Where,

$$\delta_d = \frac{\sum F_{di}}{V_i}, \quad \delta_p = \frac{\sqrt{\sum F_{pi}^2}}{V_i}, \quad \delta_p = \sqrt{(\sum E_{hi} / V_i)}$$

i = structural groups within the molecule

δ = the total solubility parameter.

F_{di} = molar attraction constant due to molar dispersion forces

F_{pi}^2 = molar attraction constant due to molar polarization forces

E_{hi} = hydrogen bonding energy.

V_i = group contribution to molar volume

The average molecular weight was used to determine the solubility parameter of different polymeric excipients while the Bagley advanced solubility parameter equation and diagrams ^[24] were used to investigate the effect of hydrogen bonding compared to the combined solubility parameters (dispersion forces and polarization forces).

2.3 Preparation of formulation blends

The dry drug/polymer powders (100 g) were blended thoroughly in a Turbula TF2 mixer (Basel, Switzerland) for 10 min. As shown in Table 2.1, the drug content for the binary blends varied from 20 – 40%. For the FMT/VA64, FMT/S630 and INM/S630 the drug content did not exceed 20% due to the difficulty with extruding the powdered formulations.

Table 2.1: Drug/polymer percentages of the HME processed formulations.

Drug	Polymer	Drug (%, w/w)	Polymer (%, w/w)
FMT	SOL	20	80
FMT	SOL	40	60
FMT	VA64	20	80
FMT	S630	20	80
Drug	Polymer	Drug	Polymer

		(%, w/w)	(%, w/w)
INM	SOL	20	80
INM	SOL	40	60
INM	VA64	20	80
INM	VA64	40	60
INM	S630	20	80

2.4 Hot-melt extrusion (HME) process

Extrusion of all INM and FMT formulations was performed using a single screw Randcastle extruder (Model RC 0750, Cedar Grove, NJ) with a 0.2 mm rod die. The temperature profile from the feeding zone to the die was 105°C/113°C/118°C/122°C/120°C for all formulations with 15 rpm screw speeds. The extrudates (strands) were milled for 5 min to produce granules using a Pulverisette 6 ball mill (Fritsch, Germany) with 400 rpm rotational speed. The micronized particles were then passed through a 250 µm sieve.

2.5 Thermal analysis

A Mettler-Toledo 823e (Greifensee, Switzerland) differential scanning calorimeter (DSC) was used to carry out DSC analyses of pure actives, physical mixtures (PM) and extrudates. 2-5 mg of samples was placed in sealed aluminium pans with pierced lids. The samples were heated at 10°C/min from 0°C to 220°C under dry nitrogen atmosphere. In addition modulated temperature scanning calorimetry (MTDSC) studies were performed from 30°C to 150°C temperature range with an underlying heating rate of 1°C/min to further analyze the samples. The pulse height was adjusted to 1-2°C with a temperature pulse width of 15-30 s.

2.6 X-ray powder diffraction (XRPD)

XRPD was used to determine the solid state of pure active substances, physical mixtures and extruded materials using a Bruker D8 Advance (Germany) in two-theta (2θ) mode. A copper anode at 40 kV and 40 mA, parallel beam Goebel mirror, 0.2 mm exit slit, LynxEye position sensitive detector with 3° opening (LynxIris at 6.5 mm) and sample rotation at 15 rpm were

used. Each sample was scanned from 2 to 40° 2θ with a step size of 0.02° (2θ) and a counting time of 0.2 seconds per step; 176 channels active on the PSD making a total counting time of 35.2 s/step.

2.7 Particle size morphology and distribution

Scanning electron microscopy (SEM) was used to study the surface morphology of the hot-melt extrudates. The samples were mounted on an aluminum stage using adhesive carbon tape and placed in a low humidity chamber prior to analysis. Samples were coated with gold, and microscopy was performed using a Jeol 5200, SEM operating at an accelerating voltage of 5 kV.

The particle size distribution of the micronized extrudate granules of all formulations was measured by dry sieving. The method involved stacking of the sieves on top of each other and then placing the test powder (100 g) on the top sieve. The nest of sieves was subjected to a standardised period of agitation (20 min) and then the weight of the material retained on each sieve was accurately determined to give the weigh percentage of powder in each sieve size range.

2.8 *In vitro* drug release studies

In vitro drug release studies were carried out in 750 ml of 0.1 M hydrochloric acid for 2 hr using a Varian 705 DS dissolution paddle apparatus (Varian Inc. North Carolina, US) at 100 rpm and 37 ± 0.5°C. After the 2 hr operation, 250 ml of 0.20 M solution of trisodium phosphate dodecahydrate were added into the vessel (buffer stage, pH 6.8) that had been equilibrated to 37 °C. At predetermined time intervals, samples were withdrawn for HPLC assay. All dissolution studies were performed in triplicate

Furthermore, the difference of the release profiles of different formulations was investigated by calculating the similarity factor (f_2). The f_2 value (Eq. (2)) is a logarithmic transformation of the sum-squared error of differences between the test T_j and reference products R_j over all time points ($n = 5$).

$$f_2 = 50 \times \log\left[\left\{1 + \left(\frac{1}{n} \sum_{j=1}^n (R_j - T_j)^2\right)^{-0.5}\right\}100\right] \quad (2.2)$$

2.9 HPLC analysis

The release of INM and FMT was determined by using HPLC, Agilent Technologies system 1200 series. A HYCHROME S50DS2-4889 (5 μm x 150 mm x 4 mm) column was used for both active substances. The wavelength was set at 260 nm and 267 nm for INM and FMT respectively. The mobile phase consisted of methanol/water/acetic acid (64/35/1 by volume) and the flow rate was maintained at 2 ml/min and the retention time was 4-5 min. For INM and FMT calibration curves ($R^2 = 0.999$) were prepared with concentrations varying from 10 $\mu\text{g}/\text{ml}$ to 50 $\mu\text{g}/\text{ml}$ and 20 μl injection volumes.

3.0 Results and Discussion

3.1 Miscibility studies by calculating solubility parameters (δ)

The estimation of the solubility parameters (δ) was used to predict the miscibility of the active substances and the polymeric carriers [12,25,26]. Calculated solubility parameters indicate the probability of a drug molecule to be miscible with a large polymer molecule. In the calculation of solubility parameters three different forces are considered. It is believed that the compounds with similar values for solubility parameters are likely to be miscible because the miscibility is caused by balancing the energy of mixing released by inter molecular interactions between the components and the energy released by intra molecular interactions within the components [27]. The Hansen three dimensional solubility parameters are calculated by group contributions of dispersion forces, polar forces and hydrogen bonding forces using the Van Krevelen/Hoftyzer (1976) method [25].

The estimated solubility parameters are depicted in Table 2.2 and it can be seen that for all drug – polymer combinations the $\Delta\delta$ values vary from 3.2 – 5.2 $\text{MPa}^{0.5}$ as derived by the Van Krevelen/Hoftyzer approach. Greenhalgh [26] classified compounds according to their difference in solubility parameters. The authors found out that compounds with a $\Delta\delta < 7 \text{MPa}^{0.5}$ were likely to be miscible, but likely to be immiscible with a $\Delta\delta > 10 \text{MPa}^{0.5}$. Since the determined solubility parameter differences between each drug and polymer are less than $7 \text{MPa}^{0.5}$, all three polymers are likely to be miscible with both of the APIs. Interestingly the $\Delta\delta$ values for INM and the two vinylpyrrolidone copolymer grades are slightly different although both appear to be miscible. This was attributed to the different molecular weights and the degree of cross – linking of the two polymers. Similar differences can be observed for FMT and the vinylpyrrolidone copolymers.

Furthermore, by means of thermodynamic considerations Bagley *et al.*^[24] concluded that the effects of δ_d and δ_p show close similarity and so introduced the combined solubility parameter δ_v , where

$$\delta_v = \sqrt{\delta_d^2 + \delta_p^2} \quad (2.3)$$

The parameter for components of intermolecular hydrogen bonding δ_h and the combined parameter δ_v are plotted in a diagram to project the three-dimensional solubility parameter space into a two-dimensional plot which is called Bagley diagram (Fig. 2.1).

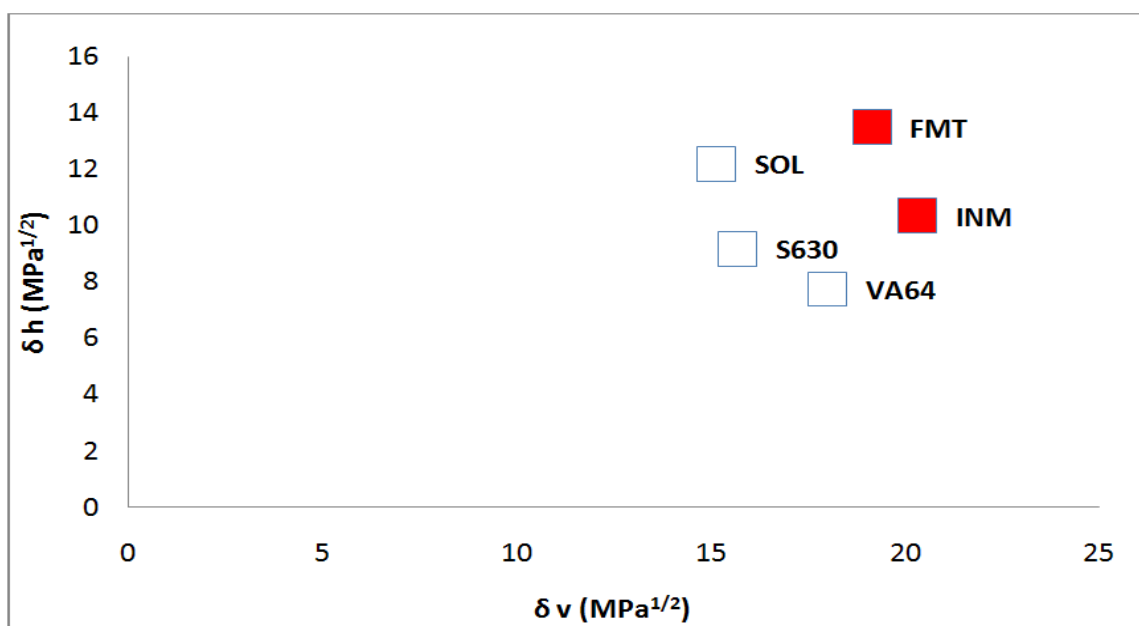


Fig. 2.1: Location of polymers (open symbols) and APIs (closed symbols) within the Bagley plot.

The two – dimensional approach through plotting the Bagley diagram can provide more accurate prediction of the drug – polymer miscibility. The drug polymer miscibility can be predicted by the distance ($R_{a(v)}$) using the Pythagorean theorem in the Bagley diagram and the two components are likely to be miscible when $R_{a(v)} \leq 5.6 \text{MPa}^{0.5}$ ^[28]. Where

$$R_{a(v)} = \sqrt{[(\delta_{v2} - \delta_{v1})^2 + (\delta_{h2} - \delta_{h1})^2]} \quad (2.4)$$

Only small differences can be observed for FMT and INM and all three polymers where the $R_{a(v)}$ values are less than $5.6 \text{MPa}^{0.5}$ suggesting again drug – polymer miscibility for each formulation (Table 2.2). The estimated $R_{a(v)}$ value for the FMT/VA64 is $5.87 \text{MPa}^{0.5}$ suggesting

immiscibility of the two components. However, the difference from the value given by Albers (2008) is marginal and the components were considered miscible.

Table 2.2: Calculated solubility parameters of drug/polymers and compound distances in Bagley diagram.

Sample	δd	δp	δv	δh	δ_{average}	$\Delta\delta_{\text{(INM)}}$	$\Delta\delta_{\text{(FMT)}}$	Ra(v)	Ra(v)
	(MPa ^{0.5})	(MPa ^{0.5})	(MPa ^{0.5})	INM (MPa ^{0.5})	FMT (MPa ^{0.5})				
INM	18.99	7.37	20.34	10.34	22.84	-	-	-	-
FMT	11.93	15.00	19.17	13.49	23.44	-	-	-	-
VA64	18.0	0.64	18.01	7.73	19.60	3.24	3.84	3.49	5.87
SOL	15.14	0.45	15.15	12.18	19.43	3.41	3.99	5.54	4.23
S630	13.0	8.80	15.70	9.17	18.18	4.66	5.26	4.79	5.54

Nevertheless, both approaches confirmed the miscibility of the binary mixtures for all formulations. It is worth mentioning that the manufacturing of solid dispersions via HME depends also on the processing parameters such as temperature profile and screw rotation speed which are not taken into account in the estimated solubility parameters by Van Kreveln/Hoftyzer or Bagley. Thus, further process optimization is required for the manufacturing of solid dispersions in order to increase drug solubility.

As can be seen in Table 1, no plasticizer was incorporated in the binary mixtures due to low glass transition temperatures of the selected polymers. All formulations were easily extruded at temperatures around 120°C even at high drug loadings.

[Please see supplementary chapter 10, section 10.2 for examples of the calculation of solubility parameters of different drug and polymers by using Van Krevelen/ Hoftyzer equation]

3.2 Particle size morphology and particle size analysis

SEM was used to examine the surface morphology of the drug and extrudates. The particle morphology of INM and FMT is illustrated in Fig 2.2. The particles size range for all extruded materials varied from 50-200 μ m after optimizing the milling process. The extrudates containing SOL, VA64 and S630 exhibited no drug crystals on the extrudate surface at 20 and 40% drug loading with INM. Similarly, no FMT crystals were observed on the surface of polymeric extrudates at all drug concentrations.

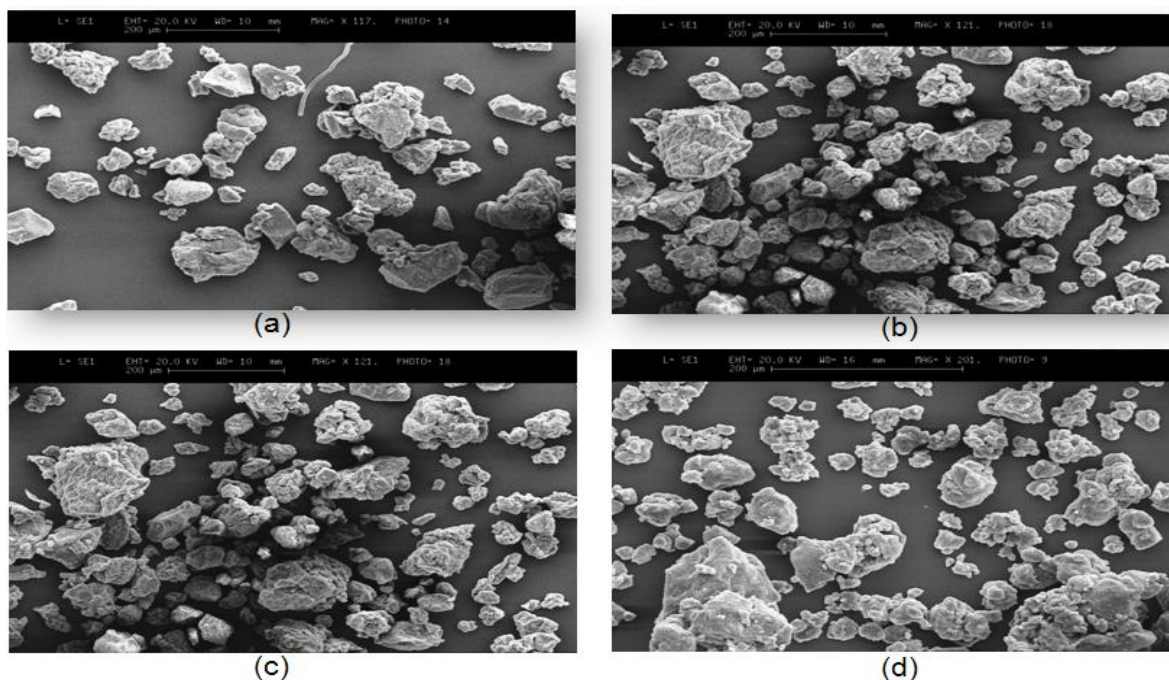


Fig. 2.2: SEM images (magnification x 500) of extruded formulations: (a) SOL/INM 20% (b) SOL/INM 40% (c) FMT/VA64 20% and (d) FMT/S630 20%.

The particle size distribution (depicted in Fig. 2.3) shows particle sizes lower than 500 μ m for most formulations ranging from 40 – 400 μ m. A small percentage can be seen at sizes <40 μ m as the milling process was optimized to reduce fines in the final extruded batches.

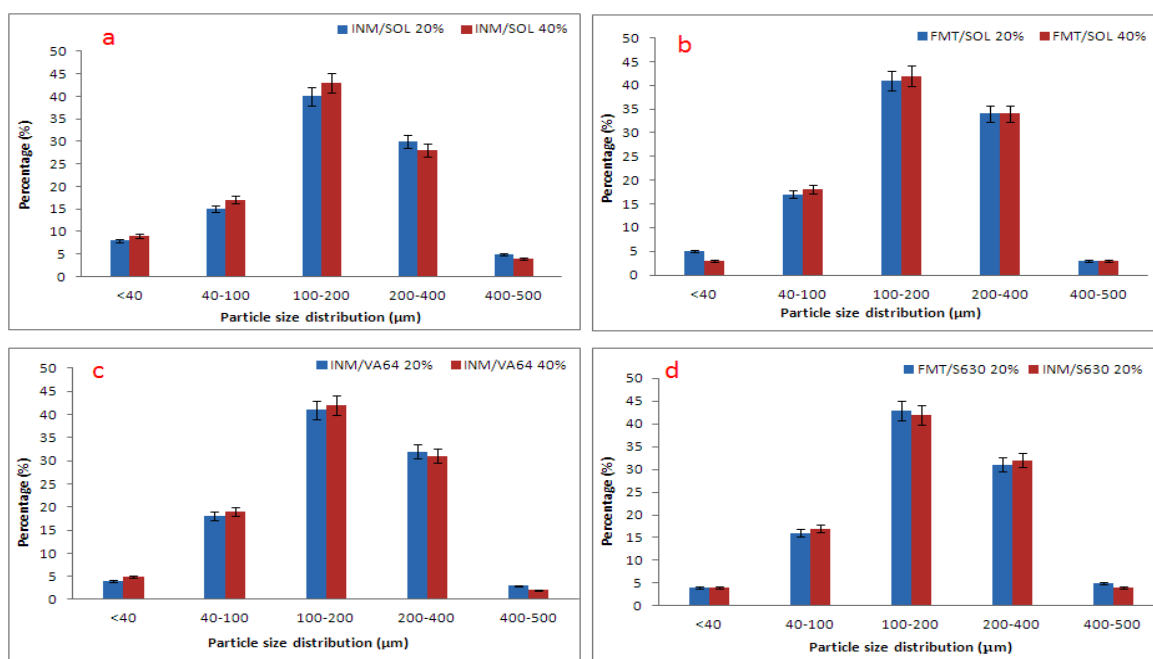


Fig. 2.3: Particles size distribution of extruded formulations after milling (5 min; 400 rpm): (a) INM/SOL 20-40%, (b) FMT/SOL 20-40%, (c) INM/VA64 20-40%, and (d) INM/S630 20%, FMT/S630 20%.

3.3 X-ray powder diffraction (XRPD)

The drug – polymer extrudates (E), including pure drugs and physical mixtures (PM) of the same composition were studied by X–ray analysis and the diffractograms were recorded to examine INM and FMT crystalline state. As can be seen from Fig. 2.4a –b the diffractogram of pure INM and FMT showed distinct peaks at 10.17, 11.62, 17.02, 19.60, 21.82, 23.99, 26.61, 29.37, 30.32 , 33.55 2θ and 5.97, 11.59, 15.73, 17.97, 20.03, 20.83, 24.04, 30.15, 32.19, 35.27 2θ respectively. As shown in Fig. 2.4a, the physical mixtures of all INM formulations showed identical peaks at lower intensities suggesting that both drugs retain their crystallinity at loads of 20 – 40%. In contrast, no distinct intensity peaks were observed in the diffractograms of the extruded formulations even at high drug loadings. The absence of INM and FMT intensity peaks indicates the formation of a solid dispersion where the drugs are present in amorphous state or molecularly dispersed into the polymer matrix.

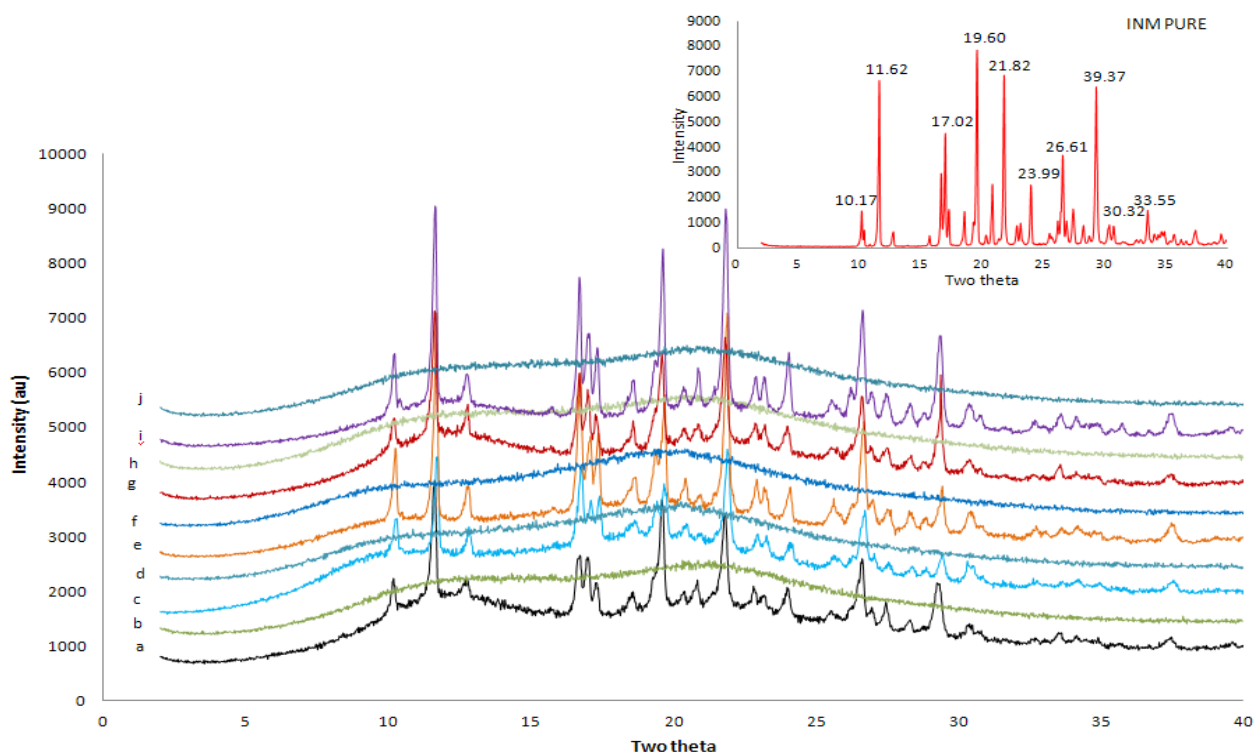


Fig. 2.4a: Diffractograms of INM formulations: pure INM (inset), (a) INM/S630 20% PM (b) INM/SC30 20% E (c) INM/ SOL 20% PM (d) INM/SOL 20% E (e) INM/SOL 40% PM (f) INM/SOL 40% E (g) INM/VA64 20% PM (h) INMO/VA64 20% E (i) INM/VA64 40% PM (j) INM/VA64 40% E (milling time 5 min at 400 rpm).

The diffraction patterns of all FMT physical mixtures exhibited crystalline peaks (Fig. 2.4b) with reduced intensities corresponding to FMT. Similar to INM the diffractograms of the extruded FMT formulations were characterized by the absence of drug intensity peaks indicating amorphous or molecularly dispersed state.

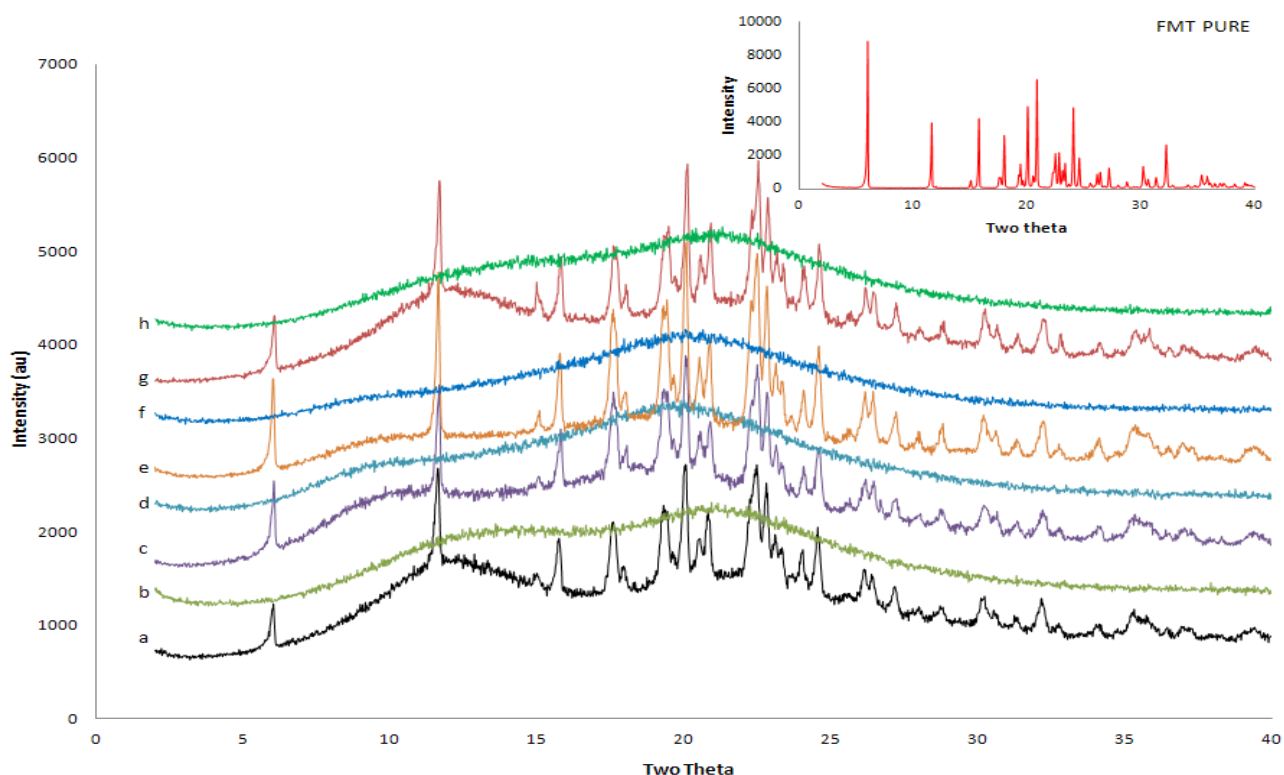


Fig. 2.4b: Diffractograms of FMT formulations: pure FMT (inset), (a) FMT/S630 20% PM (b) FMT/S63020% E (c) FAM/SOL 20% PM (d) FMT/SOL 20% E (e) FMT/SOL 40% PM (f) FMT/SOL 40% E (g) FMT/VA64 20% PM (h) FMT/VA64 20% E (milling time 5 min at 400 rpm).

3.4 Differential Scanning Calorimetry (DSC)

DSC was used to determine the solid state of both drugs, within the extruded formulations and compared with those of the physical mixtures. The DSC thermograms of pure INM and FMT showed sharp melting endothermic peaks at 162°C (polymorphic form γ) and 165.5°C respectively with a fusion enthalpy (ΔH) of about 109.6 J/g and 158.5 J/g (Fig. 2.5a). Modulated temperature DSC (MTDSC) was used to analyse reversible heat flow of the pure polymers where amorphous SOL, VA64, and S630 exhibited glass transitions (T_g) at 68.7, 105.0 and 105.5°C (Fig. 2.5a), respectively. As can be seen in Table 2.3 all drug – polymer physical mixtures exhibited melting peaks of INM and FMT at lower temperatures and reduced ΔH values as the ratio of carrier increased.

However, the DSC thermograms of the PM showed broad endothermic transitions from 127-163°C and 124-151°C that correspond to INM and FMT, respectively (Fig. 2.5 b-e). The absence of sharp melting endotherms in the active formulations suggests that both drugs are partially dissolved in the melted polymers.

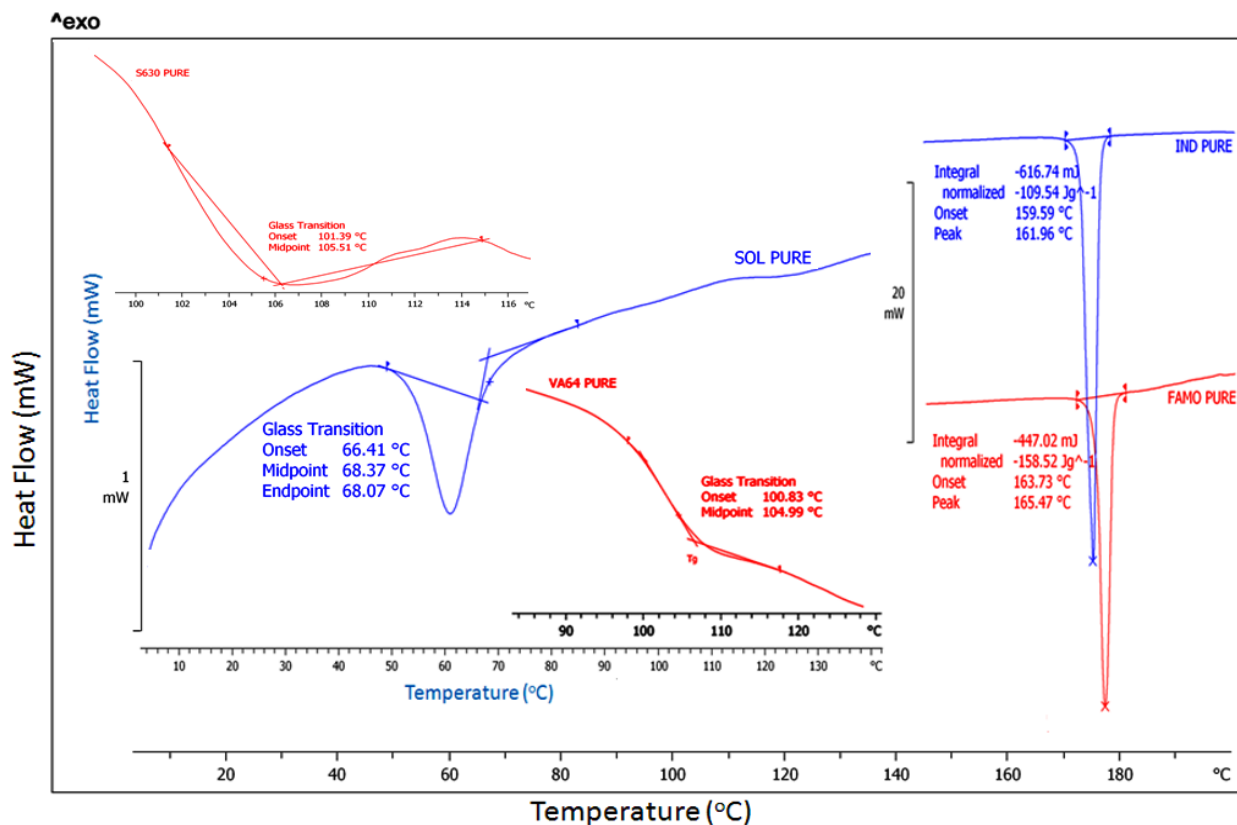


Fig. 2.5a: MTDSC thermograms of pure polymers and drugs.

In the case of INM/VA64 extrudates, a single T_g was observed for both loadings indicating drug – polymer miscibility. When the two components are miscible the T_g of the extruded sample should, according to the Gordon – Taylor equation ^[29] be between their T_g s. For INM 20% and 40% loadings, the T_g s were lowered to 56.2°C and 57.2°C, respectively denoting INM – VA64 miscibility. The INM glass transition temperature has been previously estimated at 42.3°C. The presence of a single T_g for the INM/VA64 extrudates suggests the presence of a glassy solid solution where INM is molecularly dispersed within the polymer matrices.

Table 2.3: DSC thermal transitions for drugs, polymers and active formulations.

Formulations	Glass transition		Melting endotherm (°C)	Enthalpy (ΔH , Jg ⁻¹)
	(°C)			
INM	-		162.0	109.6
FMT	-		165.5	158.5
SOL	68.7		-	
VA64	105.0		-	
S630	105.5		-	
Physical mixtures (PM) and extruded formulations (EF)				
	PM	EF	PM	Enthalpy EF (ΔH , Jg ⁻¹)
INM/SOL 20%	60.6	52.7	162.4	2.1
INM/SOL 40%	60.6	51.7	154.6	2.3
INM/ VA64 20%	56.2	55.4	131.8	1.6
INM/ VA64 40%	57.2	55.2	127.4	2.5
INM/S630 20%	70.8	56.6	130.8	2.1
FMT/SOL 20%	60.4	49.6	150.9	2.0
FMT/SOL 40%	60.2	48.5	155.3	1.6
FMT/VA64 20%	55.3	53.9	124.3	2.0
FMT/S630 20%	69.2	51.9	143.8	1.4

In addition, the determined T_g values (Fig. 2.5b) showed plasticization effect for INM as T_g decreased with increase in drug concentration.

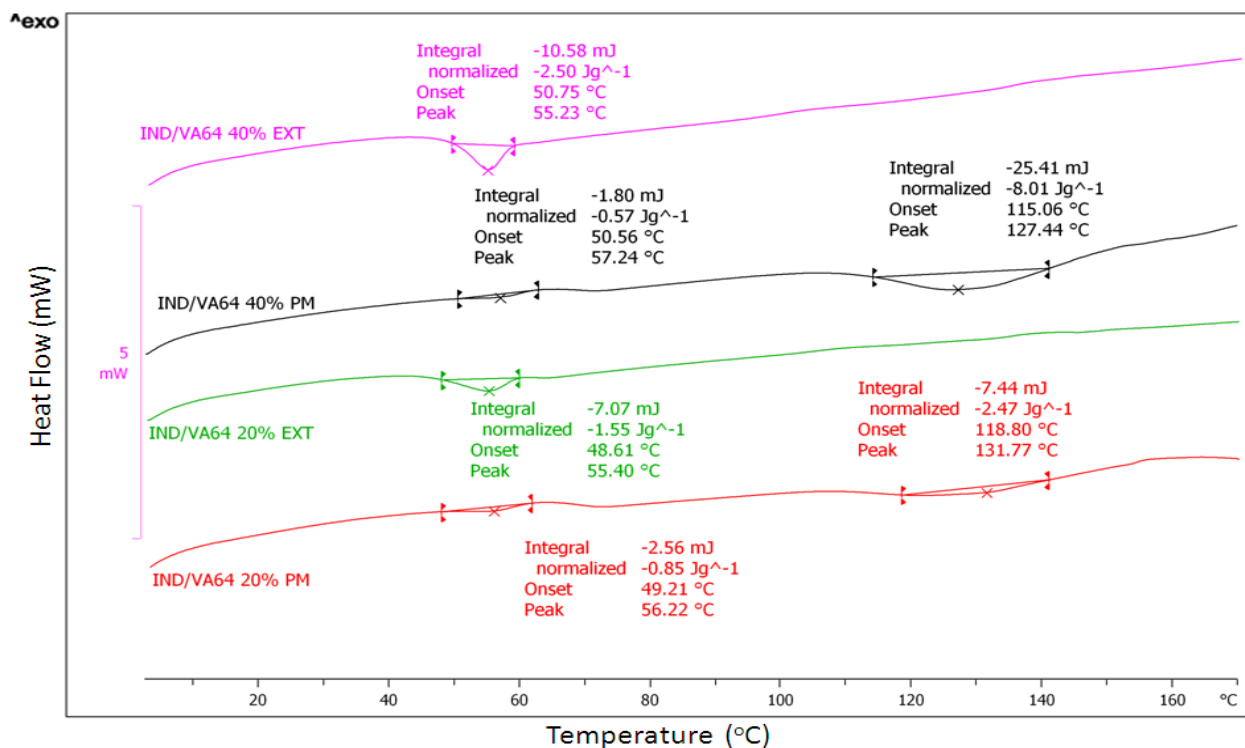


Fig. 2.5b: DSC thermograms of INM and VA64 (physical mixtures and extrudates).

This phenomenon was also observed for INM/SOL extrudates where a single T_g was detected at 52.70°C and 51.71°C for 20% and 40% INM loadings as shown in Fig. 2.5c. Both T_gs were found between the INM and polymer T_gs indicating the presence of molecularly dispersed INM.

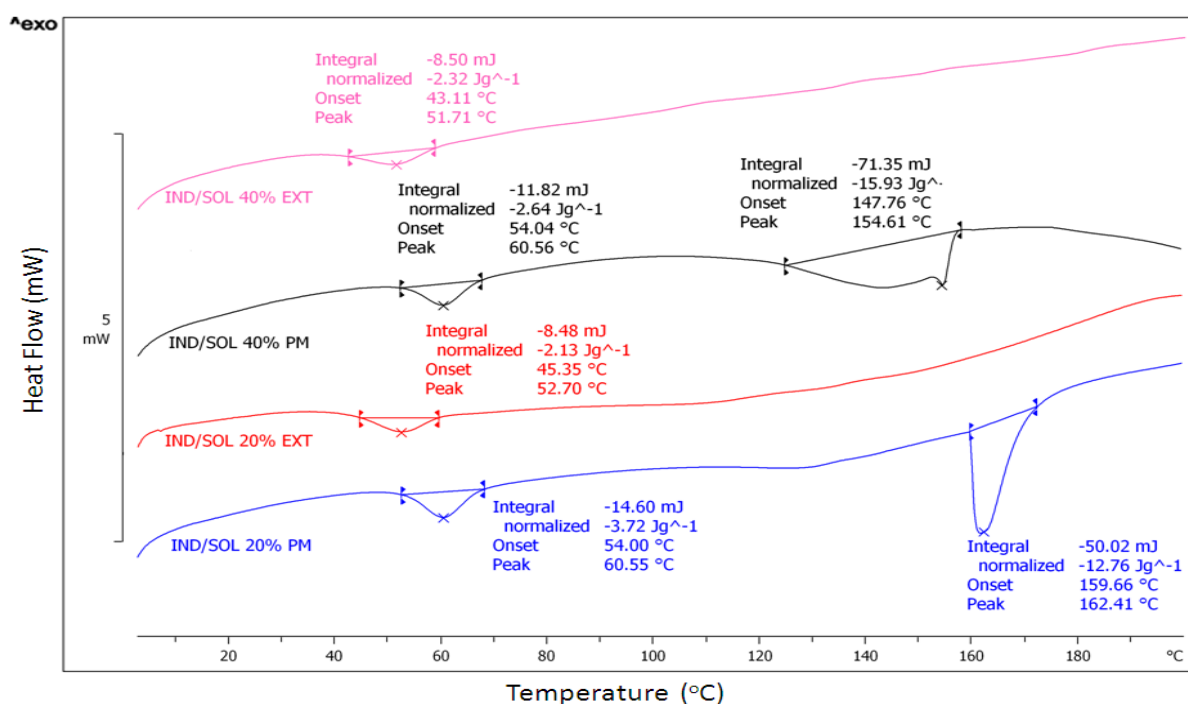


Fig. 2.5c: DSC thermograms of INM and SOL (physical mixtures and extrudates).

By comparing the Tgs at different loadings, INM showed a plasticization effect for Soluplus. By analyzing the thermograms of the INM/S630 extrudates (Fig. 2.5d) it was concluded that INM was also molecularly dispersed in the carrier due to the single Tg at 56.57°C and the absence of the drug melting endotherm.

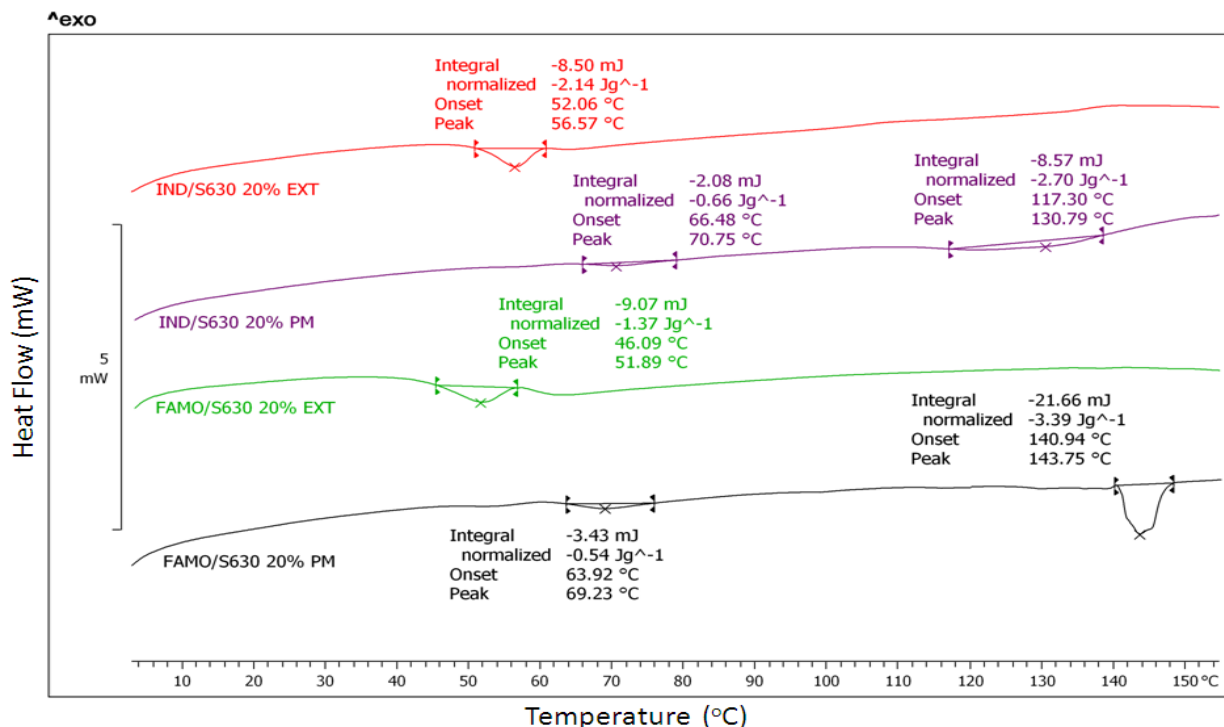


Fig. 2.5d: DSC thermograms of INM and FMT with Plasdone S630 (physical mixtures and extrudates).

Further evaluation of the DSC thermograms for the FMT – polymer extrudates confirmed the existence of glassy solid solutions for all formulations. For each binary mixture only a single Tg was observed without any endothermic peak related to FMT (Fig. 2.5e). The Tgs of FMT/SOL at 20% and 40% loadings were detected at 49.55°C and 48.54°C respectively suggesting plasticization effect of FMT. In contrast, the thermograms of physical mixtures showed distinct FMT melting endotherms shifted at lower temperatures.

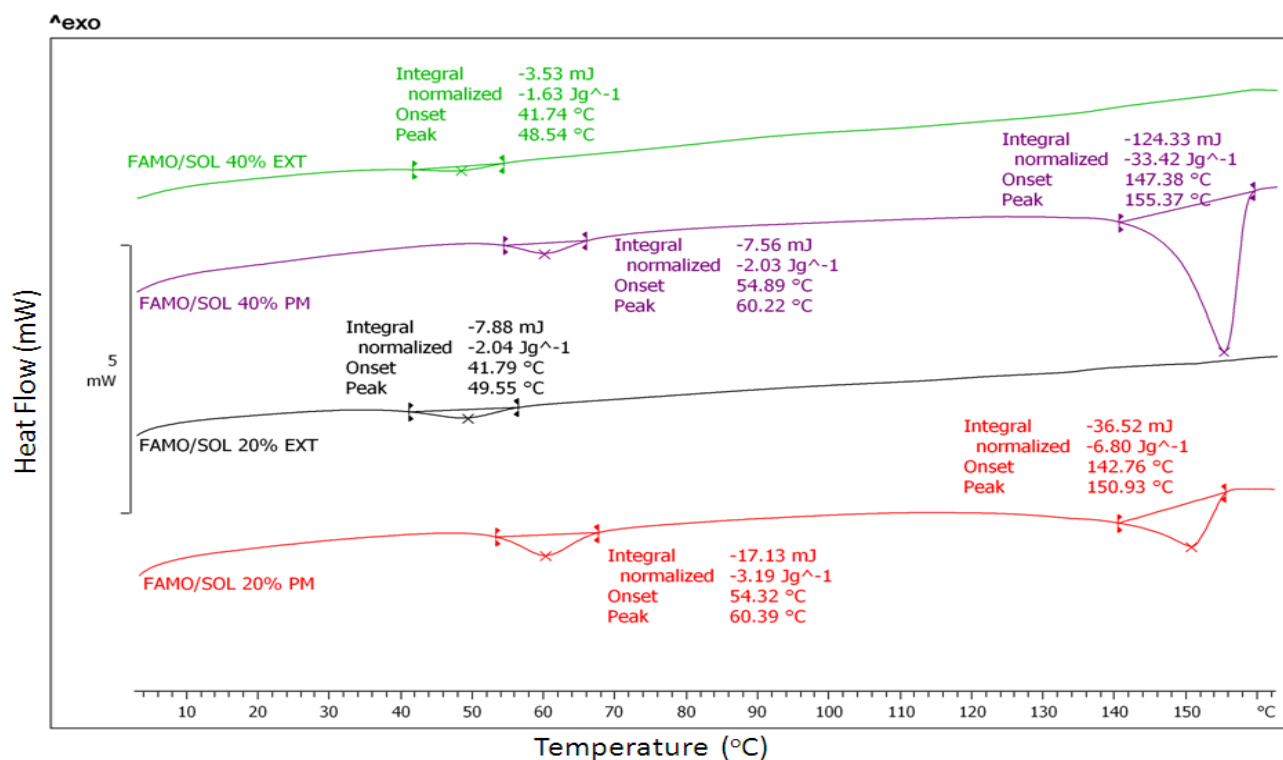


Fig. 2.5e: DSC thermograms of FMT and SOL (physical mixtures and extrudates).

3.5 *In vitro* dissolution studies

The dissolution profiles of INM and FMT from SOL, VA64 and S630 extruded (EXT) granules are shown in Fig. 2.6a- b. The dissolution rates of pure APIs were also investigated to signify the increase of the dissolution rates of the extruded formulations.

Due to its low water solubility, the bulk INM powder showed very slow dissolution rates up to 5% within five hours. In contrast, the dissolution profiles of INM extruded formulations exhibited enhanced dissolution rates compared to the bulk INM powder as shown in Fig 2.6a. The extrudates of SOL, VA64 and S630 polymers at 20% INM loadings exhibited increased dissolution rates with 30 – 40% released in 120 min and 55 – 70% in 300 min. SOL showed slightly increased released rates compared to VA64 and S630 without significant differences as shown by a Kruskal – Wallis nonparametric test ($p > 0.05$) (GraphPad, InStat, Software, US). Interestingly, the INM loading level was shown to have an effect on the dissolution rates. The drug dissolution rate at high drug loadings tended to increase with an increase in the INM level. This phenomenon was attributed to the plasticization effect of INM on VA64. Therefore, at 40% INM loading the drug release rate of INM/SOL and INM/VA64 granules was 55–65% in 120 min and 75–80% in 300 min.

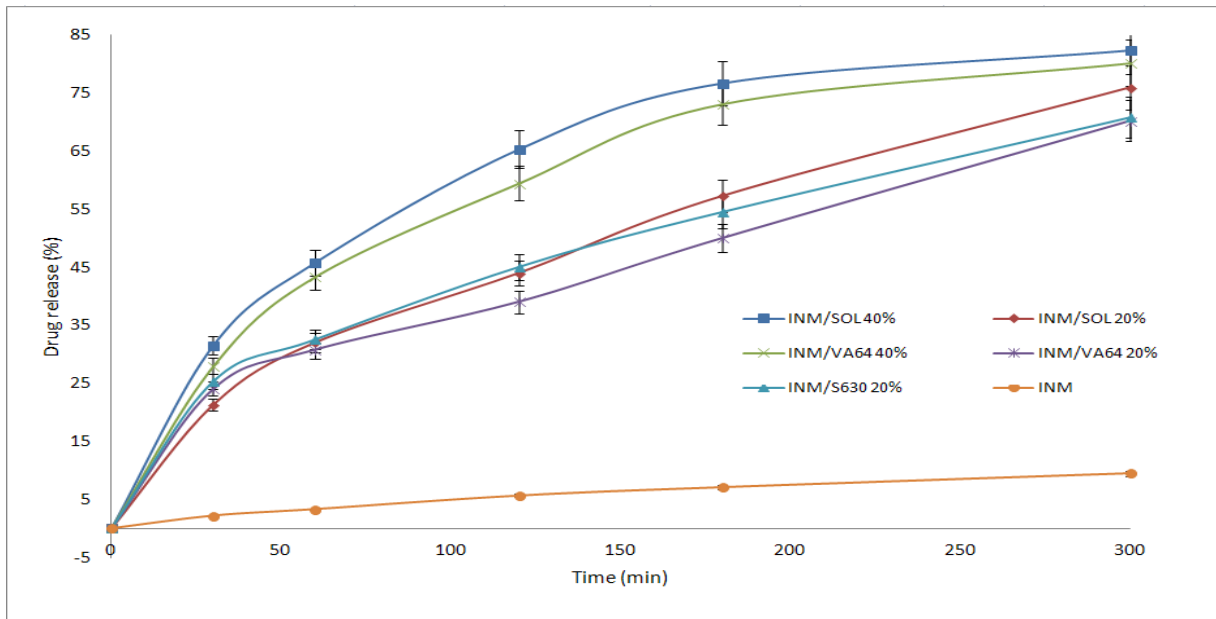


Fig. 2.6a: Drug release profile of pure INM, INM/SOL 20%, INM/VA64 20%, INM/S630 20%, INM/VA64 40% and INM/SOL 40% EXT.

FMT demonstrated low dissolution rates with about 22% released in 300 min whereas FMT/SOL 20% and FMT/VA64 20% presented about six times faster dissolution rates compared to pure API with more than 70% released within 120 min (Fig. 2.6b). The FMT/S630 20% extrudates showed slightly lower dissolution rates compared to the other formulations but significantly higher than the pure active substance.

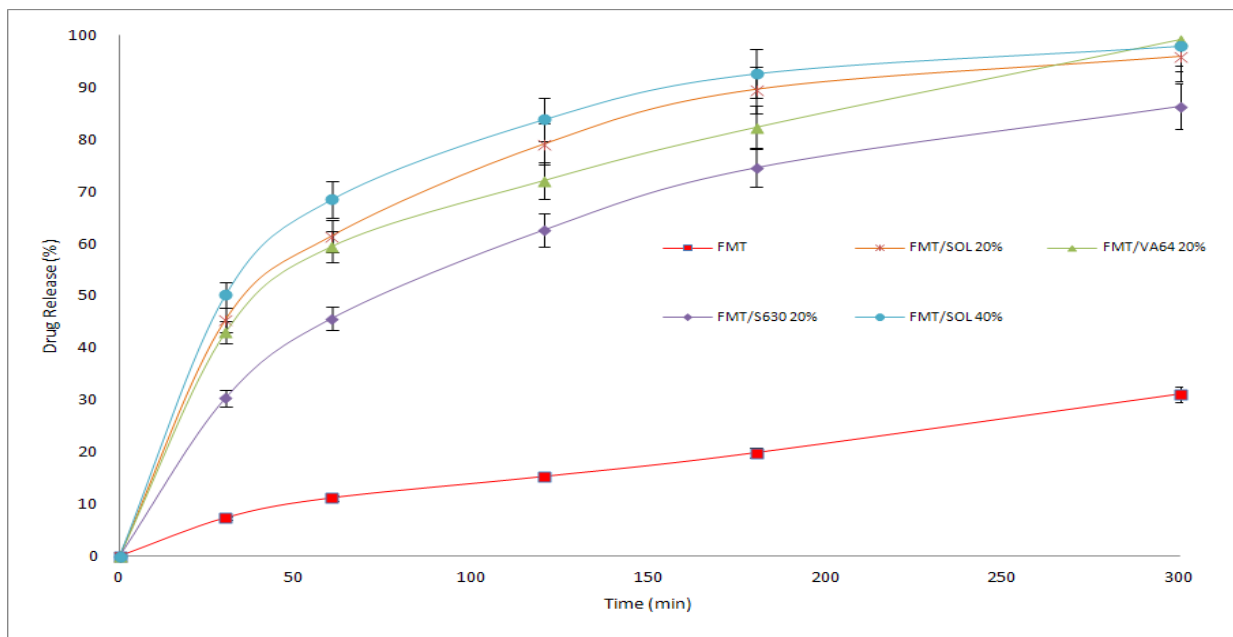


Fig. 2.6b: Drug release profiles of pure FMT, FMT/VA64 20%, FMT/SOL 20% and FMT/S630 20% EXT.

Nevertheless, more than 80% FMT was released from all drug/polymers formulations after 300min. Similar to INM the FMT/SOL granules at 40% loading showed faster dissolution rates to the 20% loading which was attributed to the drug’s plasticization effect.

Furthermore, the difference of the release profiles of different formulations was investigated by calculating the similarity factor (f_2). According to the FDA guidelines, release curves are considered similar when the calculated f_2 is 50–100 [30]. The formulation containing pure APIs differs significantly from that of the active extruded formulations as all of the calculated f_2 values fall into 10-20.07 range (Table 2.4).

Table 2.4: Similarity factor (f_2) for comparing release curves with respect to drug loading of INM and FMT formulations

Formulations	Difference Factor (f_2)	
	INM	FMT
INM/S630 20%	18.67	-
INM/VA64 20%	20.07	-
INM/VA64 40%	13.48	-
INM/SOL 20%	17.91	-
INM/SOL 40%	12.10	-
INM PURE	Ref	-
FMT/S630 20%	-	17.27
FMT/VA64 20%	-	12.72
FMT/SOL 20%	-	11.63
FMT/SOL 40%	-	10.09
FMT PURE	-	Ref

4.0 Conclusions

In the current chapter HME processing was employed as a means to increase the dissolution rates of two water insoluble drugs. INM and FMT were extruded with SOL, VA64 and S630 at different loadings up to 40% without the presence of traditional plasticizers. The extrusion process was optimized to produce amorphous solid dispersions of the drug substances. Further physico-chemical characterization studies confirmed the theoretical drug – polymer miscibility for all binary mixtures as predicted by Greenhalgh and Bagley approaches. In addition, INM and FMT demonstrated plasticization effects and were found to be molecularly dispersed within the polymer matrices. Increased aqueous solubility was observed in both APIs mixtures with all three polymers and the extruded solid dispersions resulted in greater dissolution rates over the bulk drugs.

Therefore, through the appropriate selection of a polymeric carrier solid dispersions of both INM and FMT can be prepared by hot-melt extrusion to improve the dissolution properties of the poorly water-soluble drugs. Further work is warranted to determine whether the oral bioavailability of INM/FMT is increased for the solid dispersions with enhanced dissolution characteristics.

5.0 References

1. Leuner C & Dressman J. Improving drug solubility for oral delivery using solid dispersions. *Eur J Pharm Biopharm* 2000; 50: 47–60.
2. Hong SW, Lee BS, Park SJ, Jeon HR, Moon KY, Kang MH, Park SH, Choi SU, Song WH, Lee J, Choi YW. Solid dispersion formulations of megestrol acetate with copovidone for enhanced dissolution and oral bioavailability. *Arch Pharm Res* 2011; 34(1):127-35.
3. Dittgen M, Fricke S, Gerecke H, Osterwald H. Hot spin mixing: a new technology to manufacture solid dispersions. *Pharmazie* 1995; 50(3): 225–226.
4. Breitenbach J. Melt extrusion: from process to drug delivery technology. *Eur J Pharm Biopharm* 2002; 54(2): 107–117.
5. Sekikawa H, Fukuda W, Takada M, Ohtani K, Arita T, Nakano M. Dissolution behavior and gastrointestinal absorption of dicumarol from solid dispersion systems of dicumarol-polyvinylpyrrolidone and dicumarol-beta-cyclodextrin. *Chem Pharm Bull* 1983; 31(4): 1350–1356.

6. Caron V, Tajber L, Corrigan OI, Healy AM. A comparison of spray drying and milling in the production of amorphous dispersions of sulfathiazole/polyvinylpyrrolidone and sulfadimidine/polyvinylpyrrolidone. *Mol Pharm* 2011; 8(2):532-42.
7. Wu K, Li J, Wang W, Winstead DA. Formation and characterization of solid dispersions of piroxicam and polyvinylpyrrolidone using spray drying and precipitation with compressed antisolvent. *J Pharm Sci.* 2009; 98(7):2422-31.
8. Gong K, Viboonkiat R, Rehman IU, Buckton G, Darr JA. Formation and characterization of porous indomethacin- PVP coprecipitates prepared using solvent-free supercritical fluid processing. *J Pharm Sci* 2005; 94(12): 2583–2590.
9. Repka MA, Battu SK, Upadhye SB, Thumma S, Crowley MM, Zhang F, Martin C, et al. Pharmaceutical applications of hot-melt extrusion: Part II. *Drug Dev Ind Pharm* 2007; 33(10): 1043-1057.
10. Qi S, Gryczke A, Belton P, Craig DQM. Characterisation of solid dispersions of paracetamol and EUDRAGIT® E prepared by hot-melt extrusion using thermal, microthermal and spectroscopic analysis. *Int J Pharm* 2008; 354: 158–167.
11. Forster A, Hempenstall J, Rades T. Characterization of glass solutions of poorly water-soluble drugs produced by melt extrusion with hydrophilic amorphous polymers. *J Pharm Pharmacol* 2001a; 53(3): 303–315.
12. Forster A, Hempenstall J, Tucker I, Rades T. Selection of excipients for melt extrusion with two poorly water-soluble drugs by solubility parameter calculation and thermal analysis. *Int J Pharm* 2001b; 226(1–2): 147–161.
13. Rambali B, Verreck G, Baert L, Massart DL. Itraconazole formulation studies of the melt-extrusion process with mixture design. *Drug Dev Pharm* 2003; 29(6): 641–652.
14. Six K, Daems T, de Hoon J, Van Hecken A, Depre M, Bouche MP, Prinsen P, Verreck G, Peeters J, Brewster ME, Van den Mooter G. Clinical study of solid dispersions of itraconazole prepared by hot-stage extrusion. *Eur J Pharm Sci* 2005; 24(2–3): 179–186.
15. Wang L, Cui FD, Hayase T, Sunada H. Preparation and evaluation of solid dispersion for nitrendipine-carbopol and nitrendipine-HPMCP systems using a twin screw extruder. *Chem Pharm Bull (Tokyo)* 2005; 53(10): 1240–1245.
16. Jaimini M, Rana AC, Tanwar YS. Formulation and evaluation of famotidine floating tablets. *Curr Drug Deliv* 2007; 4(1); 51-55.
17. Wenning LA, Murphy MG, James LP, Blumer JL, Marshall JD, Baier J, Scheimann, AO, et al. Pharmacokinetics of famotidine in infants. *Clin Pharmacol* 2005;44(4):395-406.

18. Amidon GL, Lunnernas H, Shah VP, and Crison JR. A theoretical basis for a biopharmaceutic drug classification: the correlation of in vitro drug product dissolution and in vivo bioavailability. *Pharm Res*1995; 12:413–420.
19. El-Badry M, Fetih G, Fathy M. Improvement of solubility and dissolution rate of indomethacin by solid dispersions in Gelucire 50/13 and PEG4000. *Saudi Pharm J* 2009; 17: 217-225.
20. Deasy PB, Law MFL. Use of extrusion-spheronization to develop an improved oral dosage form of Indomethacin. *Int J Pharm* 1997; 148: 201-209.
21. Mady FM, Abou-Taleb AE, Khaled KA, Yamasaki K, Iohara D, Taguchi K, Anraku, M, et al. Evaluation of carboxymethyl-beta-cyclodextrin with acid function: improvement of chemical stability, oral bioavailability and bitter taste of famotidine. *Int J Pharm* 2010; 397(1-2): 1-8.
22. Hansen CM. The universality of the solubility parameter. *Ind Eng Chem Res Dev* 1969; 8: 2-11.
23. Hoftyzer PJ, Krevelen DWV. *Properties of polymers*. Amsterdam: Elsevier, 1976:
24. Bagley EB, Nelson TP & Scigliano JM. Three-dimensional solubility parameters and their relationship to internal pressure measurements in polar and hydrogen bonding solvents. *J Paint Technol* 1971; 43: 35-42.
25. Zheng X, Yang R, Tang X and Zheng L. Part I: Characterization of Solid Dispersions of Nimodipine Prepared by Hot-melt Extrusion. *Drug Dev Ind Pharm* 2007; 33:791–802.
26. Greenhalgh DJ, Peter W, York TP, Solubility parameters as predictors of miscibility in solid dispersions. *J Pharm Sci* 1999; 88 (11): 1182–1190.
27. Hancock BC, York P, Rowe RC. The use of solubility parameters in pharmaceutical dosage form design. *Int J Pharm* 1997; 148(1): 1–21.
28. Albers, J. *Hot-melt Extrusion with Poorly Soluble Drugs*. Heinrich-Heine- Universitat Dusseldorf, Germany 2008.
29. Forster A, Hempenstall J, Tucker I, Rades T. The potential of small-scale fusion experiments and Gordon–Taylor equation to predict the suitability of drug/polymer blends for melt extrusion. *Drug Dev Ind Pharm* 2001c; 27:549– 560.
30. *Guidance for Industry. Dissolution Testing of Immediate Release Solid Oral Dosage Forms* U.S. Department of Health and Human Services Food and Drug Administration, Center for Drug Evaluation and Research (CDER). 1997.

CHAPTER 3: DEVELOPMENT AND EVALUATION OF ORALLY DISINTEGRATING TABLETS (ODTs) CONTAINING IBUPROFEN GRANULES PREPARED BY HOT-MELT EXTRUSION

1.0 Introduction

The development of oral disintegrating tablets (ODTs) has received increased interest among researchers and pharmaceutical industries over the last decade. ODTs are designed to disintegrate or dissolve rapidly on contact with saliva, in the absence of additional water, compared to the traditional tablet forms. ODTs provide several advantages as they combine the properties of both liquid and conventional tablet formulations ^[1-2]. ODTs are quickly ingested upon introduction on the tongue, thus eliminating the need to chew the tablet, swallow it intact, or take with water. Furthermore, administration of ODTs is favourable to paediatric and geriatric patients or people who find swallowing difficult and for the treatment of patients where compliance is difficult.

However, as a result of the rapid ODT disintegration, the active substance comes in contact with the taste buds and the need for a pleasant taste becomes a key aspect for patient palatability. Thus the taste-masking of bitter active substances is a critical hurdle to overcome for the successful development of ODT formulations. In general, oral administration of bitter active substances through ODT formulations should provide an improved degree of palatability, increased patient compliance and a concomitantly beneficial therapeutic effect. In the past, the methods of taste-masking in fast dissolving/disintegrating tablets included sweeteners and flavors. Nevertheless, these additives were not a sufficient means for complete taste-masking. Recent advances in technology have presented viable formulation alternatives to taste-mask bitter drugs. Several approaches have been reported which involve complexation ^[3, 4], freeze-drying ^[5], microencapsulation ^[6, 7], fluidized-bed coating ^[8,9] and supercritical fluids ^[10, 11] for taste-masking purposes.

Hot-melt extrusion (HME) is widely used in the pharmaceutical industry as a process to prepare drug delivery systems such as granules, pellets, sustained release tablets and even transmucosal/transdermal systems. Among the other applications HME has been used to increase the bioavailability of water insoluble active substances ^[12 - 14] by creating molecular dispersions. There are a few studies reported where ibuprofen (IBU) extrudates were prepared by HME using various polymeric matrices ^[15 - 18] to obtain a powdered material. However, in these studies, IBU formulations were developed to provide sustained release profiles. Recently, hot-melt extrusion was introduced as an alternative taste masking technique ^[19] where, for example, anionic active substances can interact with the functional groups of positively charged polymers. These

interactions facilitate the creation of hydrogen bonding and consequently mask the active's bitter taste.

The aim of this study was to increase IBU dissolution rate and to incorporate the taste masked granules produced into robust ODT formulations. IBU is a well-known and widely used nonsteroidal anti-inflammatory drug (NSAID) with <1 mg/ml water solubility at room temperature (25°C) [20]. At present, IBU's over-the-counter ODTs are marketed as Nurofen® (Meltlets) to treat migraine, headache and rheumatic/muscular pain.

Here we report the development of an orally disintegrating tablet developed by HME of IBU-methacrylic pH-sensitive copolymer (EUDRAGIT® EPO) mixtures and the evaluation of the ODTs produced. To evaluate taste a sensory test was implemented using 10 healthy volunteers, which revealed significant taste-masking of the active in the formulations developed. For the development of ODTs the effect of the amount of superdisintegrant(s) on ODT hardness, friability and disintegration times were assessed in order to identify the optimum formulation. The use of superdisintegrants is a well known approach to formulate ODTs [2] where the physicochemical nature of the disintegrant determines the disintegration mechanism and consequently affects the disintegration times.

2.0 Materials and methods

2.1 Materials

Ibuprofen (IBU) was purchased from Shasun Chemicals & Drugs Ltd. (London, UK). Eudragit EPO polymer was kindly donated from Evonik Pharma Polymers (Darmstadt, Germany). Crospovidone (Polyplasdone XL10), croscarmellose, (Vivasol, JRS Pharma, Rosenberg, Germany), crosslinked polyvinylpyrrolidone (Kollidon CL and CL-SF, BASF, Germany) Pearlitol C160 (Roquette, France), Microcrystalline cellulose (Avicel 102, FMC), sodium stearyl fumarate (PRUV, JRS Pharma, Rosenberg, Germany), calcium hydrogen phosphate dehydrate (Emcompress, JRS Pharma, Rosenberg, Germany) were also donated and used as tablet excipients. SiO₂ and MgSt were purchased from Sigma Aldrich, UK. Nurofen® Hotmelts Lemon with 200 mg taste masked IBU were purchased from Boots UK Ltd. for the comparative studies. The HPLC solvents were analytical grade and purchased from Fisher Chemicals (UK). Artificial saliva (pH 5.8) was used as a solvent medium in order to simulate oral disintegration. All materials were used as received.

2.2 Hot-Melt extrusion

Hot-melt extrusion was carried out using a 18 mm Leistritz twin-screw extruder. Screws were co-rotated at a speed of 200 rpm; the temperature applied was 140°C. At this temperature, dissolution of the IBU in the polymer occurred. The drug-excipients composition consisted of IBU/EPO/Talc and IBU/EPO/Talc at a ratio of 25/25/50 and 50/40/10(% wt/wt). The extrudates were collected as strands with diameter of approximately 1.5 mm and milled under cryogenic milling (Retsch ZM 200 Ultracentrifugal, Germany) conditions (6000 rpm, 10 min) to obtain the final taste-masked granules.

2.3 Particle size distribution measurements

The particle size distribution of the produced IBU granules was measured by dry sieving. The method involved stacking of the sieves on top of each other and then placing the test powder (100 g) on the top sieve. The nest of sieves was subjected to a standardised period of agitation (20 min) and then the weight of the material retained on each sieve was accurately determined to give the weight percentage of powder in each sieve size range.

2.4 Tablet preparation

Development batches were prepared using batch sizes of 200 g. All materials were passed through a mesh sieve with an aperture of 800µm before use. The batches were blended with sodium stearyl fumarate (0.5%) in a Turbula TF2 mixer (Basel, Switzerland) for 5 minutes. Blends were directly compressed on a Flexitab trilayer tablet press (Oystar - Manesty, Germany) using 13 mm normal flat punches. Dwell time was set at 30 ms and the compaction force varied from 4-12kN.

2.5 Flow properties and compressibility

Compressibility index I (Carr's index) values of the different formulations were determined by measuring the tapped bulk and poured bulk volumes of the powders after subjecting to 100 taps in a graduated measuring cylinder using the following equation ^[21]:

$$I = \left(1 - \frac{V}{V_o}\right) \times 100 \quad (3.1)$$

V is the freely settled volume of a given mass of a powder and V_o is the tapped volume of the same mass of powder.

2.6 Evaluation of tablets

The prepared tablets were evaluated for the uniformity of thickness, hardness (Erweka TBH 28, Frankfurt, Germany), friability (Erweka friabilator, model A3R, Frankfurt, Germany), and disintegration time (Erweka, model ZT4, Heusenstamm, Germany) according to USP22 tests/2010. The diametral compression test defined by Fell and Newton [22] was used to determine the tensile strength T , using the formula:

$$T = \frac{2P}{\pi Dt} \quad (3.2)$$

Where P (kP) is the applied stress, D (cm) is the diameter of the tablet, and t (cm) is the tablet thickness. Three tablets from each batch were subjected to tensile strength determination.

The solid fraction (SF) and porosity (ϵ) were calculated based on the true density (ρ_{true}), tablet volume (v), and tablet weight (W_t) as below [23]:

$$SF = \frac{W_t}{\rho_{true} \times v} \quad (3.3)$$

$$\epsilon = 1 - SF \quad (3.4)$$

2.7 *In vitro* tablet disintegration test

The tablet disintegration test was carried out using a TA-XD*Plus* texture analyzer (Stable Micro Systems) similar to a recent study [24]. The apparatus was calibrated with a 5 kg load cell and fitted with a flat-bottomed cylindrical stainless steel probe (P/25, 12mm in diameter and 25mm in height). In summary, the completely dry tablet is placed on the perforated grid and it is not in contact with the disintegration medium. The probe descends until a trigger force is detected where it gets in contact with the tablet placed on the grid and pushes the whole system downwards. The tablet then touches the medium and starts disintegrating. At this point, the TA apparatus is set to maintain a predetermined nominal force (50 g) for a given period of time (60 s). For all the disintegration studies artificial saliva (pH 5.8) was used as a solvent medium in order to simulate oral disintegration.

2.8 *In vivo* tablet disintegration and bitterness evaluation

In vivo disintegration and taste masking evaluation was performed on 10 healthy human volunteers [25, 26] from whom informed consent was first obtained (approved by the Ethics

Committee of the University of Greenwich). The study is also in accordance with the Code of Ethics of the World Medical Association (Declaration of Helsinki). The healthy volunteers of either sex (age 18–25) were selected, trained and one tablet was held in the mouth after rinsing and the time required for complete disintegration of the tablet was recorded. The time when the tablet placed on the tongue disintegrated without leaving any lumps was taken as the end point. The disintegrated material was held in the mouth for another 60 seconds, and then spat out. The mouth was rinsed with water without swallowing the disintegrated material and, finally, the roughness levels were recorded on a numerical scale ranging from 0 to 3 where 0, 1, 2, and 3 indicate no, slight, moderate, and high roughness, respectively.

The equivalent of 200 mg of pure IBU was held in the mouth for 10 seconds and then spat out, and 1 ODT (containing equal amounts of IBU) was held in the mouth until complete disintegration (three tablets per trained volunteer). Bitterness was recorded immediately and at several intervals for 15 minutes according to the bitterness intensity scale from 0 to 3 where 0, 0.5, 1, 2, and 3 indicate no, threshold, slight, moderate, and strong bitterness.

2.9 Differential scanning calorimetry (DSC)

The physical state of the pure drugs and the coated granules were examined by differential scanning calorimetry (DSC). The thermographs of each powder were obtained by using a Mettler-Toledo 823e (Greifensee, Switzerland) differential scanning calorimeter. Samples accurately weighed (2-3 mg) were placed in pierced aluminium pans and heated from 20 to 260 °C at a scanning rate of 10 °C min⁻¹ in a nitrogen atmosphere.

2.10 X-ray powder diffraction

Samples of pure and loaded IBU were evaluated using a Bruker D8 Advance in theta-theta mode, Cu anode at 40 kV and 40 mA, parallel beam Goebel mirror, 0.2 mm exit slit, LynxEye Position Sensitive Detector with 3 degree opening and LynxIris at 6.5 mm, sample rotation at 15rpm. The sample was scanned from 5 to 45° 2-theta with a step size of 0.02 degrees 2-theta and a counting time of 0.2 seconds per step; 176 channels active on the position sensitive detector making a total counting time of 35.2 seconds per step.

2.11 *In vitro* drug release studies

In vitro drug release studies were carried out in 750 ml of 0.1 M hydrochloric acid for 2 hr using a Varian 705 DS dissolution paddle apparatus (Varian Inc. North Carolina, US) at 100 rpm and 37 ± 0.5°C. After 2 hr operation, 250 ml of 0.20 M solution of trisodium phosphate

dodecahydrate were added into the vessel (buffer stage, pH 6.8) that has been equilibrated to 37 °C. At predetermined time intervals samples were withdrawn for HPLC assay. All dissolution studies were performed in triplicate

2.12 HPLC analysis

The amounts of released IBU were determined by HPLC. An Agilent Technologies system equipped with a NUCLEODUR[®] C18 Pyramid, 5 µm x 125 m x 4 mm column at 254 nm was used for the IBU HPLC assay. The mobile phase consisted of acetonitrile/water (1% acetic acid) (50:50, v/v). The flow rate was 1.0 ml/min and the retention time of IBU was 6.0 minutes. The IBU calibration curves ($R^2=0.999$), at concentrations varying from 10 µg/ml to 200µg/ml, were used to evaluate all the samples with 10µl injection volume.

3.0 Results and discussion

3.1 Hot-melt extrusion process

The HME process was conducted at 140°C to produce smooth extrudates at two different IBU loadings of 25 and 40%. The Eudragit[®] EPO is an amorphous copolymer based on dimethylaminoethyl methacrylate and neutral methacrylic esters with a low glass transition temperature of 48.6°C [27]. Eudragit[®] EPO was chosen as the primary matrix-forming polymer due to its cationic nature that could facilitate drug-polymer interactions. In addition, EPO's solubility in gastric media up to pH 5 renders it an excellent carrier in order to provide immediate release of the active substance. Finally EPO is extremely thermally stable to withstand the HME process. For the purposes of the study no plasticizer was used as IBU has been found to present plasticising effects compared to traditional plasticizers [28]. Usually, plasticizers are low molecular weight compounds that convert rigid polymers into flexible ones by reducing their glass transition temperature. IBU has shown concentration-dependent plasticizing properties as it is homogeneously dispersed on a molecular level in the ethylcellulose matrix by creating hydrogen bonding. However, it was important to add an anti-tacking agent such as talc to avoid tackiness of the EPO polymer.

The tackiness of acrylic polymers increases with the amount of plasticizer and in this case with the IBU amount due to the softening of the polymer [29]. This effect is eliminated by adding the appropriate talc amounts. The extruded materials still presented some tackiness and thus micronization was carried out under cryogenic milling conditions. The particle size distribution obtained is depicted in Fig. 3.1 and shows low percentages of fine particles with only 4.5 % below 40µm. Similarly, a small particle fraction of 5% was observed between 400-500µm. The majority of the particles lay in the size range of 100-400µm.

The PM of formulation II (40% IBU) showed exactly the same comparable peaks with that of the pure drug (Fig. 3.2) indicating no drug-polymer interaction while IBU retains its crystallinity. In the diffractogram of Formulation I (25% IBU) only three intensity peaks could be identified at 9.43° , 18.80° , 28.57° 2θ values, all of them belonging to talc. The characteristic IBU peaks disappeared indicating the presence of an amorphous state of IBU and possible drug-polymer interactions.

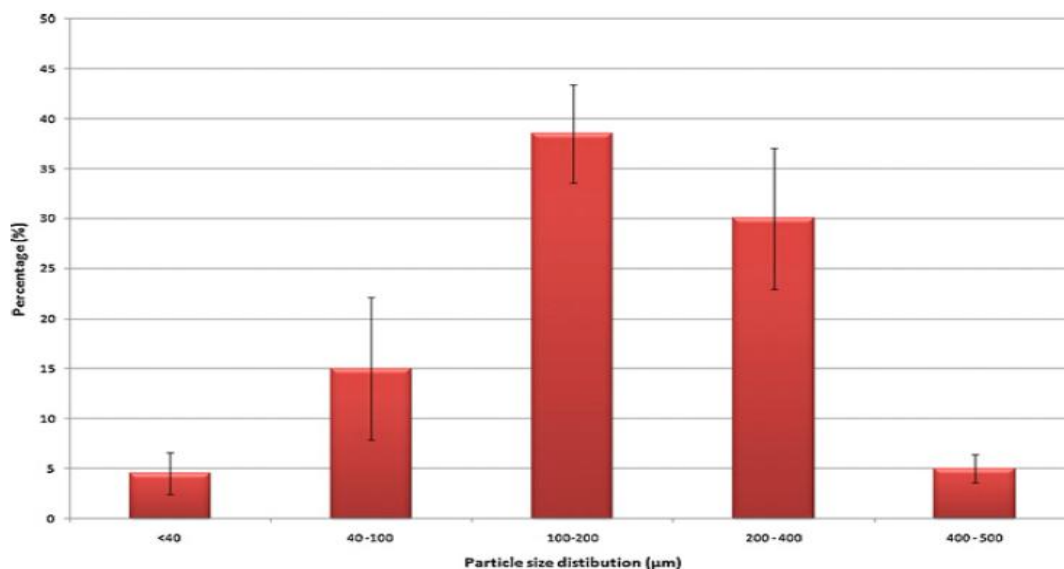


Fig. 3.1: Particles size distribution of micronized IBU/EPO (40% loading) extrudates (Milling time 10 min at 6000 rpm).

The IBU/EPO extrudates, including the physical mixture (PM) of the same composition and the pure active, were studied by X-ray analysis. The diffractograms were recorded to examine the IBU crystallinity. As can be seen from Fig. 3.2, the characteristic IBU intensity peaks could be identified at 6.03° , 12.09° , 16.48° , 17.55° , 18.75° , 20.02° , 22.13° , 24.47° , 24.99° 2θ degrees.

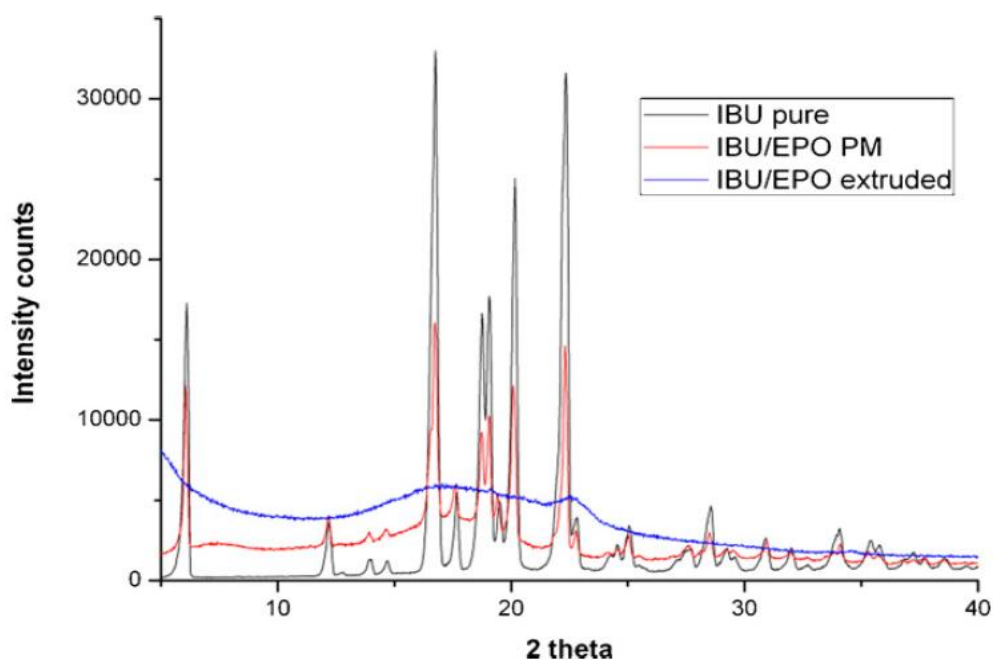


Fig. 3.2: X-ray diffraction patterns of pure IBU, physical IBU/EPO mixture and extruded IBU/EPO granules, respectively.

When IBU was processed at 40% loading, no significant peaks were apparent in the diffractogram indicating amorphous IBU even at high drug loadings. The diffractograms did not present any changes after one year storage and no IBU re-crystallization was observed. DSC was also used to study the IBU state within the EPO matrix. In Fig. 3.3 the IBU melting point was determined at 77.36°C and at 76.69°C for the physical mixture. The shift of the melting point is attributed to the IBU's plasticization effect. For the physical mixture the EPO glass transition temperature was unchanged at 54.97°C in comparison to the pure EPO (54.83°C). The thermogram of extruded IBU/EPO (40% loading) showed the absence of IBU melting and the existence of a single glass transition, T_g . In fact, T_g was lowered at 29.49°C clearly indicating that EPO has been plasticized by the IBU. The presence of a single T_g confirms the complete miscibility of IBU/EPO and the creation of a glassy solution where IBU is molecularly dispersed within EPO [27, 30].

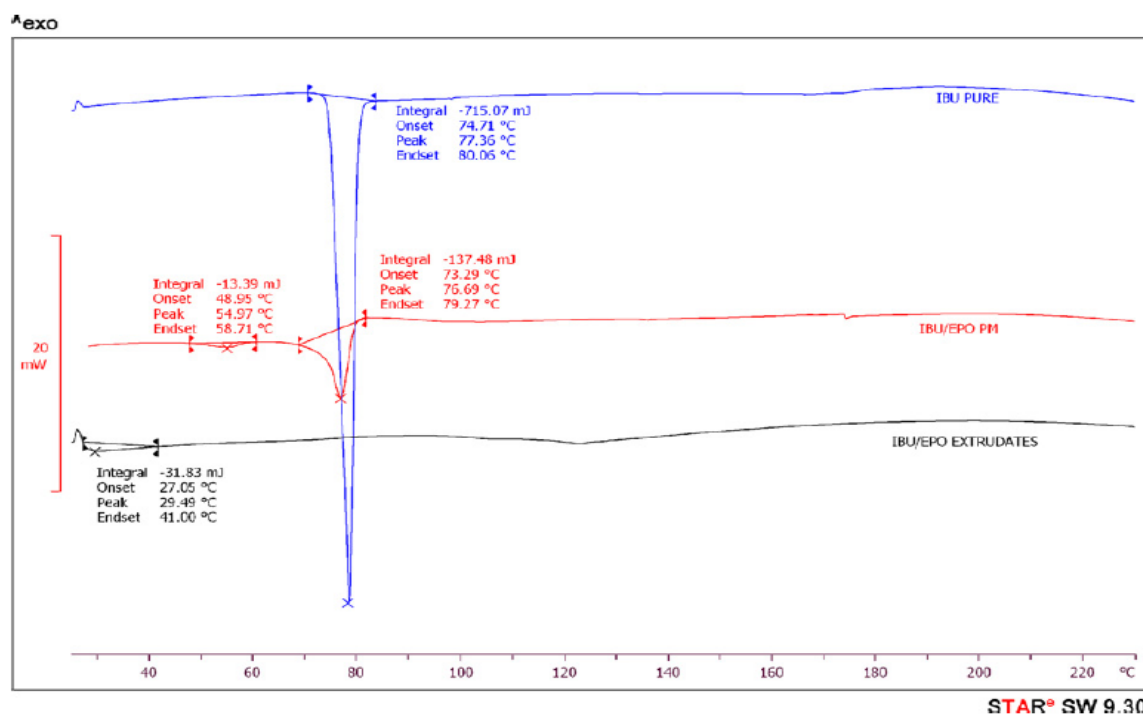


Fig. 3.3: DSC thermograms of pure IBU, physical IBU/EPO mixture and extruded IBU/EPO granules, respectively.

The IBU/EPO interactions and the existence of molecularly dispersed IBU have been confirmed by FTIR studies elsewhere [31]. The FT-IR findings elucidated a possible taste masking mechanism attributed to the intermolecular ionic interactions between the IBU's functional carboxylic and the EPO's dimethylamino groups. IBU can act as a hydrogen donor with the hydrogen bonding acceptor dimethylamino group. The deprotonation of the -COOH facilitates the formation of a carboxylate salt and consequently builds a taste masking effect on the molecularly dispersed IBU.

3.2 Powder and ODTs characterization

The IBU/EPO extrudates (40% loading) were blended with five different superdisintegrants at concentrations varying from 2-20% (w/w) as shown in Table 3.1 prior to tablet compaction. All batches were characterized in terms of compressibility by Carr's index determination. The excellent batch flowability and compressibility properties were attributed to the presence of microcrystalline cellulose, MCC, (Avicel 102), which is an excellent filler/flow-aid for direct compression with an average particle size of 90 µm. The addition of mannitol (Pearlitol C160) contributed as well to the improved tablet compressibility.

Table 3.1: Composition of ODT formulations

IBU/Excipients	F1	F2	F3	F4	F5	F6	F7	F8	F9	F10	F11	F12	F13	F14	F15	F16	F17	F18	F19	F20
	(%)																			
IBU*/EPO	75,0	75,0	75,0	75,0	75,0	75,0	75,0	75,0	75,0	75,0	75,0	75,0	75,0	75,0	75,0	75,0	75,0	75,0	75,0	75,0
Avicel 102	12,5	10,5	8,5,0	2,5	12,5	10,5	8,5,0	2,5	12,5	10,5	8,5,0	2,5	12,5	10,5	8,5,0	2,5	12,5	10,5	8,5,0	2,5
XL10	2,0	5,0	10,0	20,0	-	-	-	-	-	-	-	-	-	-	-	-	-	-	-	-
Vivasol	-	-	-	-	2,0	5,0	10,0	20,0	-	-	-	-	-	-	-	-	-	-	-	-
XL	-	-	-	-	-	-	-	-	2,0	5,0	10,0	20,0	-	-	-	-	-	-	-	-
CL-SF	-	-	-	-	-	-	-	-	-	-	-	-	2,0	5,0	10,0	20,0	-	-	-	-
CL	-	-	-	-	-	-	-	-	-	-	-	-	-	-	-	-	2,0	5,0	10,0	20,0
Mannitol	10,0	9,0	6,0	2,5	10,0	9,0	6,0	2,5	10,0	9,0	6,0	2,5	10,0	9,0	6,0	2,5	10,0	9,0	6,0	2,5
Pruv	0,5	0,5	0,5	0,5	0,5	0,5	0,5	0,5	0,5	0,5	0,5	0,5	0,5	0,5	0,5	0,5	0,5	0,5	0,5	0,5

*IBU loading was 40%

As a general rule, the powder compressibility decreased when the amount of superdisintegrants was increased in all formulations (Table 3.2). In many cases the presence of MCC (disintegrant nature) and mannitol (soluble diluents) has been reported to facilitate tablet disintegration. However, this was not observed in our studies as the formulations prepared in the absence of superdisintegrants showed high disintegration times (data not shown). As a result the improved disintegration times observed in this study should not be attributed to the existence of the aforementioned excipients.

Table 3.2: Physical properties of powder blends and compressed tablets (n = 3).

	F2	F6	F7	F10	F11	F13	F14
Bulk density (g/cm ³)	29.00	35.00	36.30	33.70	37.30	38.30	42.30
Tapped density (g/cm ³)	25.00	30.30	31.70	30.30	32.00	34.30	38.00
Density (g/cm ³)	1.35	1.40	1.40	1.35	1.33	1.36	1.35
Carr's Index (%)	13.8	13.40	12.60	10.10	14.20	10.44	10.16
Tensile strength (kP/cm ²)	6.05	10.40	9.44	8.97	7.21	9.73	9.93
Porosity	0.14	0.13	0.13	0.16	0.13	0.15	0.15

As is shown in Table 3.1 superdisintegrants with concentrations varying from 5-20%, under different compaction forces, were tested to evaluate their effect on the ODTs disintegration times. In general, the concentration of a superdisintegrant influences the relationship between the applied compaction force and the disintegration time ^[32]. For the purposes of the study four different grades of crosslinked N-Vinylpyrrolidone (XL, XL10, CL, CL-SF) and sodium croscarmellose (Vivasol[®]) were evaluated. The selected superdisintegrants differ in their particle size distribution, particle shape, porosity, compressibility, flowability and disintegration mechanism. The CL and CL-SF grades act as

disintegrants by absorbing water and the subsequent swelling leads to separation of the tablet particles. In contrast, XL10, XL and croscarmellose promote wicking *via* capillary action due to their high porosity. Subsequently, water is rapidly absorbed and disrupts the interparticular matrix bonds causing the tablet to fall apart [33].

The superdisintegrant concentration *versus* the compaction force profiles in Fig. 3.4(a-d) showed interesting results regarding the disintegration time performance of each superdisintegrant. At first, it can be seen that XL10 outperformed all superdisintegrants at low levels (2-5% wt/wt) while XL outperformed at high levels (10-20% w/w) respectively. The disintegration performance can be arranged in descending order for low levels as follows: XL10>XL>Vivasol>CL-SF>CL, while for high levels the order is XL>XL10>Vivasol>CL-SF>CL. For XL10 the optimum concentration level was between 5-10% w/w with disintegration times varying between 8-20 sec while for 20% w/w disintegration times were increased without exceeding 60sec. On the other hand, XL's optimum level was at 10–20% (wt/wt) showing substantial reduction to the disintegration times (Fig. 3.4C). The better performance of XL10 at low levels can be attributed to the smaller particle size of XL10 (30-50µm) compared to XL (100-130 µm) facilitating faster water absorbance. On the contrary, high XL10 levels led to increased disintegration times.

Vivasol showed good disintegration times at high levels (10-20% wt/wt) and better disintegration times at compaction forces of 10-20 kN. Interestingly the addition of Kollidon CL–SF presented excellent disintegration times at concentrations of 2% w/w with compaction forces of 8 or 12 kN. This also could be attributed to the particles morphology facilitating faster water absorptions.

Further addition of CL – SF amounts led to prolonged disintegration times but much lower than 60 sec. In contrast, the Kollidon CL grade showed poor performance for all concentrations and the entire range of compaction forces. This behaviour can be explained to some extent because of the small CL–SF (10-30µm) particle size compared to the CL grade (110 – 130µm) similar to the other two crosslinked N-Vinylpyrrolidone grades (XL, XL10).

However, the different disintegration times of the five superdisintegrants are mainly attributed to the different disintegration mechanisms and the tablet porosities. The Polyplasdone (XL10, XL) and Vivasol grades possess both swelling and wicking properties. All the disintegration studies were carried out at pH 5.6, where these cross-linked polymers have similar swelling capacities (92, 90 and 85% respectively).

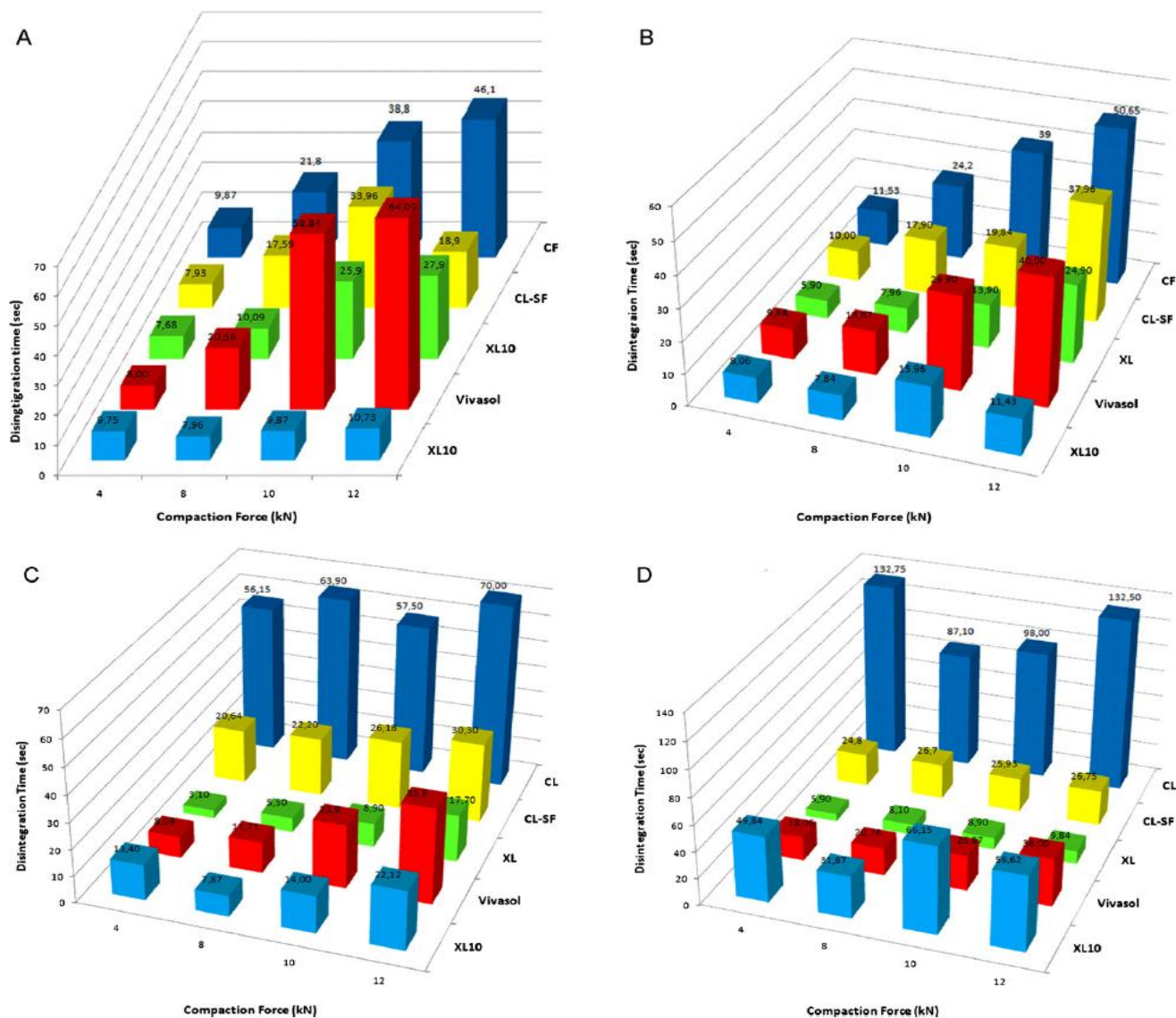


Fig. 3.4: Schematic diagram of ODT disintegration times at various compaction forces with a) 2%, b) 5%, c) 10% and d) 20% superdisintegrants.

However, swelling is not the primary disintegration mechanism for XL10 and XL. XL10 and XL can rapidly absorb water (wicking), due to their porous particle size morphology, and generate rapid volume expansion by increasing the hydrostatic pressure that causes tablet disintegration. In contrast, Vivasol has a fibrous non-porous particle structure which swells at slower rates and thus results in slower disintegration times. The Kollidon CL-SF grade has a fibrous particle shape (10-30 μm) and non-porous surface with swelling as the main disintegration mechanism. CL-SF exhibits low swelling pressure (~ 25 kPa) and relatively increased times to reach 90% of the swelling capacity (35 sec) while CL grades exhibit high swelling pressure (170 kPa) and rapid swelling times (5 sec). It would be reasonable to expect, therefore, superior tablet disintegration times for the CL grades. Nevertheless, CL-SF grades present higher water uptake capacity (~ 7.0 - 8.5 g water/g polymer) to the CL

grades (3.5-5.5 g water/g polymer) and in combination with the smaller particle size, display faster disintegration times.

Fig. 3.5(a-d) depicts the tablet hardness *versus* the compaction force at various superdisintegrant concentrations and compaction forces. It can be seen that the hardness increased with concentrations up to 5% (wt/wt) for all superdisintegrants. When high disintegrant concentrations (>10% wt/wt) were used, the tablets became softer and the hardness decreased (except CL 20% w/w) as a result of modest compressibility. Another interesting observation for all disintegrants is that the hardness increased with an increase in the applied compaction force. The results obtained from friability studies indicate dissimilar behaviour for each disintegrant. For instance, Kollidon CL and Vivasol at 2-10% wt/wt displayed no impact of disintegrant level at 8-12 kN compaction forces but displayed high friability at concentrations of 20% w/w. On the other hand, XL and CL - SF showed very low friability at 2% levels and a slight increase from 5-20% levels. In the case of XL10, the optimum friability was observed at 10% w/w levels.

The rapid disintegration times described above are also related to tablet porosity as can be seen in Table 2. High porosity is a critical ODT parameter because it facilitates liquid penetration into the tablet and results in faster disintegration. The estimated porosities for all ODT formulations were quite high, varying from approximately 0.13-0.16 without however compromising tablet mechanical properties. The hardness and friability studies demonstrated acceptable mechanical properties as mentioned above (Hardness about 7 Kp, friability <2.2%). Nevertheless, the evaluation of the superdisintegrants at various concentrations listed in Table 3.1 revealed the tablet formulations with high porosity and adequate strength.

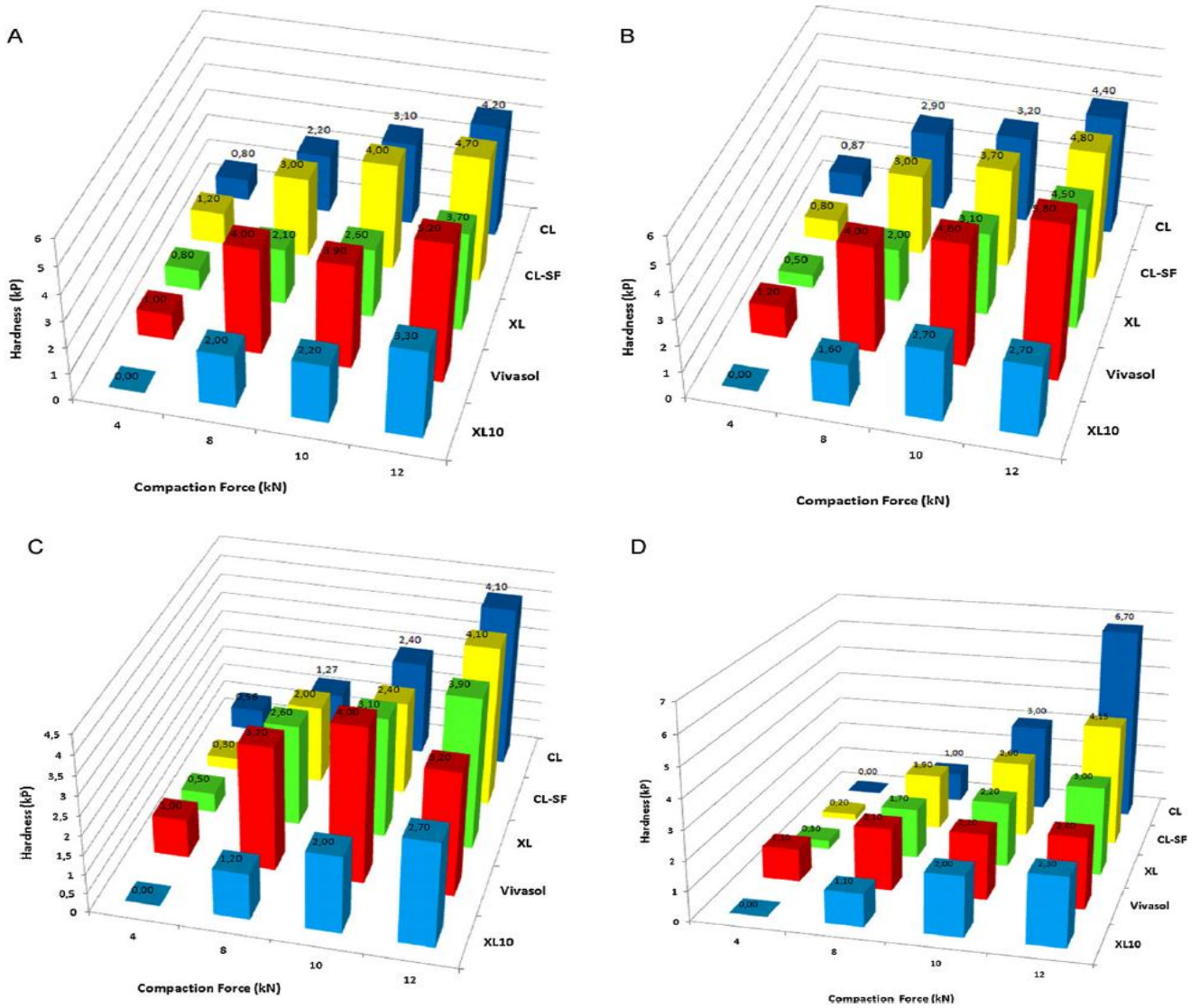


Fig. 3.5: Schematic diagram of ODTs hardness at various compaction forces with a) 2%, b) 5%, c) 10% and d) 20% superdisintegrants.

The ODTs friability was also investigated as a function of the superdisintegrant level and the applied compaction force (Fig. 6a-d). At 4 kN compaction forces, friability levels were very high for all superdisintegrants while at higher compaction forces of 8-12kN friability was significantly decreased. This is due to the compactability of the powder while punching the tablets. It is assumed that higher the compression forces better the hardness of the tablets thus lower the friability values.

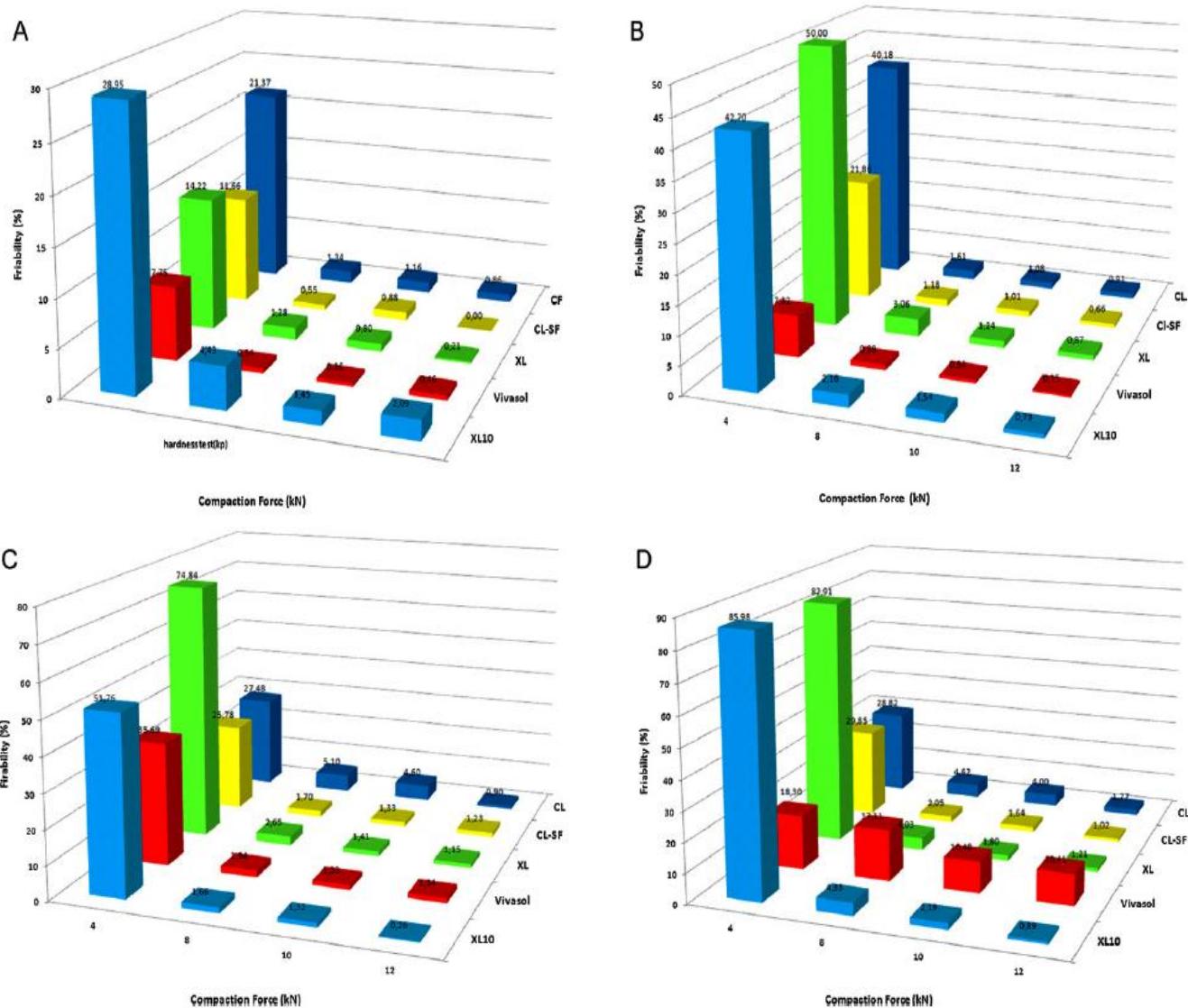


Fig. 3.6: Schematic diagram of friability of ODTs at various compaction forces with a) 2%, b) 5%, c) 10% and d) 20% superdisintegrants.

Analysis of the experimental findings in Figs. 3.4-3.6 allowed us to evaluate the robustness of the developed ODT formulations. A robust ODT should present unique features such as increased drug loading, taste masking, controlled release of API, rapid disintegration times, low friability and high crushing strength (hardness). The robustness of seven ODT formulations developed in the current study was evaluated in comparison to the commercial Nurofen® Meltlets. All tablet formulations were assessed in terms of disintegration times, hardness, friability, tablet weight and IBU loading. As can be seen in Fig. 3.7 the ODT formulations developed through HME processing presented better friability and comparable disintegration times to Nurofen® ODTs.

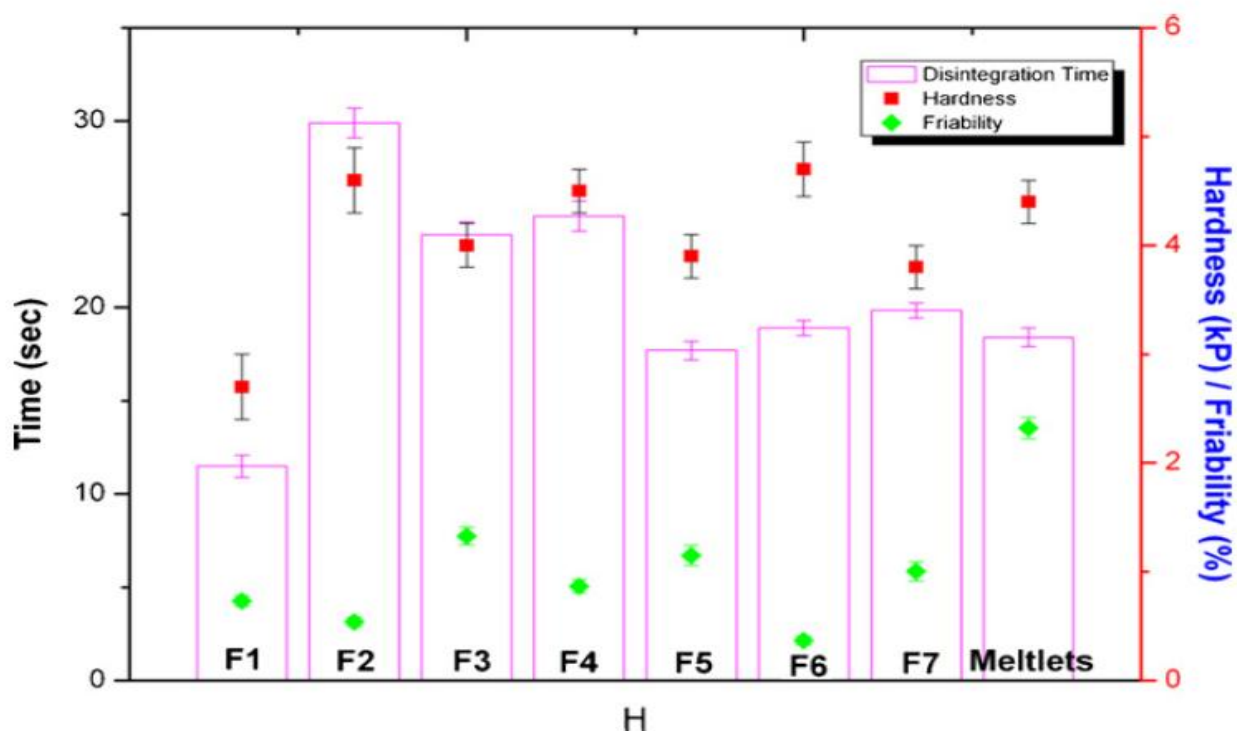


Fig. 3.7: Schematic diagram of ODTs disintegration times at various compaction forces with superdisintegrants at their optimal levels.

Interestingly, most of the ODTs developed showed relatively low hardness (2.7 - 4.0 kP) without, however, affecting tablet friability. The Nurofen® tablets showed rapid disintegration times but also low hardness (4.4 kP) and high friability values. ODTs with CL – SF at 2–5 % w/w proved to be robust with excellent disintegration times, hardness and friability. Similarly, the incorporation of XL, XL10 and Vivasol superdisintegrants produced high quality ODTs. An important aspect for the new generation ODTs is the capability to provide disintegration times of less than 30 sec without compromising tablet friability. This was feasible for the developed ODTs and Nurofen® tablets despite the high tablet weights that could possibly elevate friability levels.

3.3 *In vivo* disintegration time and taste-masking evaluation

The ODTs disintegration times were evaluated using the texture analyzer and *in vivo* disintegration methodologies. The average disintegration times in Table 3.3 did not reveal significant differences ($p > 0.05$) between the two approaches. The reason is that the texture analyzer method (artificial saliva, 37°C) simulates effectively the oral disintegration of ODTs providing a convenient means for accurate and reproducible determination of the disintegration times.

Table 3.3: Comparison of disintegration times of ODTs at various compaction forces (n=3).

Formulations	Disintegration Time	
	Texture analyzer (sec)	<i>In – vivo</i> disintegration (sec)
F2(12 kN)	11.40±0.6	13.50±1.2
F6 (10 kN)	29.90±1.3	31.80±2.5
F7 (10 kN)	23.90±1.2	25.20±1.8
F10 (12 kN)	24.90±1.0	26.60±2.3
F11 (12 kN)	17.70±0.7	19.30±2.0
F13 (12 kN)	18.90±0.6	20.10±1.5
F14 (10 kN)	19.80±0.9	20.60±1.8
Nurofen®	18.40±0.9	20.30±2.0

The taste-masking of the ODTs developed was of critical importance for this study. The embedding of the bitter IBU crystals with the EPO polymer matrix proved an efficient taste-masking platform. In Table 3.4 the perceived taste intensity studies in human volunteers showed considerable masking of IBU's bitter taste. The degree of bitterness was zero after 3 min for all formulations. In addition, the use of XL (10%) and CL-SF (5-10%) gave a smooth mouth feel. Nurofen® ODTs presented excellent taste-masking but with moderate roughness levels. The overall taste and sensory tablet evaluations showed excellent palatability.

Table 3.4: Taste evaluation of ODTs on healthy human volunteers (average value, n=10).

Formulations	Degree of bitterness (DB) / roughness (DR) after time					
	30 sec		1 min		2min	
	DB	DR	DB	DR	DB	DR
IBU	3	3	3	3	3	3

F2	0	0.5	0	1	0	1
F6	0	0.5	0	1	0	2
F7	0	0.5	0	1	0	2
F10	0	0.5	0	1	0	1
F11	0	0.5	0	0.5	0	0.5
F13	0	0.5	0	1	0	0.5
F14	0	0	0	0	0	0
Nurofen®	0	1	0	1	0	2

3.4 *In vitro* dissolution

The main objectives for this study were to increase IBU's dissolution rate, achieve sufficient taste-masking and to provide simultaneous rapid release. The amorphous IBU state within the EPO polymer matrix is expected to provide increased dissolution rates.

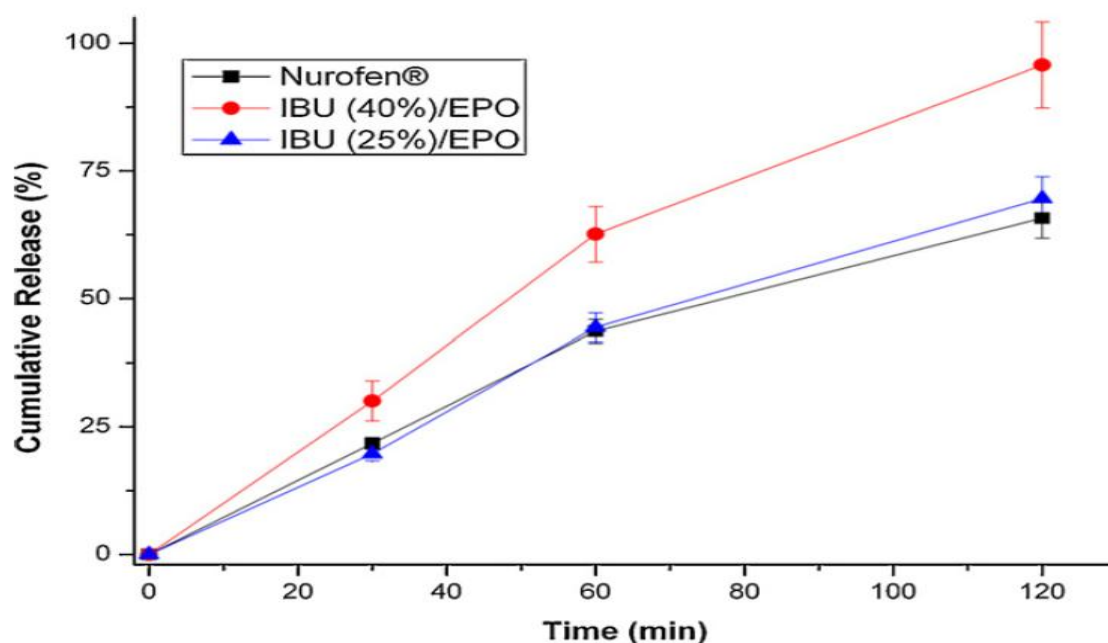


Fig. 3.8: Release profiles of ODTs with IBU/EPO extruded granules of, \blacktriangle) 25%, (\bullet) 40% drug loading and \blacksquare) Nurofen®.

In Fig. 3.8, it can be seen that ODTs of 25% and 40% loadings of extruded IBU/EPO provided rapid cumulative release profiles compared to that of pure IBU. The release of pure

IBU has been reported 22% after 2 hrs ^[34]. In addition it was observed that increased IBU loading (40% - Formulation II) provided faster release rates in contrast to the 25% loading (Formulation I). This is attributed to the increased talc amounts (50%) in Formulation I. As mentioned earlier talc serves as an anti-tacking agent and because of its hydrophobic nature retards polymer hydration and the subsequent IBU release rate. Comparison of the extruded formulations with the Nurofen® tablets demonstrated similar release rates for 25% loading but a faster rate for the 40% IBU/EPO extrudates. Application of a Kruskal-Wallis non-parametric test ($p > 0.05$) to the results showed no significant difference. Nevertheless, the HME extruded formulations showed excellent release patterns that could provide fast onset action in future clinical trials.

4.0 Conclusions

In this chapter we have demonstrated the manufacture of robust taste-masked IBU ODTs. For the purpose of the study IBU was hot-melt extruded and embedded within a Eudragit EPO polymer matrix. The *in vivo* taste-masking evaluation showed that HME processing can be used to mask efficiently the taste of bitter active substances without compromising tablet palatability. The ODTs developed showed disintegration times and crushing resistance similar to commercial Nurofen® tablets but improved tablet friability. Finally the increased IBU release rates of the developed ODTs were faster than the commercial Nurofen® tablets.

5.0 References

1. W. Habibh, R. Khankarik, J. Hontz. Fast-Dissolve Drug Delivery System. Crit Rev Ther Drug Carrier Syst. 17 (2000) 61-72.
2. D. Douroumis. Practical approaches of taste masking technologies in oral solid forms. Expert Opin Drug Deliv. 4 (2007) 417-26.
3. A. Mahesh, N. Shastri, M. Sadanandam. Development of Taste Masked Fast Disintegrating Films of Levocetirizine Dihydrochloride for Oral Use. Curr Drug Deliv. 7 (2010) 21 – 7.
4. A. Dinge, M. Nagarsenker. Formulation and evaluation of fast dissolving films for delivery of triclosan to the oral cavity. AAPS PharmSciTech. 9 (2008) 349-56.
5. Zydis fast dissolving technology
(http://www.catalent.com/documents/file/zydis_bro_v15b_Web_MedRES.pdf)

6. M.F. Al-Omran, S.A. Al-Suwayeh, A.M. El-Helw, S.I. Saleh. Taste masking of diclofenac sodium using microencapsulation. *J Microencapsul.* 19 (2002) 45-52.
7. P.P. Shah, R.C. Mashru, Y.M. Rane, A. Thakkar. Design and optimization of mefloquine hydrochloride microparticles for bitter taste masking. *AAPS PharmSciTech.* 9 (2008) 377-89.
8. S.S. Behzadi, T. Toegel, H. Viernstein. Innovations in coating technology. *Recent Pat Drug Deliv Formul.* 2 (2008) 209-30.
9. T. Hamashita, M. Matsuzaki, T. Ono, M. Ono, Y. Tsunenari, T. Aketo, S. Watano. Granulation of core particles suitable for film coating by agitation fluidized bed II. A proposal of a rapid dissolution test for evaluation of bitter taste of ibuprofen. *Chem Pharm Bull, (Tokyo).* 56 (2008) 883-7.
10. J.P. Benoit, H. Rolland, C. Thies, V. Vande Velde. Method of coating particles and coated spherical particles. US Patent: 6,087,003 (2000)
11. H. Mazen, P. York. Particle formation methods and their products. US Patent: 7,115,280 (2006)
12. A. Forster, J. Hempenstall, T. Rades. Characterization of glass solutions of poorly water-soluble drugs produced by melts extrusion with hydrophilic amorphous polymers. *J Pharm Pharmacol,* 53 (2001) 303–315.
13. M. Kinoshita, K. Baba, A. Nagayasu, K. Yamabe, T. Shimooka, Y. Takeichi et al. Improvement of solubility and oral bioavailability of a poorly water-soluble drug, TAS-301, by its melt-adsorption on a porous calcium silicate. *J Pharm Sci,* 91 (2002) 362–370.
14. J. Breitenbach, M. Magerlein. Melt extruded molecular dispersions. In I. Ghebre-Sellassie & C. Martin (Eds.), *Pharmaceutical Extrusion Technology*, New York: Marcel Dekker Inc. 2003.
15. I. Ozgüney, D. Shuwisitkul, R. Bodmeier. Development and characterization of extended release Kollidon SR mini-matrices prepared by hot-melt extrusion. *Eur. J Pharm. Biopharm.* 73 (2009) 140-5.
16. E. Verhoeven, C. Vervaet, J.P. Remon. Xanthan gum to tailor drug release of sustained-release ethylcellulose mini-matrices prepared via hot-melt extrusion: in vitro and in vivo evaluation. *Eur J Pharm Biopharm.* 63 (2006) 320-3.
17. C. De Brabander, C. Vervaet, J.P. Remon. Development and evaluation of sustained release mini-matrices prepared via hot melt extrusion. *J Cont Rel.* 89 (2002) 235-47.

18. Verhoeven, T.R.M. De Beer, E. Schacht, G. Van den Mooter, J.P. Remon, C. Vervaet. Influence of polyethylene glycol/polyethylene oxide on the release characteristics of sustained-release ethylcellulose mini-matrices produced by hot-melt extrusion: in vitro and in vivo evaluations. *Eur J Pharm Biopharm.* 72 (2009) 463-470.
19. Innovative formulations from Melt Extrusion
<http://eudragit.evonik.com/product/eudragit/en/downloads/eudragitbrochures/pages/default.aspx>.
20. A. Fini, G. Fazio, G. Feroci. Solubility and solubilisation properties of non-steroidal anti-inflammatory drugs. *Int J Pharm.* 126 (1995) 95–102.
21. N.A. Peppas, P.A. Buri. Surface, interfacial and molecular aspects of polymer bioadhesion on soft tissues *J Control Rel.* 2 (1985) 257–75.
22. J.T. Fell, J.M. Newton. Determination of tablet strength by diametral – compression test. *J Pharm Sci,* 59 (1970) 688 – 91.
23. C.K. Tye, C.C. Sun, G.E. Amidon. Evaluation of the effects of tableting speed on the relationships between compaction pressure, tablet tensile strength, and tablet solid fraction. *J Pharm Sci.* 94 (2005) 465-67.
24. G. Abdelbary, C. Eouani, P. Prinderre, J. Joachim, J.P. Reynier, P. Piccerelle. Determination of the in vitro disintegration profile of rapidly disintegrating tablets and correlation with oral disintegration. *Int J Pharm.* 292 (2005) 29–41.
25. S. Khan, P. Kataria, P. Nakhat, Y.P. Pramod. Taste Masking of Ondansetron Hydrochloride by Polymer Carrier System and Formulation of Rapid-Disintegrating Tablets. *AAPS PharmSciTech.* 8 (2007) E1 – E7.
26. H. Goel, N. Vora, V. Rana. A Novel Approach to Optimize and Formulate Fast Disintegrating Tablets for Nausea and Vomiting. *AAPS PharmSciTech.* 9 (2008) 774 – 781.
27. S. Qi, A. Gryczke, P. Belton, D.Q. Craig. Characterisation of solid dispersions of paracetamol and EUDRAGIT E prepared by hot-melt extrusion using thermal, microthermal and spectroscopic analysis. *Int J Pharm.* 354 (2008) 158-67.
28. C. De Brabander, G. Van Den Mooter, C. Vervaet, J.P. Remon. Characterization of ibuprofen as a nontraditional plasticizer of ethyl cellulose. *J Pharm Sci.* 91 (2002) 1678-85.
29. M. Wesseling, F. Kuppler, R. Bodmeier. Tackiness of acrylic and cellulosic polymer films used in the coating of solid dosage forms. *Eur J Pharm Biopharm.* 47 (1999) 73-8.

30. L. Saerens, L. Dierickx, B. Lenain, C. Vervaet, J.P. Remon, T. De Beer. Raman spectroscopy for the in-line polymer–drug quantification and solid state characterization during a pharmaceutical hot-melt extrusion process. *Eur J Pharm Biopharm.* 77(1) (2011) 158-63.
31. Pharma Polymers, 51st International, EUDRAGIT® Workshop, March 14-16, Degussa AG, Business Line Pharma Polymers, Darmstadt, Germany, 2006.
32. E.L. Parrott. In Lieberman, H. A., Lachman, L., Schwartz, J.B., (eds.), “Pharmaceutical Dosage Forms: Tablets Vol. 2,” 2nd ed., Marcel Dekker, New York, 1990 pp. 201—243.
33. Y.X. Bi, H. Sunada, Y. Yonezawa, K. Danjo. Evaluation of rapidly disintegrating tablets prepared by a direct compression method. *Drug Dev Ind Pharm.* 25 (1999) 571-81.
34. P. Kocbek, S. Baumgartner, J. Kristl. Preparation and evaluation of nanosuspensions for enhancing the dissolution of poorly soluble drugs. *Int J Pharm.* 312 (2006) 179–186.

CHAPTER 4: TASTE MASKING OF PARACETAMOL BY HOT MELT EXTRUSION: AN *IN VITRO* AND *IN VIVO* EVALUATION

1.0 Introduction

The taste masking of bitter APIs is a major challenge especially for the development of orally disintegrating tablets (ODT) in pharmaceutical industry. Several approaches have been reported which involve fluidized-bed coating, supercritical fluids and coacervation approaches where effective taste-masking is achieved by applying polymeric coating layer to create a physical barrier around the drug [1, 2]. Other alternatives involve the use of complexing agents (cyclodextrins, ion exchange resins) through the formation of inclusion complexes or resonates [3]. Recently, taste masking approaches have employed taste suppressants molecules by blocking the gap junction channels and hemichannels and thus suppressing the drugs taste [4,5]. However, there is an enormous need for more robust, cost effective and easy to scale – up taste masking technologies. HME is a continuous, one step process that has been used for the development of solid dispersions of active substances for various applications [6, 7].

Hot-melt extrusion (HME) has been employed as a novel technique for the formulation of oral solid dosage forms in pharmaceutical industries in the last decade. It was initially used in food and plastic industry but has attracted significant interest in the pharmaceutical manufacturing for the development of robust formulations. HME can be used to develop various formulations such as sustained release matrices [8–11]. It has also been introduced for taste masking purposes of bitter APIs by involving the use of taste masking polymers that create solid dispersions to prevent bitter drugs from coming in contact with the patient's taste buds [12–15].

Taste masking can be achieved through intermolecular forces (e.g. hydrogen bonding) between the active substance and the polymer matrix by processing oppositely charged compounds [1, 2]. In addition, solid dispersions in which the drug is molecularly dispersed within the polymer matrix have shown effectiveness for masking of the drug's unpleasant taste. Successful taste masking requires development of HME processing conditions, drug/polymer ratio and selection of the appropriate formulation components (Hansen solubility parameters). HME can be used for the development of robust formulations with increased patient palatability and compliance. Taste masking evaluation of pharmaceutical dosage forms is usually carried out by human taste panels (volunteers) and it can be used for further product optimization. However, the taste assessment is subject to the individuals

leading to significant variations while ethical, safety and toxicity issues should be also taken in account. Alternatively, *in vitro* electronic taste sensing systems can be employed to predict the taste of pharmaceutical formulations [3, 16, 17]. Commercially available electronic tongues (Astree e-tongue and INSENT sensing system) have been well studied and evaluated for taste masking purposes. The Astree e – tongue (AlphaMOS, France) has been systematically used to evaluate the bitterness of pure active substances in comparison to formulated products. These e – tongue studies showed very good correlation with human taste panels, reproducibility, low detection limits and high sensitivity [18].

Paracetamol (PMOL) is a white crystalline powder with bitter taste mainly used as analgesic pain reliever and antipyretic. The main uses of paracetamol are the relief of headaches, minor aches and pains. In this study PMOL was used as a model drug for the purpose of taste masking. At the moment there are several over – the – counter products of orally disintegrating tablets (ODTs) where the active pharmacological agent is taste masked through various approaches.

In the current study PMOL extrudates were prepared by optimizing the HME processing [19, 20] parameters in order to mask its taste efficiently. The extrudates were evaluated both by *in vivo* and *in vitro* studies where an electronic tongue analyzer was employed that captures the global taste profile. The electronic tongue can be a valuable tool for the development of pharmaceutical formulations by providing accurate and reliable taste patterns of the desired formulations.

2.0 Materials and Methods

2.1. Materials

Paracetamol (PMOL) was purchased from Sigma Aldrich (Gillingham, UK). Eudragit EPO polymer was kindly donated from Evonik Pharma Polymers (Darmstadt, Germany). Crosslinked polyvinylpyrrolidone (Kollidon VA64) was also donated from BASF, Germany. The HPLC solvents were of analytical grade and purchased from Fisher Chemicals (UK). All materials were used as received.

2.2. Calculation of Hansen solubility parameters

The Hansen solubility parameters of the drug and the polymers were calculated from their chemical structures to check the miscibility of drug/polymer formulations using the Hoftyzer and van Krevelen method [21]. [Please see Chapter 2, Section 2.2 for more details].

2.3. Hot-melt Extrusion (HME) process

PMOL formulations with Kollidon VA64 and Eudragit EPO were mixed properly in 100 g batches for 10 min each. A Turbula TF2 Mixer was used to blend the powder formulations for 10 min. The extrusion of all PMOL blends was performed using a Randcastle single-screw extruder (RCP0625) equipped with a 0.2 mm rod die. The drug-polymers composition consisted of PMOL/EPO and PMOL/VA64 at a ratio of 40/60, 50/50, 60/40 and 30/70, 40/60, 50/50 (% wt/wt) respectively. The temperature profile used for all formulations was 100°C/113°C/113°C/113°C/115°C (from feeding zone → Die) with screw speed of 15 rpm (rev/min). The produced extrudates (strands) were milled to obtain granules (<500 µm). Grinding by ball milling carried out with a rotational speed of 400 rpm for 5 min each.

2.4 Thermal analysis

For the purposes of analysing the solid state of drug, polymers, their physical mixtures and the extruded formulations, differential scanning calorimetry studies (DSC) and temperature modulated (MTDSC) DSC were performed. The physical state of the pure drug, physical mixtures and extrudates was examined by using a Mettler-Toledo 823e (Greifensee, Switzerland) differential scanning calorimeter. Samples were prepared in sealed aluminum pans (2-5 mg) with a pierced lid. The samples were heated at 10°C/min under nitrogen atmosphere in a temperature range between 0 and 220°C. MTDSC experiments were performed from 30°C to 160°C temperature range with an underlying heating rate of 1°C/min to further analyze the samples. The pulse height was adjusted to 1°C with a temperature pulse width of 15-30 s.

2.5 X-ray powder diffraction (XRPD)

XRPD was used to assess the solid state of the extrudates where samples of pure and loaded PMOL were evaluated using a Bruker D8 Advance in theta-theta mode, Cu anode at 40 kV and 40 mA, parallel beam Goebel mirror, 0.2 mm exit slit, LynxEye Position Sensitive Detector with 3 degree opening and LynxIris at 6.5 mm, sample rotation at 15 rpm. The sample was scanned from 2 to 40 degrees 2-theta with a step size of 0.02 degrees 2-theta and a counting time of 0.2 seconds per step; 176 channels active on the PSD making a total counting time of 35.2 seconds per step.

2.6. *In vitro* drug release studies

In vitro drug release studies were carried out in 750 ml of 0.1 M hydrochloric acid for 2 hr using a Varian 705 DS dissolution paddle apparatus (Varian Inc. North Carolina, US) at 100 rpm and $37 \pm 0.5^\circ\text{C}$. After 2 hr operation, 250 ml of 0.20 M solution of trisodium phosphate dodecahydrate were added into the vessel (buffer stage, pH 6.8) that has been equilibrated to 37°C . At predetermined time intervals samples were withdrawn for HPLC assay. All dissolution studies were performed in triplicate.

2.7. HPLC analysis

The release of PMOL was determined by HPLC. An Agilent Technologies system equipped with a HICROM S50DS2, $5 \mu\text{m} \times 150 \text{ mm} \times 4 \text{ mm}$ column at 276 nm was used for the PMOL HPLC assay. The mobile phase consisted of acetonitrile/water (1% acetic acid) (50:50, v/v). The flow rate was 1.5 ml/min and the retention time of PMOL was 3.6 minutes. The PMOL calibration curves ($R^2=0.999$), at concentrations varying from 10 $\mu\text{g/ml}$ to 50 $\mu\text{g/ml}$, were used to evaluate all the samples with 20 μl injection volume.

2.8. *In vivo* taste masking evaluation

In vivo taste masking evaluation was performed on 6 healthy human volunteers [\[22, 23\]](#) from whom informed consent was first obtained (approved by the Ethics Committee of the University of Greenwich, Ref No: UG09/10.5.5.12). The study is also in accordance to the Code of Ethics of the World Medical Association (Declaration of Helsinki). The healthy volunteers of either sex (3 males and 3 females, age 18–25) were selected, trained and the extruded granules were evaluated (no exclusion criteria). The equivalent of 200 mg of pure PMOL or PMOL extrudates (containing equal amounts of PMOL) were held in the mouth for 60 seconds and then spat out. The selection of samples was random and in between two samples analysis mineral water was used to wash each volunteer's mouth. The bitterness was recorded immediately according to the bitterness intensity scale from 0 to 5 where 0, 1, 2, 3, 4 and 5 indicate none, threshold, slight, moderate, bitter and strong bitterness, respectively.

2.9. *In vitro* taste masking evaluation: Astree e-tongue

The assays were realized on Astree e-tongue system equipped with an Alpha M.O.S. sensor set #2 (for pharmaceutical analysis) composed of 7 set of sensors (ZZ, AB, BA, BB, CA, DA, JE) on a 48-positions autosampler using 25 ml-beakers. Acquisition times were fixed at 120s. All the data generated on the Astree system were processed using

multidimensional statistics on AlphaSoft V12.3 software. Each sample (granules) was tested on the Astree e-tongue at least 4 times with three replicates for each sample for the statistical analysis. The average values between 100 and 120 s were used to build the maps. Astree sensors were cleaned up in deionised water between each sample measurement. Each sample was diluted for 60 seconds under magnetic stirring in 25 ml of deionised water to reach API concentration corresponding to a final PMOL dose of 200 mg. The mixtures were filtered with Buchner funnel fitted with filter paper of 2.5 μm pore size.

3.0 Results and Discussion

3.1. Solubility parameters and extrusion process

The PMOL miscibility with EPO and VA64 was investigated prior to extrusion by estimating the Hansen solubility parameter using the method of Hoftyzer and van Krevelen for pure PMOL and both polymers. The prediction of drug/polymers miscibility in solid dispersions has successfully been achieved by the solubility parameters (δ) [24-27]. This miscibility is caused by balancing the energy of mixing released by inter-molecular interactions between the components by the energy released by intra molecular interactions within the components [21]. Three dimensional partial solubility parameters by Hansen (1969) calculated by group contributions of dispersion forces, polar forces and hydrogen bonding forces was provided by Van Krevelen/Hoftyzer (1976) and Fedors (1974). The theoretical approach of the solubility parameter suggests that compounds with similar δ values are likely to be miscible. The reason is that the energy of mixing from intramolecular interactions is balanced with the energy of mixing from intermolecular interactions. It was demonstrated that compounds with $\Delta\delta < 7 \text{ MPa}^{1/2}$ were likely to be miscible and compounds with $\Delta\delta > 10 \text{ MPa}^{1/2}$ were likely to be immiscible [28]. Thus, solubility parameters provide a simple and generic capability for rational selection of carriers in the preparation of solid dispersions [29]. As can be seen in Table 4.1, the difference between the calculated solubility parameters of the polymers and the drug indicate that PMOL is likely miscible with both polymers. By using the Van Krevelen/Hoftyzer the $\Delta\delta$ values for PMOL and EPO/VA64 are 6.86 and 6.17 respectively.

However, a two dimensional approach proposed by Bagley *et al.* [30] was used also to predict drug – polymer miscibility as shown in Table 4.1. By using the two – dimensional approach Bagley *et al.* observed that δ_p and δ_d have similar thermodynamic effects in contrast to δ_h and introduced the volume – dependent solubility parameter, δ_v , where

$$\delta_v = \sqrt{\delta_d^2 + \delta_p^2} \quad (4.1)$$

Table 4.1: Calculated solubility parameters of drug/polymers

Sample	δ_d (MPa ^{1/2})	δ_p (MPa ^{1/2})	δ_v (MPa ^{1/2})	δ_h (MPa ^{1/2})	δ_t (MPa ^{1/2})	$\Delta \delta$	Distance $R_{a(v)}$
PMOL	19.43	9.71	29.14	13.88	25.77	-	-
EPO	17.89	0.65	18.54	6.08	18.91	6.86	13.16
VA64	18.0	0.64	18.64	7.73	19.60	6.17	12.17

$$R_{a(v)} = \sqrt{[(\delta_{v2} - \delta_{v1})^2 + (\delta_{h2} - \delta_{h1})^2]}$$

This method was further developed by Breitzkreutz [31] and Albers [32] and used in predicting the duration of intestinal absorption for various drugs. The two-dimensional approach can provide more accurate prediction of the drug-polymer miscibility. The drug polymer miscibility can be predicted by the distance ($R_{a(v)}$) using the Pythagorean Theorem and the two components are considered miscible when $R_{a(v)} \leq 5.6 \text{MPa}^{1/2}$. In our case it is obvious from Table 4.1 that the δ_p values of the drug – polymer combinations differ significantly indicating an effect on the predicted miscibility. HME quite often requires the addition of a plasticizer to lower the glass transition temperature of the polymers and thus to conduct the extrusion process at lower temperatures [6, 24]. However, plasticizers were not incorporated in our studies as both polymers present low glass transition temperature allowing samples to be processed at low extrusion temperature ranges. The absence of plasticizer did not affect the extrusion process.

3.2. Thermal analysis and X – ray solid state characterization studies

DSC studies were performed to investigate the physical state of the drug within the polymer matrix. As can be seen in Fig. 4.1a the DSC thermogram of pure PMOL (calibrated by the peak onset) showed a sharp melting peak at 169°C (fusion enthalpy 33.40 J/g) with an onset of peak at 168°C where the amorphous EPO showed an endothermic peak at 48.4°C (onset 44.1°C) which corresponds to the glass transition temperature (T_g).

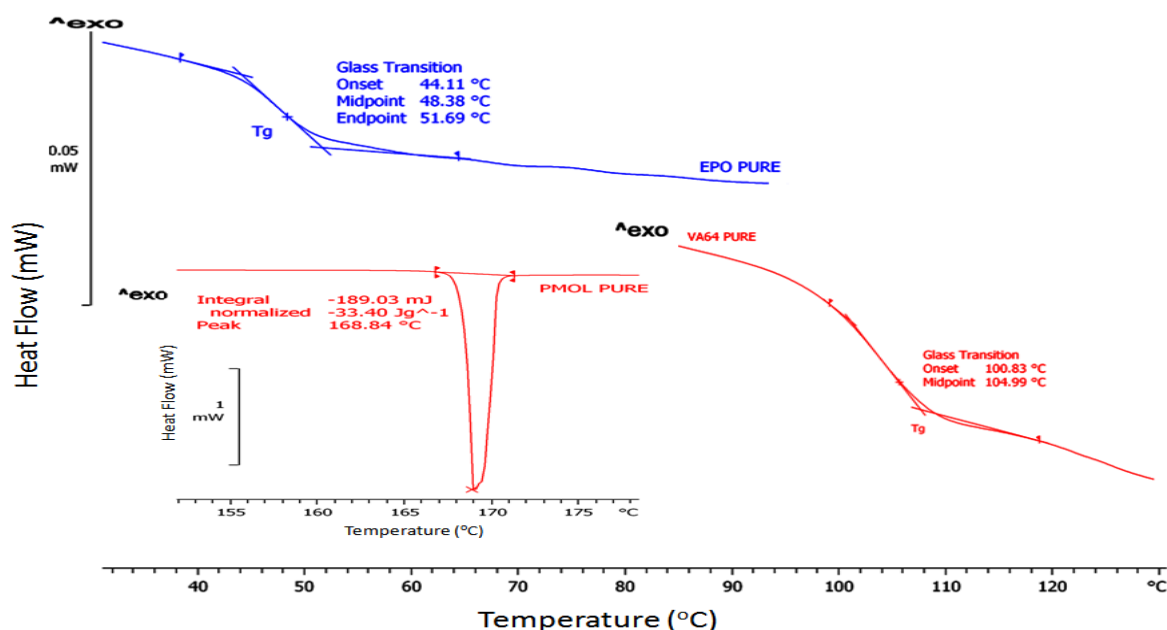


Fig. 4.1a: MTDSC thermograms of pure PMOL (inset) and Eudragit EPO, Kollidon VA64

Previous studies [33–34] of pure PMOL reported the existence of three crystal forms, the Form III which is highly unstable (melting point at 148°C), the metastable orthorhombic (Form II) with melting point at 160°C and the stable monoclinic (Form I) with melting point at 170°C while the amorphous form has a glass transition at 23°C. The polymorphic form of PMOL that was used in the current study was the monoclinic Form I. The DSC scans of the PMOL/EPO extrudates (Fig. 4.1b) showed melting endotherms at 143.3°C, 148.5°C and 151.5°C, respectively that correspond to 40, 50 and 60% PMOL loadings.

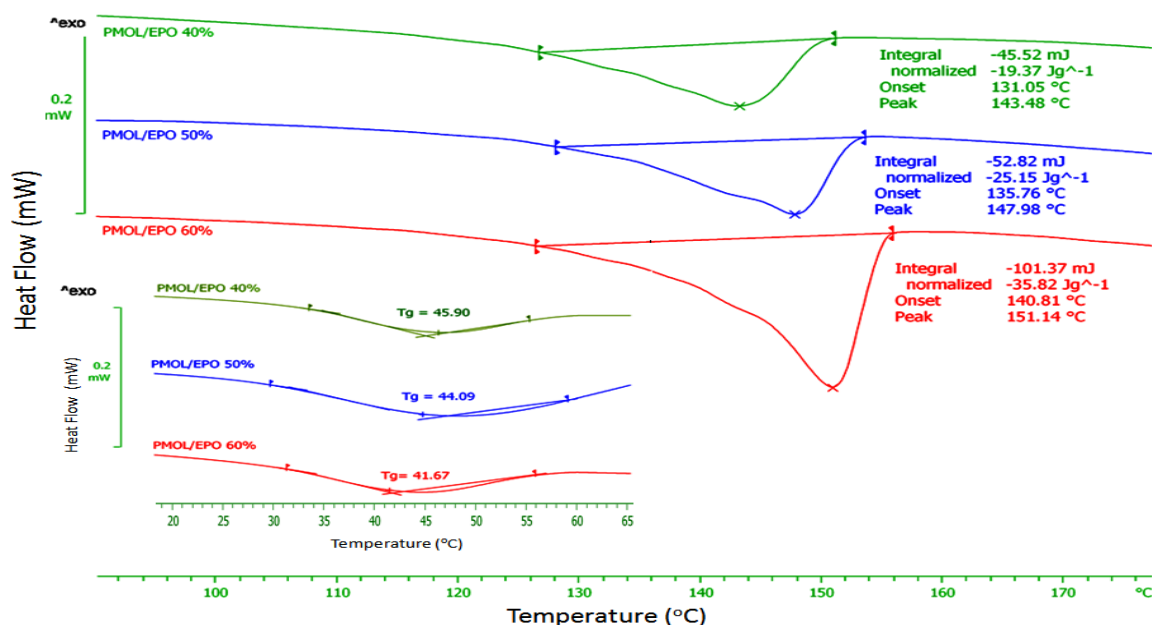


Fig. 4.1b: MTDSC thermograms of PMOL/EPO extrudates at different PMOL loadings.

The observed melting peaks are shifted to lower temperatures and the peak shapes are broader compared to those of pure PMOL suggesting the presence of crystalline PMOL. The observed melting peak of PMOL occurred between 143–152°C which is due to the presence of Form I PMOL in the polymer matrix. However, the shifts of the melting endothermic peaks can also be attributed to possible PMOL–EPO interactions without any changes in the crystal modifications. The presence of Form I was confirmed by the X–ray characterization studies as described below. If the PMOL/EPO components are miscible the Tg of the extruded samples can be derived by the Gordon – Taylor equation ^[35] and it will show a single Tg that varies between the Tg of the pure components. The EPO glass transition temperatures for the PMOL loaded samples (30-60%) are shifted at lower temperatures (45.9°C, 44.1°C, 41.7°C) and are slightly different from the estimated Gordon – Taylor theoretical values at 36.0°C, 33.7°C, 31.6°C respectively. In addition, only a single Tg was observed for all PMOL/EPO ratios while the Tgs decreased with increase in PMOL concentrations showing partial drug – polymer miscibility and PMOL plasticization effect. In total, the shifts of the melting PMOL peaks and EPO glass transition temperatures suggest the co–existence of molecularly dispersed and crystalline PMOL within the polymer matrix. Similar observations were reported by Qi et al. ^[36] for PMOL/EPO extrudates where PMOL was presented in two physical forms simultaneously. The calculated amorphous/crystallinity degrees ^[37] of the extruded formulations are shown in Table 4.2. It is obvious that the presence of crystalline PMOL is increased with the PMOL loading in each formulation.

Table 4.2: Crystalline/amorphous percentage of the extruded PMOL formulations

Formulation	Amorphous (%)	Crystalline (%)	Tg (°C)	Tm (°C)
PMOL/EPO 40%	79.5	20.5	45.9	143.3
PMOL/EPO 50%	75.5	24.5	44.1	148.5
PMOL/EPO 60%	52.0	48.0	41.7	151.5
PMOL/VA64 30%	100.0	-	85.8	-
PMOL/VA64 40%	100.0	-	95.2	-
PMOL/VA64 50%	100.0	-	93.5	-

Tg: polymer glass transition, Tm: PMOL melting point

In contrast, the PMOL/VA64 extrudates showed two Tg peaks, one close to the Tg of bulk VA64 (105°C) and the other between 27 – 42°C depending on the PMOL loadings. Pure

VA64 showed a baseline shift at 105°C which is reported as T_g and there is another endothermic peak visible at about 200°C which correspond to decomposition of the polymer. As Fig. 4.1c shows the low temperature T_g is related to the PMOL loading with descending order of PMOL (30%)>PMOL (40%)>PMOL (50%) →(41.1°C, 37.7°C, 27.6°C) and are elevated at higher temperature in comparison to amorphous PMOL T_g (25°C). The transformation of PMOL from Form I to amorphous is supported by the disappearance of the melting endothermic peak at 169°C. As a result we could rule out the presence of molecularly dispersed PMOL within the VA64 matrix which can be recognised by the presence of one single mixed-phase T_g. In our case, the two consecutive glass transitions indicate the presence of amorphous mixtures and an amorphous/amorphous phase separation. This observation is not unusual as similar results have been observed for itraconazole/EPO100 solid dispersions [38].

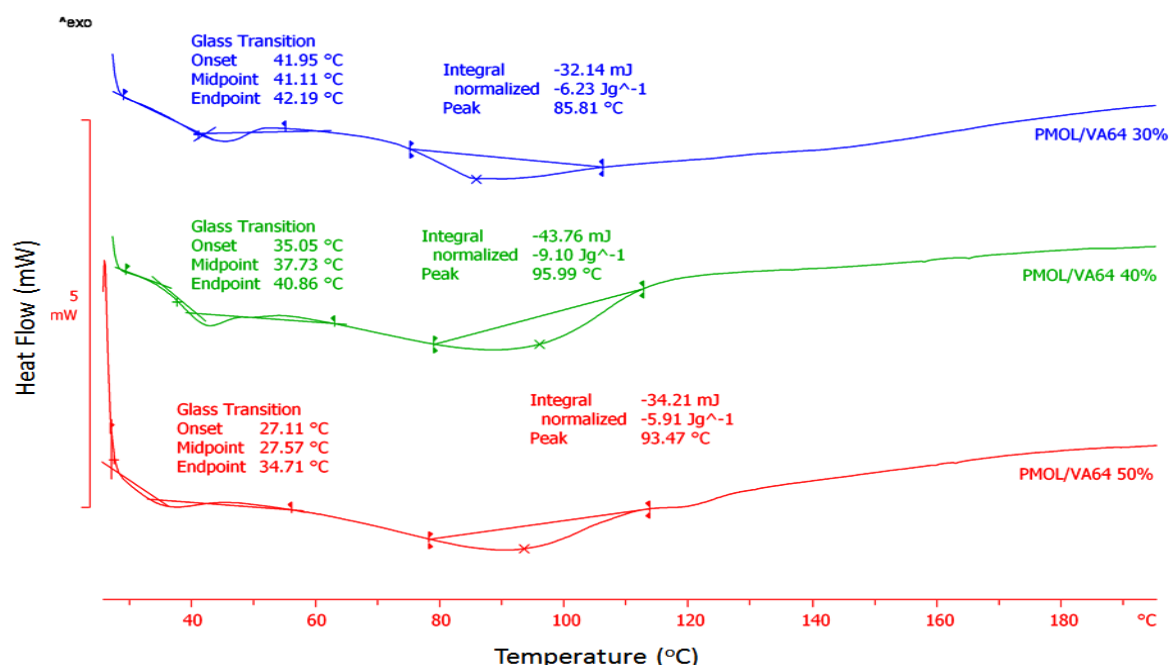


Fig. 4.1c: MTDSC thermograms of PMOL/VA64 extrudates at different PMOL loadings.

XRPD was employed to investigate the crystalline state of PMOL within the polymer matrices. The standard XRPD patterns of pure PMOL, physical mixtures with Eudragit EPO, and extrudates are depicted in Fig. 4.2a.

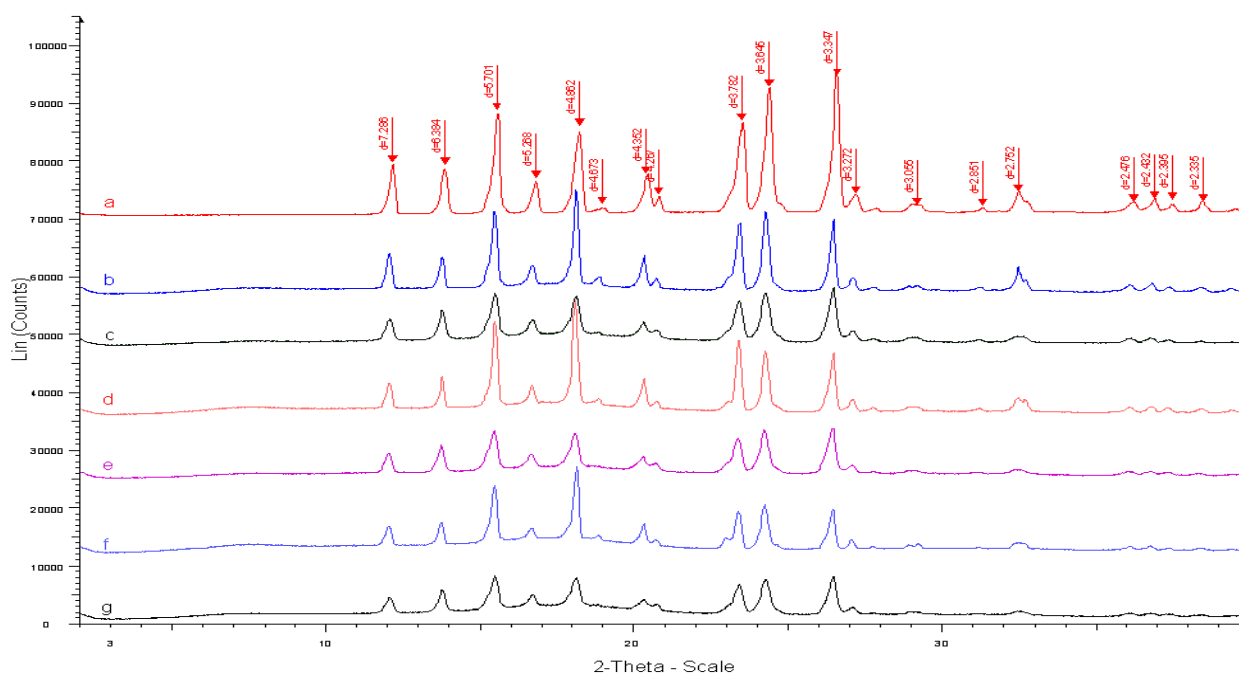


Fig. 4.2a: Powder XRPD patterns of PMOL/EPO solid dispersion (SD) and physical mixtures (PM) systems: (a) PMOL pure (b) PMOL/EPO 60% PM (c) PMOL/EPO 60% Ext. (d) PMOL/EPO 50% PM (e) PMOL/EPO 50% Ext.50% (f) PMOL/EPO 40% PM (g) PMOL/EPO 40% Ext.

Crystalline PMOL has distinct crystalline peaks at 2θ angles of 12.11, 13.82, 15.52, 18.20, 20.42, 23.51, 24.39 and 26.59° and a series of smaller peaks at different 2θ angles ranging from 26.78 - 38.45° . The diffraction patterns of the physical mixtures of drug and polymers in three different ratios presented identical crystalline peaks to those of pure PMOL but at a lower intensity. The XRD patterns of extruded formulations showed increased amorphous trends compared to the pure PMOL due to the dispersion of the drug into the polymer matrix. Furthermore the diffraction patterns of all the PMOL–EPO extrudates confirmed the presence of Form I within the polymer matrices as no new distinct crystalline peaks at different 2θ could be observed [33]. The PMOL intensity peaks supported the DSC investigations where crystalline drug was detected in the binary mixtures. In contrast, for the PMOL–VA64 extrudates no distinct peaks were observed suggesting the presence of amorphous PMOL as shown in Fig. 4.2b. The absence of crystalline PMOL was detected for all drug loadings even at 50% PMOL. The combined DSC and X–ray characterization studies revealed different PMOL crystalline states mainly depending on the polymeric carrier and its miscibility with the active substance.

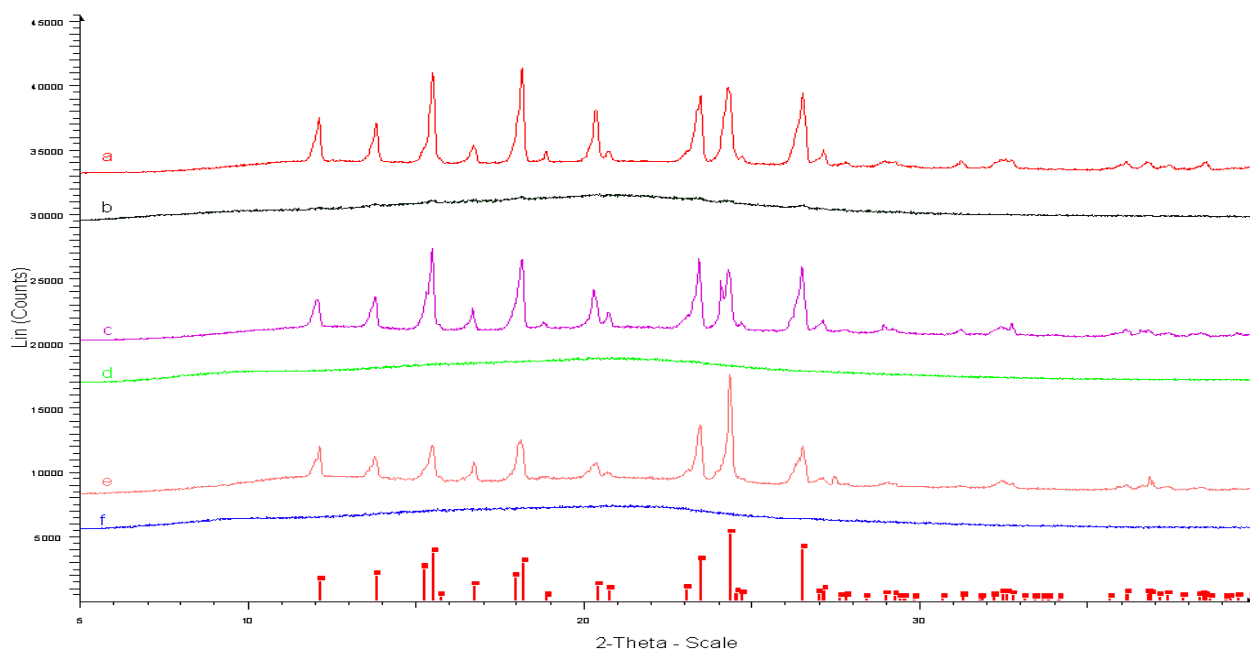


Fig. 4.2b: Powder XRPD patterns of PMOL pure (DIF), PMOL/VA64 extruded (ext) and physical mixtures (PM) samples: (a) PMOL/VA64 50% PM (b) PMOL/VA64 50% ext (c) PMOL/VA64 40% PM (d) PMOL/VA64 40% Ext (e) PMOL/VA64 30% PM and (f) PMOL/VA64 30% Ext.

3.3. *In vivo* and *in vitro* taste masking evaluation

The masking efficiency of the developed granules was evaluated *in vivo* with the assistance of six healthy human volunteers (age 18–25). The *in vivo* statistical data collected for the pure active substance, bulk polymers and the extruded formulations are summarized in Table 3. The data analysis showed significant suppression of the bitter taste for PMOL and strong influence of the polymeric carriers indicating the importance of drug loading in the final formulation.

Both polymers showed improved taste masking capacity for certain formulations with descending order VA64>EPO. The PMOL/EPO extrudates presented masking effect for active concentrations up to 50% with panellists' scores showing slight bitterness. In Fig. 4.3 it can be seen that PMOL/EPO extrudates showed better taste suppression at 40% loading while at 60% no masking effect was observed. The PMOL/VA64 extrudates demonstrated similar masking effect where for PMOL loadings from 40 – 50% the recorded scores suggested slight bitterness. The PMOL/VA64 (30%) extrudates showed improved masking effect with panellists' scores indicating threshold values.

Interestingly, no difference was observed in the *in vivo* taste scores for both polymers at the same PMOL loadings. For example at 40% PMOL loading the average panellists' score was identical for EPO and VA64 extrudates respectively.

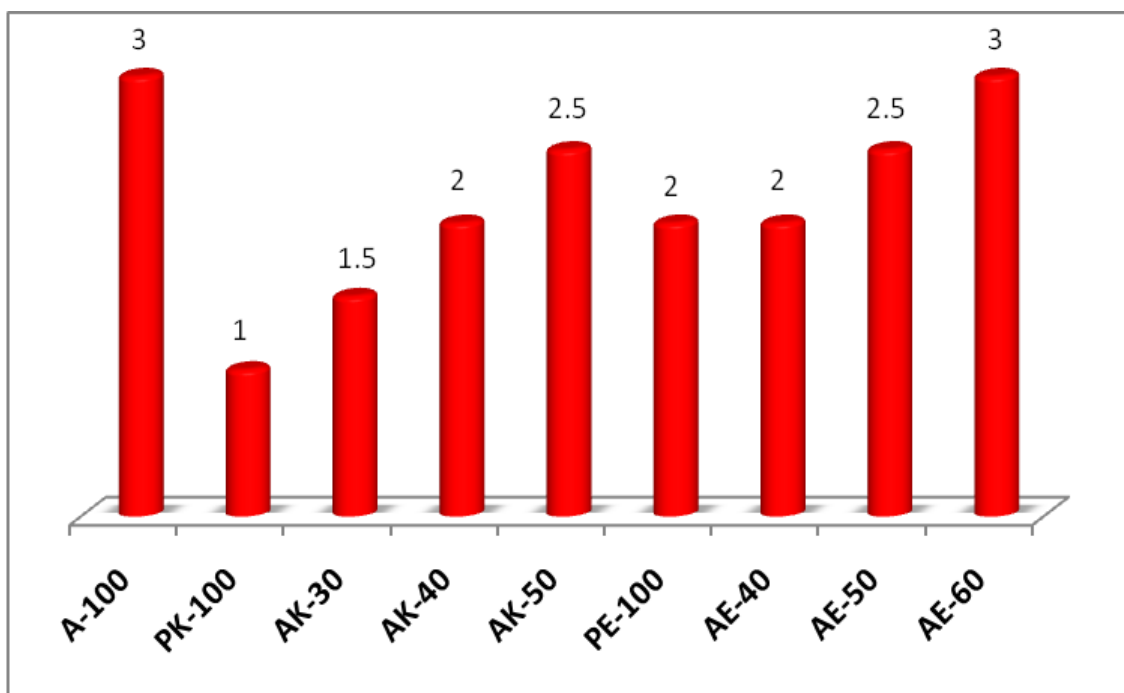


Fig. 4.3: Schematic representation of the taste scores of pure API, bulk polymers and the extruded formulations.

A novel *in vitro* approach to evaluate the taste masking efficiency of various pharmaceutical dosage forms and avoid problems related to human panelists is the use of electronic sensor arrays ^[39-42] known as electronic tongues (e – tongue). Similar studies were performed by other researchers where a principal component analysis (PCA) of active formulations against the placebo was presented through PCA maps in order to determine the taste masking potency of various components ^[43-45]. For the purposes of the study pure PMOL, bulk polymers and extruded granules were processed as described in the previous section. The signal of the different formulations was represented on taste maps based on a projection obtained by PCA as depicted in Fig. 4.4a- b. These maps showed the relative repartition and proximity of bitterness for each formulation.

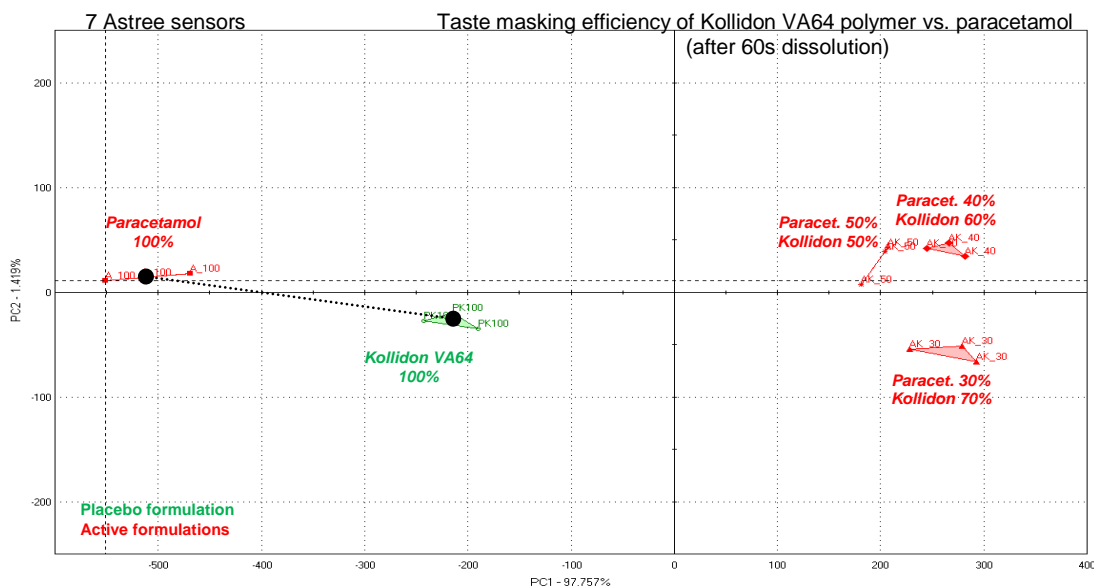


Fig. 4.4a: Electronic tongue “taste map”: Global signal comparison (PCA analysis of the electrode responses) between pure PMOL and extruded formulations with VA64 polymer after dissolution for 60 s.

According to Fig. 4.4a the active sample (100% PMOL) and placebo polymer (VA64) are well separated indicating a big distance and taste differences. Also, the taste map indicates significant discrimination between the placebo and the active extruded formulations. All three drug-polymer extruded samples are close to each other while relatively far from PMOL. This means a significant taste evolution and a masking improvement towards pure PMOL. Similar to Kollidon VA64 samples the same conclusions were observed for EPO polymer, despite a lowest distance from pure active to placebo formulation (Fig. 4.4b).

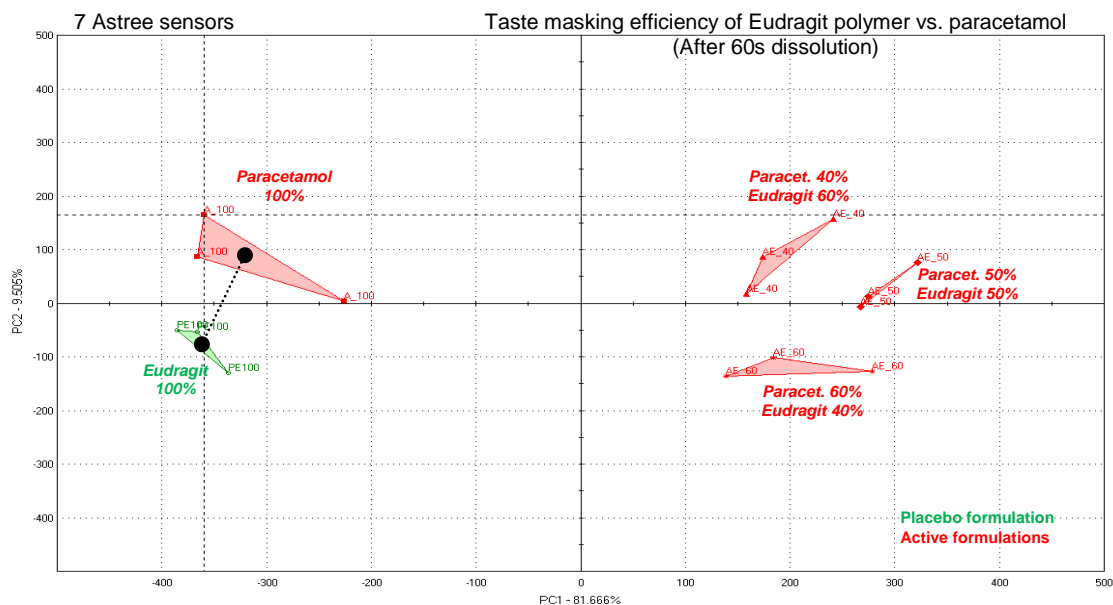


Fig. 4.4b: Electronic tongue “taste map”: Global signal comparison (PCA analysis of the electrode responses) between pure and extruded formulations with EPO polymer after dissolution for 60 s.

The distance between active and polymer formulations are indicative of the taste potency of each polymer. The closer the formulation is located to the placebo and the larger the distances to the pure unpleasant PMOL are, the better the taste masking is [46]. A taste improved effect is thus observed for each of the three PMOL-VA64 extrudates compared to polymer alone (DI>80%). As shown in Fig. 4.6 a taste improvement is perceptible with VA64 with the highest average distance obtained for PMOL/VA64 at 30/70%.

In Fig.4.5 it can also be seen that the PMOL/EPO extrudates showed closer distances and lower DI to pure API. However, these distances suggest improved masking effect with the best result achieved for PMOL loading at 50%.

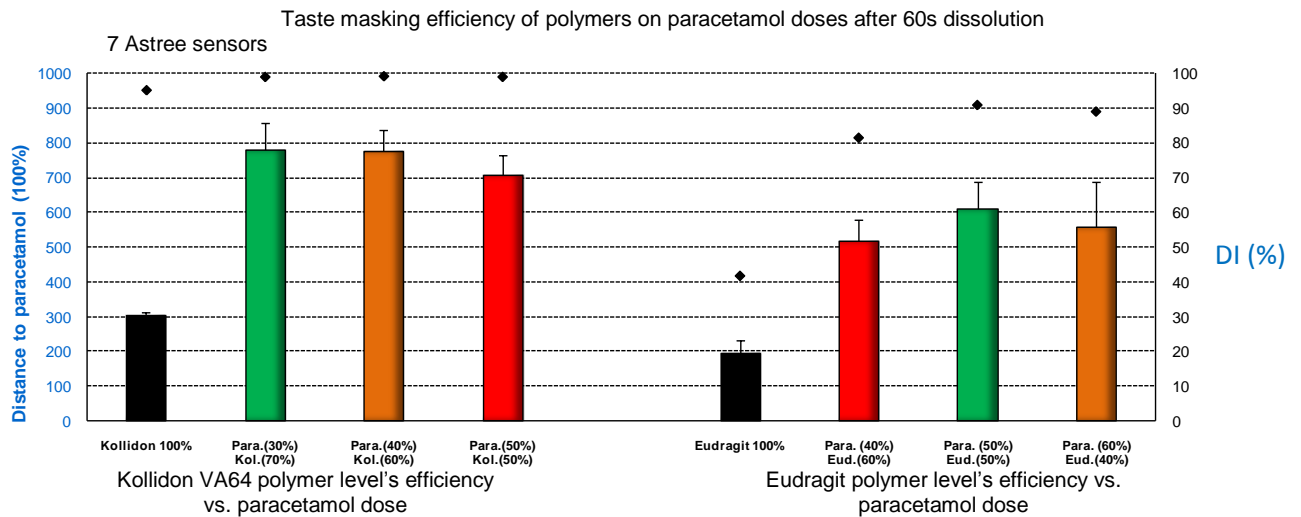


Fig. 4.5: Distance and discrimination comparison between signal of 100% PMOL formulation and each polymer’s formulation on Astree E-Tongue (after 60s).

This last result is slightly different than the panelists’ scores. Furthermore, a sensory correlated model based on Partial Least Square (PLS) was built to evaluate the correlation with sensory scores as depicted in Fig. 4.6. The correlation model is valid ($R^2 < 0.8$) despite dispersion and low discrimination between formulations (p value > 0).

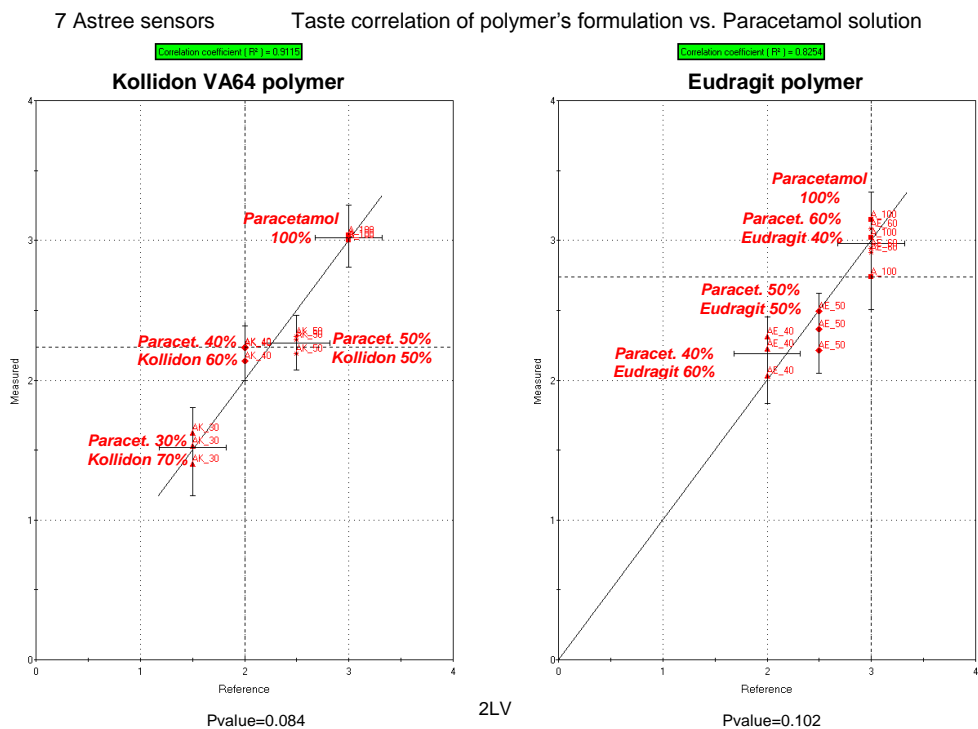


Fig. 4.6: Correlation of human sensory data “Reference” with Astree electronic tongue measurements (“Measured”).

The *in vitro* e-tongue evaluation was in good agreement with the *in vivo* tests and it was able to identify the optimum taste masked formulations. The e-tongue can be proved an efficient approach to develop palatable and pleasant – tasting products by replacing taste panelists.

3.4. Dissolution studies

Dissolution profiles of PMOL from PMOL/EPO 40-60% and PMOL/VA64 30-50% are shown in Fig. 4.7a, b. The dissolution rates of PMOL for both EPO and VA64 extrudates were rapid and approximately 80% PMOL was released in 15 min while more than 92% was released in 30 min. Only a slightly lower release rate was observed for the PMOL/EPO at 50 – 60% loadings which can be attributed to the higher crystalline matter of PMOL in the extrudates.

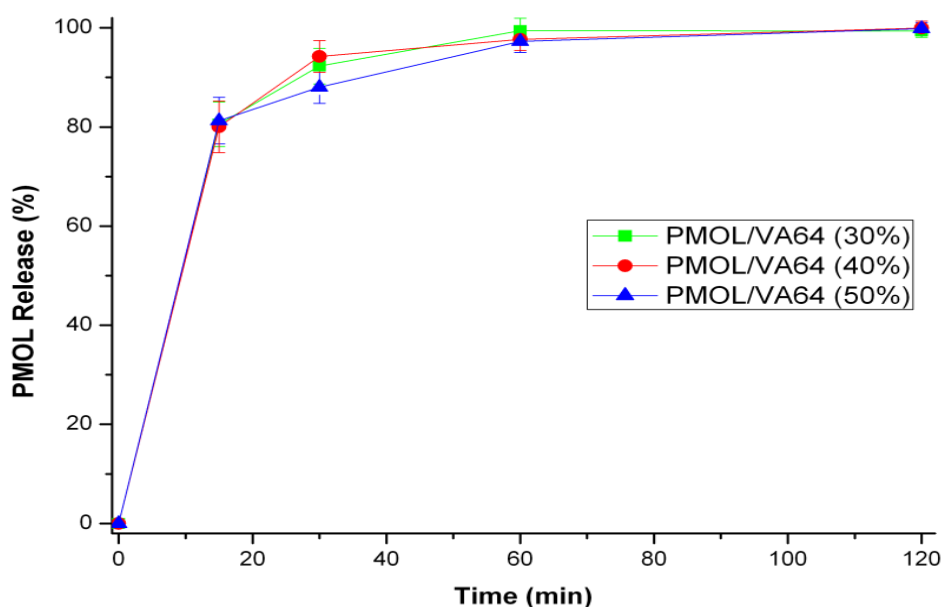


Fig. 4.7a: Dissolution profiles of PMOL in PMOL/EPO extrudates (n=3).

As a result each of the extruded formulations can be applied for fast onset action dosage forms. Furthermore, PMOL release patterns for the first 60s were investigated to determine the actual drug amount released during the *in vitro* taste masking evaluation. The PMOL release was found to be dependent on the polymer grade and the actual drug loading. In the case of PMOL/EPO extrudates the release varied between ~ 9 – 14% and the released drug amounts increased with increase in the drug loading. Similarly, the PMOL/VA64

exhibited the same trends but slower PMOL release patterns which varied from ~ 5 – 7%. The study of the onset PMOL release is important in order to verify the ability of both polymers to be used as masking agents.

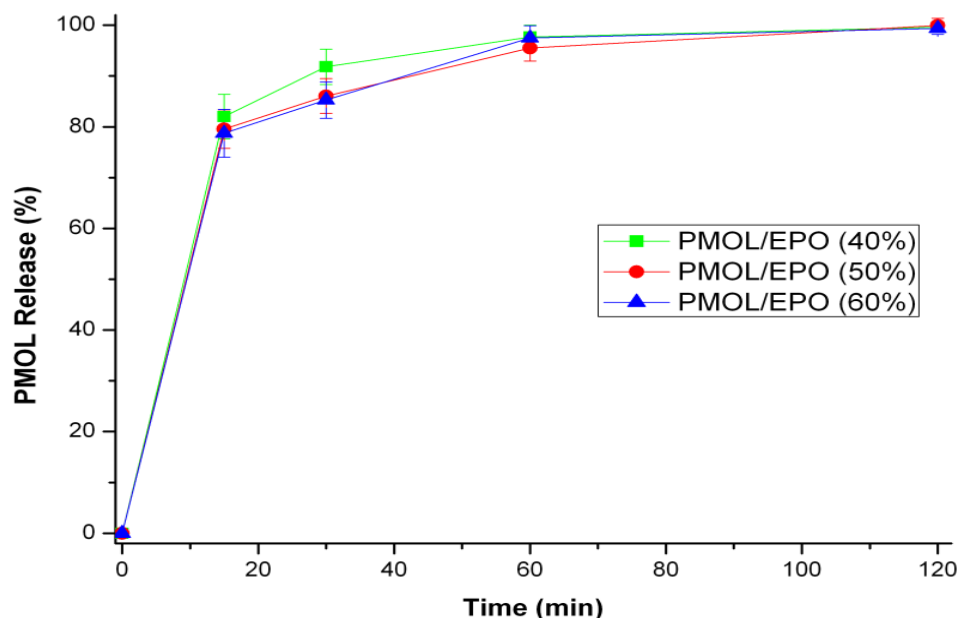


Fig. 4.7b: Dissolution profiles of PMOL in PMOL/VA64 extrudates (n = 3).

4.0 Conclusions

In this chapter HME was employed as a processing technique to manufacture taste masked PMOL formulation by embedding the active substance either in Eudragit EPO or Kollidon VA64 polymer carriers. PMOL was found to be in crystalline or amorphous state depending on the polymer used for extrusion. The optimized formulations were evaluated in terms of taste masking efficiency both by *in vivo* human panellists and an electronic tongue. The extruded formulations of VA64 demonstrated better taste masking compared to those of EPO while the e – tongue was found to be a valuable tool for taste masking assessments and formulation development.

5.0 References

1. D. Douroumis, Practical approaches of taste masking technologies in oral solid forms. *Expert Opin. Drug Deliv.* 4 (2007), pp. 417–426.
2. D. Douroumis, Orally disintegrating dosage forms and taste-masking technologies. *Expert Opin Drug Deliv.* 8 (2010), pp. 665-75.

3. K. Woertz, C. Tissen, P. Kleinebudde, J. Breitzkreutz, Rational development of taste masked oral liquids guided by an electronic tongue. *Int. J. Pharm.*, 400 (2010), pp. 114-23.
4. T. Sato, K. Nishishita, Y. Okada, K. Toda, Effect of gap junction blocker - glycyrrhetic acid on taste disk cells in frog. *Cell. Mol. Neurobiol.*, 29 (2009), pp. 503–512.
5. V. Lyall, T. –H. T. Phan, Z. Ren, S. Mummalaneni, P. Melone, S. Mahavadi, K. S. Murthy, J.A. DeSimone, Regulation of the putative TRPV 1t salt taste receptor by phosphatidylinositol 4, 5-bisphosphate. *J. Neurophysiol.*, 103 (2010), pp. 1337–1349.
6. M.A. Repka, S.K. Battu, S.B. Upadhye, S. Thumma, M.M. Crowley, F. Zhang, C. Martin, J.W. McGinity, Pharmaceutical applications of hot-melt extrusion: Part II. *Drug Dev Ind Pharm.*, 33 (2007), pp. 1043-57.
7. M.M. Crowley, F. Zhang, M.A. Repka, S. Thumma, S.B. Upadhye, S.K. Battu, J.W. McGinity, C.Martin, Pharmaceutical applications of hot-melt extrusion: part I. *Drug Dev. Ind. Pharm.*, 33 (2007), pp. 909-26.
8. A. Almeida, S. PossemiersS, M.N. Boone, T. De Beer, T. Quinten, L. Van Hoorebeke, J.P. Remon, C. Vervaet. Ethylene vinyl acetate as matrix for oral sustained release dosage forms produced via hot-melt extrusion. *Eur. J. Pharm. Biopharm.*, 77 (2011), pp. 297-305.
9. E. Verhoeven, T.R. De Beer, E. Schacht, G. Van den Mooter, J.P. Remon, C. Vervaet. Influence of polyethylene glycol/polyethylene oxide on the release characteristics of sustained-release ethylcellulose mini-matrices produced by hot-melt extrusion: In vitro and in vivo evaluation. *Eur J Pharm. Biopharm.* 72 (2009), pp. 463 - 470.
10. E. Verhoeven, T.R.M. De Beer, G. Van den Mooter, J.P. Remon, C. Vervaet. Influence of formulation and process parameters on the release characteristics of ethylcellulose sustained-release mini-matrices produced by hot-melt extrusion. *Eur. J. Pharm. Biopharm.*, 69 (2008), pp. 312-319
11. J. Liu, F. Zhang, J.W. McGinity. Properties of lipophilic matrix tablets containing phenylpropanolamine hydrochloride prepared by hot-melt extrusion. *Eur. J. Pharm. Biopharm.*, 52 (2001), pp. 181-190.
12. A. Gryczke, S. Schminke, M. Maniruzzaman, J. Beck, D. Douroumis, Development and evaluation of orally disintegrating tablets (ODTs) containing Ibuprofen granules prepared by hot melt extrusion. *Coll Surf B Biointerfaces.*, 86 (2011), pp. 275-84.

13. A. Michalk, V.-R. Kanikanti, H.-J. Hamann, P. Kleinebudde. Controlled release of active as a consequence of the die diameter in solid lipid extrusion. *J. Control Release.*, 132 (2008), pp. 35-41.
14. R. Witzleb, V.R. Kanikanti, H.J. Hamann, P. Kleinebudde. Solid lipid extrusion with small die diameters--electrostatic charging, taste masking and continuous production. *Eur. J. Pharm. Biopharm.*, 77 (2011), pp. 170-7.
15. J. Breitreutz, F. El-Saleh, C. Kiera, P. Kleinebudde, W. Wiedey. Pediatric drug formulations of sodium benzoate: II. Coated granules with a lipophilic binder. *Eur. J. Pharm. Biopharm.*, 56 (2003), pp. 255-60.
16. K. Woertz, C. Tissen, P. Kleinebudde, J. Breitreutz, A comparative study on two electronic tongues for pharmaceutical formulation development. *J. Pharm. Biomed. Anal.*, 55 (2011), pp. 272-81.
17. T. Harada, T. Uchida, M. Yoshida, Y. Kobayashi, R. Narazaki, T. Ohwaki, A new method for evaluating the bitterness of medicines in development using a taste sensor and a disintegration testing apparatus, *Chem. Pharm. Bull.*, 58 (2010), pp. 1009–1014.
18. K. Woertz, C. Tissen, P. Kleinebudde, J. Breitreutz, Performance qualification of an electronic tongue based on ICH guideline Q2, *J. Pharm. Biomed. Anal.* 51 (2010), pp. 497–506.
19. H. Liu, P. Wang, X. Zhang, F. Shen, C.G. Gogos Effects of extrusion process parameters on the dissolution behavior of indomethacin in Eudragit E PO solid dispersions. *Int. J. Pharm.*, 383 (2010), pp. 161-9.
20. H. Suwardie, P. Wang, D.B. Todd, V. Panchal, M. Yang, C.G. Gogos. Rheological study of the mixture of acetaminophen and polyethylene oxide for hot-melt extrusion application. *Eur. J. Pharm. Biopharm.*, (2011) (in press)
21. P.J. Hoftyzer, D.W.V Krevelen, Properties of polymers, Elsevier, Amsterdam, 1976.
22. S. Khan, P. Kataria, P. Nakhat, Y.P. Pramod, Taste Masking of Ondansetron Hydrochloride by Polymer Carrier System and Formulation of Rapid-Disintegrating Tablets, *AAPS PharmSciTech.*, 8 (2007), pp. E1 – E7
23. H. Goel, N. Vora, V. Rana, A Novel Approach to Optimize and Formulate Fast Disintegrating Tablets for Nausea and Vomiting, *AAPS PharmSciTech.*, 9 (2008) 774–781.
24. A. Forster, J. Hempenstall, I. Tucker, T. Rades, Selection of excipients for melt extrusion with two poorly water-soluble drugs by solubility parameter calculation and thermal analysis. *Int. J. Pharm.*, 226 (1–2) (2001), pp. 147–161.

25. B.C. Hancock, P. York, R.C. Rowe, The use of solubility parameters in pharmaceutical dosage form design, *Int. J. Pharm.*, 148 (1997), pp. 1–21.
26. H. Suzuki, H. Sunada, Comparison of nicotinamide, ethylurea and polyethylene glycol as carriers for nifedipine solid dispersions systems, *Chem. Pharm. Bull.* 45(1997), pp. 1688–1693.
27. H. Suzuki, H. Sunada, Influence of water-soluble polymers on the dissolution of nifedipine solid dispersions with combined carriers, *Chem. Pharm. Bull.*, 46 (1998) 482–487.
28. D.J. Greenhalgh, W. Peter, T.P. York, Solubility parameters as predictors of miscibility in solid dispersions, *J. Pharm. Sci.*, 88 (1999), pp. 1182–1190.
29. X. Zheng, R. Yang, X. Tang, L. Zheng, Part I: Characterization of Solid Dispersions of Nimodipine Prepared by Hot-melt Extrusion. *Drug Dev. Ind. Pharm.*, 33 (2007), pp. 791–802.
30. E.B. Bagley, T.P. Nelson and J.M. Scigliano, Three-dimensional solubility parameters and their relationship to internal pressure measurements in polar and hydrogen bonding solvents. *J. Paint. Technol.*, 43 (1971), pp. 35–42
31. J. Breitzkreutz, Prediction of intestinal drug absorption properties by three dimensional solubility parameters. *Pharmaceutical Research*, 15 (1998), pp. 1370–1375.
32. Albers, J., 2008. Hot-melt Extrusion with Poorly Soluble Drugs. Heinrich-Heine-Universität Dusseldorf, Germany
33. A. Rossi, A. Savioli, M. Bini, D. Capsoni, V. Massarotti, R. Bettini, A. Gazzaniga, M.E. Sangalli, F. Giordano, Solid-state characterization of paracetamol metastable polymorphs formed in binary mixtures with hydroxypropylmethylcellulose. *Thermochim. Acta*, 406 (2001), pp. 55–67.
34. P.D. Martino, A.M. Guyot-Hermann, P. Conflant, M. Drache, J.C. Guyot, A new pure paracetamol for direct compression: the orthorhombic form, *Int. J. Pharm.*, 128 (1996), pp. 1–8.
35. A. Forster, J. Hempenstall, I. Tucker, T. Rades, The potential of small-scale fusion experiments and Gordon–Taylor equation to predict the suitability of drug/polymer blends for melt extrusion, *Drug Dev. Ind. Pharm.*, 27 (2001), pp. 549–560.
36. S. Qi, A. Gryczke, P. Belton, D.Q. Craig, Characterisation of solid dispersions of paracetamol and EUDRAGIT E prepared by hot-melt extrusion using thermal, microthermal and spectroscopic analysis. *Int. J. Pharm.*, 354 (2008), pp. 158–67.

37. Y. Kong, J.N. Hay, The measurement of the crystallinity of polymers by DSC, *Polymer*, 43 (2002), pp. 3873 – 3878.
38. S. Janssens, A. De Zeure, A. Paudel, J. Van Humbeeck, P. Rombaut, G. Van den Mooter, Influence of preparation methods on solid state supersaturation of amorphous solid dispersions: a case study with itraconazole and eudragit E100. *Pharm. Res.*, 27 (2010), pp. 775-85.
39. P.C. Kayumba, N. Huyghebaert, C. Cordella, J.D. Ntawukuliryayo, C. Vervaet, J.P. Remon JP, Quinine sulphate pellets for flexible pediatric drug dosing: formulation development and evaluation of taste-masking efficiency using the electronic tongue. *Eur. J. Pharm. Biopharm.*, 66 (2007), pp. 460-5.
40. K. Woertz, C. Tissen, P. Kleinebudde, J. Breitzkreutz, A comparative study on two electronic tongues for pharmaceutical formulation development, *J. Pharm. Biomed. Anal.*, 55 (2011), pp. 272-281.
41. K. Woertz, C. Tissen, P. Kleinebudde, J. Breitzkreutz, Performance qualification of an electronic tongue based on ICH guideline Q2, *J. Pharm. Biomed. Anal.*, 51 (2010), pp. 497 - 506.
42. O. Rachid, F.E. Simons, M. Rawas-Qalaji, K.J. Simons, An electronic tongue: evaluation of the masking efficacy of sweetening and/or flavoring agents on the bitter taste of epinephrine, *AAPS PharmSciTech.*, 11 (2010), pp. 550-7.
43. L. Li, V. Naini, S. U. Ahmed, Utilization of a modified special-cubic design and an electronic tongue for bitterness masking formulation optimization. *J. Pharm. Sci.*, 96(2007), pp. 2723-2734
44. J.Y. Zheng, M. P. Keeney, Taste masking analysis in pharmaceutical formulation development using an electronic tongue. *Int. J. Pharm.*, 310 (2006), pp. 118-124
45. J. K. Lorenz, J. P. Reo, O. Hendl, J. H. Worthington, V. D. Petrossian, Evaluation of a taste sensor instrument (electronic tongue) for use in formulation development. *Int. J. Pharm.*, 367 (2009), pp. 65-72.
46. K. Woertz, C. Tissen, P. Kleinebudde, J. Breitzkreutz, Taste sensing systems (electronic tongues) for pharmaceutical applications. *Int. J. Pharm.*, 417 (2011), pp. 256-71.

CHAPTER 5: AN *IN VIVO* AND *IN VITRO* TASTE MASKING EVALUATION OF BITTER MELT EXTRUDED APIs

1.0 Introduction

The taste of a pharmaceutical formulation has major influence on patient compliance to the medication and therefore the taste masking of bitter APIs is a major challenge especially for the development of orally administered dosage forms in pharmaceutical industry ^[1]. In reality, most or many of the active pharmaceutical substances have either an unpleasant taste, such as bitterness, sourness or saltiness. Some of them may often cause an irritating mouth feeling, including metallic and/or spicy taste or astringency. For these reasons, the need for a pleasant taste becomes a key aspect for patient palatability ^[2]. Taste masking of various bitter active ingredients can be carried out using various techniques depending on the type of APIs and the type of formulation ^[3].

Currently, various taste masking methods are available. The most commonly used conventional methods are film coating ^[4] and adding sugars, flavours or sweeteners ^[3] which are often limited due to regulatory requirements. Freeze-drying ^[1], microencapsulation ^[5, 6], fluidized bed coating ^[1], high shear mixing ^[7], supercritical fluids ^[8, 9] and spray drying ^[10] have been reported to be used as successful techniques for the purposes of taste-masking various bitter active substances. In addition to the afore mentioned conventional methods, different advanced and chemical taste masking approaches such as drug complexation by cyclodextrines ^[11, 12], ion exchange resins ^[13], prodrugs and different salt formations ^[14] have been reported in the literature. Similarly, HME was introduced as useful tool to produce polymeric extrudates with taste masking properties in a continuous process ^[15]. Different polymeric systems have already been implemented for taste masking purposes via the hot-melt extrusion (HME) processing and have been proved effective taste-masking approach by applying polymeric coating layer that creates a physical barrier around the drug.

Gryckze *et al.* (2011) successfully claimed taste masking of ibuprofen was achieved through intermolecular forces (e.g. hydrogen bonding) between the active substance and the polymer matrix by processing oppositely charged compounds ^[2]. Later, similar results were observed by Maniruzzaman *et al.* (2012) where the authors successfully managed to mask the bitterness of paracetamol by applying the same mechanism ^[1]. In addition, solid dispersions where the drug is molecularly dispersed within the polymer matrix have shown effective masking of the drug's unpleasant taste. Successful taste masking requires development of

HME processing conditions, drug/polymer ratio and selection of the appropriate formulation components. HME can also be used for the development of robust formulations with increased patient palatability and compliance.

Taste masking evaluation of pharmaceutical dosage forms is usually carried out by human taste panels as well as electronic taste sensing systems which can be employed to predict the taste of pharmaceutical formulations [1]. Commercially available electronic tongues such as a Astree e-tongue have been well studied and evaluated for taste masking purposes which showed very good correlation with human taste panels, reproducibility, low detection limits and high sensitivity [16, 17]. Furthermore, in comparison to final extruded formulations the Astree e-tongue (AlphaMOS, France) has been systematically used to evaluate the bitterness of pure active substances.

Cetirizine HCl (CTZ) and Verapamil HCl (VRP) are white crystalline powders with very bitter taste mainly used as antihistaminic group drug and used for treating high blood pressure, chest pain, and irregular heart rhythms, respectively. In this study both CTZ and VRP were used as model drugs for the purpose of taste masking.

The purpose of this study was to develop and optimize CTZ and VRP based melt extruded granules in order to mask the bitter tastes. The extrudates were evaluated both by *in vivo* and *in vitro* studies where an electronic tongue analyzer was employed that captures the global taste profile correlating the *in vivo* data.

2.0 Materials and methods

2.1 Materials

Cetirizine HCl (CTZ) and Verapamil HCl (VRP) were purchased from Sigma Aldrich (London, UK). Eudragit L100 (L100) and Eudragit L100-55 (Acryl EZE-EZE) was kindly donated by Evonik Pharma Polymers (Darmstadt, Germany) and Colorcon Ltd respectively. The HPLC solvents were analytical grade and purchased from Fisher Chemicals (UK). All materials were used as received.

2.2 Calculation of solubility parameters

The Hansen solubility parameters (δ) of both drugs as well as the polymers were calculated by using the Hoftyzer and van Krevelen method [18, 19] as described in Chapter No 2 (section 2.2). Bagley advanced solubility parameter diagrams [20] were used to investigate the effect of the hydrogen bonding compared to the combined solubility parameters

(dispersion forces and polarization forces) derived from Bragley equation. [Please see Chapter 4, Section 2.2 for details].

2.3 Preparation of formulation blends and hot-melt extrusion (HME) processing

CTZ and VRP formulations with L100 and EZE to be extruded were mixed properly in 100 g batches for 10 min each. A Turbula (TF2, Basel) mixer was used to blend the powder formulations. The drug-polymers composition consisted of CTZ/L100, CTZ/EZE, VRP/L100 and VRP/EZE at a ratio of 10/90 wt/wt. Extrusion of all CTZ and VRP formulations were performed using a Randcastle single-screw extruder (RCP0625) equipped with a 5 mm rod die in 100°C/150°C/150°C/160°C/155°C (Feeder → Die) temperature profiles. The screw speed maintained for all extrusion was 15rpm. The produced extrudates (strands) were grinded by using a ball milling system to obtain granules (<500 µm). Grinding by ball milling was carried out with a rotational speed of 400 rpm for 5 min each.

2.4 Scanning electron microscopy (SEM)

In order to examine the surface morphology of drug, polymers and extrudates by SEM the samples were mounted on an aluminum stage using adhesive carbon tape and placed in a low humidity chamber prior to analysis. Samples were coated with gold-palladium prior to the scans, and microscopy was performed using a LEO Supra 35 (Cambridge Instruments S 360F). The system was operated at an accelerating voltage of 5 kV.

2.5 Differential scanning calorimetry (DSC)

The physical state of the pure drug, physical mixtures and extrudates were examined by using a Mettler-Toledo 823e (Greifensee, Switzerland) differential scanning calorimeter. Samples were prepared in sealed aluminum pans (2-5 mg) with a pierced lid. The samples were heated at 10°C/min under nitrogen atmosphere in a temperature range between 25 and 250°C.

2.6 X-ray powder diffraction (XRPD)

XRPD was also used to assess the solid state of the extrudates where samples of pure and loaded APIs were evaluated using a Bruker D8 Advance (Germany) in two-theta (2θ) mode, Cu anode at 40 kV and 40 mA, parallel beam Goebel mirror, 0.2 mm exit slit, LynxEye Position Sensitive Detector with 3 degree opening and Lynx Iris at 6.5 mm, sample

rotation at 15rpm. The sample was scanned from 2 to 40 degrees 2-theta with a step size of 0.02 degrees 2-theta and a counting time of 0.2 seconds per step; 176 channels active on the PSD making a total counting time of 35.2 seconds per step.

2.7 *In vivo* taste masking evaluation

In vivo taste masking evaluation for pure APIs, polymers and all active extruded formulations was performed in accordance to the Code of Ethics of the World Medical Association (Declaration of Helsinki). Six (6) healthy volunteers of either sex (age 18–25) were selected (Male = 3, female = 3) from whom informed consent was first obtained (approved by the Ethics Committee of the University of Greenwich, Ref: UG09/10.5.5.12) and trained. The equivalent of 100 mg of pure CTZ, VRP or CTZ/VRP extrudates (containing equal amounts of APIs) were held in the mouth for 60 seconds and then spat out. The selection of samples was random and in between of two samples analysis mineral water was used to wash each volunteer's mouth. The bitterness was recorded immediately according to the bitterness intensity scale from 1 to 5 where 1, 2, 3, 4 and 5 indicate none, threshold, moderate, bitter and strong bitterness.

2.8 *In vitro* taste masking evaluation: Astree E-Tongue

The assays were realized on an Astree e-tongue system equipped with an Alpha M.O.S. sensor set #2 (for pharmaceutical analysis) composed of 7 specific sensors (ZZ, AB, BA, BB, CA, DA, JE) on a 48-positions autosampler using 25 ml beakers. Acquisition times were fixed at 120 s. All the data generated on Astree system were treated using multidimensional statistics on AlphaSoft V12.3 software. Each solution was tested on Astree e-tongue at least 4 times. 3 replicates were taken into account for the statistical treatment. The average values between 100 and 120 s were used to build the maps. Astree sensors were cleaned up in deionised water between each sample measurement.

2.8.1 *Sample preparation for Astree e-tongue*

In vitro taste masking evaluation was carried out with an Astree e-tongue equipped with 7 different sensor sets. To be as close as to the panellists taste's conditions, each drug was diluted for 60s under magnetic stirring in 25 ml of deionised water to reach API concentration corresponding to a final dose of 100 mg. Then solutions were filtered with Buchner funnel fitted with filter paper at 2.5µm pore size (Table 5.1). One single analysis was done for each API.

Table 5.1: Sample preparation for taste masking analysis

Code	Type	Description	Drug (%)	Placebo (%)	Drug (mg)	Placebo (mg)	Total (mg)	Final Volume (ml)	pH
AD100	Active	CTZ	100	0	100	0	100	25	3.8
PDA90	Placebo	EZE	0	90	0	900	900	25	5.8
ADA10	A. Form	CTZ/EZE	10	90	100	900	1000	25	3.4
PDE90	Placebo	L100	0	90	0	900	900	25	3.0
ADE10	A. Form	CTZ/L100	10	90	100	900	1000	25	1.8
AP100	Active	VRP	100	0	100	0	100	25	3.3
PPA90	Placebo	EZE	0	90	0	900	900	25	5.8
APA10	A. Form	VRP/EZE	10	90	100	900	1000	25	2.6
PPE90	Placebo	L100	0	90	0	900	900	25	2.8
APE10	A. Form	VRP/L100	10	90	100	900	1000	25	1.7

2.9 *In vitro* drug release studies

In vitro dissolution study was carried out by using a Varian 705 DS dissolution paddle apparatus (Varian Inc. North Carolina, US) at 100 rpm and $37 \pm 0.5^\circ\text{C}$. The dissolution medium pH was maintained as 1.2 by using 750 ml of 0.1 M hydrochloric acid for 2 hr. After 2 hr operation, 150 ml of 0.20 M solution of dehydrogenate sodium ortho phosphate was added into the vessel to give the final pH of 6.8 that has been equilibrated to 37°C . At predetermined time intervals, samples were withdrawn for HPLC assay. All dissolution studies were performed in triplicate. The difference in the release profiles of different formulations were investigated by calculating the similarity factor (f_2) The f_2 value (Eq. 1) is a logarithmic transformation of the sum-squared error of differences between the test T_j and reference products R_j over all time points ($n=6$).

$$f_2 = 50 \times \log\left[\left\{1 + \left(\frac{1}{n} \sum_{j=1}^n (R_j - T_j)^2\right)^{-0.5}\right\}100\right] \quad (5.1)$$

2.10 HPLC analysis

The release of CTZ and VRP was determined by HPLC. An Agilent Technologies system equipped with a HYPHASE 4889, 5 μm x 150 mm x 4 mm column at 276 nm and 266 nm was used for the CTZ and VRP HPLC assay, respectively. The mobile phase consisted of methanol/water/ triethylamine (70:30:0.25, v/v). The flow rate was 1.5 ml/min and the retention time of CTZ and VRP was about 4 minutes. The CTZ and VRP calibration curves ($R^2 = 0.999$), at concentrations varying from 10 $\mu\text{g/ml}$ to 50 $\mu\text{g/ml}$, were used to evaluate all the samples with 20 μl injection volume.

3.0 Results and discussion

3.1 Solubility parameters and extrusion process

The theoretical approach derived from the solubility parameter suggests that compounds with similar δ values are likely to be miscible. The reason is that the energy of mixing from intramolecular interactions is balanced with the energy of mixing from intermolecular interactions [21, 22]. Greenlagh (1999) demonstrated that compounds with $\Delta\delta < 7 \text{ MPa}^{1/2}$ were likely to be miscible and compounds with $\Delta\delta > 10 \text{ MPa}^{1/2}$ were likely to be immiscible [23].

As it can be seen in Table 5.2 the difference between the calculated solubility parameters of the polymers and the drug indicate that both CTZ and VRP are likely to form solid solutions with both polymers. By using the Van Krevelen/Hoftyzer the $\Delta\delta$ values for CTZ/L100, CTZ/ EZE, VRP/L100 and VRP/EZE are 2.07, 0.97, 3.4 and 2.3 $\text{MPa}^{1/2}$, respectively.

Furthermore, a more advanced two dimensional approach proposed by Bagley *et al.* [20] was used also to predict drug – polymer miscibility as shown in Table 5.2. By using the two – dimensional approach Bagley *et al.* introduced the volume – dependent solubility parameter, δ_v , where

$$\delta_v = \sqrt{\delta_d^2 + \delta_p^2} \quad (5.2)$$

Table 5.2: Solubility parameters calculations summary for both drugs and polymers

Comp.	δ_p (MPa ^{1/2})	δ_d (MPa ^{1/2})	δ_h (MPa ^{1/2})	δ_v (MPa ^{1/2})	δ (MPa ^{1/2})	$\Delta\delta$ <i>CTZ</i> (MPa ^{1/2})	$\Delta\delta$ <i>VRP</i> (MPa ^{1/2})	$R_{a(v)}$ <i>CTZ</i>	$R_{a(v)}$ <i>VRP</i>
CTZ	5.42	17.50	9.60	18.32	20.68	-	-	-	-
VRP	5.12	17.31	6.95	18.05	19.35	-	-	-	-
L100	0.41	19.31	12.03	19.31	22.75	2.07	3.4	5.33	5.12
EZE	0.25	18.22	11.69	18.22	21.65	0.97	2.3	5.22	4.95

$$R_{av} = \sqrt{(\delta_{v2} - \delta_{v1})^2 + (\delta_{h2} - \delta_{h1})^2}$$

In this equation, δ_p and δ_d were observed to have similar thermodynamic effects in contrast to δ_h . The two – dimensional approach can provide more accurate prediction of the drug – polymer miscibility by calculating the distance ($R_{a(v)}$) using the Pythagorean Theorem (24, 25). In this theory two components are considered miscible when $R_{a(v)} \leq 5.6 \text{MPa}^{1/2}$. In this study it is obvious from Table 6.2 that even though the δ_p values of the drug – polymer combinations differ significantly it does not affect the predicted miscibility.

3.2 Scanning electron microscopy (SEM)

Surface morphology was examined by SEM for both the drug and extrudates (EXT). The extrudates containing L100 and EZE exhibited no drug crystals on the extrudate surface with CTZ (Fig. 5.1). Similarly, no VRP crystals were observed on the surface in all drug/polymer extrudates, indicating that VRP is also highly miscible with both anionic methacrylate co-polymers in order to form solid solutions. Thus, the SEM observations were also quite sensitive to elucidate the presence of drug/polymer miscibility as well as the formation of drug/polymers amorphous solid dispersions by complementing the thermal investigations.

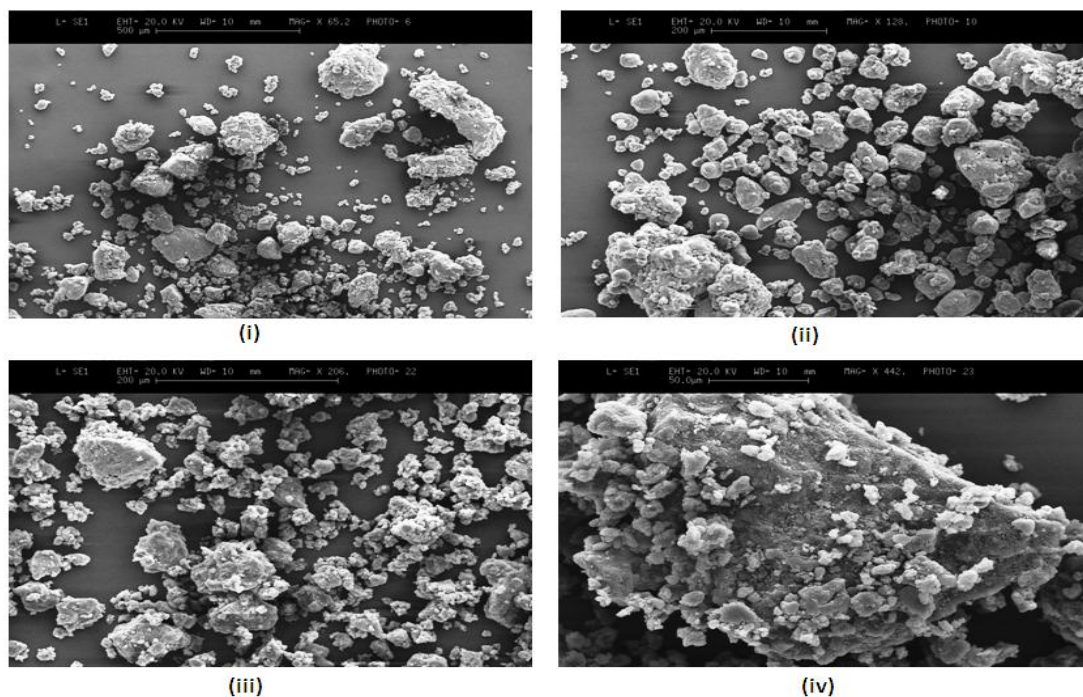


Fig. 5.1: SEM images (magnification x 500) of (i) CTZ/L100 EXT, (ii) CTZ/EZE EXT, (iii) VRP/L100 EXT and (iv) VRP/EZE EXT.

3.3 Differential scanning calorimetry (DSC)

Differential scanning calorimetry (DSC) was used to analyse the solid state of pure APIs, polymers, their binary mixtures and active extruded formulations. The overall findings from DSC results are summarized in Table 5.3.

Table 5.3: Summary of DSC results of pure drugs, polymers and formulations

Formulations	Glass transition	Melting endotherm/ enthalpy
	(°C)	(°C / ΔH , Jg ⁻¹)
CTZ	55.36	225.6/104.2
VRP	51.65	145.9/106.5
L100	164.38	-
EZE	83.97	59.2

Physical mixtures (PM) and extruded formulations (EF)

	PM	EF	PM
	(°C /ΔH, Jg ⁻¹)	(°C /ΔH, Jg ⁻¹)	(°C /ΔH, Jg ⁻¹)
CTZ/L100	113.60	105.72/6.85	222.90/31.23
CTZ/EZE	73.19	64.78/2.64	187.55/9.74
VRP/L100	113.68	74.73/8.15	146.41/14.39
VRP/CTZ	72.98	64.11/3.42	161.30/11.95

The DSC scan of pure CTZ and VRP in Fig. 5.2a showed an endothermic peak corresponding to its melting point at 225.6°C ($\delta H = 104.2$ J/g) and 145.9°C ($\delta H = 106.5$ J/g), respectively. Similarly, the pure polymers showed a Tg at 83.97°C corresponding to Eudragit L100-55 and 164.83°C corresponding to Tg of L100, respectively (Fig. 5.2a).

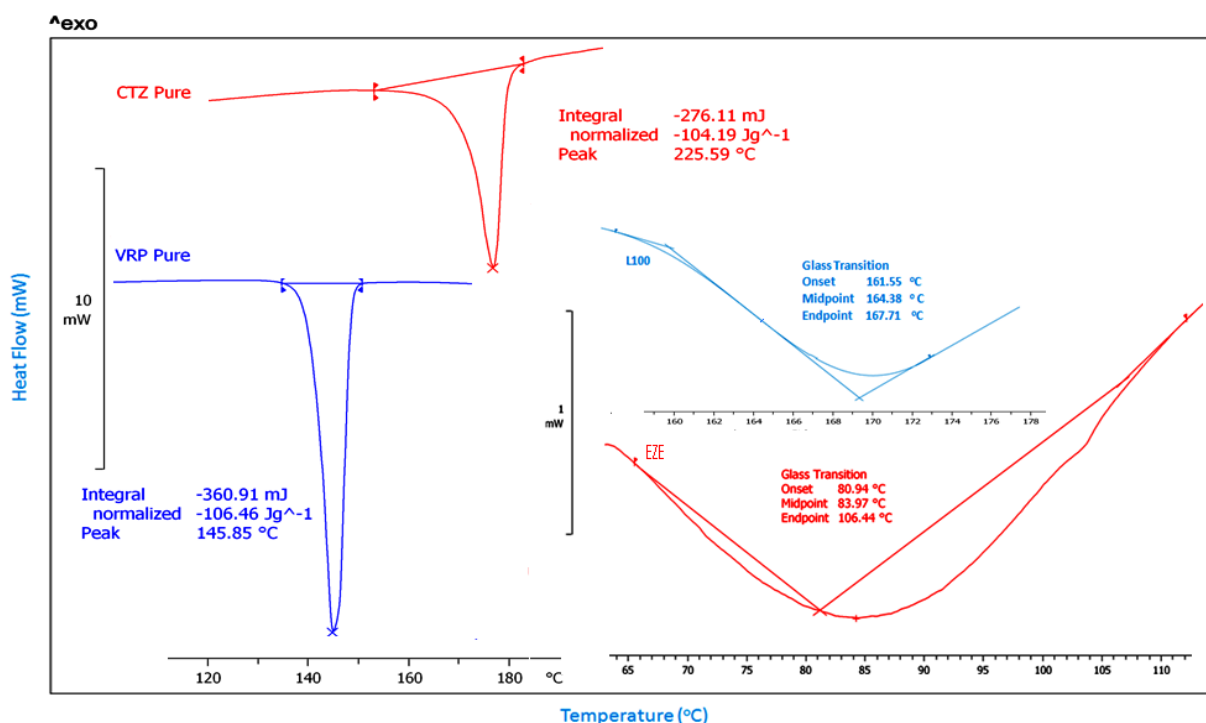


Fig. 5.2a: DSC thermograms of pure APIs and polymers.

There was also a sharp melting peak present in EZE diffractogram at 59.2°C (data not shown) which could be due to the presence of crystalline plasticizers and other ingredients in the co-processed formulation of Acryl-EZE. Later, this melting peak was also visible in physical mixtures (PM) of both drugs (Fig. 5.2 b-c). Eventhough, all binary physical

drugs/polymers blends exhibits endothermic peaks (Fig 5.2b-c) corresponding to the initial substances at slightly shifted temperatures indicating the drug existence in its crystalline form, the melting peaks were absent in all extruded formulations.

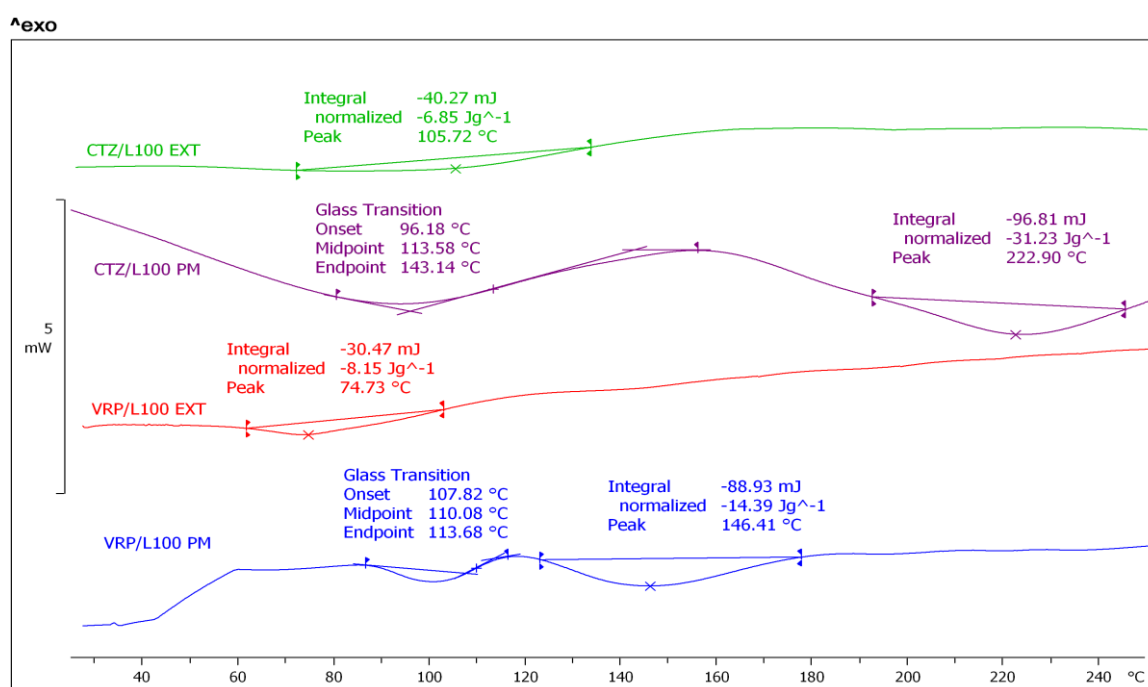


Fig. 5.2b: Thermograms of CTZ and VRP in L100 polymers systems.

Furthermore, the extruded formulations exhibited a broad Tg peak ranging from 64 to 105°C indicating the conversion of the originally crystalline drugs into their amorphous forms during the HME process. The range of one single Tg in the extruded formulation is in between the Tgs of drugs (CTZ at 55.36°C and VRP at 51.65°C) and polymers. This also confirms the formation of solid dispersions of drugs into the polymer matrices [21, 26] and also the drug/polymers miscibility. According to the Gordon Taylor equation, the miscible drug/polymers extrudates would exhibit a broad single Tg at the intermediate position of the Tgs of amorphous drug and polymers [22]. Nevertheless, the characteristic peak of CTZ and VRP cannot be found in the thermograms of the extruded formulations, indicating that extruded formulation is different in physicochemical properties from the physical mixture of drug/polymer. This could be attributed to the amorphous dispersion of the drugs in molecular basis onto the polymer matrices.

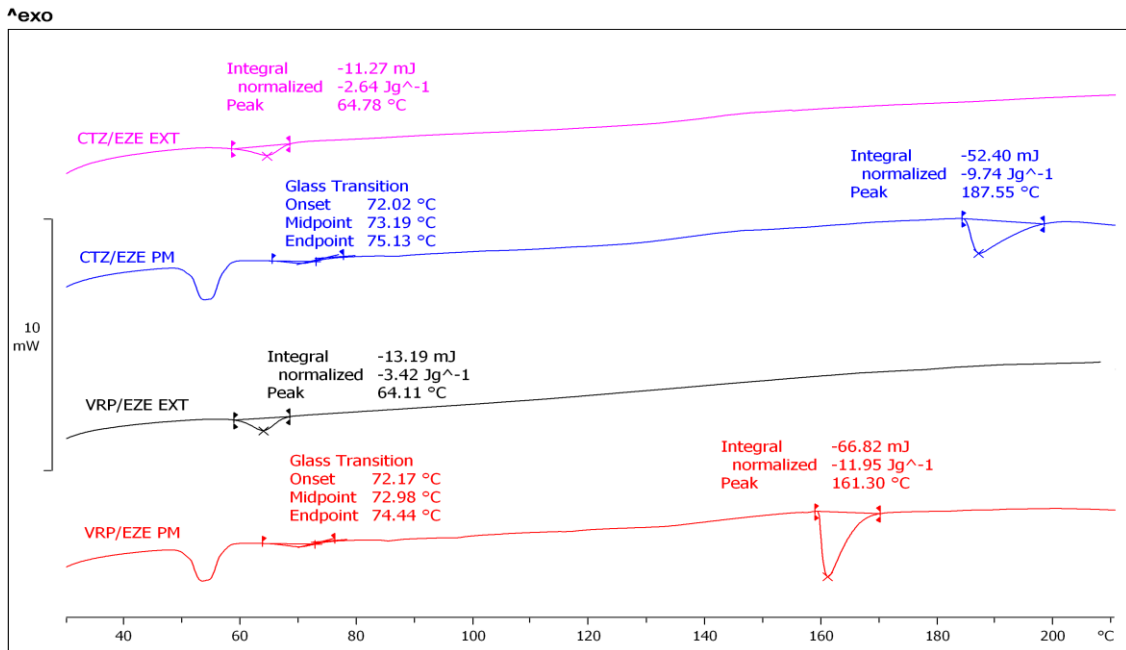


Fig. 5.2c: Thermograms of CTZ and VRP in EZE (L100-55) polymers systems.

3.4 X-ray powder diffraction (XRPD) analysis

The findings from DSC has always been supplement by XRD studies. Therefore, drug – polymer extrudates, including pure drugs and physical mixtures of the same composition were studied by X-ray analysis and the diffractograms were recorded to examine both APIs physical (crystalline or amorphous) state. As depicted in Fig. 5.3a–b the diffractogram of pure CTZ and VRP presented distinct peaks ranging from 7- 38.5 2θ and 8.75-39.5 2θ, respectively.

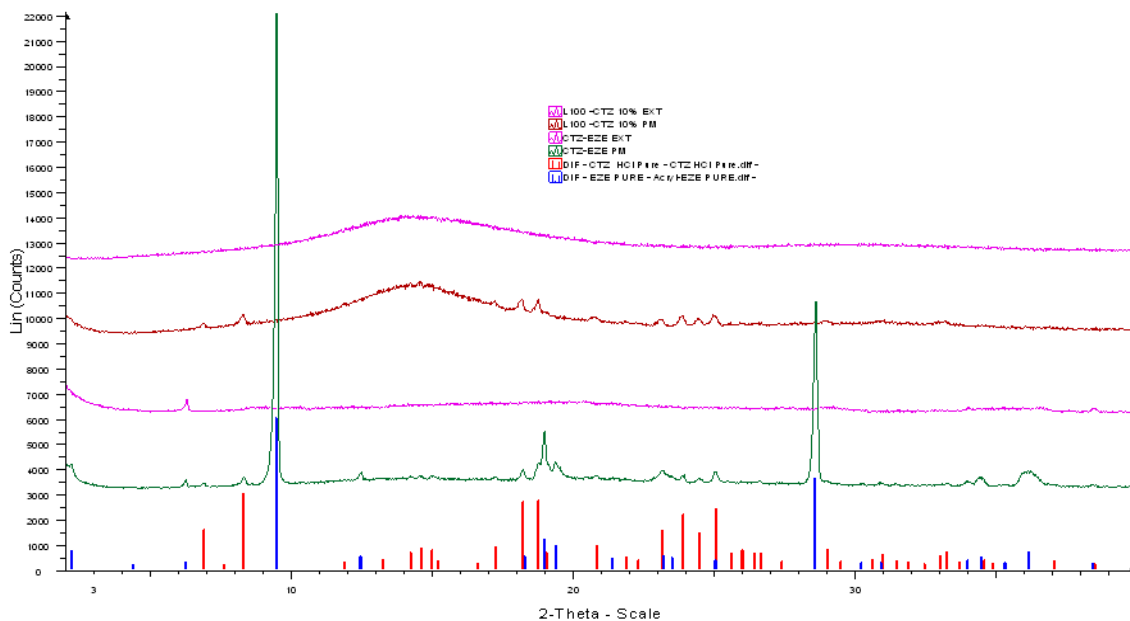


Fig. 5.3a: Diffractograms of CTZ/polymer formulations.

As shown in Fig. 5.3a and b the PM of all formulations presented identical peaks at lower intensities suggesting that both drugs retain their crystalline properties. The Acryl EZE based systems for both drugs in PM exhibits distinct crystalline peaks due to the presence of crystalline plasticizer with co-processed amorphous L100-55 along with the active substances. No crystalline distinct peaks were found in the extruded formulations in EZE systems. In contrast no distinct intensity peaks for both CTZ and VRP were observed in the diffractograms of the extruded formulations in L100 based formulations. The absence of CTZ and VRP intensity peaks indicates the presence of amorphous APIs in the extruded solid dispersion which confirms the DSC results.

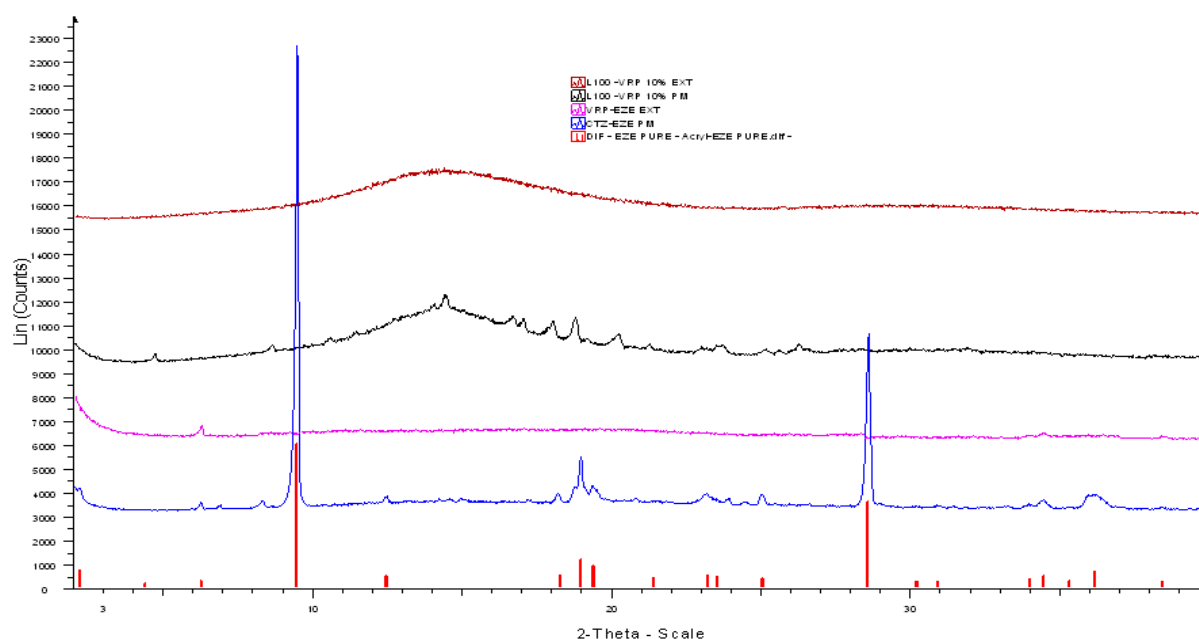


Fig. 5.3b: Diffractograms of VRP/polymers formulations.

3.5 *In vivo* taste masking evaluations

The masking efficiency of the developed granules was evaluated *in vivo* with the assistance of six healthy human volunteers (age 18 – 25). Bitterness was recorded for a period of two minutes according to the bitterness intensity scale from 1 to 5 where 1, 2, 3, 4, and 5 indicate no, threshold, slight, moderate, and strong bitterness ^[1]. The statistical data collected from the *in vivo* study for the pure active substances and the extruded formulations are depicted in Fig. 5.4. The data analysis showed significant suppression ($p > 0.05$) of the bitter taste for both APIs & influence of the polymeric carriers and importance of drug loading in the final formulation. Both polymers showed effective taste masking capacity with descending order L100>EZE. Furthermore, the HME formulations presented excellent

masking effect for active concentrations (10%) of both APIs. In Fig. 6.4 sensory data obtained from six volunteers interestingly showed the taste masking efficiency of L100 substantially better than EZE for both of the APIs used. This could be attributed to the pH dependant dissolution properties of EZE ($\text{pH} \geq 6$) compared to that of L100 ($\text{pH} \geq 6.5$) as the saliva represents a pH approximately 6 in healthy individuals. However, the sensory scores for both of the active APIs in different formulations are within the range (below 2) which has been demonstrated as optimum by *in vitro* evaluations.

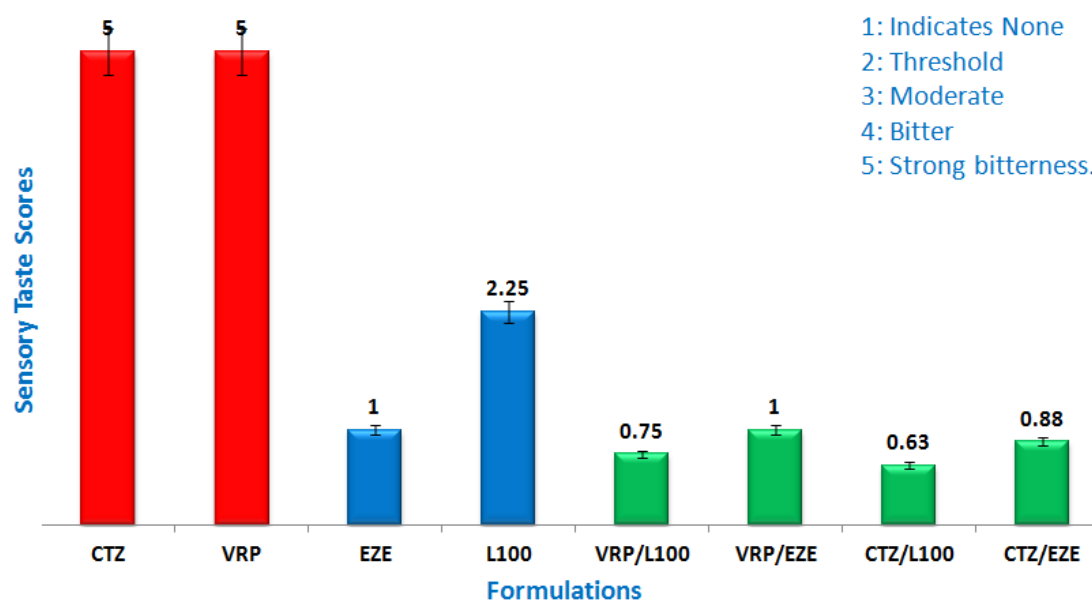


Fig. 5.4: Sensory taste scores of human volunteers for all formulations and pure materials.

3.6 *In vitro* taste evaluations

To evaluate the *in vitro* taste masking, Astree e-tongue data were explored for both of the drugs using Principal Component Analysis (PCA) associated to complementary data processing. The distances between active and polymer solutions were calculated as they are indicative of taste masking power of the coating dose. Also, a Discrimination Index (DI in %) was determined for each solution. This indicator takes into account the average difference between the pairs to compare the dispersion of each sample as well. The closer the DI values to 100%, the longer the distance between groups and the lower the dispersion (less masking effects). The DI therefore helps to assess the level of significance of difference between the groups. Sensory correlated models based on Partial Least Square (PLS) were also built to evaluate the correlation with sensory scores. The results are presented in the following sections for each drug.

The taste map shows significant discrimination between placebo and active solutions. Liquid sensors are able to detect the presence of the drug in the coated formulations. Focusing on pure drug in water the complex with Eudragit polymer (L100) at 90% shows a better taste improvement compared to Acryl EZE coating (Fig. 5.5a). The distance proximity with placebo is about four times less important.

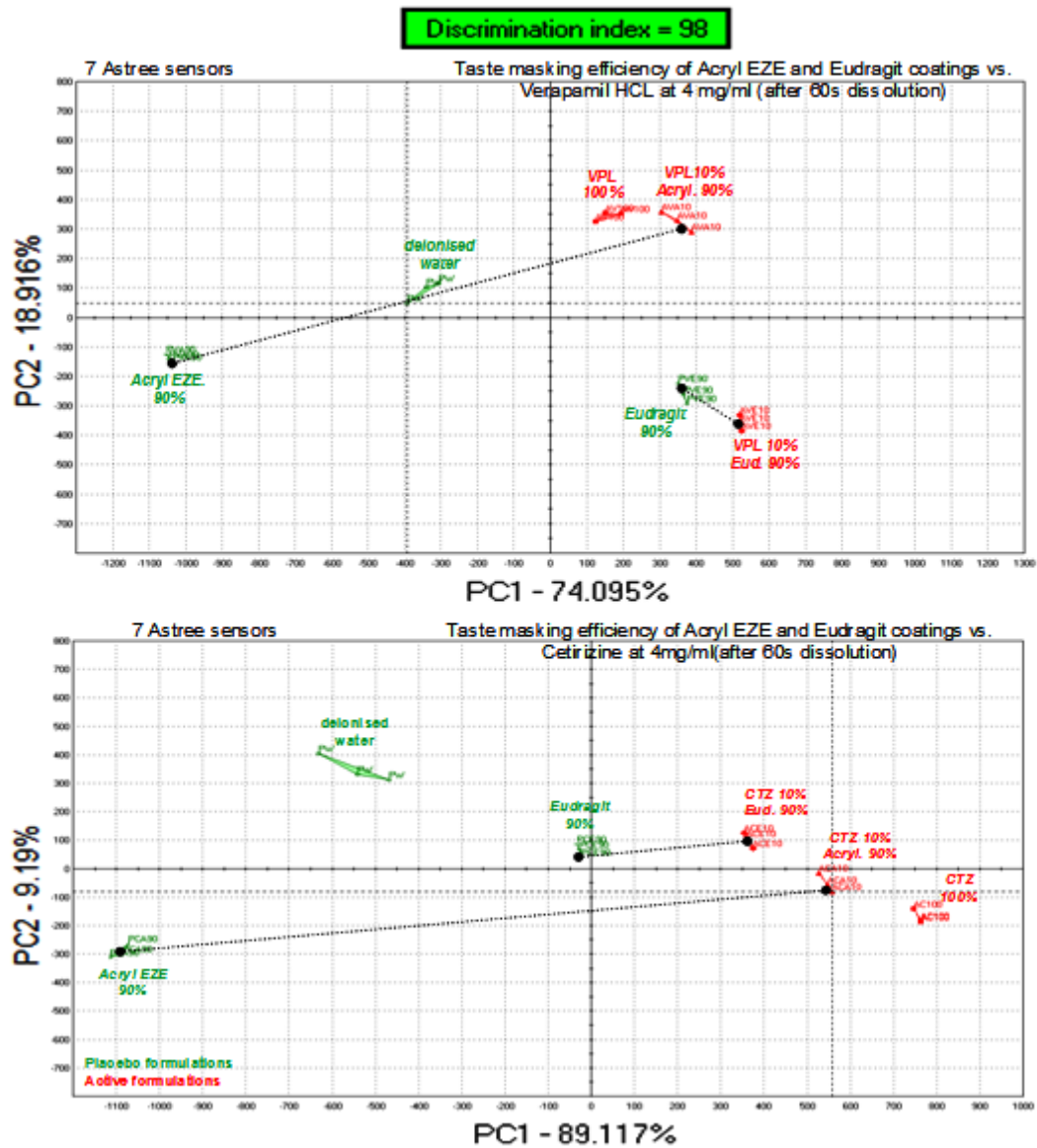


Fig. 5.5a: Signal comparison between active and placebo formulations with Eudragit L100 and Acryl-EZE coatings on cetirizine HCl and verapamil HCl (dissolution for 60s).

The correlation model is considered as valid and fits with panel perception (Fig 5.5b; $R^2 > 0.8$). But it should be taken with care as all data on sensory tests (number of panelists, variability on measurement) were not communicated.

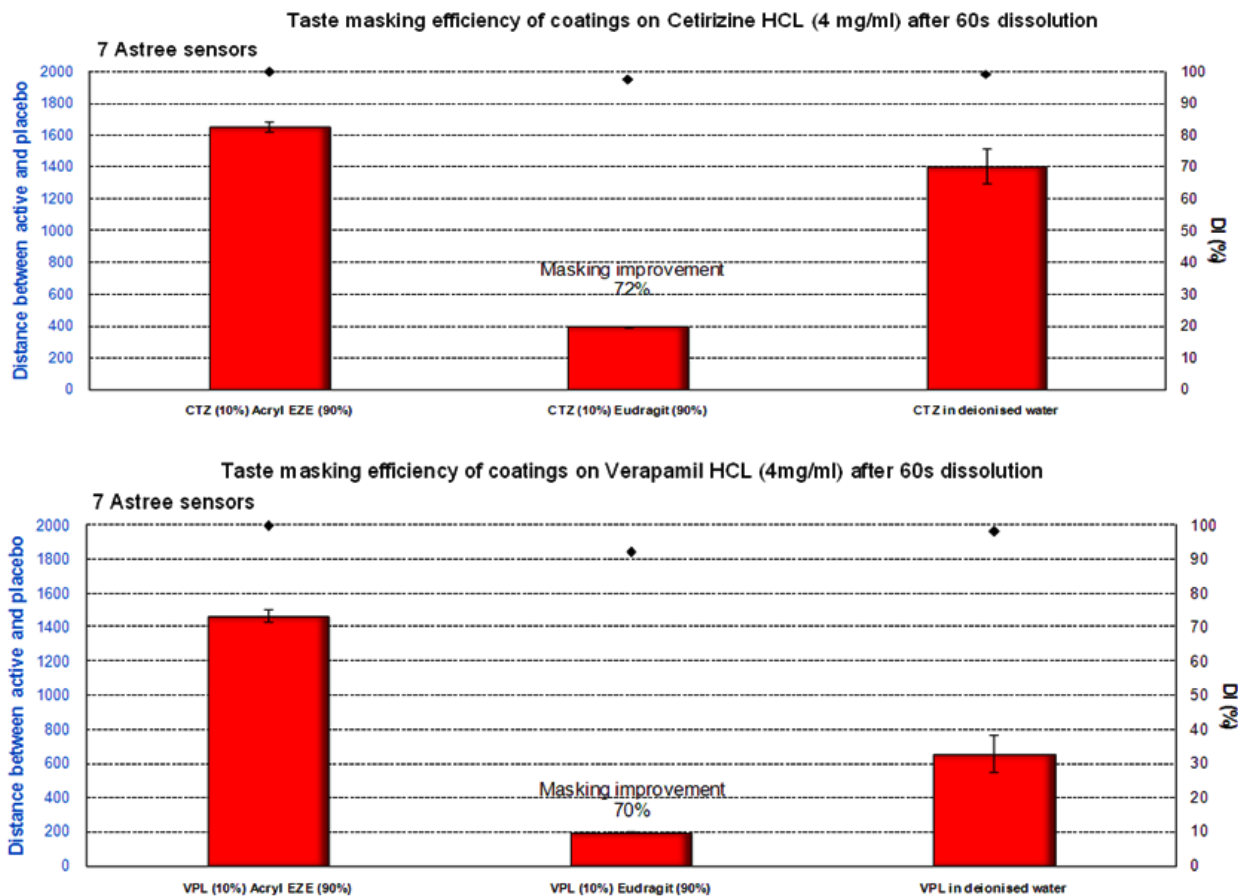


Fig. 5.5b: Distance and discrimination comparison between signal of pure cetirizine HCL and verapamil HCL formulation and each polymer's formulation on Astree e-tongue (after 60s dissolution).

However, CTZ at 10% in Eudragit L100 is perceived as less bitter compared to pure API which implies a good masking. On the other hand, CTZ in Acryl-EZE 90% is perceived by panelists as equivalent as Acryl-EZE taste but Astree system shows significant differences. The acidity of the media with Eudragit is close to drug pH in solution which may influence the global taste perception. As acid threshold is lower for liquid sensors, it explains the increased gap observed on PCA for Acry-EZE formulations.

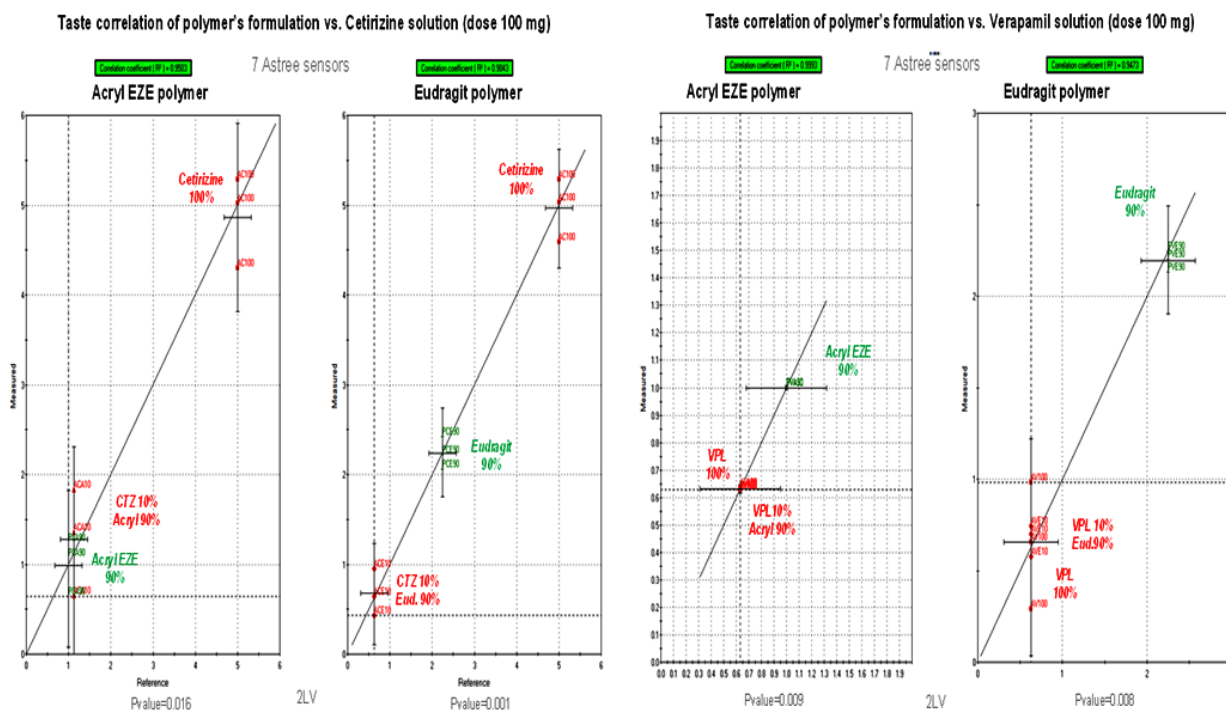


Fig. 5.5c: Correlation of human sensory data “Reference” with Astree Electronic tongue measurements (“Measured”) for both drugs.

The variation observed within solutions is important especially between Acryl-EZE solutions (Fig 5.5c). Eudragit solutions have a better proximity with a significant improvement of VRP taste. This trend is likely to be linked with a pH influence as variation between pure Acryl in water (~6) and the media with the drug is more acidic (<3), which leads to a higher separation of couples. The difference of taste is less perceptible with Eudragit polymer as depicted in Fig. 5.5a.

PLS models showed a good correlation (Fig. 5.5c). Verapamil HCl was found to be not bitter by the panelists. The impact of Acryl coating didn’t affect the taste as Acryl-EZE itself was also found to be not bitter which was not the case for Eudragit (threshold-moderate bitterness). However, the PLS highlights the same conclusions: sensory panel was sensitive to taste perception with Eudragit. The findings from standard deviations studies of both the drugs along with polymeric formulations are summarized in Table 5.4. The results showed good interpretation of taste masking of all excipients as SD < 50: Fair, SD < 30: good

Table 5.4: Mean standard deviation (SD) and relative standard deviation (RSD) for each solution.

CTZ after 60s dissolutions			
Formulations	Mean SD	Mean RSD (%)	Interpretations of SD
AC100	9	1.8	Good
ACA10	10	1.8	Good
ACE10	8	1.3	Good
PCA90	16	1.8	Good
PCE90	8	1.2	Good
PW	31	2.4	Fair
VRP after 60s dissolutions			
AV100	9	0.6	Good
AVA10	18	1.2	Good
AVE10	8	0.6	Good
PVA90	7	0.4	Good
PVE90	11	0.9	Good
PW	17	1.0	Good

$$RSD = \frac{SD}{\bar{x}} \times 100$$

3.7 *In vitro* drug release profiles

The dissolution rates of CTZ for both L100 and EZE extrudates were quite fast and approximately 65% drug was released in 60 min while more than 80% was released in 3 hr (Fig 5.6a). Only a slightly higher release rate was observed for VRP based formulations which can be attributed to the less stronger interaction compared to CTZ with polymers in the extrudates ^[27]. The VRP release obtained after 3hr was above 95% (Fig 5.6b). As a result each of the extruded formulations can be applied for fast onset action dosage forms.

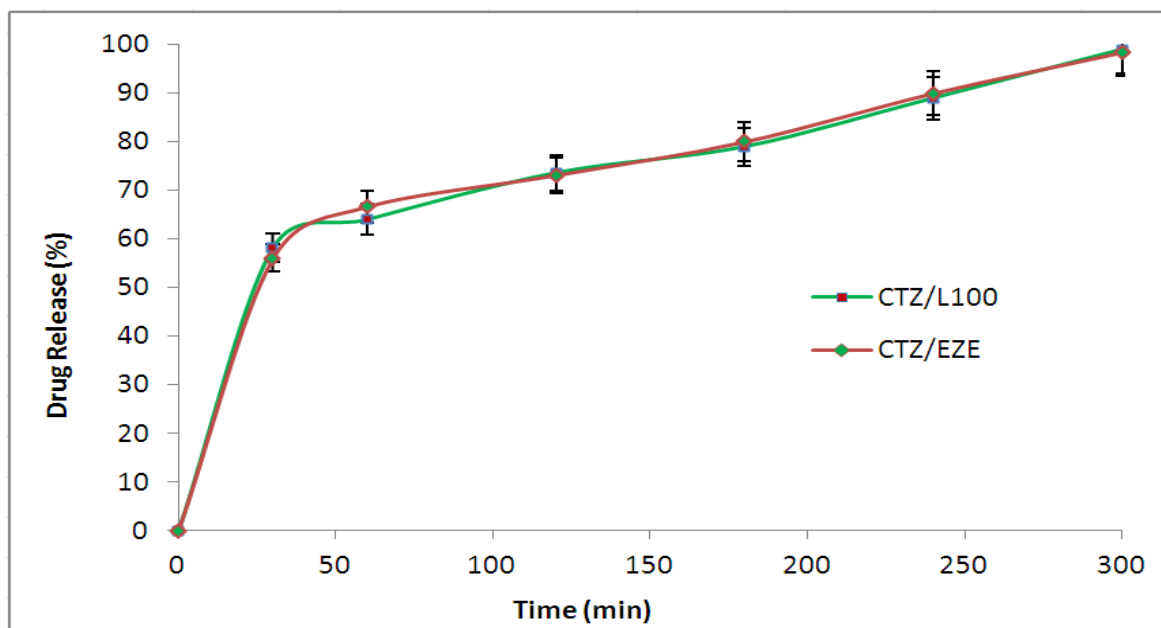


Fig. 5.6a: Release profiles of CTZ extruded formulations (paddle speed 100 rpm, pH 1.2 (6.8 after 2 hr), n=3).

Furthermore, the difference of the release profiles of different formulations was investigated by calculating the similarity factor (f_2). According to the FDA guidelines, release curves are considered similar when the calculated f_2 is 50–100 [28]. The calculated difference factor of all extruded formulation are summarised in Table 5.5.

Table 5.5: Similarity factor (f_2) for comparing release curves of CTZ and VRP formulations

Formulations	Difference Factor (f_2)	Formulations	Difference Factor (f_2)
CTZ/L100	Ref	CTZ/L100	74.11
CTZ/EZE	74.11	CTZ/EZE	When CTZ/L100 is Ref
VRP/L100	49.16	VRP/L100	86.77
VRP/EZE	48.80	VRP/EZE	When VRP/L100 is Ref

The derived release profile of extruded formulation containing CTZ/L100 differs significantly from VRP/L100 and VRP/EZE formulations whereas CTZ/L100 is quite similar to CTZ/EZE. Similarly, VRP/L100 formulation exhibits similar release profile of VRP/EZE formulation as the calculated f_2 value falls into 86.77 which in the 50-100 range according to the aforementioned FDA guidelines.

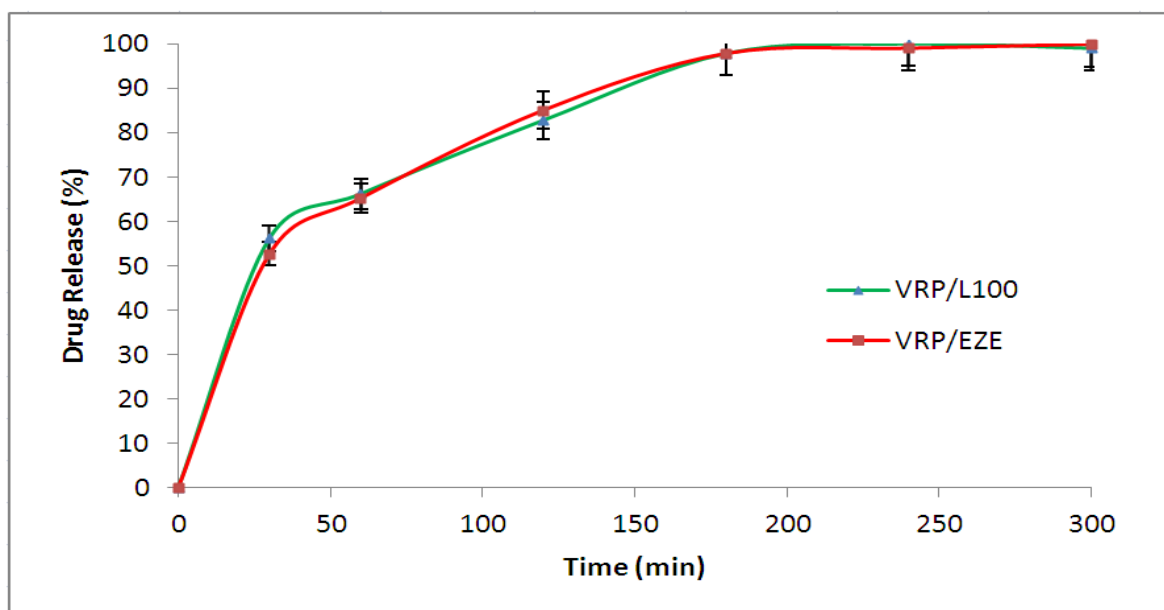


Fig. 5.6b: Release profiles of VRP extruded formulations (paddle speed 100 rpm, pH 1.2 (6.8 after 2 hr), n=3).

4.0 Conclusions

In this current chapter hot melt extrusion has been employed as a robust processing technique for the manufacture of taste masked formulations based on VRP and CTZ. Both of the APIs were found to be in amorphous state after extrusion due to the formation of solid dispersions. The optimized formulations evaluated by both *in vivo* and *in vitro* taste masking tests correlated with each other. The extruded formulations of L100 demonstrated better taste masking compared to those of EZE while the e – tongue was found to be a valuable tool for taste masking assessments and formulation development.

5.0 References

1. Maniruzzaman M, Boateng JS, Bonnefille M, Aranyos A, Mitchell JC, Douroumis D. Taste Masking Evaluation of Hot Melt Extruded Paracetamol using an Electronic Tongue. *AAPS Journal*. 2011,13: 5357.
2. Gryczke A, Schminke S, Maniruzzaman M, Beck J, Douroumis D. Development and evaluation of orally disintegrating tablets (ODTs) containing Ibuprofen granules prepared by hot melt extrusion. *Coll Surf B Biointerfaces*. 2011; 86(2):275-84.
3. Ayenew Z, Puri V, Kumar L, Bansal AK. Trends in pharmaceutical taste masking technologies: a patent review. *Recent Pat Drug Deliv Formul*.2009; 3: 26–39.

4. Douroumis DD, Gryczke A, Schminke S. Development and evaluation of cetirizine HCl taste-masked oral disintegrating tablets. *AAPS PharmSciTech*. 2011;12:141-151.
5. Al-Omran MF, Al-Suwayeh SA, El-Helw AM, Saleh SI. Taste masking of diclofenac sodium using microencapsulation. *J Microencapsul*. 2002;19:45–52.
6. Shah PP, Mashru RC, Rane YM, Thakkar A. Design and optimization of mefloquine hydrochloride microparticles for bitter taste masking. *AAPS PharmSciTech*. 2008;9:377–389.
7. Albertini B, Cavallari C, Passerini N, Voinovich D, González-Rodríguez ML, Magarotto L, Rodriguez L. Characterization and taste-masking evaluation of acetaminophen granules: comparison between different preparation methods in a high-shear mixer. *Eur J Pharm Sci*. 2004;21:295–303.
8. Benoit JP, Rolland H, Thies C, Vande Velde V. Method of coating particles and coated spherical particles. US Patent. 2000;6(087):003.
9. Mazen H, York P. Particle formation methods and their products. US Patent. 2006;7(115):280
10. Bora D, Borude P, Bhise K. Taste masking by spray-drying technique. *AAPS PharmSciTech*. 2008; 9: 1159–1164.
11. Ono N, Miyamoto Y, Ishiguro T, Motoyama K, Hirayama F, Iohara D, Seo H, Tsuruta S, Arima H, Uekama K. Reduction of bitterness of antihistaminic drugs by complexation with β -cyclodextrins. *J Pharm Sci*. 2010;100: 1935–1943.
12. Woertz K, Tissen C, Kleinebudde P, Breitzkreutz J. Rational development of taste masked oral liquids guided by an electronic tongue. *Int J Pharm*. 2010; 400: 114–123.
13. Suthar AM, Patel MM. Formulation and evaluation of taste masked suspension of metronidazole. *Int J Appl Pharm*. 2011; 3: 16–19.
14. Menegon RF, Blau L, Janzanti NS, Pizzolitto AC, Corrêa MA, Monteiro M, Chung MC. A nonstaining and tasteless hydrophobic salt of chlorhexidine. *J Pharm Sci*. 2011; 100: 3130–3138.
15. Michalk A, Kanikanti VR, Hamann HJ, Kleinebudde P. Controlled release of active as a consequence of the die diameter in solid lipid extrusion. *J Cont Release*. 2008; 132: 35–41.
16. Woertz K, Tissen C, Kleinebudde P, Breitzkreutz J. Taste sensing systems (electronic tongues) for pharmaceutical applications. *Int J Pharm*. 2011; 417: 256– 271

17. Woertz K, Tissen C, Kleinebudde P, Breitzkreutz J. Performance qualification of an electronic tongue based on ICH guideline Q2. *J Pharm Biomed Anal.* 2010; 51: pp. 497–506.
18. Hansen CM. The universality of the solubility parameter. *Ind Eng Chem Res Dev.* 1969; 8: 2-11.
19. Hoftyzer PJ, VanKrevelen DW. *Properties of polymers*, Elsevier, Amsterdam, 1976.
20. Bagley EB, Nelson TP & Scigliano JM. Three-dimensional solubility parameters and their relationship to internal pressure measurements in polar and hydrogen bonding solvents. *J Paint Technol.* 1971; 43: 35-42.
21. Maniruzzaman M, Rana MM, Boateng JS, Mitchell JC, Douroumis D. Dissolution enhancement of poorly water-soluble APIs processed by hot-melt extrusion using hydrophilic polymers. *Drug Dev Ind Pharm.* 2012. In press.
22. Zheng X, Yang R, Tang X and Zheng L. Part I: Characterization of Solid Dispersions of Nimodipine Prepared by Hot-melt Extrusion. *Drug Dev Ind Pharm.* 2007; 33:791–802.
23. Greenhalgh DJ, Peter W, York TP. Solubility parameters as predictors of miscibility in solid dispersions, *J Pharm Sci.* 1999; 88: 1182–1190.
24. Breitzkreutz J. Prediction of intestinal drug absorption properties by three dimensional solubility parameters. *Pharm Res.* 1998; 15:1370-1375.
25. Albers J. *Hot-melt Extrusion with Poorly Soluble Drugs*. Heinrich-Heine- Universitat Dusseldorf, Germany. 2008.
26. Forster A, Hempenstall J, Tucker I, Rades T. Selection of excipients for melt extrusion with two poorly water-soluble drugs by solubility parameter calculation and thermal analysis. *Int J Pharm.* 2001; 226 (1–2):147–161.
27. Gryczke A. *Innovative Formulations by Melt Extrusion with EUDRAGIT® Polymers*. RÖHM GmbH & Co. KG, Darmstadt. 2005.
28. *Guidance for Industry. Dissolution Testing of Immediate Release Solid Oral Dosage Forms* U.S. Department of Health and Human Services Food and Drug Administration, Center for Drug Evaluation and Research (CDER). 1997.

CHAPTER 6: DRUG-POLYMER INTERMOLECULAR INTERACTIONS IN HOT-MELT EXTRUDED SOLID DISPERSIONS

1. Introduction

Over the last decades hot-melt extrusion (HME) has emerged as an influential processing technology in developing solid dispersions of active pharmaceutical ingredients (APIs) into polymer matrices and has already been demonstrated to provide time controlled, modified, extended and targeted drug delivery resulting in improved bioavailability [1, 2]. The formation of active solid dispersions through HME and therefore configuration of complexes due to macromolecular orientational relations in polymer networks has been of great interest in pharmaceutical research and development. Polymer complexes are classified by the nature of the association. The major classes of polymer complexes are the stereocomplexes, intermolecular hydrogen-bonded complexes and polyelectrolyte complexes [3,4].

The polyelectrolyte–drug complexes have been the focus of several researchers and still very limited data is available concerning the understanding of the underlying mechanisms involved in the formation of drug-polyion complexes [5]. Different techniques have already been reported successfully to describe various drug-polymer interactions and analyse the drug-polyelectrolyte complexes. Pavli *et al.* described oppositely charged doxazosin mesylate (DM), a cationic drug and polyelectrolytes carrageenans interaction by special DM ion-selective membrane electrode methods constructing the binding isotherms treated by the Zimm–Bragg theory and cooperative binding model [5]. Some other techniques which have already been established to analyse drug-polymers interactions are the dialysis equilibrium technique [6, 7], Fourier transform infra-red spectroscopy (FTIR) and UV spectroscopy [8, 9], solid state NMR [10], drug–polymer interaction parameter model [11] and more importantly x-ray photo electron spectroscopy [10, 12].

The X-ray photoelectron spectroscopy (XPS) can be employed as a valuable tool for the characterisation of polymer surfaces and it has made a significant contribution to the investigation of biomedical polymers but most importantly provides a quantitative elemental analysis and also information on the chemical bonding within the surface layers of the polymer as well as the prediction of the changes onto the material surface [10]. The increasing importance of XPS for many types of intermolecular interactions based analysis arises for several reasons; such as it can provide information about the actual composition and chemical state of surfaces and interfaces that dominate properties of interacting materials even in nano

scale or lower. XPS is more accurate and sensitive to presents precise surface analysis results of different type complexes compared to that of NMR and FTIR.

The types of the interaction to form polymeric complexes in the solid dispersions would normally depend on many factors such as nature of the polymer, degree of substitution, polymer chain configuration and length ^[13]. The H-bonding would also be more prominent in the longer side-chain polymers, where a larger number of groups are available for the interaction to occur. Furthermore, HME processing has been proved to facilitate drug-polymer interactions leading to increase solubility of water insoluble drugs, taste masking of bitter actives and stable solid dispersions.

Therefore, in order to investigate the type of potential drug-polymer interactions a comprehensive study was carried out using two model cationic drugs (propranolol HCl and diphenhydramine HCl) with with the anionic polymers, Eudragit L 100-55, Eudragit L100. The identification and understanding of this type of interactions can find ground in the development of solid dispersions in pharmaceutical industry

2. Experimental sections

2.1 Materials

Propranolol HCl (PRP) and Diphenhydramine HCl (DPD) were purchased from Sigma Aldrich (Gillingham, Kent, UK). Eudragit L100 (L100) and Eudragit L100-55 (L100-55) were kindly donated by Degussa (Evonik, Germany) and Colorcon Ltd (Dartford, UK), respectively. The HPLC solvents were analytical grade and purchased from Fisher Chemicals (UK).

2.2 Determination of drug-polymer miscibility by Hansen solubility parameters (δ)

The partial solubility parameters (δ) of PRP and DPD as well as the anionic polymers were calculated by using Hoftyzer and Vankrevelen method ^[14] considering their chemical structural orientations in order to determine the theoretical drug/polymer miscibility. *[Please see Chapter 5, section 2.2 for details].*

2.3 Hot-melt extrusion process

Prior to the extrusion process, the dry drug/polymer powders (100g) were blended properly in a Turbula TF2 mixer (Basel, Switzerland) for 10 minutes. The drug polymer compositions consisted of PRP/L100 and PRP/L100-55 in the ratio of 10/90 (% wt/wt). Similarly, DPD/L100 and DPD/L100-55 were used in the ratio of 10/90 (% wt/wt). Extrusion

of all PRP and DPD formulations was performed using a single screw Randcastle extruder (RCP 0625, Cedar Grove, NJ) with a 0.2 mm rod die. The temperature profile from the feeding zone to die was 100°C/150°C/150°C/160°C/155°C for all formulations with L100 and L100-55 with 15 rpm screw speed. The extrudates (strands) were milled for 5 min to produce granules using a Pulverisette 6 ball mill (Ritsch, Germany) with 400 rpm rotational speed. The micronized particles were then passed through a 250 µm sieve to separate out the particles to use under this threshold.

2.4 Scanning electron microscopy (SEM)

SEM was used to study the surface morphology of the hot-melt extrudates. The samples were mounted on an aluminum stage using adhesive carbon tape and placed in a low humidity chamber prior to analysis. Samples were coated with gold–palladium, and microscopy was performed using a LEO Supra 35 (Cambridge Instruments, S360) operating at an accelerating voltage of 5 kV.

2.5 Thermal analysis by differential scanning calorimetry (DSC)

A Mettler-Toledo 823e (Greifensee, Switzerland) differential scanning calorimeter was used to carry out DSC runs of pure actives, physical mixtures and extrudates. Sealed aluminium pans were used to prepared sample. 2-5 mg of samples was prepared with a unpierced lid. The samples were heated at 10°C/min from -40°C to 220°C under nitrogen atmosphere.

2.6 X-ray powder diffraction (XRPD)

XRPD was used to determine the solid state of pure active substances, physical mixtures and extruded materials using a Bruker D8 Advance (Germany) in two theta-theta (2θ) mode. For the study purposes a Cu anode at 40 kV and 40 Ma, parallel beam Goebel mirror, 0.2 mm exit slit, LynxEye Position Sensitive Detector with 3° opening (LynxIris at 6.5 mm) and sample rotation at 15 rpm were used. Each sample was scanned from 2 to 40° 2θ with a stepsize of 0.02° 2θ and a counting time of 0.1 seconds per step; 176 channels active on the PSD making a total counting time of 35.2 seconds per step.

2.7 Molecular modelling

The monomeric structures of L100, L100-55, PRP and DPD were constructed by program Gaussview (Frisch's group, Gaussian Inc. Wallington CT) ^[15]. Hydrogen bonding

patterns were identified after energy optimisation at the B3LYP 6-31G* level using Gaussian 09. In all of the drug/polymers combinations primarily two different H bonding were detected with up to 2α °A distance. All possible H bondings were shown in dash line in the constructed figures.

2.8 X-ray photoelectron spectroscopy (XPS) analysis

X-ray photoelectron spectra (XPS) were measured on a Kratos Axis Ultra-DLD using a monochromatic Al K_{α} X-ray source (120 W) and an analyser pass energy of 160 eV (survey scans) or 20 eV (high resolution scans); the pressure during analysis was 1×10^{-9} Torr. All data were referenced to the C (1s) signal at 285.0 eV attributable to unsaturated C-C/C-H bonds [16]. Quantification and curve fitting was performed in CasaXPS™ (Version 2.3.15) using elemental sensitivity factors supplied by the manufacturer.

2.9 Nuclear magnetic resonance (NMR) studies

NMR spectra were recorded on a Jeol ECA 500 NMR spectrometer, incorporating a 5mm inverse probe (The ^1H operating frequency was 500 MHz). ^1H NMR spectra of the drugs, polymers and drug/polymer formulations were recorded using the standard Jeol pulse sequence. All samples were dissolved in CD_3OD , degassed and then maintained at 25°C during data acquisition. Samples were referenced with respect to the solvent. The solution concentration of the drugs was 2 mg/ml, the polymer was 18mg/ml, and the drug/polymer formulation was 20 mg/ml (the overall drug content in the formulations was 10%). ^1H T_1 relaxation experiments were recorded for all samples using a standard inverse recovery experiment. Recovery delays (τ) were investigated between 10 ms and 20 s. The relaxation delay was set to be $> 5T_1$. T_1 s were calculated from curve fitting, peak intensities, obtained from the spectra recorded for different recovery delays. Jeol, curve fitting software was utilised during this process.

3. Results and discussion

3.1 Determination of drug-polymer miscibility by Hansen solubility parameters (δ)

To predict the miscibility of the active substances and the polymeric carriers the Hansen solubility parameter was used [14, 17, 18]. According to the Vankrevelen/ Hoftyzer equation the calculated solubility parameters for PRP and DPD are $21.94 \text{ MPa}^{1/2}$ and $17.75 \text{ MPa}^{1/2}$, respectively whereas the solubility parameters for L100 and L100-55 are $22.75 \text{ MPa}^{1/2}$ and $21.65 \text{ MPa}^{1/2}$, respectively. Since the determined difference in solubility

parameters between each drug and polymer are less than $7\text{MPa}^{1/2}$ (about $0\text{-}5\text{ MPa}^{1/2}$), both polymers are likely to be miscible with both of the APIs [19]. Thus, miscibility studies by solubility parameters provide a simple and generic approach for rational selection of carriers in the preparation of solid dispersions through the intermolecular interactions. In the miscible drug-polymers based solid dispersions cationic active substances (PRP, DPD) can interact with the functional groups of the negatively charged polymers. These interactions facilitate the creation of hydrogen bonding between the active amide group of the APIs and carboxylic group of the polymers and consequently mask the API's bitter taste [20].

3.2 Scanning electron microscopy (SEM)

SEM was used to examine the surface morphology of the drug and extrudates. The extrudates containing L100 and L100-55 exhibited no drug crystals on the extrudate surface with PRP (Fig. 6.1). Similarly, no DPD crystals were observed on the surface of polymeric extrudates in all drug/ polymers extrudates, indicating that DPD is also high miscible with both anionic methacrylate co-polymers. Thus, the SEM observations were also quite sensitive to elucidate the presence of drug/polymer miscibility by complementing DSC and XRPD investigations.

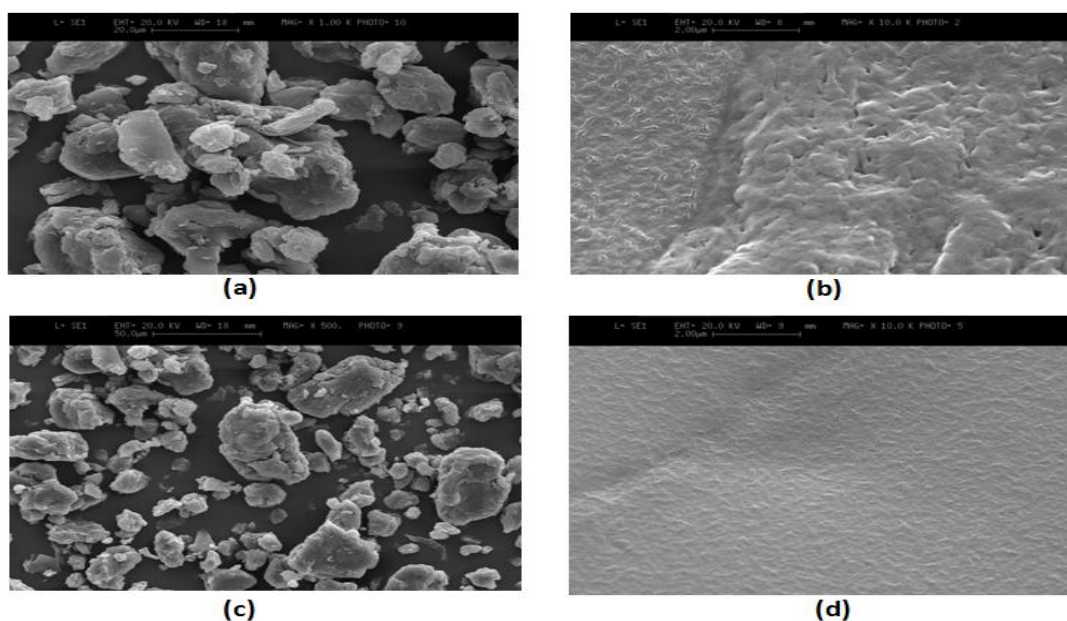


Fig. 6.1: SEM images of (a) PRP/L100 (Magnification x 2000), (b) PRP/L100-55 (Magnification x 10K), (c) DPD/L100 (Magnification x 500) and (d) DPD/L100-55 (magnification x 10K) extruded formulations.

3.3 Differential scanning calorimetry (DSC)

DSC was employed in order to analyse the solid state of the processed drug/polymers binary mixtures (PM) and drug/polymer extrudates (EXT). The DSC thermograms of PRP and DPD in Fig. 6.2a showed an endothermic peak corresponding to melting points at 166.65°C ($\Delta H = -126.25$ J/g) and 170.83°C ($\Delta H = -124.59$ J/g) respectively. The bulk polymers showed Tgs at 83.97°C and 164.83°C corresponding to L100-55 and L100 respectively (Fig. 6.2a).

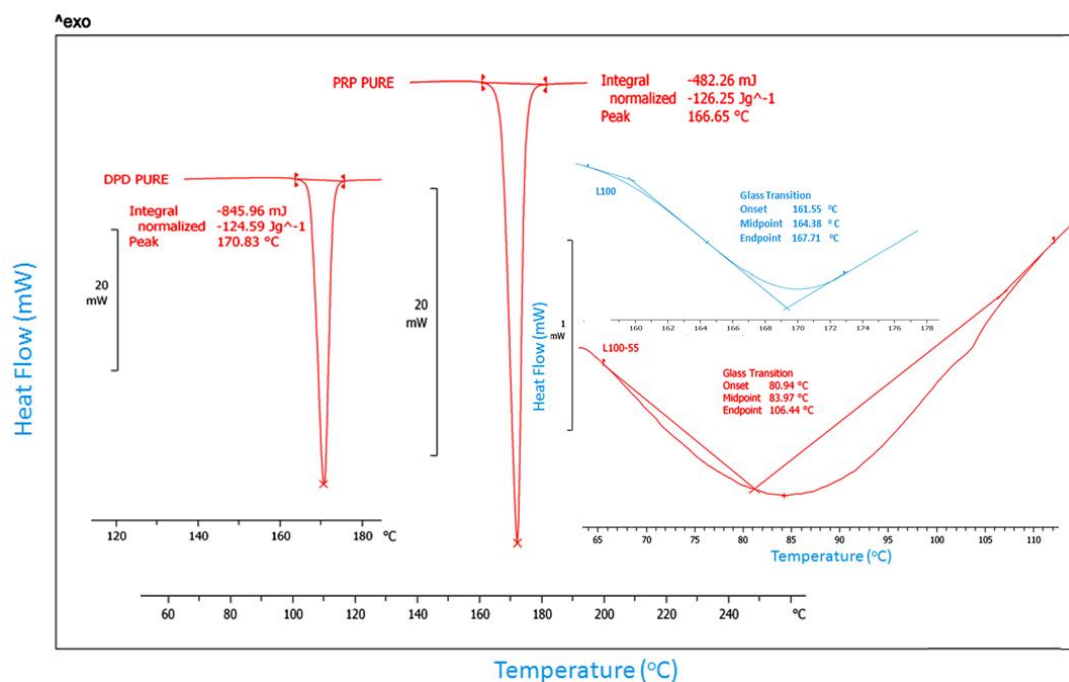


Fig. 6.2a: DSC thermograms of pure drugs and pure polymers.

The binary physical blends of DPD/L100 and DPD/L100-55 in Fig. 6.2b exhibited DPD endothermic peaks shifted at slightly lower temperatures of 139.19°C ($\Delta H = -15.14$ J/g), 153.62 °C ($\Delta H = 16.16$ J/g), respectively, indicating drug/polymer interaction to a small extent. The same shift at lower temperatures was observed for the Tgs of the polymers at 114.46°C for L100 and 71.98°C for L100-55.

Furthermore, the extruded DPD/L100 (and L100-55) complexes exhibited single glass transition peaks at 62.11 and 76.56°C, respectively, which denotes the presence of drug/polymers miscibility and formation of solid dispersions. Single Tg also indicates the presence of the APIs in amorphous forms [21]. When the two components are miscible the Tg of the extruded sample lies between the Tgs of the individual components (DPD has a Tg at 14.80°C) according to the Gordon – Taylor equation [19]. Similarly, PRP/polymers exhibited single Tg peaks at 65.70°C (L100) and 54.52°C (L100-55) attributed to the presence of PRP in molecularly dispersed state within both polymer matrices (Supp. Fig. 1). The Tg of

PRP was determined at 34.74°C. Overall, DSC analysis confirmed the creation of molecular dispersions for all extruded formulations.

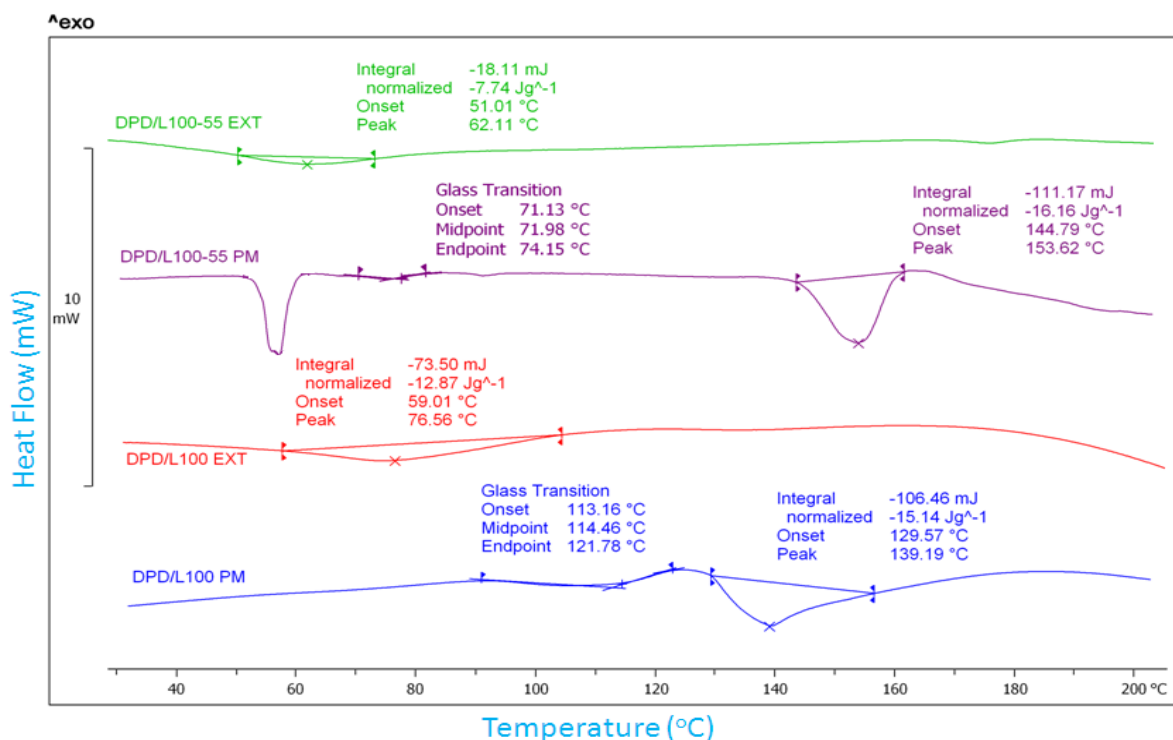


Fig. 6.2b: DSC thermograms of DPD/L100 (PM), DPD/L100 (EXT), DPD/L100-55 (PM) and DPD/L100-55 (EXT).

3.4 X-ray powder diffraction (XRPD)

To examine PRP and DPD crystalline state diffractograms of pure drugs, the drug – polymer extrudates and their binary physical mixtures were recorded by X–ray powder diffraction analysis. As can be seen from Fig. 5.3, the diffractograms of pure PRP and DPD presented distinct peaks at 8.38°, 9.71°, 12.51°, 16.72°, 19.49°, 21.26°, 22.06°, 23.59°, 25.07°, 27.07°-39.07° 2θ and 10.41°, 12.39°, 18.61°, 20.34°, 22.03°, 24.87°, 26.55°, 31.45° 2θ, respectively. As shown in Fig. 6.3 the PM of all PRP formulations presented identical peaks at lower intensities suggesting that both drugs retained their crystallinity at loads of 10%. In contrast no distinct intensity peaks were observed in the diffractograms of the extruded formulations. The absence of PRP and DPD intensity peaks indicates the formation of a solid dispersion where the drugs are present in amorphous ^[22] state or molecularly dispersed into the polymer matrix.

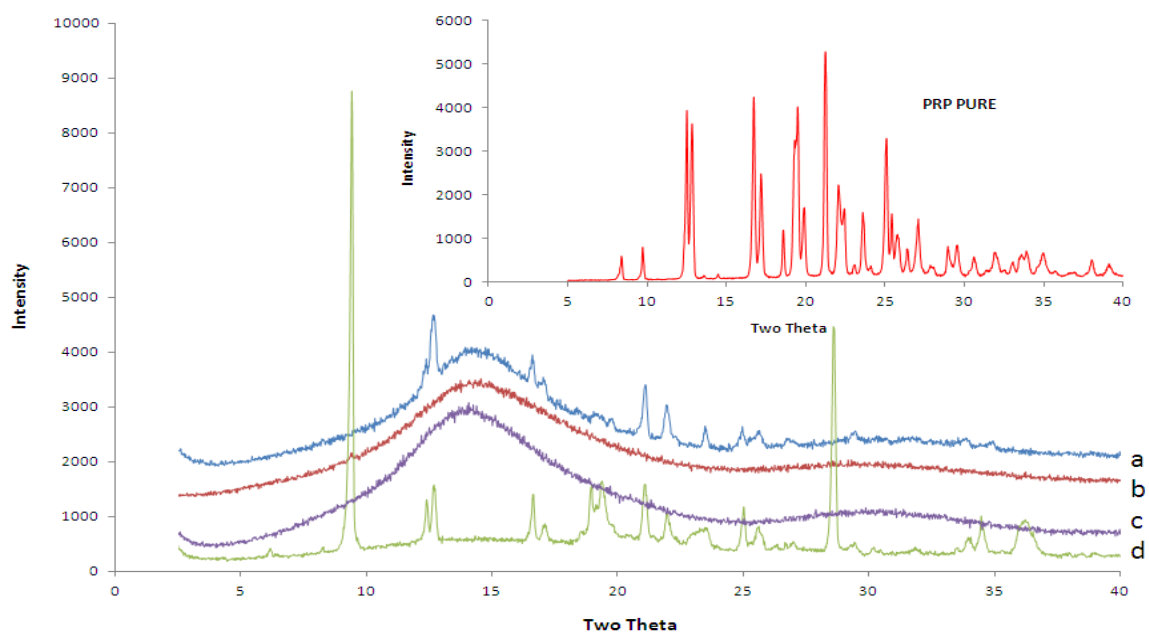


Fig. 6.3a: Diffractograms of PRP formulations: PRP pure (inset), (a) PRP/L100 PM (b) PRP/L100 extrudates (c) PRP/L100-55 extrudates (d) PRP/L100-55 PM.

Similarly, the diffraction patterns of all DPD physical mixtures exhibited crystalline peaks (Fig. 6.3b) with reduced intensities corresponding to DPD. The PRP the diffractograms of the extruded DPD formulations were characterized by the absence of drug intensity peaks again indicating amorphous [22] or molecularly dispersed state.

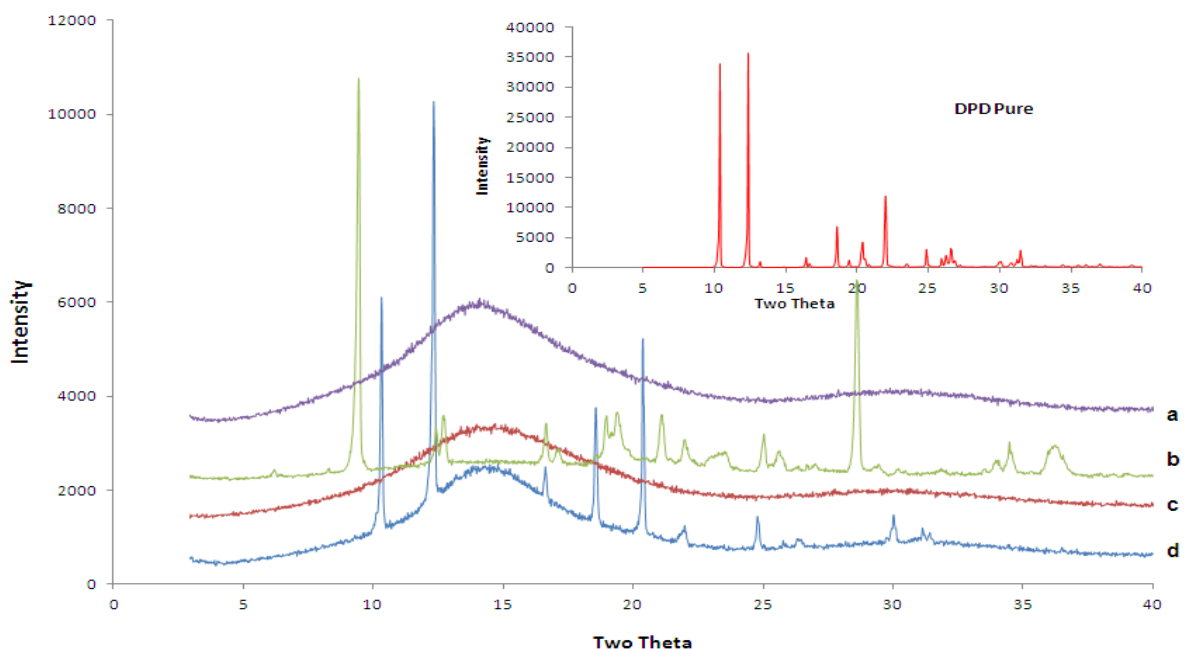


Fig. 6.3b: Diffractograms of DPD formulations: DPD pure (inset), (a) DPD/L100-55 extrudates (b) DPD/L100-55 PM (c) DPD/L100 extrudates and (d) DPD/L100 PM.

3.5 Intermolecular interactions of hot-melt extrudates

3.5.1 Molecular modelling

Depending on the initial positioning of the PRP molecule, two hydrogen bonding patterns were identified (Fig. 6.4) after energy optimisation at the B3LYP 6-31G* level using Gaussian09 [23, 24]. Both the hydroxyl group and amine group within the drug molecule could form strong hydrogen bonds with the monomer, as indicated by the optimal distances between the H-bond donor and acceptor. Furthermore, the chloride ion was placed within the proximity of the H bonds in structures. After re-optimisation, the H-bonding interaction formed with the hydroxyl group was broken due to the presence of the chloride ion while the H-bond interaction with the amine group was not affected (Fig. 6.4) Therefore, calculations indicate that the hydrogen bond identified based on PRP, DPD, L100 and L100-55 formulations is most likely formed between the amine group of the drug molecule and the carbonyl groups of the polymer.

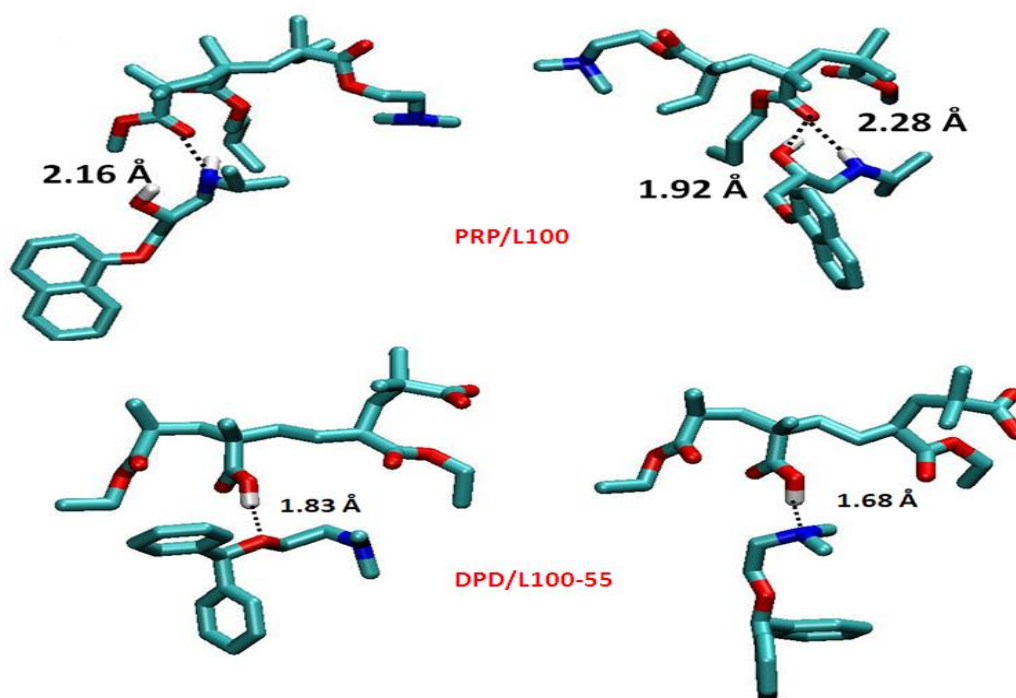


Fig. 6.4: Molecular modelling of drugs/polymers (Gaussian 09).

3.5.2 X-ray photoelectron spectroscopy (XPS)

The surface elemental ratios of PRP, DPD, polymers and the extruded formulations determined experimentally by XPS [25] are shown in Table 6.1 and are compared with the theoretical values derived from the structural formula [26]. The experimental results were in

good agreement with the anticipated theoretical values. PRP predominantly contained O (8.56%) and C (83.53%) atoms. Similarly, DPD contained C (88.05%) and O (4.34%) atoms.

Table 6.1: Position and percentage area of O, C, N and Cl atoms of bulk APIs, polymers and extrudates

	O, 1s	C, 1s	N, 1s	Cl, 2p
Formulation	Area (%)	Area (%)	Area (%)	Area (%)
PRP	8.56	83.53	4.16	3.75
DPD	4.34	88.05	4.20	3.41
L100	24.83	75.17	-	-
L100-55	51.48	25.78	-	-
PRP/L100	23.51	75.87	0.63	-
PRP/L100-55	43.14	39.41	0.23	0.24
DPD/L100	23.66	75.82	0.53	-
DPD/L100-55	45.05	35.00	-	0.26

The main differences in the spectra are observed in the C (1s) peaks around ~284.85 (C-C or Ring) and 290.85 eV (-COO- / O-C-O groups). Fig. 6.5a shows that extruded formulation of PRP/L100 produced C peaks at ~284.85 eV with increased intensity. The high intensity of the peak is an indication of the concentration of a particular species, suggesting reaction of ester/carboxylic acid functionalities from polymers and drugs to yield C-OH or C-O-C like hydrocarbon chains in the extruded materials ^[12].

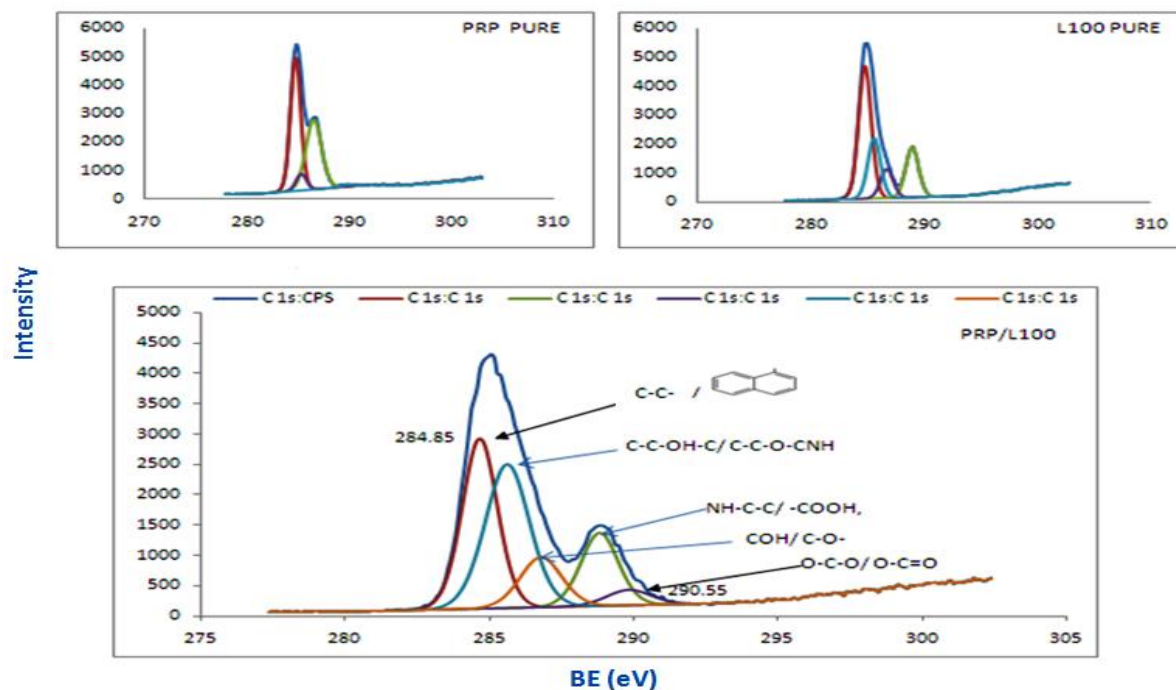


Fig. 6.5a: XPS BE peaks of C 1s PRP, L100 and PRP/L100 formulations.

Both DPD and L100 show a C-C/C-C-H peak at BE = ~285.10 eV ^[27] while they appear slightly shifted at ~284.97 eV in DPD/L100 formulation (Fig 6.5b).

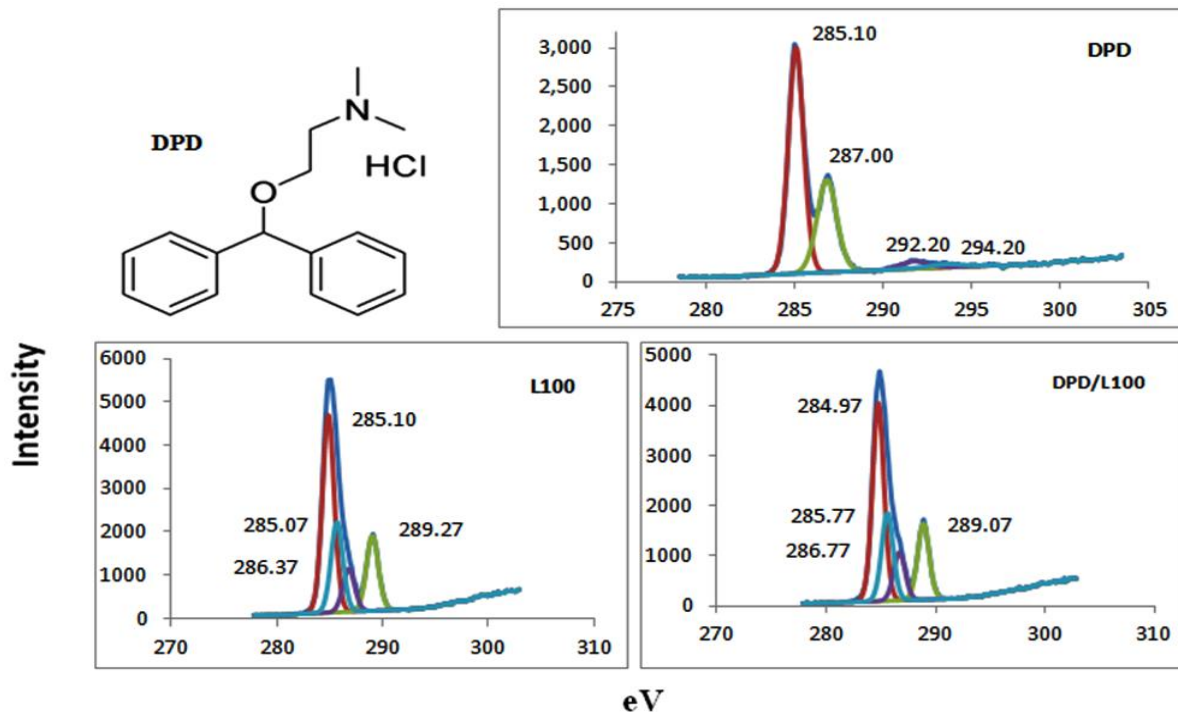


Fig. 6.5b: C 1s BE peaks of DPD, L100 and DPD/L100 formulations.

Since L100 contained higher proportions of C atoms compared to DPD, the peak shifts could be due to the positive charge effect of electropositive atom next to C-C/C-C-H bonds in extrudates. In the extruded formulation peaks representing C-Ring structures at BE= ~ 292.20, 294.20 eV from DPD and bonds at 289.27 eV from L100 have been eliminated by C-O-O/ O=C-O-O structures in the DPD/L100 formulation at about ~ 289.07 eV. At the same time peaks at 285.07 eV and 286.37 eV from DPD have shifted by +0.60eV and +0.40 eV respectively in the final formulation. This could be attributed to the interaction of C-C bonds shifting to a -C-O-O-/ N-C=O/ =OC (O)-O-OH complex structure.

In comparison to the pure L100-55 polymer (Supp. Fig. 3), in the PRP/L100-55 extrudates few specific peaks are submerged exhibiting new formed peaks due to the drug-polymer interactions where most of the C-COO or C-O bonds peaks have been shifted slightly. The BE peaks at ~285.0 eV represent C-C structures and two other slightly more shifted peaks at ~286.67eV and ~288.97eV represent new formed C-COO- or -C-O bonds in the PRP/L100-55 extruded formulation [27, 28]. In addition, peaks at BE= ~285.07eV (-C-C) from pure polymer in combination with peaks from pure drug at ~284.94eV (-C-C), ~285.84 eV formed a new peak at BE= ~285.0 eV representing new formed -C-C bonds in the extruded formulation. At the same time peaks at ~285.87eV, ~286.77eV from L100-55 and peaks at ~286.84eV from pure drug exhibit a new peak at BE= ~286.67eV (-C-COO/ -C=O) in the extruded formulation. Similarly, the peak at ~288.97 eV of the extruded powders is due to the interactions of two groups from drug/polymer at ~290.64eV and ~289.17eV respectively.

DPD/L100-55 formulation has showed peaks at ~285.07 eV represents C-C structure and two other slightly more shifted peaks at ~286.77eV and 289.70eV represent newly formed C-COO- or -C-O bonds [12].

The O (1s) peak at ~533.34 eV in PRP represents mainly a C-O-C structure while for the bulk L-100 polymer the peak at BE = ~533.63 eV suggests COOH/ COOCH structures (Supp. Fig.2). In the extruded formulations, a slight peak shift of +0.27eV from BE=532.67eV (in polymer) indicates the formation of C-OH or C-O-C at BE = ~532.90 eV. The presence of O (1s) peak at BE= ~534.40 eV in the extruded formulation (peak shift +0.77eV from both pure API and polymer) represents the ester/carboxylic acid functionalities. This is due to the interaction of drug-polymer molecules within the extruded polymer matrix. A possible outline of bonds could be represented as follows:



For the extruded DPD/L100 samples the following shifts can be observed; from the BE assignment peaks of O atoms in L100, only two peaks at BE = ~ 532.67 eV and ~533.63 eV are visible and have been shifted to ~532.27 eV and ~533.77 eV respectively¹² in the extruded samples. Mainly -OH/ -O-OH/-C=O bonds are changed to -C-C(O)-O bonds in the extruded formulation. The peak at BE= ~533.30 eV in DPD represents C-O bonds which was later shifted to ~533.77eV BE (DPD/L100) (Fig. 6.5c).

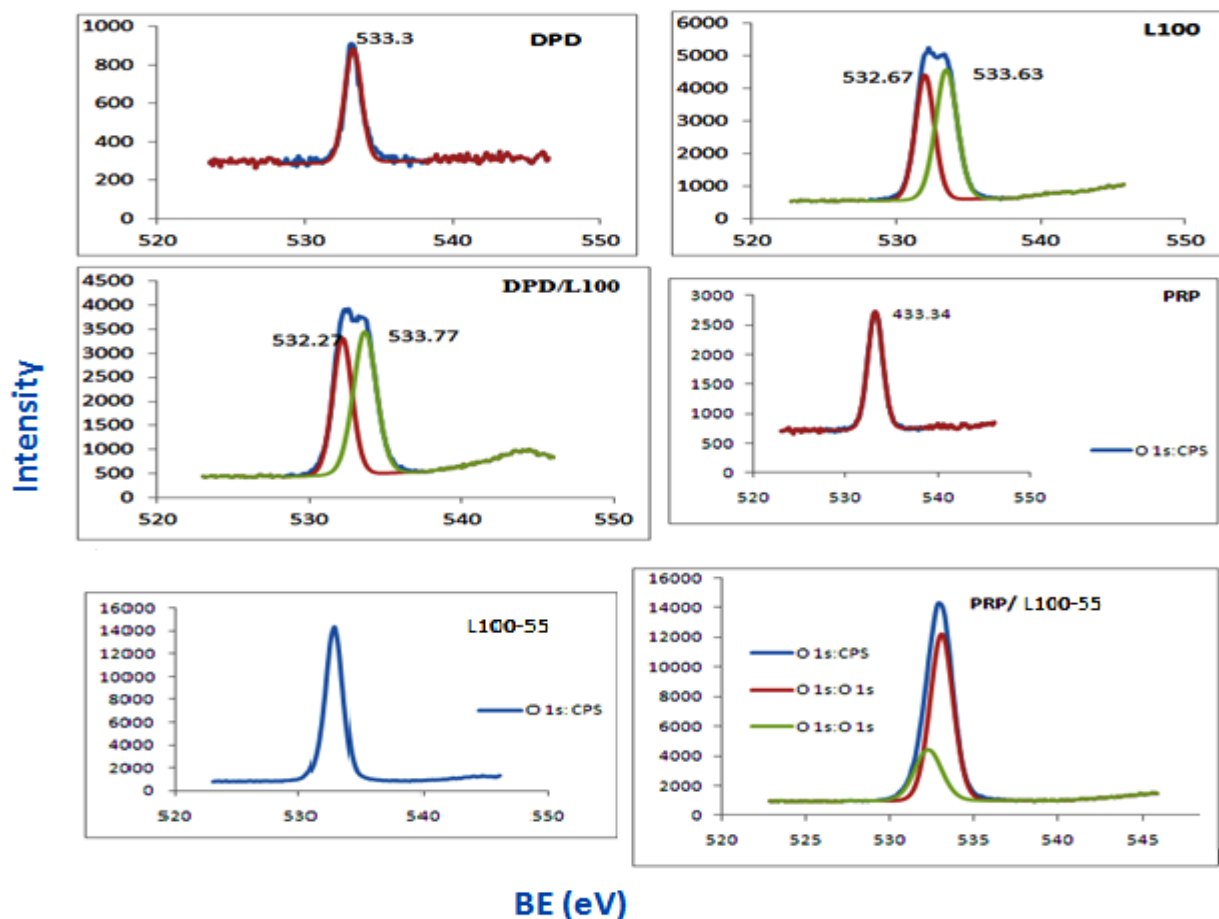


Fig. 6.5c: O 1s peaks of DPD, L100, DPD/L100 and PRP, L100-55, PRP/L100-55 formulations.

In the case of PRP/L100-55 formulations (Fig 6.5c), it is obvious that O (1s) BE peaks at ~532.87 eV from L100-55 and peaks at ~533.34 eV from PRP are shifted at ~532.70 eV and ~533.20 eV respectively at the point of extrusion. The newly formed peak at ~533.10eV (~532.70 eV + ~533.20 eV) is the combination of two C-O bonds from drug-polymer complex representing new C-O-O-C bonds. One single O (1s) BE peak for DPD/L100-55 formulation (Supp. Fig. 4) at BE= 533.01 eV resulted from the combined peak shifts of DPD (BE = ~533.3eV) and L100-55 (BE= ~532.87eV). Another newly formed peak

at ~533.01 eV is the combination of C-O/-O-O bonds from polymer/drug and represents C-O-O-C or C(O)-O-O bonds [27, 28].

The N (1s) binding energy (BE) of ~402.035 eV (Fig.6.5d) in PRP suggests the protonation of the NH⁺ group while Cl (2p) energy of ~198.035 eV significantly supports that conclusion [26]. The N (1s) energy of ~402.8 eV in PRP/L100 extrudates represents further protonation effect of N atom as NH₄⁺ which is described by the equation (ii) below. The N (1s) binding energy (BE) of ~402.6 eV (Fig. 5d) in DPD suggests similar effect in relation to the protonation of the NH⁺ group while the slightly reduced Cl (2p) energy of ~197.495 eV compared to pure PRP also significantly supports the statement.



The N 1s peak at BE= ~402.80 eV is in good agreement with the previously observed protonation of amide group by Beamson and Briggs [16]. The BE peak at ~402.80 eV (higher than typically observed for amines BE= ~399 eV - 400.5 eV and much more for -NH₂⁺ group) for N1s is an indication of C-O-NH₂⁺ structure whereas the O atom peak at ~534.40 eV shows the same [16]. These results strongly indicate an interaction between the amide group of the API and ester/carboxyl group of the polymer (L100) through the available H-interactions or hydrogen bridges (Fig. 6.5d).

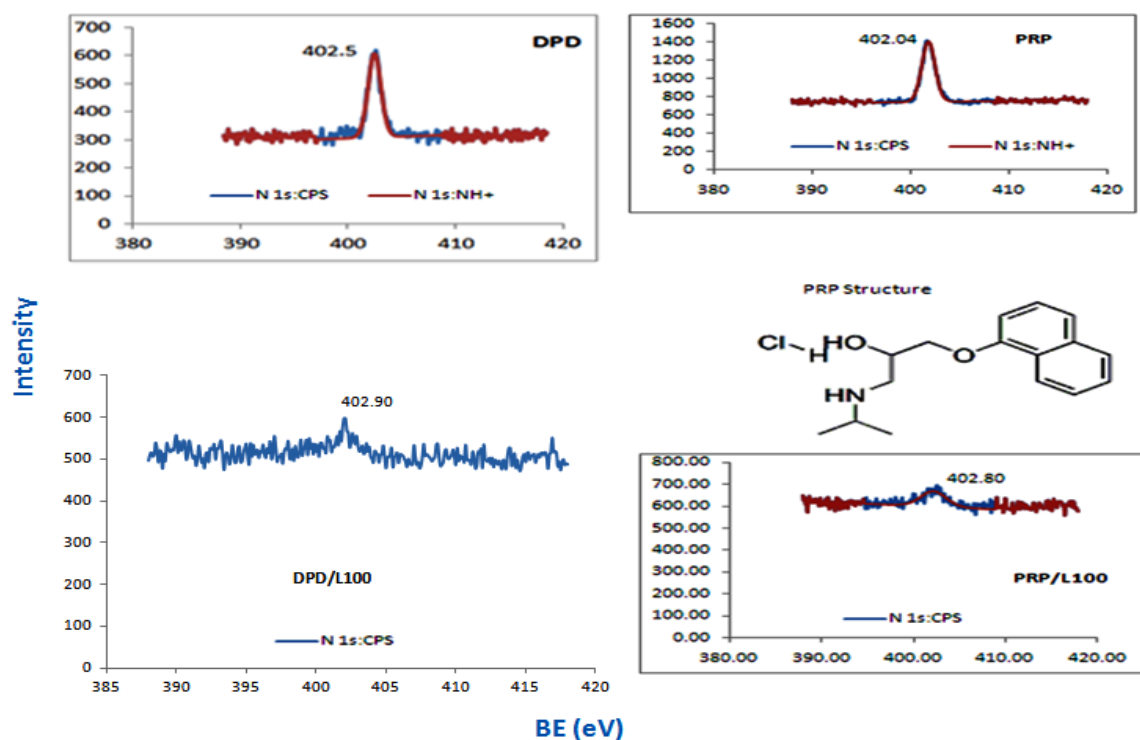


Fig. 6.5d: N 1s peaks of PRP and DPD formulations.

N 1s peaks from PRP/L100-55 and DPD/L100-55 also complement the observations from PRP/L100 and DPD/L100 formulations. The N (1s) energy of ~402.9 eV in DPD/L100 formulation represents a positive shift of the peak position to the right by +0.40 eV. This is due to the additional protonation effect of N atom converted to NH_4^+ . The N 1s peak at BE= ~402.90 eV suggests protonation of the amide group as observed for the PRP/L100 formulation. The BE peak at ~402.90 eV for N1s is an indication of C-O-NH_2^+ structure with longer peak shift than that of PRP/L100. As before, we concluded that a strong interaction between the amide group of API and ester/carboxyl group of polymer through the available H-interactions has taken place.

The protonation effects of N 1s in the extruded formulations were significant and showed high peak shifts which are summarised in Table 6.2. From the binding energy assignments determined by XPS it is presumed that the higher the peak shifts the more significant the protonation ^[29], therefore stronger intermolecular interactions.

Table 6.2: N 1s peak shifts in all extruded formulations with both drugs

PRP Formulations			DPD Formulations		
Form.	Peak Position (eV)	Net shift (eV)	Form.	Peak Position (eV)	Net shift (eV)
PRP Pure	~ 402.04	-	DPD Pure	~ 402.5	-
PRP/L100	~ 402.80	+ 0.76	DPD/L100	~ 402.9	+ 0.40
PRP/L100-55	~ 402.47	+ 0.43	DPD/L100-55	~ 402.77	+ 0.27

From Table 6.2 it is obvious that the peak shifts of N 1s in PRP/L100 are higher compared to the other formulations demonstrating the a high protonation effect and thus stronger drug – polymer interaction. The ascending order of the protonation effects in the extudates is PRP/L100>PRP/L100-55>DPD/L100>DPD/L100-55. Therefore, even though both drugs were found molecularly dispersed through DSC studies the XPS analysis showed different magnitude of interactions even with counterpart polymer grades. The XPS observations demonstrate a direct relation of the drug – polymer miscibility and intermolecular interactions.

Finally, the XPS analysis confirmed the molecular modelling predictions and verified the presence of H – bonding between the drug – polymer functional groups facilitated by HME processing.

3.5.3 Nuclear magnetic resonance (NMR) studies

^1H NMR spectroscopy can be used to monitor changes in molecular chemical environments by studying the movement of NMR signals (chemical shift) such as the changes in the ^1H NMR spectra of drug and drug/polymer solutions. Chemical shift (δ) locations of drug and polymer ^1H signals were identified and $\Delta\delta$ values were calculated after comparison with the spectra from the drug/polymer formulations.

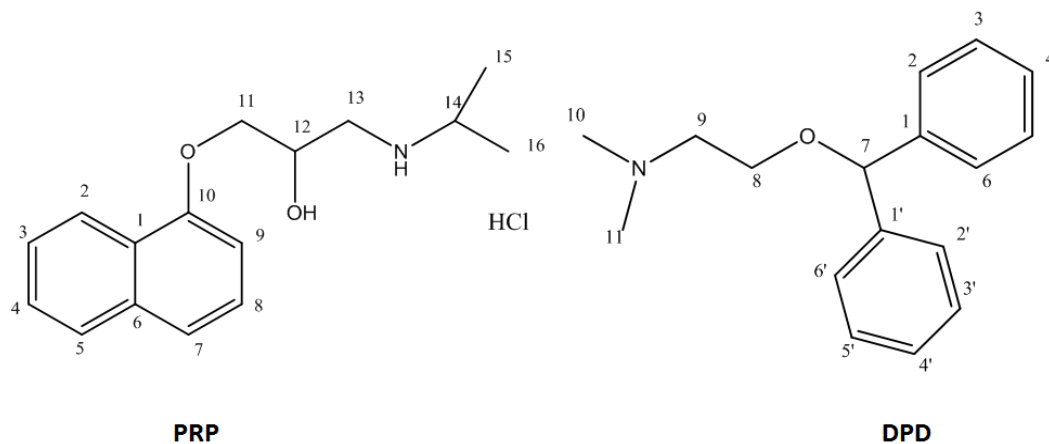


Fig. 6.6a: Molecular structure of PRP and DPD (NMR peak assignment).

Table 6.3 presents ^1H NMR chemical shift data and assignments for PRP, DPD, L100 and L100-55 (data not shown). Assignments have been annotated with respect to the molecular structures of both drugs presented in Fig. 6.6a. It should be noted, that the broad ^1H NMR signals from the L100 sample have been tentatively assigned with respect to the polymeric repeat unit. There are a number of well resolved multiplets that are also observed in the ^1H NMR spectrum of the commercial polymer, Eudragit L100, but the origin of these signals cannot be obtained. The ^1H NMR spectra for drug/polymer complexes follow very similar assignments as seen for the individual molecules (Table 6.3). For example, peak broadened, PRP, aromatic signals can be observed at 8.28 ppm (H2), 7.81 ppm (H5), 7.39 ppm (H8) and 6.95 ppm (H9), in the PRP/L100 complex.

Table 6.3: ^1H NMR assignments for drugs and polymer (samples were dissolved in CD_3OD).

Propranolol HCl		Diphenhydramine HCl		Eudragit L100	
Chemical shift/ ppm	Assignment	Chemical shift/ ppm	Assignment	Chemical shift/ ppm	Assignment
1.38	H15, 16	2.87	H10, 11	0.80 -1.40	H1, 3
3.23 – 3.40	H13 a,b	3.38	H9	1.80 – 2.24	H2
3.49	H14	3.75	H8	3.62	H4
4.17- 4.26	H11 a,b	5.52	H7		
4.40	H12	7.27	H4, 4'		
6.94	H9	7.34	H3, 3', 5, 5'		
7.38	H8	7.39	H2, 2', 6, 6'		
7.44 -7.51	H3, 4, 7				
7.81	H5				
8.27	H2				

In Fig. 6.6b significant changes can be observed for the peak widths found in the ^1H NMR spectra of the drug and the drug/polymer formulations. This can be easily seen with respect to the aromatic ^1H signals found only in the drug, resulting in the chemical shift locations between 6.5 and 8.5 ppm. The peak width is proportional to transverse relaxation (T_2), which arises as the result of magnetic field differences in the sample. As T_2 becomes shorter (faster relaxation), the peak width increases. The peak broadening of the ^1H NMR signals after formulation could be attributed to changes in local magnetic fields arising from intramolecular and intermolecular interactions in the sample. Indeed, it has been stated that changes in the T_2 can be attributed to decreases in rotational freedom of small molecules in the presence of a 'receptor' to which they can interact ^[30].

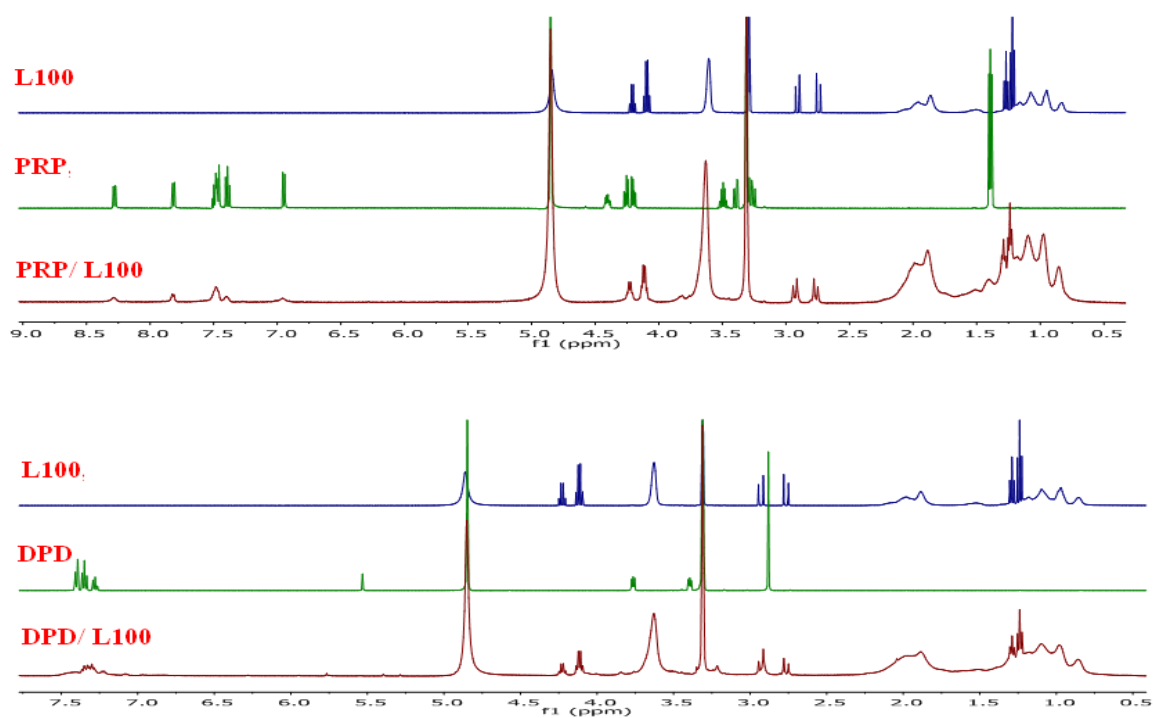


Fig. 6.6b: ^1H NMR spectra of all PRP and DPD formulations.

To investigate the potential interactions found within the drug/polymer formulation, ^1H NMR inverse recovery experiments were carried out to analyse spin relaxation times [31, 32]. Differing relaxation rates of nuclear spins can be related to aspects of molecular structure and additionally to internal molecular motion. The rationale of these experiments was to look at potential changes of the drugs molecular motion, before and after HME processing. Indeed, it would be assumed that the free drug (with a low molecular weight) would have quite a high molecular motion leading to fairly high T_1 relaxation delays. After extrusion, any possible interactions between the drug and polymer would result in a decrease in the amount of molecular motion observed for the drug. T_1 relaxation times are particularly sensitive to intermediate molecular motions which result in short T_1 s. Molecules which have fast or slow molecular motion can have comparable T_1 s (Supp. Fig. 5-8).

In Table 6.4, significant changes ($p > 0.05$) between the T_1 relaxation times for the drugs and the drug/polymer solutions can be observed. It is expected that low molecular weight present relatively fast molecular motion in solution. The decrease in T_1 of the extruded drug – polymer blends indicates a slowing in the molecular motion of the compounds. This result would infer that there is some type of molecular interaction between the drugs and polymers in methanol solutions, although the proximity of the interactions cannot be elucidated.

Table 6.4: A comparison of T₁ relaxation times for drug and drug/polymer solutions.

Sample	¹ H NMR T ₁ range of drug protons
Propranolol HCl	1.0 - 3.7 seconds
Propranolol HCl/ Eudragit L-100	0.05 – 0.5 seconds
Diphenhydramine HCl	1.5 – 4.3 seconds
Diphenhydramine HCl / Eudragit L-100	0.4 – 1.6 seconds

4.0 Conclusions

HME has successfully been employed as a robust technique to form solid dispersions of both APIs into polymer matrix through intermolecular interactions. The existence of amorphous APIs into the polymer matrices has been confirmed by thermal analysis. The NMR method and molecular modelling indicated the presence of intermolecular interactions between drug and polymer molecules. The XPS analysis has finally confirmed the mechanism of the interaction through H-bonding between the carboxyl group of the anionic methacrylate co-polymer and the amide group of the active substances.

5.0 References

- 1) Maniruzzaman, M.; Rana, M. M.; Boateng, J. S.; Mitchell, J. C.; Douroumis, D. Dissolution enhancement of poorly water-soluble APIs processed by hot-melt extrusion using hydrophilic polymers. *Drug Dev. Ind. Pharm.* 2012. In press.
- 2) Lakshman, J. P.; Cao, Y.; Kowalski, J.; Serajuddin, A.T. Application of melt extrusion in the development of a physically and chemically stable high-energy amorphous solid dispersion of a poorly water-soluble drug. *Mol Pharm.* 2008, 5(6), 994-1002.
- 3) Bekturov, E. A.; Bimendana, L.A. Interpolymer complexes. *Adv. Polym. Sci.* 1981, 43, 100-147.
- 4) Tsuchida, E.; Abe, K. Interactions between macromolecules in solution and intermolecular complexes, *Adv. Polym. Sci.* 1982, 45, 1-119.
- 5) Pavli, M.; Baumgartner, S.; Kosa, P.; Kogejc, K. Doxazosin–carrageenan interactions: A novel approach for studying drug–polymer interactions and relation to controlled drug release. *Int. J. Pharm.* 2011, 421, 110– 119.

- 6) Bonferoni, M.C.; Rossi, S.; Ferrari, F.; Bettinetti, G.P.; Caramella, C. Characterization of a diltiazem–lambda carrageenan complex. *Int. J. Pharm.* 2000, 200, 207–216.
- 7) Lelham, N.C.; Sundelof, L.O. Some aspects on characterization and properties of charged polysaccharides. An investigation of the system carrageenan/ amitriptyline/water with relation to amphiphile adsorption and charge density. *Int. J. Pharm.* 1995, 115, 103–111.
- 8) Takka, S. Propranolol hydrochloride/anionic polymer binding interaction. *Il Farmaco.* 2003, 58, 1051-1056.
- 9) Puttipatkachorna, S.; Nunthanidb, J.; Yamamoto, K.; Peckd, G. E. Drug physical state and drug–polymer interaction on drug release from chitosan matrix films. *J of Controlled Release.* 201, 75, 143–153.
- 10) Baer, D. R.; Engelhard, M.H. XPS analysis of nanostructured materials and biological surfaces *Journal of Electron Spectroscopy and Related Phenomena.* 2010, 178, 415–432.
- 11) Li, J.; Masso, J. J.; Guertin, J. A. Prediction of drug solubility in an acrylate adhesive based on the drug–polymer interaction parameter and drug solubility in acetonitrile. *Journal of Controlled Release.* 2003, 83, 211–221.
- 12) Davies, M. C.; Wilding, I. R.; Short, R. D.; Khan, M. A.; Watts, J. F.; Melia, C. D. An analysis of the surface chemical structure of polymethacrylate (Eudragit) film coating polymers by XPS. *International Journal of Pharmaceutics.* 1989, 57, 183-187.
- 13) Takka, S.; Rajbhandari, S.; Sakr, A. Effect of anionic polymers on the release of propranolol hydrochloride from matrix tablets. *Eur. J. Pharm. Biopharm.* 2001, 52, 75-82.
- 14) Maniruzzaman, M.; Boateng, J. S.; Bonnefille, M.; Aranyos, A.; Mitchell, J. C.; Douroumis, D. Taste masking of paracetamol by hot-melt extrusion: an in vitro and in vivo evaluation. *Eur J Pharm Biopharm.* 2012, 80(2), 433-42.
- 15) Gauss View, Version 5, Roy Dennington, Todd Keith and John Millam, *Semichem Inc.*, Shawnee Mission KS, 2009.
- 16) Beamson, G.; Briggs, D. High resolution XPS of organic polymers: The Scienta ESCA 300 Database. *J. Chem. Educ.* 1993, 70, PA25.
- 17) Wang, L.; Cui, F. D.; Hayase, T.; Sunada, H. Preparation and evaluation of solid dispersion for nitrendipine-carbopol and nitrendipine-HPMCP systems using a twin screw extruder. *Chem. Pharm. Bull.* 2005, 53(10), 1240–1245.

- 18) Forster, A.; Hempenstall, J.; Tucker, I.; Rades, T. Selection of excipients for melt extrusion with two poorly water-soluble drugs by solubility parameter calculation and thermal analysis. *Int J Pharm* 2001, 226(1–2), 147–161.
- 19) Zheng, X.; Yang, R.; Tang, X.; Zheng, L. Part I: Characterization of Solid Dispersions of Nimodipine Prepared by Hot-melt Extrusion. *Drug Dev Ind Pharm* 2007, 33, 791–802.
- 20) Gryczke, A.; Schminke, S.; Maniruzzaman, M.; Beck, J.; Douroumis D. Development and evaluation of orally disintegrating tablets (ODTs) containing Ibuprofen granules prepared by hot melt extrusion. *Colloids Surf B. Biointerfaces*. 2011, 86(2),275-84.
- 21) Tabary, N.; Mahieu, A.; Willart, J-F.; Dudognon, E.; Danède, F.; Descamps, M.; Bacquet, M.; Martel, B. Characterization of the hidden glass transition of amorphous cyclomaltoheptaose. *Carbohydrate Res*. 2011, 346, 2193–2199.
- 22) Delplacea, C.; Kreyea, F. Klosea, D.; Danedec, F.; Descampsc, M.; Siepmanna, J.; Siepmanna, F. Impact of the experimental conditions on drug release from parenteral depot systems: From negligible to significant. *Int. J. of Pharm*. 2012, 432, 11– 22.
- 23) Frisch, M. J.; Trucks, G. W.; Schlegel, H. B.; Scuseria, G. E.; Robb, M. A.; Cheeseman, J. R.; Scalmani, G.; Barone, V.; Mennucci, B.; Petersson, G. A.; Nakatsuji, H.; Caricato, M.; Li, X.; Hratchian, H. P.; Izmaylov, A. F.; Bloino, J.; Zheng, G.; Sonnenberg, J. L.; Hada, M.; Ehara, M.; Toyota, K.; Fukuda, R.; Hasegawa, J.; Ishida, M.; Nakajima, T.; Honda, Y.; Kitao, O.; Nakai, H.; Vreven, T.; Montgomery, J., J. A. ; Peralta, J. E.; Ogliaro, F.; Bearpark, M.; Heyd, J. J.; Brothers, E.; Kudin, K. N.; Staroverov, V. N.; Kobayashi, R.; Normand, J.; Raghavachari, K.; Rendell, A.; Burant, J. C.; Iyengar, S. S.; Tomasi, J.; Cossi, M.; Rega, N.; Millam, N. J.; Klene, M.; Knox, J. E.; Cross, J. B.; Bakken, V.; Adamo, C.; Jaramillo, J.; Gomperts, R.; Stratmann, R. E.; Yazyev, O.; Austin, A. J.; Cammi, R.; Pomelli, C.; Ochterski, J. W.; Martin, R. L.; Morokuma, K.; Zakrzewski, V. G.; Voth, G. A.; Salvador, P.; Dannenberg, J. J.; Dapprich, S.; Daniels, A. D.; Farkas, Ö.; Foresman, J. B.; Ortiz, J. V.; Cioslowski, J.; Fox, D. J. *Gaussian 09, Revision B.1, Gaussian, Inc., Wallingford CT, 2009*.
- 24) R. Dennington, T. Keith, J. Millam. Gauss View, Version 5, Semichem Inc., Shawnee Mission KS. 2009.
- 25) Choong, C.; Griffiths, J-P.; Moloney, M. G.; Triffitt, J.; Swallow, D. Direct introduction of phosphonate by the surface modification of polymers enhances biocompatibility. *Reactive & Functional Polymers*. 2009, 69, 77–85.

- 26) Vandecasteele, N.; Reniers, F. Plasma-modified polymer surfaces: Characterization using XPS. *Journal of Electron Spectroscopy and Related Phenomena*. 2010, 178–179, 394–408.
- 27) Ghods, P.; Isgor, O.B.; Brown, J.R.; Bensebaa, F.; Kingston, D. XPS depth profiling study on the passive oxide film of carbon steel in saturated calcium hydroxide solution and the effect of chloride on the film properties. *Applied Surface Science*, 2011, 257, 4669–4677.
- 28) Sabbatini, L.; Zambonin, P. G. XPS and SIMS surface chemical analysis of some important classes of polymeric biomaterials. *Journal of Electron Spectroscopy and Related Phenomena*, 1996, 81, 285-301.
- 29) A.Gryczke. Degussa technical brochure (Melt Extrusion with Eudragit). Germany. 2006
- 30) Brettmann, B.; Bell, E.; Myerson, A.; Trout, B. Solid-State NMR Characterization of High-Loading Solid Solutions of API and Excipients Formed by Electrospinning. *Pharmaceutical Nanotechnology*. 2012, 101, 1538-1545.
- 31) Qi, S.; Belton, P.; Nollenberger, K.; Clayden, N.; Reading, M.; Craig, D. Q. M. Novel characterisation of phase separation in hot melt extruded solid dispersions: a thermal, microscopic and NMR relaxometry study. *Pharm Res*. 2010, 27, 1869–83.
- 32) Qi. S.; Gryczke, A.; Belton, P.; Craig, D. Q. M. Characterisation of solid dispersions of paracetamol and EUDRAGIT® E prepared by hotmelt extrusion using thermal, microthermal and spectroscopic analysis. *Int J Pharm*. 2008, 354, (1–2):158–67.

CHAPTER 7: EVALUATION OF THE INTERRELATION BETWEEN INTERMOLECULAR INTERACTIONS AND TASTE MASKING EFFICIENCY OF TWO ANIONIC POLYMERS IN MELT EXTRUDED SOLID DISPERSIONS

1.0 Introduction

To date, masking the unpleasant taste of bitter APIs has been a real challenge for patient compliance and therefore various taste masking approaches have already been developed. The most commonly technologies are film casting by adding flavours or sweeteners [1,2]. Freeze-drying [2], spray drying [4], microencapsulation [5, 6], fluidized bed coating [2], high shear mixing [7] and supercritical fluids [8] have also been reported to be used for taste-masking purposes. HME has been introduced as a novel approach to mask the taste of bitter actives by enhancing drug-polymer interactions [9].

It has been reported in the literature that HME technique has successfully managed to mask the bitterness of ibuprofen and paracetamol through intermolecular forces (e.g. hydrogen bonding) between the active substance and the polymer matrix [2, 10]. In these studies the active substances were molecularly dispersed within the polymer matrices resulting effective taste masking of the drug's unpleasant taste. Solid lipid extrusion is also another suitable HME approach to produce extrudates of bitter APIs with improved taste properties. Recently, Breitzkreutz *et al.* developed taste masked lipid based formulation by extrusion with NXP 1210, a BCS class II drug (anti inflammatory) [11].

The taste masking evaluation of pharmaceutical dosage forms is evaluated both by *in vivo* and/or *in vitro* taste analysis. For the *in vitro* taste masking analysis commercially available electronic tongues have been employed to evaluate the masking effect. The e - tongues demonstrate very good correlation with human taste panels, reproducibility, low detection limits and high sensitivity [12, 13].

Various techniques have already been reported successfully to describe various drug-polymer interactions such as the dialysis equilibrium technique [14, 15], UV spectroscopy [16, 17], solid state NMR [18], drug-polymer interaction parameter model [19], Fourier Transform Infrared (FT-IR) and more importantly X-ray photo electron spectroscopy [16, 20]. X-ray photoelectron spectroscopy (XPS) has proved a potent tool for the characterisation of polymer surfaces and it has made a significant contribution to the analysis of biomedical polymers. Similarly FT-IR has been accepted as sensitive technique to elucidate the structural changes in the active formulations [16]. The lattice-based Flory-Huggins (F-H) theory is a well known theory describing polymer-solvent or polymer-polymer interactions based on the

Gibbs free energy change before and after mixing ^[21]. It has been reported in the literature that F-H theory could successfully be applied in order to determine the interaction parameter therefore signifying the interactions strengths between two compounds during their melting. A small molecule drug-polymer pair is analogous to a solvent-polymer system and has potential to be described by the F-H theory. The recent publications applying the F-H theory in this area focus on obtaining the F-H interaction parameter, χ , by the melting point depression method ^[22, 23]. Extractions of the maximum information out of the F-H theory and prediction of the thermodynamics of pharmaceutical binary systems is still of great interests in pharmaceutical research and developments.

In this study, both the FT-IR and XPS were used to identify the strength and types of the possible drug-polymer interactions. Similarly the F-H interaction parameter of the model system determined at two different conditions using the Nishi-Wang ^[24] equation based on melting point data and Hildebrand and Scott ^[25] correlation, respectively was further evaluated to interrelate them with the taste masking efficiencies of two different anionic model polymers (Eudragit L100-55, Eudragit L100) in the extruded solid dispersions of propranolol HCl and diphenhydramine HCl.

2.0 Materials and methods

2.1 Materials

Propranolol HCl (PRP) and Diphenhydramine HCl (DPD) were purchased from Sigma Aldrich (London, UK). Eudragit L100 (L100) and Eudragit L100-55 were kindly donated by Evonik Pharma Polymers (Darmstadt, Germany) and Colorcon Ltd respectively. The HPLC solvents were analytical grade and purchased from Fisher Chemicals (UK). All materials were used as received.

2.2 Hansen solubility parameters: prediction of drug/polymer miscibility

The Hoftyzer and van Krevelen method was used to calculate all drug polymer solubility parameters by considering the chemical structural orientations ^[26] and two – dimensional approach introduced by Bagley *et al.* ^[27] was used to predict the combined thermodynamic effects on the drug-polymers miscibility over hydrogen bonding energy. *[Please see Chapter 6, Section 2.2 for more details].*

2.3 Flory Huggins (F-H) theory for the prediction of drug/polymer interaction parameter

The F–H interaction parameter, χ , was correlated with temperature dependence, as in many simplified cases. The interaction parameter of the model system was determined at two different conditions using the Nishi–Wang ^[24] Eq. 7.1 equation based on melting point depression data and Hildebrand and Scott ^[25] Eq. 7.2 correlations with solubility parameter, respectively. The F-H interaction parameter (χ) for all of the drug/polymers binary mixtures were calculated by using the following equations. The value determined by Eq. 7.1 represents the interactions between the two substances, specifically at the melting temperature, which may not be extrapolated to other temperatures.

$$\frac{1}{T_m} - \frac{1}{T_m^0} = -\frac{Rv_{drug}}{\Delta H_{drug}v_{poly}} \left[\ln \phi_{drug} + \left(1 - \frac{1}{m_{poly}}\right) \times (1 - \phi_{drug}) + \chi_{drug-poly}(1 - \phi_{drug})^2 \right] \quad (7.1)$$

Where, v is the molar volume of the repeating unit, m is the degree of polymerization, ϕ is the volume fraction and χ is the crystalline– amorphous polymer interaction parameter, T_m and T_m^0 is the crystalline melting peak and amorphous Tg in the system, respectively.

F-H interaction parameter (χ) can be also estimated by the method developed by Hildebrand and Scott according to Eq. 7.2 ^[25].

$$\chi = \frac{v(\delta_{drug} - \delta_{poly})^2}{RT} \quad (7.2)$$

Where, R is the gas constant, T is the absolute temperature, and v the volume per lattice site and δ_{drug} and δ_{poly} are solubility parameters of drugs and polymers respectively.

2.4 Differential Scanning Calorimetry (DSC)

The physical state of the pure drug, physical mixtures and extrudates were examined by using a Mettler-Toledo 823e (Greifensee, Switzerland) differential scanning calorimeter. Samples were prepared in sealed aluminum pans (3-5 mg) with a pierced lid. The samples were heated at 10°C/min in a temperature range between 0 and 220°C under nitrogen atmosphere.

2.5 Hot-melt extrusion (HME) processing

Drug/polymer blends were blended in 100 g batches for 10 min each with a Turbula (TF2, Basel) mixer. The extrusion of all batches was performed using a Randcastle single-screw extruder (RCP0625) equipped with a 5 mm rod die at 100°C/150°C/150°C/160°C/155°C (Feeder --> Die) temperature profiles and screw speeds at 15 rpm. The drug-polymer composition consisted of PRP/L100, PRP/L100-55, DPD/L100 and DPD/L100-55 at ratios of 10/90 wt/wt. The produced extrudates (strands) were grinded by using a Ball Milling system (Retsch, Germany) to obtain granules (< 500 µm at a rotational speed of 400 rpm for 5 min.

2.6 Particle morphology and size distribution

SEM was used to study the surface morphology of all hot-melt extrudates. The samples were mounted on an aluminum stage using adhesive carbon tape and placed in a low humidity chamber prior to analysis. Samples were coated with gold, and microscopy was performed using a Leica Cambridge Instruments (S360F), SEM operating at an accelerating voltage of 5 kV.

In order to determine the particle size distribution of the micronized extrudate granules a dry sieving method was applied. The method involved stacking of the sieves on top of each other and then placing the test powder (100 g) on the top sieve. The nest of sieves was subjected to a standardised period of agitation (20 min) in order to give the weight percentage of powder in each sieve size range.

2.7 *In vivo* taste masking evaluation

In vivo taste masking evaluation for pure APIs, polymers and all active extruded formulations was performed in accordance to the Code of Ethics of the World Medical Association (Declaration of Helsinki) ^[28]. Six (6) healthy volunteers of either sex (age 18–25) were selected (Male = 3, female = 3) from whom informed consent was first obtained (approved by the Ethics Committee of the University of Greenwich, Ref: UG09/10.5.5.12) and trained. The equivalent of 100 mg of pure DPD, PRP or DPD/PRP extrudates (containing equal amounts of APIs) were held in the mouth for 60 seconds and then spat out. The selection of samples was random and in between of two samples analysis mineral water was used to wash each volunteer's mouth. The bitterness was recorded immediately according to

the bitterness intensity scale from 1 to 5 where 1, 2, 3, 4 and 5 indicate none, threshold, moderate, bitter and strong bitterness.

2.8 *In vitro* taste masking evaluation: TS-5000Z sensing system

The assays were realized on TS-5000Z taste sensing system equipped with a BASIC sensor set (for pharmaceutical analysis) which are suitable for basic APIs composed of 10 specific sensors (AAE, CT0, CA0, C00, AE1, AC0, AN0, BT0, GL1) on a 48-positions autosampler using 25 ml beakers. Acquisition times were fixed at 120s with a BT0 negatively charged sensor. All the data generated on TS-5000Z system were treated using multidimensional statistics. Each solution was tested on TS-5000Z at least 4 times and triplicates were taken into account for the statistical treatment. Sensors were then cleaned up in reference solutions (30 mM KCl + 0.3 mM tartaric acid) between each sample measurement. The samples were dissolved in 50 mL of 10 mM KCl aq. solutions and further diluted to prepare 0.03, 0.1, 0.3, and 1 mM solutions as standards. Then solutions were filtered with Buchner funnel fitted with filter paper at 2.5 μm pore size.

2.9 Molecular modelling

The monomer of L100, dimer of L100-55, PRP and DPD were constructed by program Gaussview ^[29]. Hydrogen bonding patterns were identified by placing the drug molecule within the proximity of the L100 and L100-55, respectively and then energy optimised at the B3LYP/6-31G* level using Gaussian09 ^[30]. Based on these optimised configurations of drug-polymer interactions, the binding energy was calculated using $E_{\text{binding}} = -[E_{\text{complex}} - (E_{\text{drug}} + E_{\text{polymer}})]$ with each energy term obtained at the M06-2x/6-31G** level ^[31] after single point calculations. A counterpoise procedure ^[32] was employed to correct for the effect of basis set superposition error (BSSE). In all of the drug/polymers combinations primarily two different H bonding were detected with the donor-acceptor distance at $\sim 2 \text{ \AA}$. All possible H bondings were shown in dash line in Table 4.

2.10 Fourier Transform Infra-Red (FT-IR) analysis

FTIR analysis was performed on the drug, polymer, drug_/polymer physical mixtures, and complex using Perkin Elmer PE1600 (Massachusetts 02451 USA) Fourier Transform Infrared Spectra according to the KBr disc method from 400 – 3600 wavelength/ cm^{-1} range.

2.11 X-ray photoelectron spectroscopy (XPS) analysis

X-ray photoelectron spectra (XPS) were measured on a Kratos Axis Ultra-DLD using a monochromatic Al K_{α} X-ray source (120 W) and an analyser pass energy of 160 eV (survey scans) or 20 eV (high resolution scans); the pressure during analysis was 1×10^{-9} Torr. All data were referenced to the C(1s) signal at 285.0 eV attributable to unsaturated C-C/C-H bonds [33]. Quantification and curve fitting was performed in CasaXPSTM (Version 2.3.15) using elemental sensitivity factors supplied by the manufacturer.

3.0 Results and discussions

3.1 Predictions of drug/polymer miscibility: solubility parameters

The calculated solubility parameters of APIs and polymers are shown in Table 7.1. The difference between the calculated solubility parameters of the polymers and the drug indicate that both PRP and DPD are likely to be miscible with both polymers since the difference of the calculated solubility parameters are not more than $7\text{MPa}^{1/2}$.

Table 7.1: Solubility parameters calculations summary for both drugs and polymers

Comp.	δ_p ($\text{MPa}^{1/2}$)	δ_d ($\text{MPa}^{1/2}$)	δ_h ($\text{MPa}^{1/2}$)	δ_v ($\text{MPa}^{1/2}$)	δ ($\text{MPa}^{1/2}$)	$\Delta\delta$		$R_{a(v)}$	
						PRP ($\text{MPa}^{1/2}$)	DPD ($\text{MPa}^{1/2}$)	PRP	DPD
PRP	3.67	19.30	9.90	19.64	21.94	-	-	-	-
DPD	4.05	16.39	5.44	16.89	17.75	-	-	-	-
L100	0.41	19.31	12.03	19.31	22.75	0.81	5.0	3.26	4.67
L100-55	0.25	18.22	11.69	18.22	21.65	0.29	3.9	3.59	4.22

$$R_{av} = \sqrt{(\delta_{v2} - \delta_{v1})^2 + (\delta_{h2} - \delta_{h1})^2}$$

Being slightly diverted from the Van-Krevelen equation, Bagley proposed a more advanced two dimensional equation to predict the drug-polymers miscibility known as Bagley equation [27].

The two – dimensional approach can provide more accurate prediction of the drug – polymer miscibility by calculating the distance ($R_{a(v)}$) in Bagley diagram using the

Pythagorean Theorem. In this theory two components are considered miscible when $R_{a(v)} \leq 5.6 \text{MPa}^{1/2}$ [26].

3.2 Flory Huggins (F-H) theory for the prediction of drug/polymers interaction parameter

In order to determine the F-H interaction parameter between both drugs and polymers the heat of fusion of crystalline PRP and DPD as well as the Tg of both polymers and melting peaks of APIs (Table 2) were determined by DSC experiments. In the DSC thermograms the pure PRP and DPD showed a sharp melting peak at 166.65°C and 170.83°C, respectively with a net heat of fusion / enthalpy (ΔH) values of 126.25 J/g and 124.59 J/g, respectively. The Tg observed for both polymers are at 164.38°C for L100 and 83.97°C for L100-55 (Acryl EZE).

Molecular volumes of the two different polymers L100 and L100-55 as well as active substances were estimated from functional group contribution. As shown in Table 7.2 the molecular volumes of PRP and DPD are 269.96 cm³ and 284.24 cm³, respectively. By implementing both the Eqs. 7.1 & 7.2, the average value of χ is calculated as shown in Table 7.3.

In this case, since the drug content is essentially low (ϕ , Drug = 10%), the accurate determination of the onset point of the melting endothermic peak became difficult. However, accurate interaction parameter by using F-H theory has successfully been implemented in our study as the interaction parameter depends on multiple factors such as crystalline melting temperature of APIs, Tg of polymers, molecular volumes and degree of polymerisations etc which have successfully been determined from the thermal analysis of drug-polymer binary mixtures. The negative interaction parameter in Table 7.3 indicates that there is a net attraction force between species in a binary mixture which is favourable for all compositions at observed melting temperature of both APIs and also same for the Tg's of both polymers [34]. Therefore the higher the absolute value of χ , the stronger the interactions between drug/polymers species. In Table 7.3, it can be seen that L100 facilitates stronger interactions with both the drugs compared to those of L100-55. To make the case stronger this observation was confirmed by both approaches (Nishi-Wang and Hildebrand-Scott).

Table 7.2: DSC findings of all APIs and polymers as well as general information of all polymers and active substances

Compound	Heat of Fusion (ΔH) J/g	Melting peaks ($^{\circ}C$)	Glass transition (T_g) $^{\circ}C$	Molecular weight/volume (cm^3)
PRP	126.25	166.65	34.74	295.34/269.96
DPD	124.59	170.83	14.80	291.35/284.24
L100	-	-	164.38	12500/100000
L100-55	-	-	83.97	320000/271186

Table 7.3: Calculation of F–H interaction parameter of different Drug–Polymer extruded formulations

Form.	Volume Fractions (ϕ)	Nishi-Wang (χ)	Hildebrand – Scott (χ)
RPR/L100	10:90	-0.2240	-2.89×10^{-4}
PRP/L100-55	10:90	-0.0826	-3.70×10^{-5}
DPD/L100	10:90	-0.2099	-1.10×10^{-4}
DPD/L100-55	10:90	-0.0774	-6.7×10^{-5}

3.3 SEM and particle size analysis

SEM was used to examine the surface morphology of all extruded formulations as depicted in Fig 1. The particles size range for all extruded materials varied majorly from 50-200 μm after optimizing the grinding process. The extrudates containing both L100 and L100-55 exhibited no drug crystals on the extrudate surface after extrusion with PRP (Fig 7.1a-b). Similarly, no DPD crystals were observed on the surface of polymeric extrudates in both polymeric systems. The particle size distribution depicted in Fig. 7.2 shows particle sizes for

all formulations ranging from 40 – 400 μm . A very small percentage can be seen at sizes $<40\mu\text{m}$ as the milling process was optimized to reduce fines in the final extruded batches.

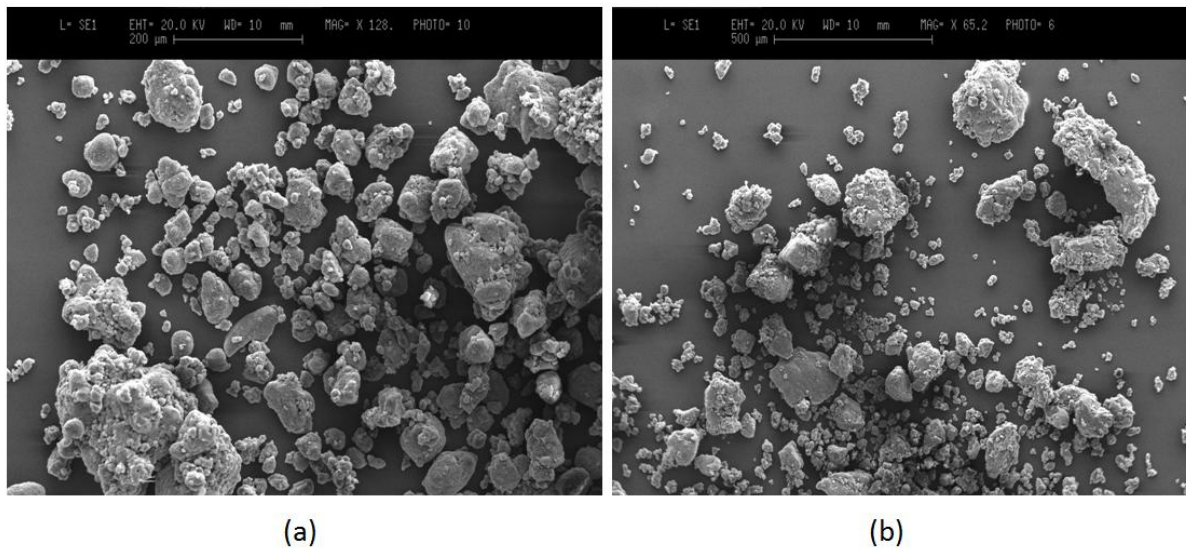


Fig. 7.1: SEM images (magnification x 500) of the extruded formulations (a) PRP/L100 and (b) DPD/L100-55.

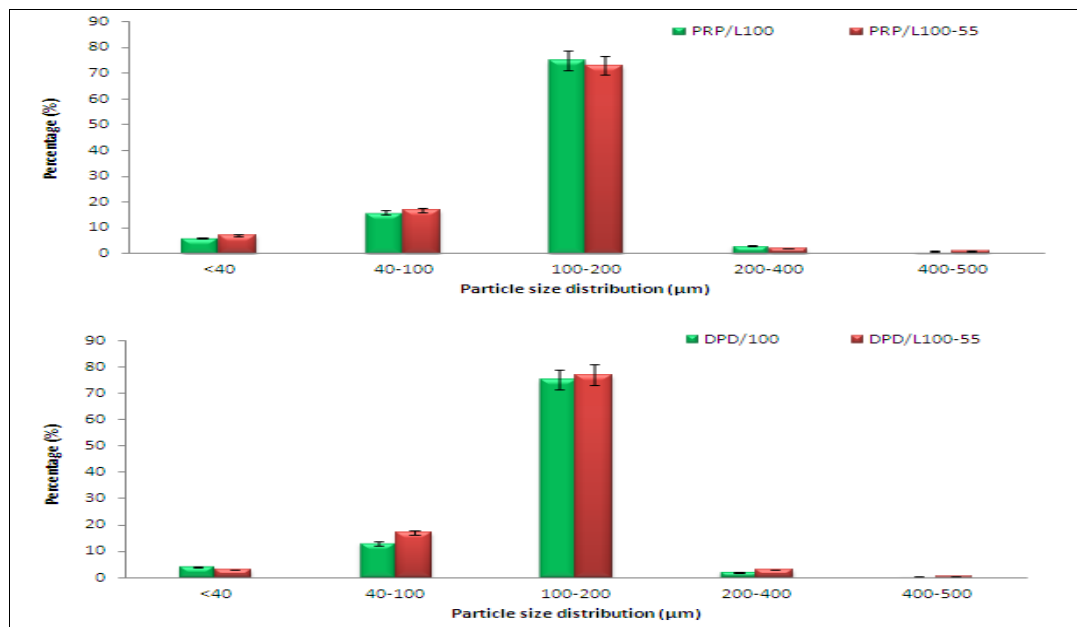


Fig. 7.2: Particle size distribution of L100 and L100-55 based formulations with both drugs (milling time 5 min, 400 rpm).

3.4 *In vivo* and *in vitro* taste masking evaluation

The masking efficiency of the developed granules was evaluated *in vivo* with the assistance of six healthy human volunteers (age 18 – 25). The statistical data collected from the *in vivo* study for the pure active substances and the extruded formulations are depicted in Fig. 3a. The data analysis showed significant suppression of the bitter taste for both APIs & influence of the polymeric carriers and importance of drug loading in the final formulation. Both polymers showed effective taste masking capacity with descending order L100>EZE. Furthermore, the HME formulations presented excellent masking effect for active concentrations (10%) of both APIs. In Fig. 7.3a sensory data obtained from six volunteers interestingly showed the taste masking efficiency of L100 significantly better than EZE for both of the APIs used. This could be attributed to the pH dependant dissolution properties of EZE (pH \geq 6) compared to that of L100 (pH \geq 6.5) as the saliva represents a pH approximately 6.0 in healthy individuals. However, the sensory scores for both of the active APIs in different formulations are within the range (below 2) which has been demonstrated as optimum by *in vitro* evaluations.

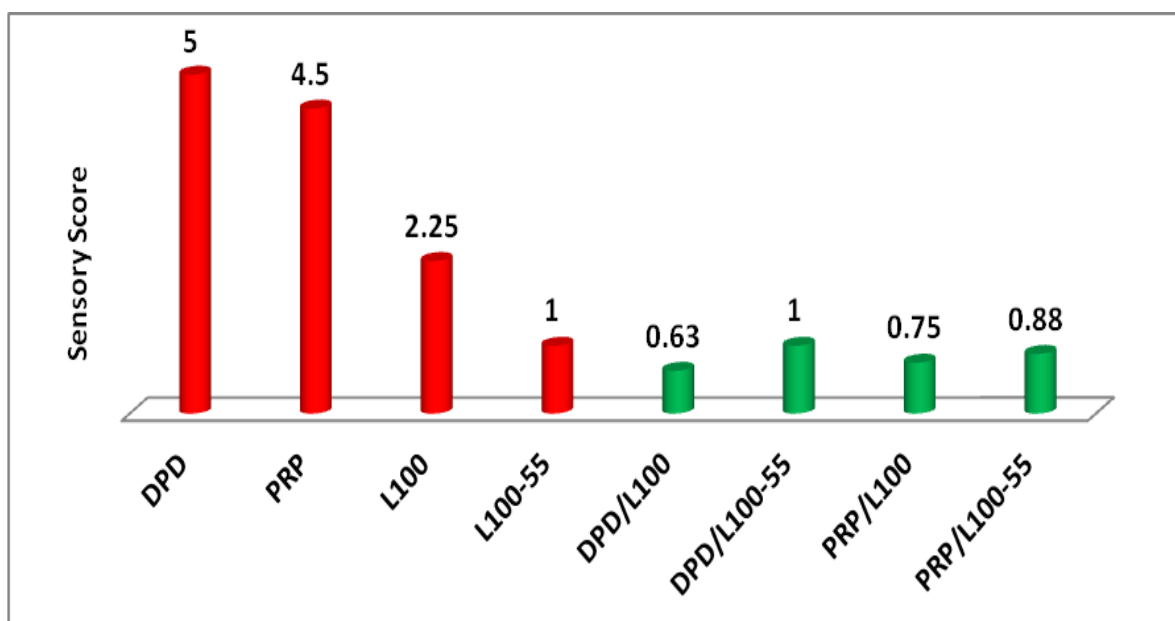


Fig. 7.3a: Sensory scores of all formulations by panellist (n = 6).

The *in vitro* masking effect of the extruded formulations in artificial saliva was evaluated by using the INSENT TS-5000Z e-tongue and the interpretation of the experimental findings is discussed below. The distances percentage (%) between active substances and formulation solutions were estimated in four phases of time distances (0.5 min, 1 min, 10 min and 30 min) as they are indicative of taste masking power of the extruded

formulations. In addition, the Discrimination Index (DI in %) was determined for each solution.

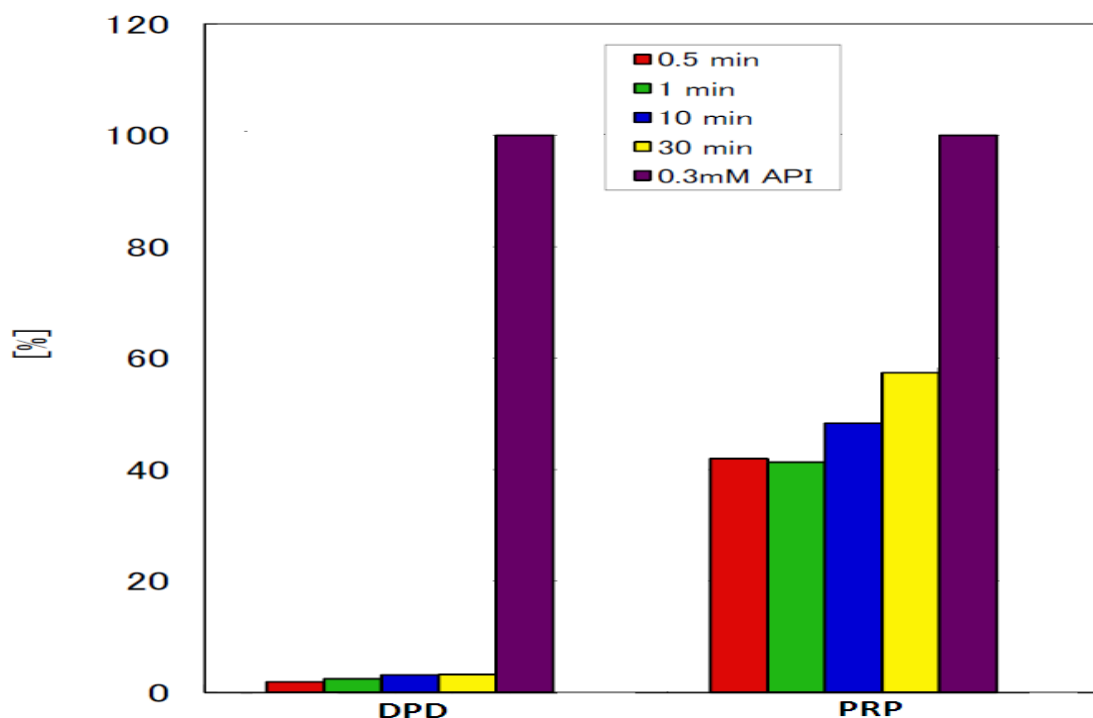


Fig. 7.3b: Normalised DI (%) of all drug/L100 formulations in four different time scale.

This indicator takes into account the average difference between the pairs to compare each other as well as the discrimination index (DI) of each sample. The closer the DI values to 0%, the longer the distance between groups and the higher the discrimination (high masking effects). The DI will help then to assess the significance of difference between the groups. The results are presented in the following sections for each drug in (Fig. 7.3b and Fig. 7.3c).

In Fig. 7.3b the bitter taste suppression of DPD in the active formulation with L100 is quite significant even after 30 min as the DI index (%) is only about 2% (very close to 0%-means no taste). Similarly, PRP/L100 extruded formulation did not show that much closer taste suppression compared to the L100 system but still about 60% DI has been determined by the BT0 sensor thus indicating taste masking.

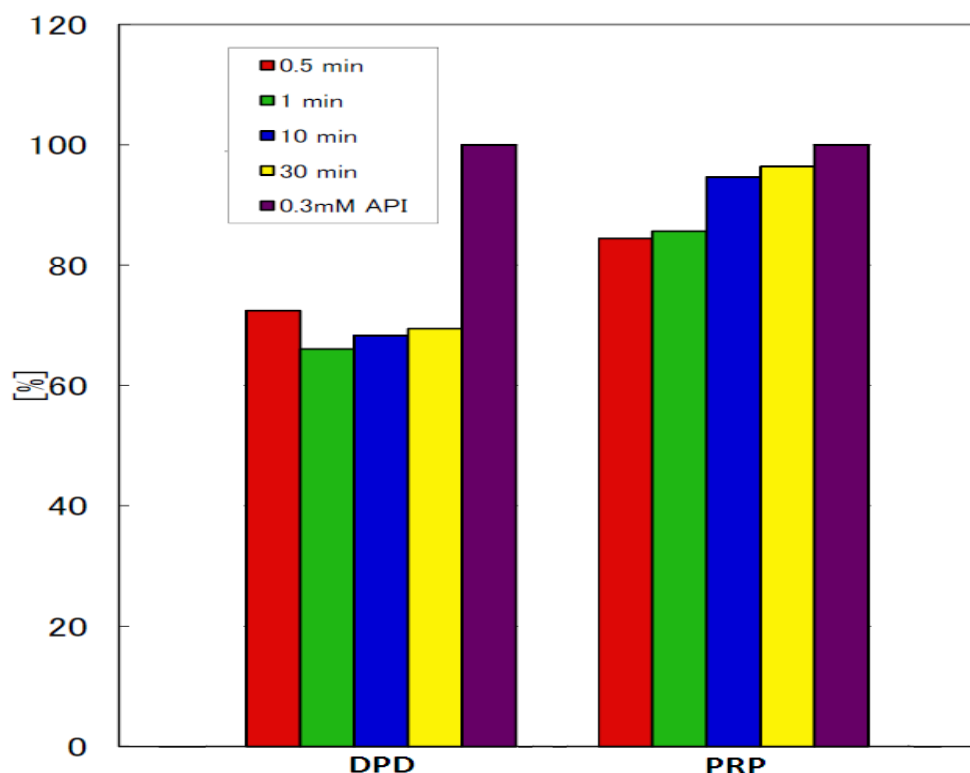


Fig. 7.3c: Normalised DI (%) of all drug/L100-55 formulations in four different time scale.

The taste graph shows significant discrimination between all active formulations and active substance solutions (Fig. 7.3c). The bitter taste of DPD has successfully been masked up to 35% (DI 65%) while for PRP only 5% (DI 95%). EZE has demonstrated its taste masking efficiency for both the APIs but not as significant as L100.

Liquid sensors are able to detect the presence of the drug in the coated formulations (up to 0.3 mM API). Focusing on pure drug in reference solution (artificial saliva) the complex with L100 (Fig. 7.3b) at 90% shows a better taste improvement compared to Acryl EZE coating (Fig. 7.3c). This could be highly attributed to the pH dependency of both polymers. L100 is soluble in pH above 6.5 while L100-55 (EZE) is soluble in slightly lower pH range therefore in the artificial saliva solutions the electronic tongue sensor did perceive the taste of bitter APIs from the dissolved polymer matrices.

Sensory correlated models were built to evaluate the correlation with sensory scores. The correlation model is considered as valid and fits with panel perception (Fig 7.3d; $R^2 > 0.9$). However, the correlation studies show the same conclusions: sensory panel was sensible to taste perception with Eudragit L100. The correlation studies depicted in fig. 3d also complemented the sensory findings from the panelists score to conclude the statement that L100 has better taste masking efficiency than L100-55 (EZE).

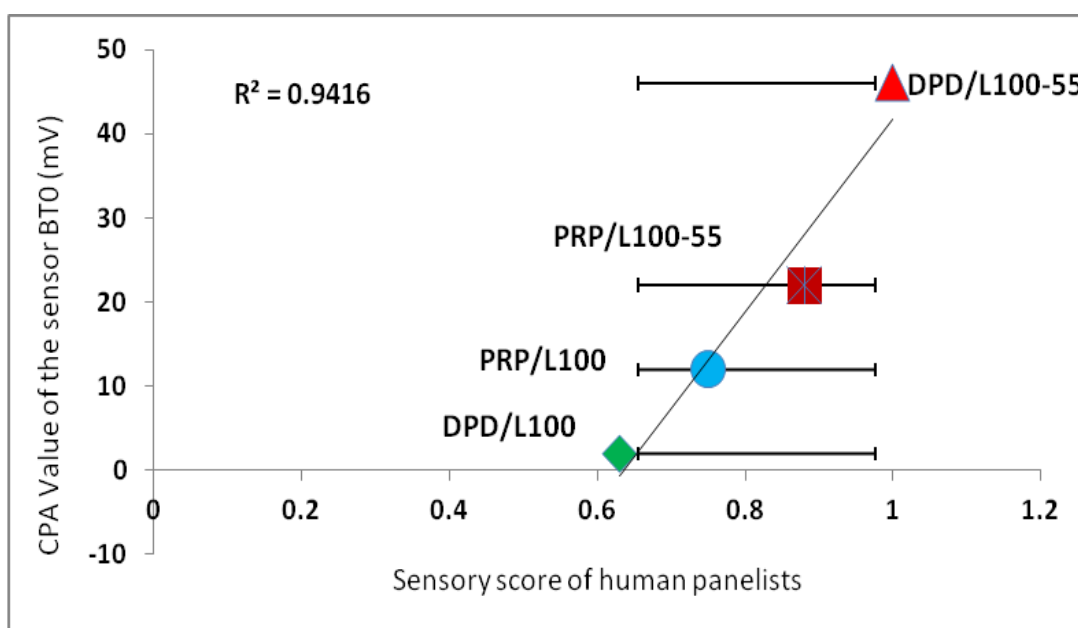


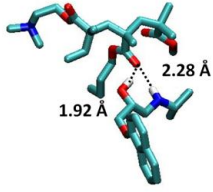
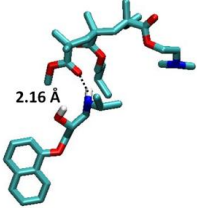
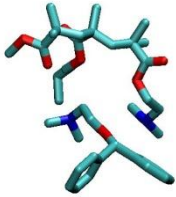
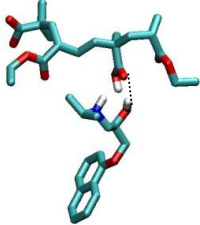
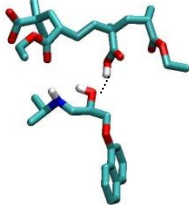
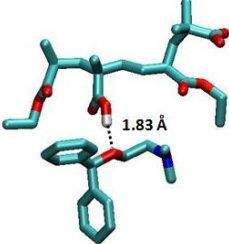
Fig.7.3d. Relationship between results of taste sensors and human taste scores for similar tastes (the standard deviations on the x- and y-axes are the difference between the panelists' scores and measurement error (n = 6), respectively).

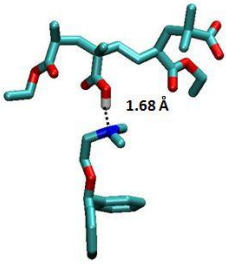
In Fig. 7.3d, TS-5000Z taste sensing system (INSENT, Japan) showed different sensitivity to each sample with a high correlation (0.94) to the taste scores, suggesting that this sensor responds selectively according to bitterness intensity and does not detect just quantitative information.

3.5 Molecular Modelling

Molecular modelling results indicated that both the hydroxyl group and amine group within the drug molecule could form strong hydrogen bonds with the monomeric form of L100 and L100-55, as indicated by the optimal distances between the H-bond donor and acceptor (Table 7.4). However, presence of the chloride ion could disrupt the H-bond between the hydroxyl group and the carboxylate group (data not shown). PRP showed a total binding energy ranging from 6.0 -15.9 kcal/mol with both of the polymers used. DPD showed a similar range (8.6 – 17.5 kcal/mol) as shown in table 7.4. In addition, both drugs require higher binding energy to interact with L100-55 in comparison to L100, as indicated by the binding energy calculation. Higher binding energy is indicative of more energy required to break the H bonds apart, therefore enhanced stiffness of the drug/polymer binary mixtures that may result in less movements of the molecules during the extrusion to form significant interactions. All conformations showed very strong binding energy specifying strong interaction possibilities between both drugs and polymers.

Table 7.4: Binding energy calculation of drug/polymer pair based on the chemical structure (Gaussian View 9).

Drug-polymer combination	Conformation (Approx.)	Binding energy (Kcal/mol)
L100-PRP^(a)		9.4
L100-PRP^(b)		6.0
L100-DPD		8.6
L100-55-PRP^(a)		15.9
L100-55-PRP^(b)		15.9
L100-55-DPD^(a)		12.0

L100-55-DPD ^(b)		17.5
----------------------------	---	------

3.6 Fourier Transform Infra-Red (FT-IR) analysis

FT-IR is one of the most potent techniques which have already been used to study interactions in drug/polymer blends by providing valuable information regarding the oppositely charged ionic drug/polymer interactions at the molecular level [35]. By showing the emergence of additional bands or alterations in wave number position or broadening of functional groups compared to the spectra of the pure drug and polymer, the FTIR spectra gives an indication of drug/polymer interactions. The FTIR spectra in the absorbance mode for the PRP/anionic polymers formulations and DPD/ polymers formulations are shown in Fig. 7.4a – 4b.

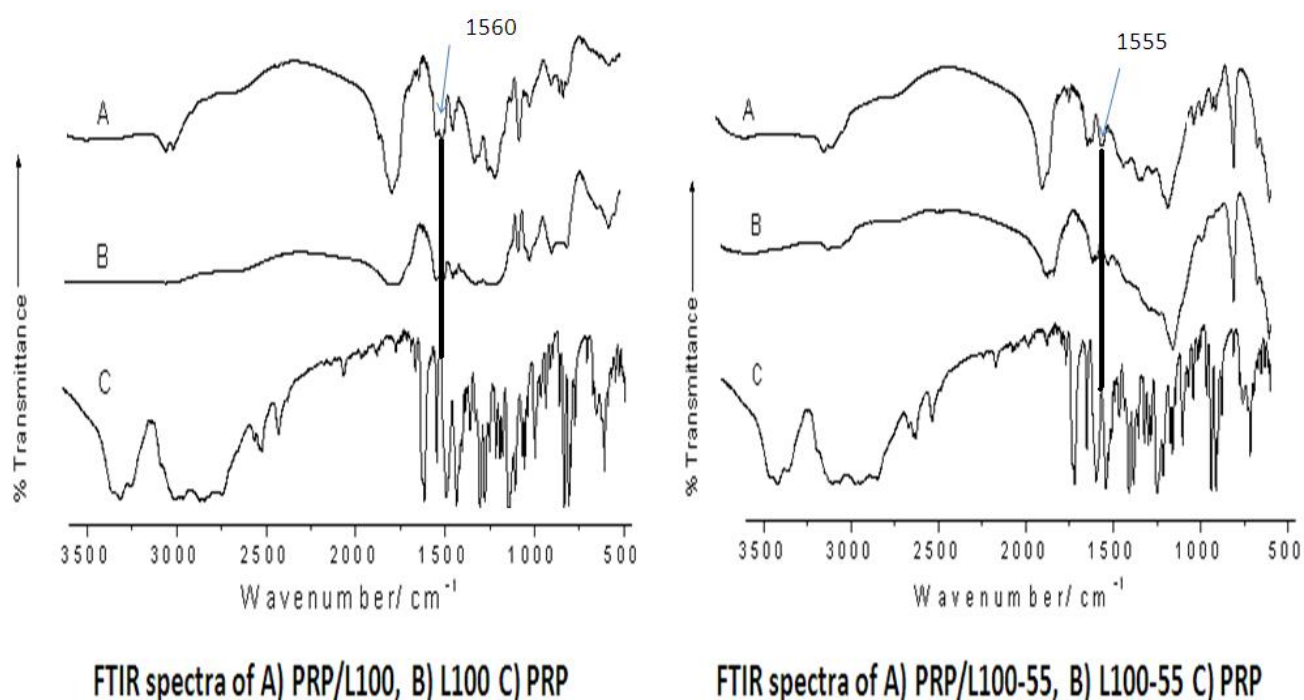


Fig 7.4a: FT-IR spectra of PRP extruded formulations.

The characteristic bands of CO- vibrations of the carboxylic acid groups are shown at $\sim 1705\text{ cm}^{-1}$ and of the esterified carboxylic groups at $\sim 1735\text{ cm}^{-1}$. The FTIR spectra of the

PRP/ polymers extruded in comparison with the pure materials are shown in Fig 4a, which show a new absorption band at 1560 and 1555 cm^{-1} for PRP/ L100 and PRP/ L100-55, respectively. This is considered to be the result of the addition of amine group to a solution of the carboxylic acid. During the ionization process the resonance is possible between the two CO- bands within COO- groups.

As a result, the characteristic CO- absorption is replaced by the band of an auto-symmetrical vibrations of the COO- structure and is used as a diagnosis of the COO- group in the 1555- 1560 cm^{-1} region of the FTIR spectra [36, 37]. A strong and extensive interaction between anionic methacrylate polymers and cationic drug PRP is therefore indicated by the presence of carboxylic groups in the structure, enabling the formation of hydrogen bonds with the amine group of the drug. Similarly, DPD/ L100 and DPD/ L100-55 extruded formulations showed emergence of new bands at 1550 cm^{-1} region (Fig. 7.5b) which significantly complement the similar interactions mechanism as PRP formulations.

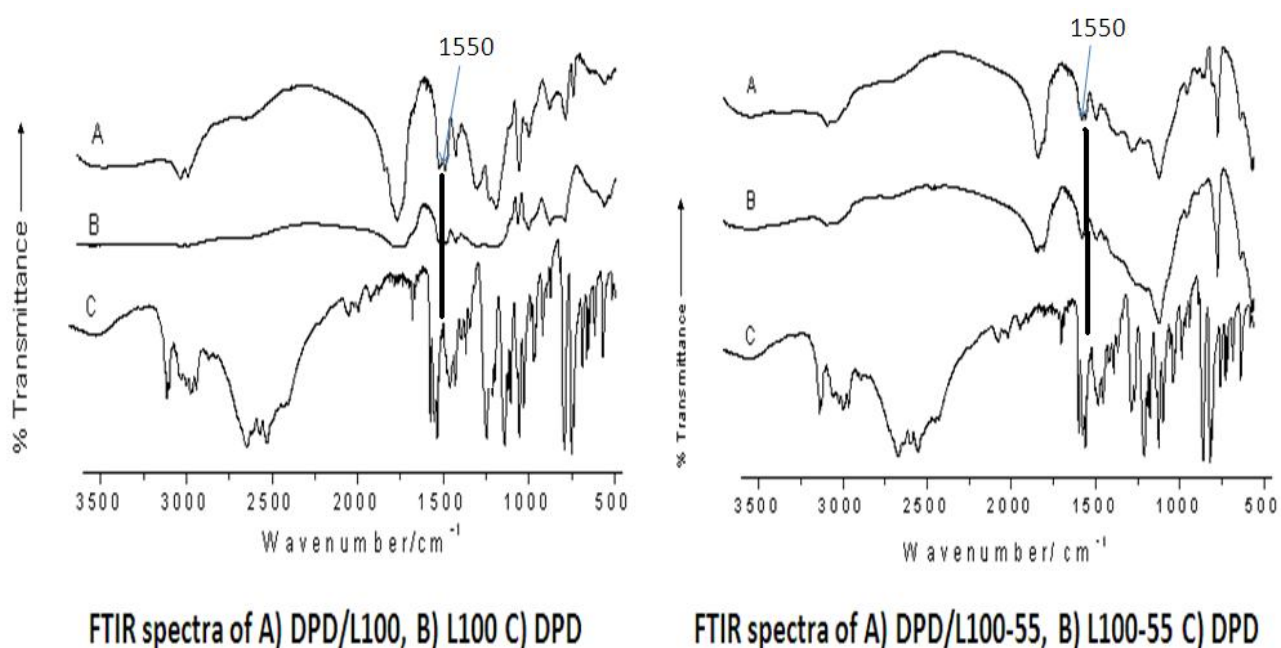


Fig 7.4b: FT-IR spectra of DPD extruded formulations.

3.7 X-ray Photoelectron Spectroscopy (XPS) analysis

In order to show the surface elemental ratios of PRP, DPD, polymers and the extruded formulations determined experimentally by XPS various surveys are depicted in Fig.7.5a-b as a comparison with the anticipated theoretical values derived from the structural formula [38].

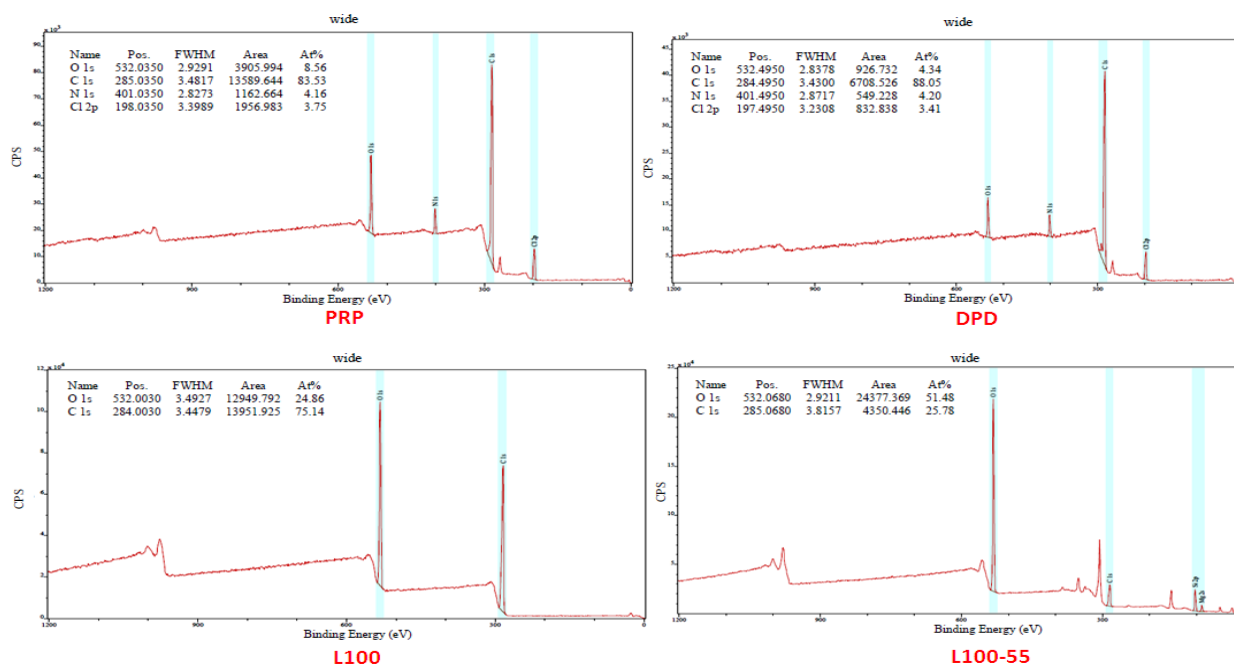


Fig 7.5a: XPS surveys of pure PRP, DPD, L100 and L100-55.

According to the surveys the PRP/L100, PRP/L100 55, DPD/L100 and DPD/L100-55 showed the amount of N atoms as 0.63%, 0.23%, 0.53% and 0.21%, respectively simply indicating lower amount of N atom present in the final extruded formulations.

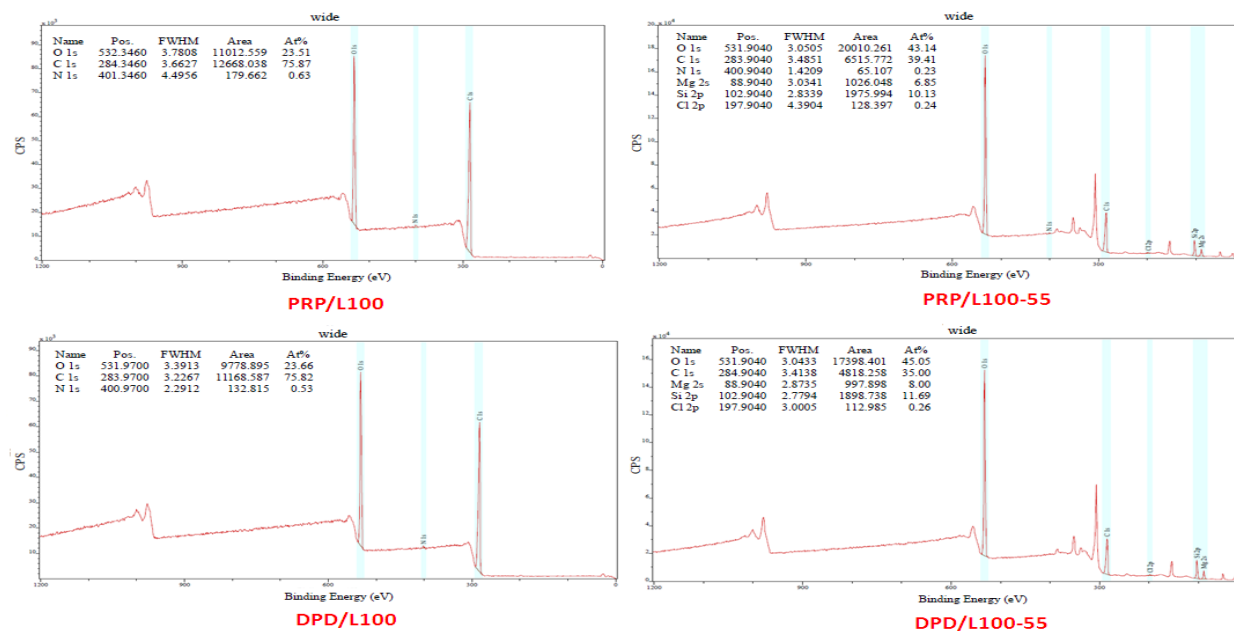


Fig. 7.5b: XPS surveys of extruded formulations.

The N (1s) binding energy (BE) of ~402.035 eV (Fig. 7.5c) in PRP and of ~402.5 eV (Fig. 5d) in DPD suggests the protonation of the NH⁺ group while the slightly higher values of N (1s) energy (~402.8 eV) in PRP/L100 extrudates represents further protonation effect of N

atom as NH_4^+ . This observed N 1s peak at BE= ~ 402.80 eV is in good agreement with the previously observed protonation of amide group by Beamson and Briggs [33]. The BE peak at ~ 402.80 eV (higher than typically observed for amines BE= ~ 399 eV - 400.5 eV and much more for $-\text{NH}_2^+$ group) for N1s is an indication of C-O-NH_2^+ structure whereas the O atom peak at ~ 534.40 eV shows the same [18, 20]. These results strongly indicate an interaction between the amide group of the API and ester/carboxyl group of the polymer (L100) through the available H-interactions or hydrogen bridges (Fig. 7.5c).

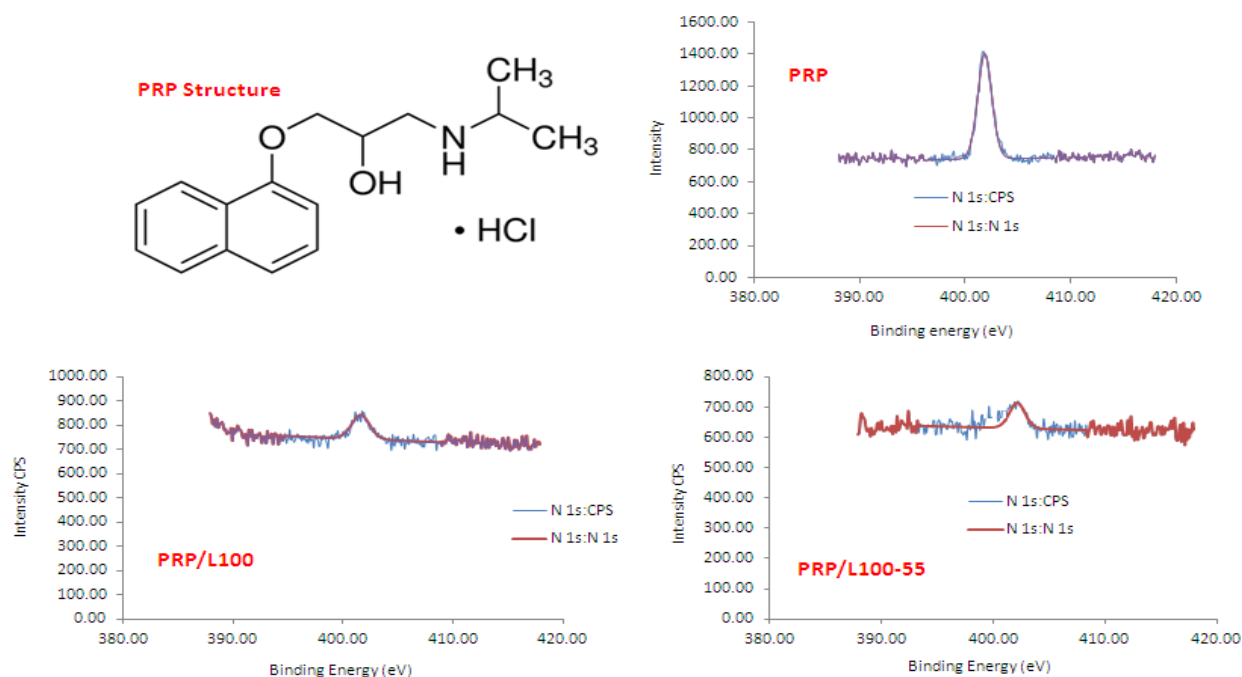


Fig. 7.5c: N 1s BE peaks of PRP and extruded formulations.

Similarly, N 1s peaks from PRP/L100-55 and DPD/L100-55 also complement the observations from PRP/L100 and DPD/L100 formulations. The N (1s) energy of ~ 402.9 eV in DPD/L100 formulation suggests protonation of the amide group as observed for aforementioned PRP/L100 formulation. The BE peak at ~ 402.90 eV (Fig. 7.5d) for N 1s is an indication of C-O-NH_2^+ structure with longer peak shift than that of PRP/L100. As before, we concluded that a strong interaction between the amide group of API and ester/carboxyl group of polymer through the available H-interactions has taken place.

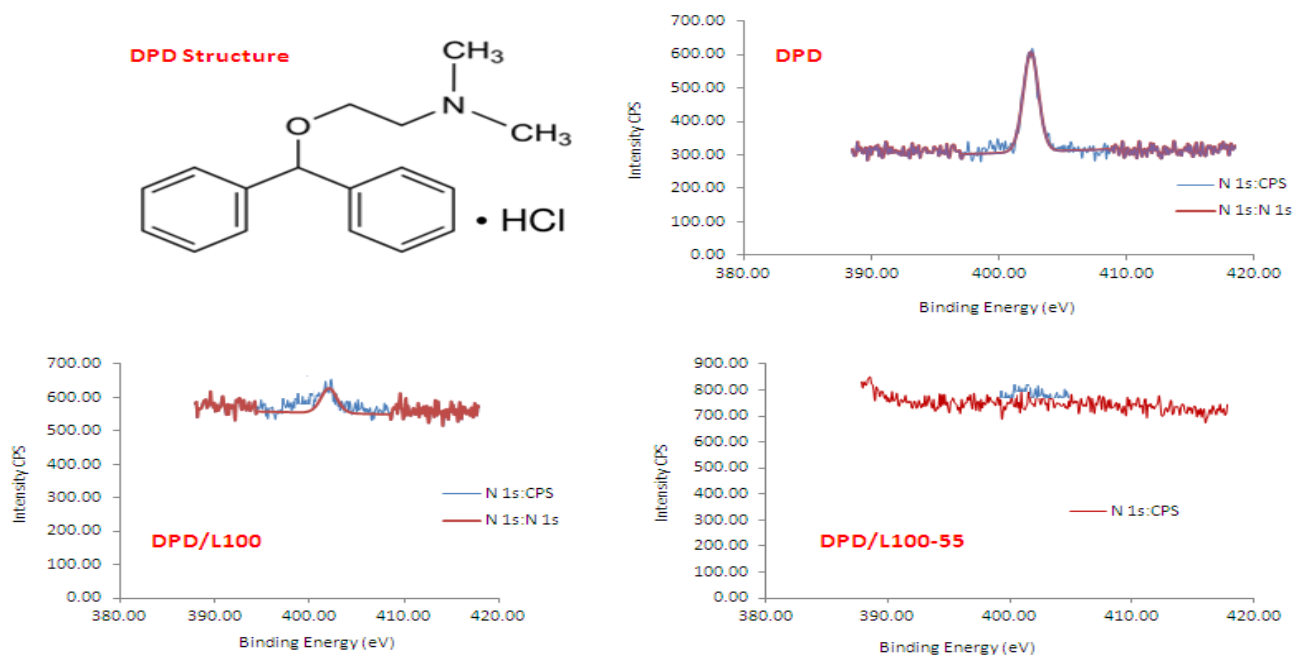


Fig. 7.5d: N 1s BE peaks of DPD and DPD based extruded formulations.

Furthermore, the calculations of N coefficients for all extruded formulations indicated the strength of the intermolecular interactions within the solid dispersions. The calculated N coefficient for all extruded formulations is summarized in table 3. From the Table 7.5 it quite clearer that the N coefficient values for L100 systems are smaller than that of L100-55 systems. It has been reported that the lower the N-coefficient, the higher the amount of protonised N atoms in cationic drugs, the stronger the interaction between polymer and APIs [39].

Table 7.5: Estimated N coefficient values of different formulations.

Formulations	N 1s Binding Energy		Calculated N Coefficient
	1 st Fitting (eV)	2 nd Fitting (eV)	
PRP/L100	63	100	0.63
PRP/L100-55	58.51	49.49	1.18
DPD/L100	45.97	54.03	0.85
DPD/L100-55	51.19	48.81	1.05

8.0 Conclusions

The presence of intermolecular interactions has successfully led the HME to be a robust technique to form solid dispersions of both APIs into polymer matrix. The existence of amorphous APIs into the polymer matrices has been confirmed by thermal analysis while an *in vivo* and *in vitro* taste masking analysis has substantially complemented each other showing the masking potential of L100 better than L100-55. The molecular modelling outlined a possible presence of intermolecular interactions between drug and polymer molecules and estimated the strength. The findings from FT-IR and XPS analysis has finally confirmed the mechanism of the interaction through H-bonding between the carboxyl group of the anionic methacrylate co-polymer and the amide group of the active substances as well as the interaction strength. These studies finally confirm that the stronger the integrations better the taste masking in an opposite charged drug/polymers based extruded solid dispersions.

9.0 References

1. Douroumis DD, Gryczke A, Schminke S. Development and evaluation of cetirizine HCl taste-masked oral disintegrating tablets. *AAPS PharmSciTech*. 2011; 12: 141–151.
2. Maniruzzaman M, Boateng JS, Bonnefille M, Aranyos A, Mitchell JC, Douroumis D. Taste masking of paracetamol by hot-melt extrusion: an *in vitro* and *in vivo* evaluation. *Eur. J Pharm. Biopharm.* 2012; 80(2): 433-42.
3. Ayenew Z, Puri V, Kumar L, Bansal AK. Trends in pharmaceutical taste masking technologies: a patent review. *Recent Pat. Drug Deliv. Formul.* 2009; 3: 26–39.
4. Bora D, Borude P, Bhise K. Taste masking by spray-drying technique. *AAPS PharmSciTech*. 2008; 9: 1159–1164.
5. Al-Omran MF, Al-Suwayeh SA, El-Helw AM, Saleh SI. Taste masking of diclofenac sodium using microencapsulation. *J Microencapsul.* 2002; 19:45–52.
6. Shah PP, Mashru RC, Rane YM, Thakkar A. Design and optimization of mefloquine hydrochloride microparticles for bitter taste masking. *AAPS PharmSciTech*. 2008; 9:377–389.
7. Albertini B, Cavallari C, Passerini N, Voinovich D, González-Rodríguez ML, Magarotto L, Rodriguez L. Characterization and taste-masking evaluation of

- acetaminophen granules: comparison between different preparation methods in a high-shear mixer. *Eur. J Pharm. Sci.* 2004; 21:295–303.
8. Mazen H, York P. Particle formation methods and their products. *US Patent.* 2006;7(115):280
 9. Michalk A, Kanikanti VR, Hamann HJ, Kleinebudde P. Controlled release of active as a consequence of the die diameter in solid lipid extrusion. *J Cont. Rel.* 2008; 132: 35–41.
 10. Gryczke A, Schminke S, Maniruzzaman M, Beck J, Douroumis D. Development and evaluation of orally disintegrating tablets (ODTs) containing Ibuprofen granules prepared by hot melt extrusion. *Coll. Surf B. Bioin.* 2011; 86(2):275-84.
 11. Vaassena J, Bartscherb J, Breitzkreutz J. Breit Taste masked lipid pellets with enhanced release of hydrophobic active ingredient. *Int. J of Pharm.* 2012; 429:99– 103
 12. Woertz K, Tissen C, Kleinebudde P, Breitzkreutz J. Taste sensing systems (electronic tongues) for pharmaceutical applications. *Int. J. Pharm.* 2011; 417: 256– 271
 13. Woertz K, Tissen C, Kleinebudde P, Breitzkreutz J. Performance qualification of an electronic tongue based on ICH guideline Q2. *J. Pharm. Biomed. Anal.* 2010; 51: pp. 497–506.
 14. Bonferoni, MC, Rossi S, Ferrari F, Bettinetti GP, Caramella C. Characterization of a diltiazem–lambda carrageenan complex. *Int. J. Pharm.* 2000; 200: 207–216.
 15. Lelham, NC, Sundelof LO. Some aspects on characterization and properties of charged polysaccharides. An investigation of the system carrageenan/amitriptyline/water with relation to amphiphile adsorption and charge density. *Int. J. Pharm.* 1995; 115: 103–111.
 16. Takka S. Propranolol hydrochloride/anionic polymer binding interaction. *Il Farmaco.* 2003; 58: 1051-1056.
 17. Puttipipatkachorna S, Nunthanidb J, Yamamoto K, Peckd GE. Drug physical state and drug–polymer interaction on drug release from chitosan matrix films. *J Cont. Rel.* 2011; 75:143–153.
 18. Baer DR, Engelhard MH. XPS analysis of nanostructured materials and biological surfaces. *J Elec. Spec. Rela. Pheno.* 2010; 178: 415–432.
 19. Li J, Masso JJ, Guertin JA. Prediction of drug solubility in an acrylate adhesive based on the drug–polymer interaction parameter and drug solubility in acetonitrile. *J Cont. Rel.* 2003; 83: 211–221.

20. Davies MC, Wilding IR, Short RD, Khan MA, Watts JF, Melia CD. An analysis of the surface chemical structure of polymethacrylate (Eudragit) film coating polymers by XPS. *Int. J Pharm.* 1989; 57: 183-187.
21. Flory PJ. *Principles of polymer chemistry*. Ithaca, New York: Cornell University Press. 1953
22. Marsac PJ, Shamblin SL, Taylor LS. Theoretical and practical approaches for prediction of drug-polymer miscibility and solubility. *Pharm Res.* 2006; 23:2417–2426.
23. Friesen DT, Shanker R, Crew M, Smithey DT, Curatolo WJ, Nightingale JAS. 2008. Hydroxypropyl methylcellulose acetate succinate-based spray-dried dispersions: An overview. *Mol. Pharm.* 2008; 5:1003–1019.
24. Nishi T, Wang TT. Melting point depression and kinetic effects of cooling on crystallization in poly (vinylidene fluoride)-poly (methyl methacrylate) mixtures. *Macromolecules.* 1975; 8:909–915.
25. Hildebrand J, Scott R. *Solubility of non-electrolytes*. 3rd ed. New York: Reinhold. 1950.
26. Maniruzzaman M, Rana MM, Boateng JS, Mitchell JC, Douroumis D. Dissolution enhancement of poorly water-soluble APIs processed by hot-melt extrusion using hydrophilic polymers. *Drug Dev. Ind. Pharm.* 2012. In press.
27. Bagley EB, Nelson TP & Scigliano JM. Three-dimensional solubility parameters and their relationship to internal pressure measurements in polar and hydrogen bonding solvents. *J Paint. Technol.* 1971; 43: 35-42.
28. WMA Declaration of Helsinki - Ethical Principles for Medical Research Involving Human Subjects. 59th WMA General Assembly, Seoul, Korea, October 2008.
29. Gauss View, Version 5, Roy Dennington, Todd Keith and John Millam, Semichem Inc. Shawnee Mission KS, 2009.
30. Frisch MJ, Trucks GW, Schlegel HB, Scuseria GE, Robb MA, Cheeseman JR et al. *Gaussian 09, Revision B.1*, Gaussian, Inc., Wallingford CT, 2009.
31. Zhao Y, Truhlar DG. The M06 suite of density functionals for main group thermochemistry, thermochemical kinetics, noncovalent interactions, excited states, and transition elements: two new functionals and systematic testing of four M06-class functionals and 12 other functional. *Chem. Acc.* 2008; 120: 215– 241.

32. Boys SF, Bernardi F. The calculation of small molecular interactions by the differences of separate total energies. Some procedures with reduced errors. *Mol. Phys.* 1970; 19:553– 566.
33. Beamson G, Briggs D. High resolution XPS of organic polymers: The Scienta ESCA 300 Database. *J. Chem. Educ.* 1993; 70: PA25.
34. Zhao Y, Inbar P, Chokshi HP, Malick W, Choi DS. Prediction of the thermal phase diagram of amorphous solid dispersions by flory–huggins theory. *J pharm. Sci.* 2011; 100, 8: 3196-3207.
35. Nair R, Nyamweya N, Goñen S, Martinez-Miranda LJ, Hoag SW. Influence of various drugs on the glass transition temperature of poly(vinylpyrrolidone): a thermodynamic and spectroscopic investigation, *Int. J. Pharm.* 2001; 225: 83-96.
36. Avram M, Mateescu GH. *Infrared Spectroscopy: Applications in Organic Chemistry*, Wiley/Interscience, New York, 1996.
37. Lee HK, Hajdu J, McGoff P. Propranolol-/methacrylic acid copolymer binding interaction, *J. Pharm. Sci.* 1991; 80:178-180.
38. Vandencastele N, Reniers F. Plasma-modified polymer surfaces: Characterization using XPS. *J Elec. Spec. Rela. Pheno.* 2010; 178–179: 394–408.
39. Gryckze A. Eudragit polymers and hot-melt extrusion brochure. Degussa. Germany 2006.

CHAPTER 8: SUSTAINED RELEASE HYDROCORTISONE TABLETS PROCESSED BY HOT-MELT EXTRUSION (HME)

1.0 Introduction

As noted previously, hot-melt extrusion (HME) has been developed as a novel technique for the formulation of oral solid dosage forms in pharmaceutical industries in recent years [1]. A wide variety of downstream processing equipment allows the manufacture of various solid dosage forms including pellets, granules, tablets, capsules and films with different pharmaceutical applications. These solid dosage forms can provide sustained, modified or targeted release by controlling both formulation and processing parameters. Despite the fact that initial research developments have focused on the effects of formulation and processing variables on the properties of final dosage forms, [2-5] more recent investigations have focused on the use of HME as a novel manufacturing technology of solid molecular dispersions through to the development of sustained release formulations as well as paediatric formulations [6,7]. Early studies through HME processing have described the preparation of matrix mini-tablets which was followed by further investigations into the properties of sustained release mini-matrices manufactured from ethyl cellulose, HPMC and ibuprofen [8,9]. Extruded mini tablets showed minimized risk of dose dumping and reduced inter- and intra-subject variability. Very recently, vegetable calcium stearate (CaSt) was reported to be used in the development of retarded release pellets using as a thermoplastic excipient processed through HME, where pellets with a paracetamol loading of 20% released only 11.54% of the drug after 8 hours due to the significant densification of the pellets. As expected, the drug release was influenced by the pellet size and the drug loading [10]. A microbicide intravaginal ring (IVRs) IVR was prepared and developed from polyether urethane (PU) elastomers for the sustained delivery of UC781 (a highly potent non-nucleoside reverse transcriptase inhibitor of HIV-1). PU IVRs containing UC781 were fabricated using a hot-melt extrusion process [11].

Chrono-pharmaceutical dosage forms are designed to release the drug at the desired time and improve therapeutic efficacy and patient compliance. Time-release formulations could be a useful tool in effecting chrono-pharmacotherapy because their unique drug release properties could take advantage of circadian rhythms in physiologic and pathologic functions. HME technique could be applied as a robust tool to formulate sustained release formulations [12, 13]. Cortisol is normally produced by the adrenal glands which regulated by the brain's hypothalamus and the pituitary gland. The hypothalamus sends "releasing hormones" to the pituitary gland which responds by secreting other hormones that regulate growth, thyroid,

testosterone and adrenal function. One of the pituitary gland's main functions is to secrete ACTH (adrenocorticotropin), a hormone that stimulates the adrenal glands. When the adrenals receive the pituitary's signal in the form of ACTH, they respond by producing cortisol. Completing the cycle, cortisol then signals the pituitary to lower secretion of ACTH. Hydrocortisone (HCS) is a synthetic form of corticosteroid administered when the body is deficient in the natural hormone. It is used to treat allergy, inflammation, asthma, collagen diseases, adrenocortical deficiency, shock and some neoplastic conditions including acute lymphoblastic leukaemia. It generally possesses low bioavailability when they are orally administered and topically applied whereas some patients are found to have severe allergic response towards intravenous injection ^[14].

The drug release rate is difficult to control in all existing conventional sustained-release tablets as drug absorption is influenced heavily by its transition rate in the gastrointestinal tract, resulting in wide variations in the oral bioavailability ^[15]. It has been reported that a multiple-unit dosage form can overcome this problem to a certain extent; however, it requires a primitive manufacturing technology ^[16, 17]. It is therefore the purpose of this study to implement HME to develop a new dosage form that overcomes these biological and technological problems. A formulation development study on the novel HCS sustained-release tablets is hereby reported along with the analysis of the release mechanism of all prepared sustained-release tablets.

2.0 Materials and methods

2.1 Materials

Hydrocortisone (HCS) was purchased from Sigma Aldrich (London, UK). Ethyl Cellulose N10 (EC N10) and Ethyl Cellulose EP7 (EC P7) were kindly donated by Harceulis (Darmstadt, Germany) and Colorcon Ltd respectively. Eudragit S100 (S100) was provided by Evonik Industries (Darmstadt, Germany). SiO₂ and MgSt were purchased from Sigma Aldrich, UK. The HPLC solvents were of analytical grade and purchased from Fisher Chemicals (UK). All materials were used as received.

2.2 Calculation of solubility parameters

[Please see Chapter 7, Section 2.2 for details].

2.3 Preparation of formulation blends and hot-melt extrusion processing

HCS formulations with EC N10 and EC P7 were mixed properly in A Turbula (TF2, Basel) mixer in 100 g batches for 10 min each, prior to the extrusion process. Drug/polymer ratios used were 10-30:90-70 wt/wt for both polymers. Extrusion of all formulations were performed using a Randcastle single-screw extruder (RCP0625) equipped with a 5-mm rod die in 112°C/132°C/132°C/135°C/140°C (from feeding zone → Die) temperature profiles. The screw speed maintained for all extrusions was 15 rpm. The extrudates (strands) produced were ground by using a ball milling system with a rotational speed of 400 rpm for 5mins each to obtain granules (<500 µm). Out of all different drug/polymer extruded formulations prepared, 10/90 wt/wt ratio was selected for both polymers in order to justify the active dosage of HCS in commercial products (10 mg).

2.4 Scanning electron microscopy (SEM) and particle size analysis

In order to examine the surface morphology of drug, polymers and extrudates by SEM the samples were mounted on an aluminium stage using adhesive carbon tape and placed in a low humidity chamber prior to analysis. Samples were coated with gold–palladium prior to the scans, and microscopy was performed using a LEO Supra 35 (Cambridge Instruments, S630F). The system was operated at an accelerating voltage of 5 kV.

2.5 Differential scanning calorimetry (DSC)

The physical state of the pure drug, physical mixtures and extrudates were examined by using a Mettler-Toledo 823e (Greifensee, Switzerland) differential scanning calorimeter. Samples were prepared in sealed aluminium pans (2-5 mg) with a pierced lid. The samples were heated at 10°C/min under nitrogen atmosphere in a temperature range between -40 and 250°C.

2.6 X-ray powder diffraction (XRPD)

XRPD was also used to assess the solid state (crystalline or amorphous) of the extrudates where samples of pure and loaded APIs were evaluated using a Bruker D8 Advance (Germany) in theta-theta mode, Cu anode at 40 kV and 40 mA, parallel beam Goebel mirror, 0.2 mm exit slit, LynxEye Position Sensitive Detector with 3 degree opening and Lynx Iris at 6.5 mm, sample rotation at 15rpm. The sample was scanned from 5 to 40 degrees 2-theta with a step size of 0.02 degrees 2-theta and a counting time of 0.2 seconds per step; 176 channels active on the PSD making a total counting time of 35.2 seconds per step.

2.7 Tablet preparation and characterization

Extruded granules were used to prepare 10mm diameter robust tablets by using a Oyester Manesty Trilayer tablet press with a final weight of 250 mg (10 mg HCS). All excipients used for the tablets were adjusted as in Table 8.1. All prepared tablets were then characterised to determine the hardness, thickness and friability. Enteric coating solution (15-25%) was then prepared by dissolving a pH dependent methacrylic polymer (Eudragit) in organic solvents (acetone, isopropyl alcohol) followed by addition of 20% plasticizer (PEG 2000) under magnetic stirring until a clear solution was made. FD&C No 2 blue dye was added and the solution was homogenized for 10 min using an Ultra Turrax homogenizer. Coating process was conducted by uniform spraying (Copley pan coater) of the coating solution onto the tablets. The process parameters were adjusted as pump flow rate 2.0 rpm, pressure 4 psi, fan speed 77%, agitation 44%, temperature 45°C. 15% coating showed better uniformity and optimum dissolution rates therefore all coated tablets will be referred as 15% coating throughout this chapter.

Table 8.1: Tablet contents for each of the extrudates.

Tablet Content	Percentage (%)	Composition	Weight (g)
Extruded Material (HCS/EC N10/ EC P7)	40.0		40.0
Eudragit RSPO	5.0		5.0
Lactose	28.5		28.5
HPMC 603	25.0		25.0
Silicon Dioxide (Sio2)	0.5		0.5
Magnesium Stearate	1.0		1.0
Total	100.0		100.0

2.8 *In vitro* drug release studies

In vitro dissolution study was carried out by using a Varian 705 DS dissolution paddle apparatus (Varian Inc. North Carolina, US) at 100 rpm and $37 \pm 0.5^\circ\text{C}$. The dissolution

medium pH was maintained as 1.2 by using 750 ml of 0.1 M hydrochloric acid for 2 hr. After 2 hr operation, 150 ml of 0.20 M solution of dehydrogenate sodium ortho phosphate was added into the vessel to give the final pH of 6.8 and the temperature equilibrated to 37°C. At predetermined time intervals, samples were withdrawn for HPLC assay and replaced with fresh dissolution medium. All dissolution studies were performed in triplicate.

2.9 HPLC analysis

The release of HCS from the prepared tablets was determined by HPLC. An Agilent Technologies system equipped with a HYPROME 4889, 5 µm x 150 mm x 4 mm column at 243 nm was used for the HCS HPLC assay. The mobile phase consisted of methanol/water/acetic acid (54:45:1, v/v/v). The flow rate was 1.5 ml/min and the retention time of HCS was about 4 minutes. The HCS calibration curve ($R^2=0.999$), at concentrations varying from 10 µg/ml to 50 µg/ml, were used to evaluate all the samples with 20 µl injection volume.

2.10 Analysis of drug release mechanism

Zero order kinetics, first order kinetics, Hixson–Crowell, Higuchi and Korsmeyer–Peppas models were used for the analysis of the dissolution mechanism taking the rate constant obtained from these models as an apparent rate constant. The drug release patterns from both coated and uncoated tablets were analyzed by release kinetics theories ^[18-22], as follows:

$$\text{Zero order kinetics: } F_t = K_0 t \quad (8.1)$$

Where F_t represents the fraction of drug released in time t and K_0 the apparent release rate constant or zero order release constant.

$$\text{First order kinetics: } \ln(1 - F) = -K_1 t \quad (8.2)$$

Where F represents the fraction of drug released in time t and K_1 is the first order release constant.

$$\text{Higuchi model: } F = K_2 t^{1/2} \quad (8.3)$$

Where F represents the fraction of drug released in time t and K_2 is the Higuchi dissolution constant.

$$\text{Hixson–Crowell model: } W_0^{1/3} - W_t^{1/3} = K_s t \quad (8.4)$$

Where, W_0 is the initial amount of drug in the pharmaceutical dosage form, W_t is the remaining amount of drug in the pharmaceutical dosage form at time t and K_s is a constant incorporating the surface volume relation.

Dividing Eq. (8.4) by $W_0^{1/3}$ and simplifying: $(1-F)^{1/3} = 1 - K_3 t$ (8.5)

Where $F=1 - (W_t/W_0)$ and F represents the drug dissolved fraction at time t and K_3 is the release constant). When this model is used, it is assumed that the release rate is limited by the drug particle dissolution rate and not by the diffusion that might occur through the polymeric matrix.

Korsmeyer–Peppas model: $F = K_4 t^n$ (8.6)

Where K_4 is a constant incorporating the structural and geometric characteristics of the drug dosage form, n is the release exponent (e.g. zero order release when $n = 1$, for tablets $n = 0.89$), indicative of the drug release mechanism and F represents the drug dissolved fraction at time t . This model is generally used to analyze the release of which mechanism is not well known or when more than one type of release phenomena is involved.

3.0 Results and discussion

3.1 Solubility parameters and extrusion process

The calculated solubility parameter of HCS, EC N10 and EC P7 were 22.60, 25.61 and 25.27 MPa^{1/2}, respectively. The difference between the calculated solubility parameters of the polymers and the drug indicates that HCS is likely to form solid dispersions with both polymers EC N10 and EC P7. By using the Van Krevelen/Hoftyzer equation, the $\Delta\delta$ values for HCS/EC N10 and HCS/EC P7 were 3.01 and 2.67 MPa^{1/2}, respectively.

3.2 Scanning electron microscopy (SEM)

Surface morphology was examined by SEM for both the drug and extrudates. The extrudates containing both polymers exhibited no drug crystals on the extrudate surface with HCS (Fig. 8.1). Similarly, the absence of HCS crystals on the surface in all drug/ polymer extrudates indicates the presence of amorphous solid dispersions of the API into the polymer matrices [13]. Thus, the SEM observations were quite sensitive to elucidate the presence of drug/polymers amorphous solid dispersions by complementing the thermal investigations (DSC, XRD).

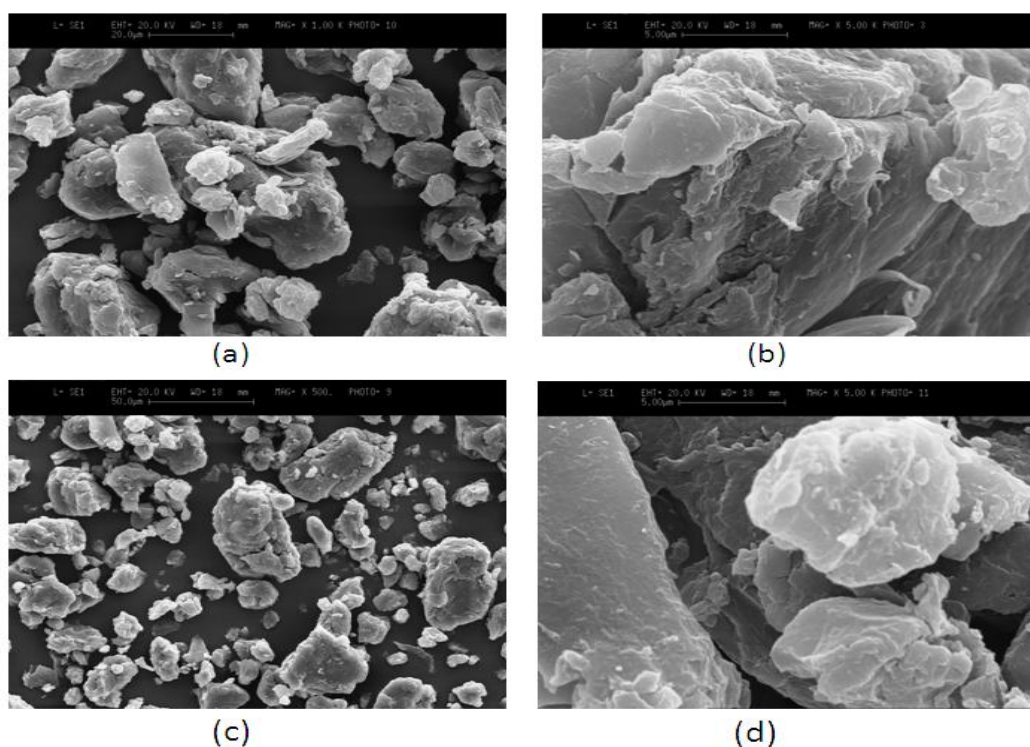


Fig. 8.1: SEM images of [(a), (b)] HCS/ EC N10 (magnification x500 and 10K, respectively) and [(c), (d)] HCS/EC P7 extruded formulations (magnification x500 and 10K, respectively).

3.3 Differential scanning calorimetric (DSC)

Differential scanning calorimetry (DSC) was used to analyse the solid state of pure API, polymers, their physical mixtures (PM) and active extruded formulations (EXT). The overall findings from DSC results are summarized in Figs 8.2a and b. The DSC scan of pure HCS in Fig. 8.2a showed an endothermic transition corresponding to its melting point [23] at 226.12°C ($\delta H = 114.92$ J/g, peak height 17.80 mW) with an onset at 223.82°C. Similarly, the pure polymers showed T_g at 133.01°C corresponding to T_g of EC N10 and 117.61°C corresponding to T_g of EC P7, respectively (Fig. 8.2a). Even though, all binary physical drugs/polymer blends exhibit endothermic peaks (Fig 8.2b) corresponding to the initial substances at slightly shifted temperatures indicating the drug existence in its crystalline form, the melting peaks were absent in all extruded formulations. In the drug/polymer physical mixture (PM) of HCS/ EC N10 formulation, two endothermic peaks were visible (Fig 8.2b), one at 202.87°C ($\delta H = 5.38$ J/g) corresponding to the melting peak of crystalline HCS present in the mixture and another one at lower temperature range at 72.27°C corresponding to the T_g of EC N10. Similar transitions were observed in the HCS/EC P7 system as well where the endothermic peak at 185.86°C ($\delta H = 13.97$ J/g) corresponds to the

HCS melting transition and 61.66°C to the T_g of EC P7. This huge shift of the melting peak of HCS in HCS/ EC P7 is due to the lower glass transition temperature value compared to that of EC N10. This also suggests that EC P7 would be more effective than EC N10 for processing HCS below the melting temperature. Furthermore, the extruded formulations exhibited a broad endothermic peak ranging from 47.83 to 49.19 °C indicating the presence of the drugs in their amorphous forms. It has been observed previously [23] that the position of shifted endothermic peak in the extruded formulations is in between the thermal transitions of amorphous drug and polymers.

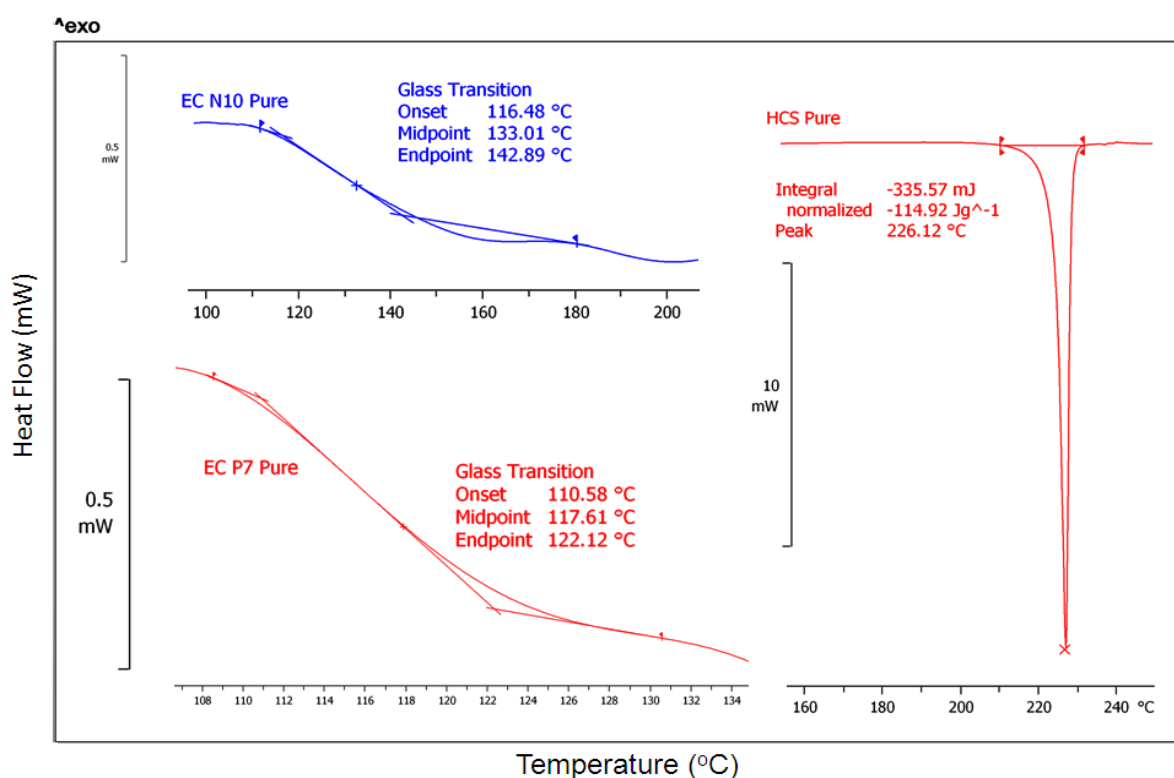


Fig. 8.2a: DSC transitions of pure polymers and drug.

This thermal phenomenon complements the formation of solid dispersion of miscible HCS in the amorphous polymer matrices [24]. Nevertheless, the characteristic peak of HCS cannot be found in the heating curve of the extruded formulations, indicating that the solid state of the extruded formulations are different having the HCS present in amorphous form compared to the drug/polymer physical mixtures.

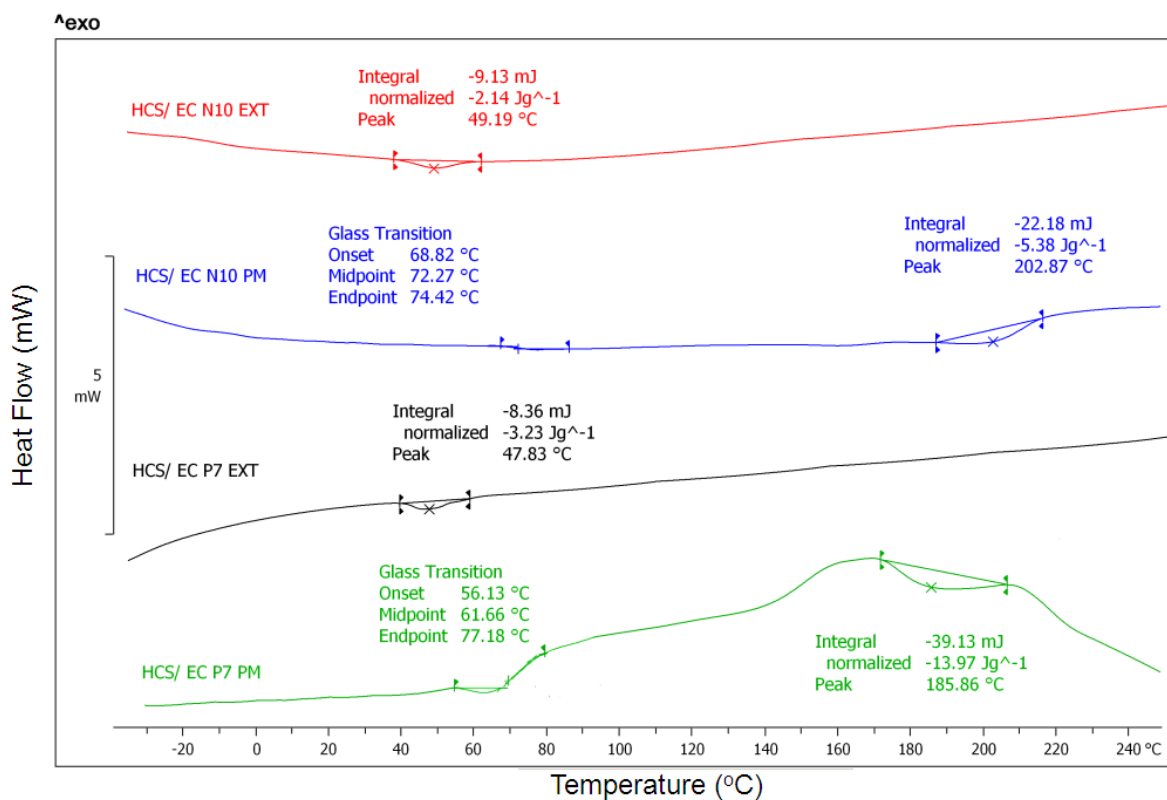


Fig. 8.2b: DSC transitions of HCS/EC N10 and HCS/ EC P7 physical mixtures (PM) and extruded formulations (EXT).

3.4 X-ray powder diffraction (XRPD) analysis

The drug – polymer extrudates, including pure drugs and physical mixtures of the same composition were studied by X–ray analysis and the diffractograms were recorded to examine the API crystalline state. As depicted in Fig. 8.3 the diffractograms of pure HCS presented distinct peaks at 5.75, 14.50, 16.08, 17.42, 18.79, 19.42, 23.22, 29.21, 30.14 2θ values.

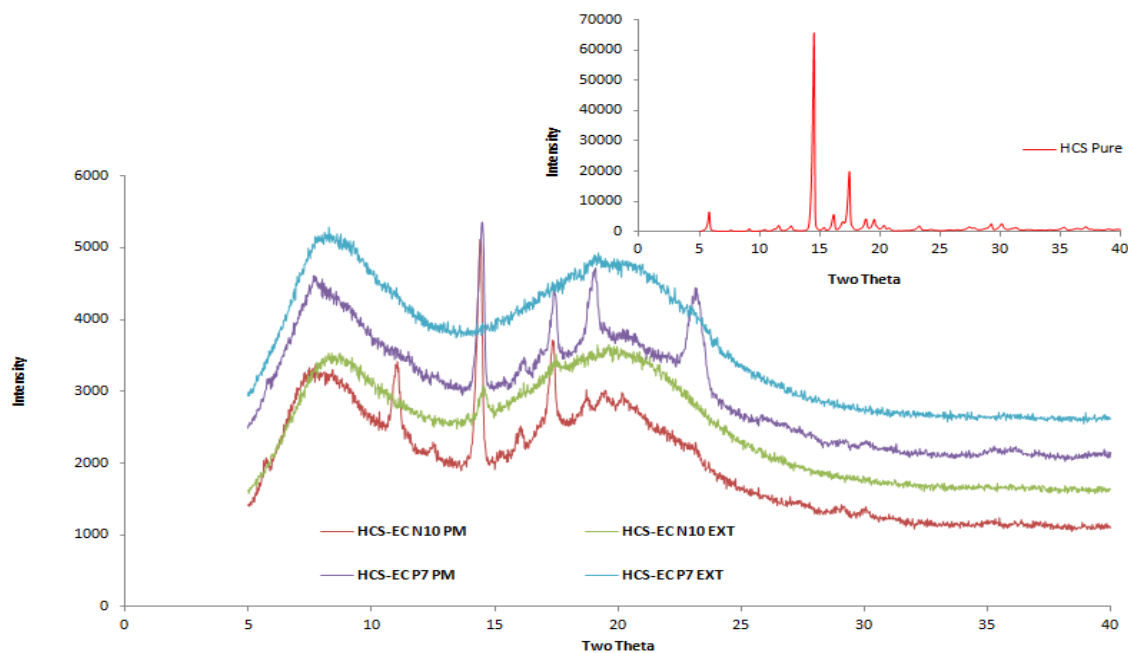


Fig. 8.3: XRD diffractograms of extruded formulations and binary mixtures [PM = physical mixtures and EXT = extruded formulations].

The physical mixture of both formulations presented identical peaks at lower intensities suggesting that both drugs retain their crystalline properties. No crystalline distinct peaks were found in the extruded formulation in EC P7 systems ($\geq 99\%$ amorphous). In contrast almost no distinct intensity peaks (apart from a very low intensity peak at about 15 2θ position) for HCS was observed in the diffractogram of the extruded formulation in EC N10 system ($\geq 97\%$ amorphous). The absence of HCS intensity peaks indicates the presence of amorphous APIs in the extruded solid dispersion.

3.5 Tablet characterization

Results obtained from tablet characterization are summarized in Table 8.2. All prepared tablets prepared were 250 mg in weight with a mean thickness of 3.44 mm ($SD = \pm 0.012$) for HCS/EC N10 formulations and 3.50 mm ($SD = \pm 0.010$) for HCS/ EC P7. The difference in the thickness of two different polymeric systems is attributed to the difference of the compactability of the powder formulations. This phenomenon has also been observed by the observed hardness values of the tablets in two different polymers. As compactability is directly proportional to hardness, the HCS/EC P7 showed higher hardness value compared to that EC N10. It is always preferential to have the hardness of normal sustained release tablet

in the range of 10-12 kP. However, in our case we observed slightly lower hardness value than expected but the all tablets still seemed to be very robust as the weight loss percentage after 10 min in friability test was only 0.01. This could be due to the presence of elastic polymers (Eudragit ESPO) in the final tablet composition. The elasticity present in the tablets has finally managed to attribute this lower hardness value with less friability and thus higher robustness.

Table 8.2: Drug/polymer’s description; tablet characterization.

Form	Weight (mg)	Thickness (mm)	Average (mm)/SD	Hardness (kP)	Average (mm)/SD	Friability (%)
HCS / EC N10	250.0	3.45	3.44/±0.012	6.2	6.0/±0.15	0.01
	250.0	3.43		6.0		
	250.0	3.45		5.9		
HCS / EC P7	250.0	3.50	3.50/±0.010	6.1	6.1/± 0.10	0.01
	250.0	3.49		6.2		
	250.0	3.51		6.0		

3.6 *In vitro* dissolution studies

Polymeric coating of the compressed tablets with 15% pH dependent polymer proved sufficient to provide 2 hrs lag time in an acidic medium (Fig. 8.4). The composition of the matrix core of the final tablet formulation included a combination of hydrophilic (HPMC) and lactose along with extruded ethylcellulose to control HCS release patterns. The combination of all three ingredients provided retarded release profiles of HCS at higher pH values when the dissolution of the coating layer occurred ^[25]. The release profile was also controlled from the polymer amount coated on the surface of the matrix tablet.

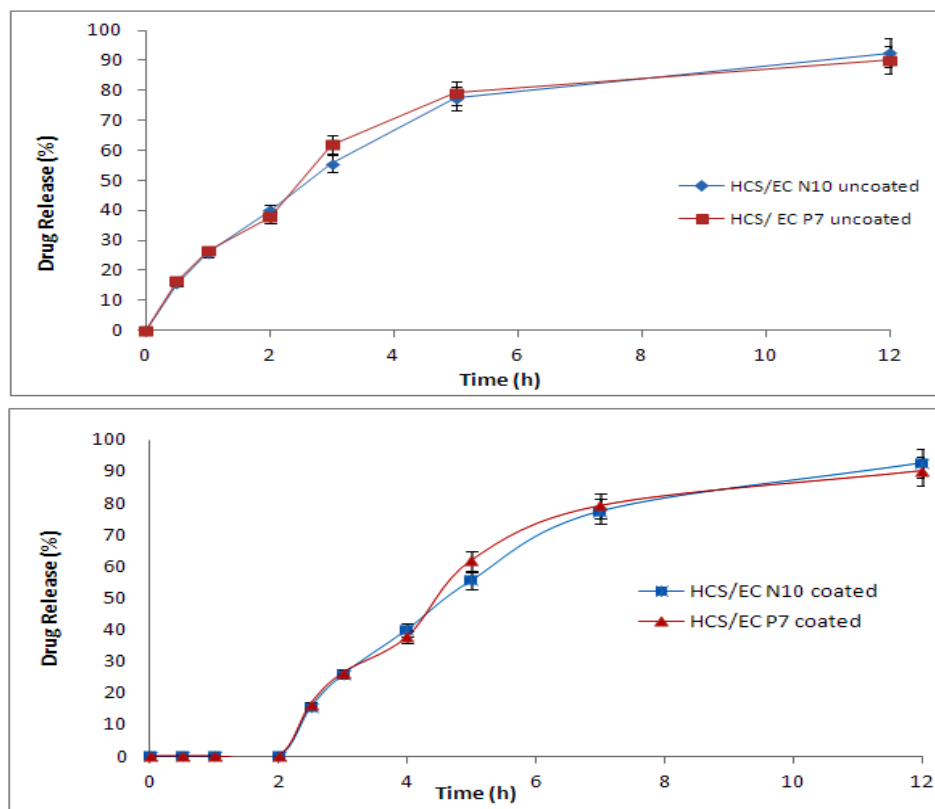


Fig. 8.4: HCS release profiles in both coated and uncoated tablets. Each result shows the mean \pm S.D. ($n = 3$).

The release mechanism from the tablets can be described as a diffusion process of the drug through the slow release polymers matrix. The slow dissolving nature of EC polymers hinders the dissolution medium penetration and consequently controls the drug dissolution and diffusion rate [25]. While processing through HME the active substance was covered by EC matrix which resulted in retarded release of HCS over 12 hrs. Moreover, the polymeric coating level indicated a controlling effect due to its slow dissolution, irrespective of the tablet composition. Lower coating levels (15%) allowed greater penetration of the dissolution medium.

3.7 Analysis of release mechanism

Analysis was performed by the above equations using water as the dissolution test medium. Obtained results for release rate constants as well as R^2 values for all tablets are summarized in table 8.3. Neither coated nor uncoated tablets fit with equation (8.1), zero order release model, which represents zero order kinetics. Concerning equations (8.2)–(8.6), regression analyses were performed in the ranges in which linearity was observed. The first order kinetics model plot shows the relationship between the logarithm of the drug residual

rate and time on the basis of Eq. (8.2). Fig. 8.5a shows the results with both coated and uncoated tablet.

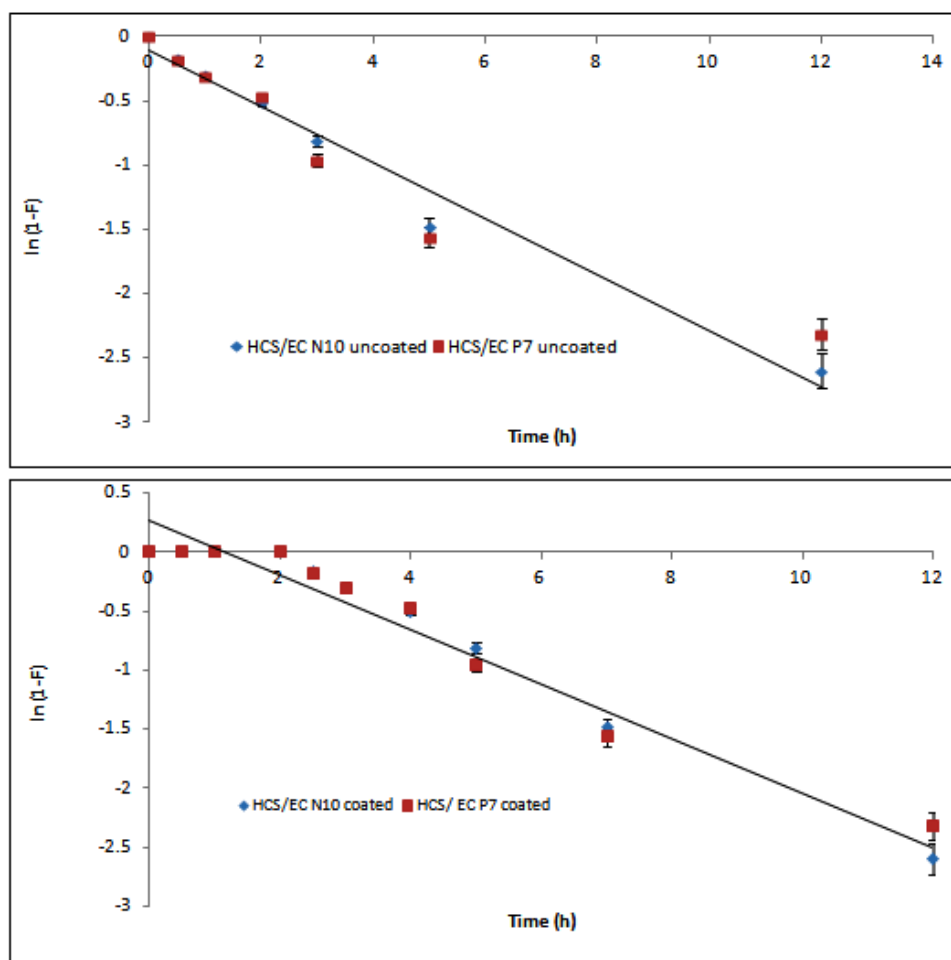


Fig. 8.5a: Semi logarithmic plot of the unreleased fraction of HCS as a function of time according to a first order kinetics model. Each result shows the mean \pm S.D. ($n = 3$).

Analyses were performed in the ranges in which linearity was maintained with both coated and uncoated tablets. The HCS release from both tablets was affected slightly by coating. In uncoated tablet, satisfactory linearity was observed throughout the test ($R^2 = 0.9709 - 0.9922$) as shown in table 8.3 for both polymers, and the release pattern was apparently linear release. In the coated tablets, satisfactory linearity was not observed up to two hours of dissolution study as no HCS was released due to the pH dependant polymer coating. After two hours, with the increase pH, HCS started releasing and therefore a satisfactory linearity between the logarithm of drug residual rate and time was observed throughout the rest of the test ($R^2 = 0.9153 - 0.9295$).

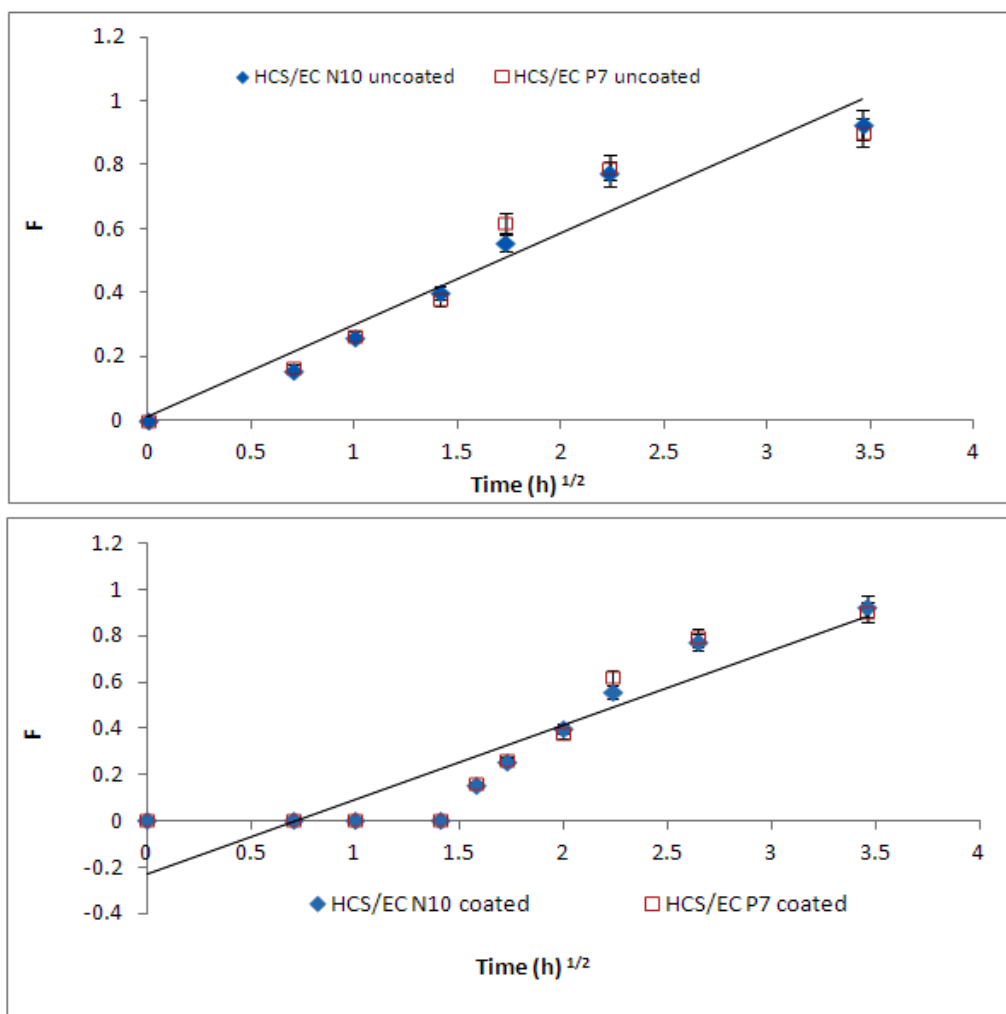


Fig. 8.5b: A plot of the HCS released as a function of time according to the Higuchi model. Each result shows the mean \pm S.D. ($n = 3$).

The Higuchi model plot shows the relationship between the drug release rate and the square root of time on the basis of Eq. (8.3) which is depicted in Fig. 8.5b. It shows the results of HCS release from HME tablets. Analyses were performed in the ranges in which linearity was maintained with both coated and uncoated tablets ($R^2 = 0.9040 - 0.9498$). The release from the coated tablet was slightly affected by the coating as expected; however, the release from uncoated tablet was quite linear throughout the test.

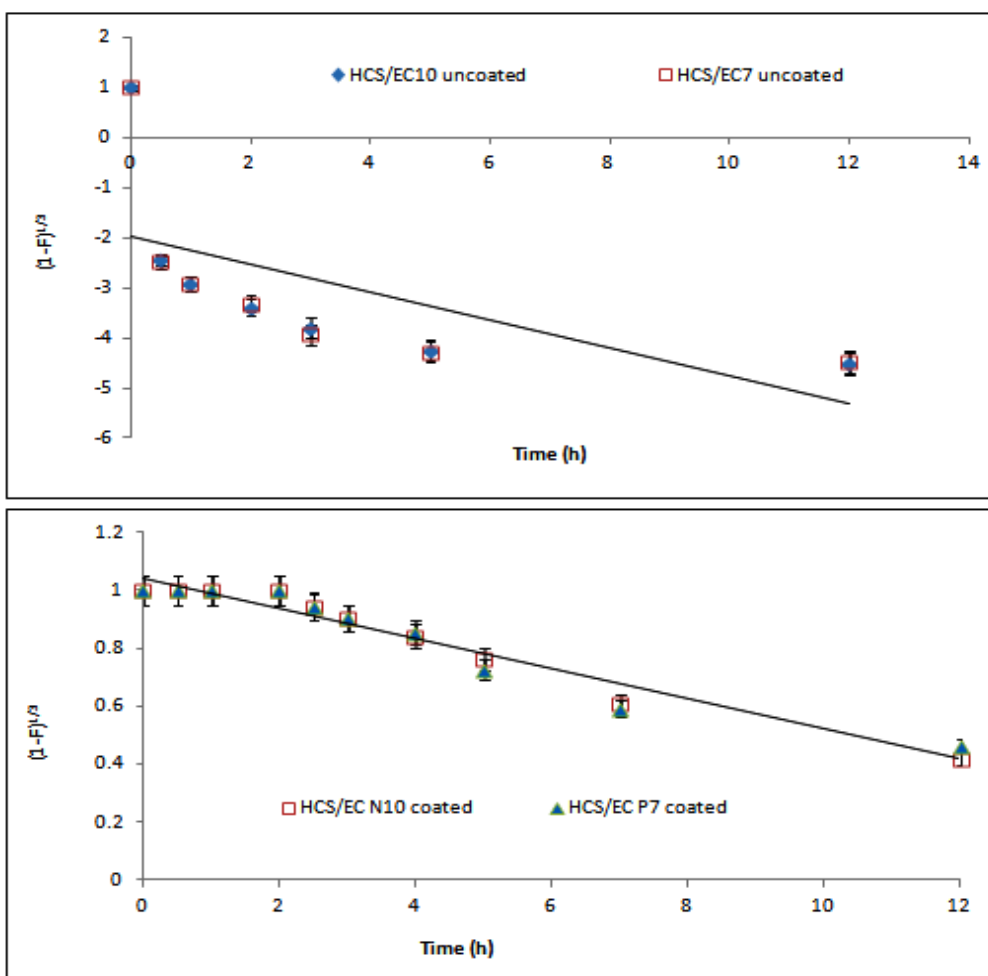


Fig. 8.5c: A plot of the cubic root of unreleased fraction of HCS from tablets as a function of time according to the Hixson–Crowell model. Each result shows the mean \pm S.D. ($n = 3$).

According to the Hixson–Crowell model plot which shows the relationship between the cubic root of the drug residual rate and time on the basis of Eq. (8.5) results are depicted in Fig 8.5c. Hixson and Crowell showed that the law of cubic root is valid in uniform particles. This equation is based on the assumption that the release occurs only in the vertical direction relative to the matrix surface, and that the release progresses with proportional decreases in all dimensions of the matrix, which maintains its shape ^[17]. Analyses were performed in the ranges in which linearly was maintained with both tablets. The release from coated tablets was not linear as the R^2 value was found to be (0.8829 - 0.8964). On the other hand, the HCS release from coated tablets according to the Hixson-Crowell model is quite linear throughout the whole test ($R^2 = 0.9622 - 0.9838$). According to the Hixson-Crowell theory of drug release it is presumed that the release progression has been maintained with the decreases in all dimensions of the matrix due to the applied coating on the tablet surfaces and thus maintained the shapes of the tablets.

Eq. (6) is a Korsmeyer–Peppas model equation concerning the diffusion mechanism, and it has been evaluated concerning pharmaceutical preparations of many matrix types. When both terms of Eq. (8.6) are converted to logarithms, the equation becomes $\ln F = \ln K_4 + n \ln t$, and the slope n can be determined by plotting the logarithm of the release rate against the logarithm of time (Fig. 8.5d).

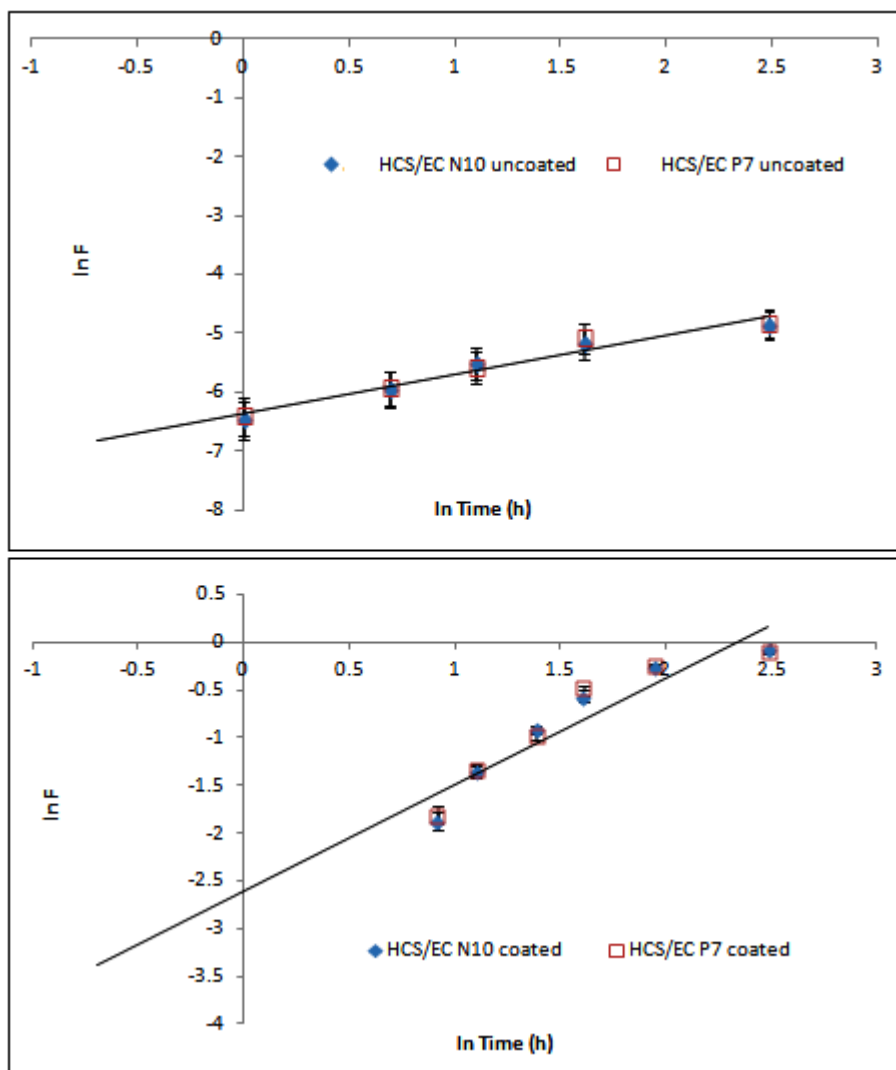


Fig. 8.5d: A plot of the logarithm of HCS released as a function of the logarithm of time according to the Korsmeyer–Peppas model. Each result shows the mean \pm S.D. ($n=3$).

The exponent (n) determined by this equation suggests that both the uncoated and coated tablets show Fick's diffusion when $n = 0.40-0.45$ (for tablets). It has been reported that a non-Fickian type release which is also known as anomalous transport occurs only when $0.45 < n < 0.89$, case-II transport can be observed when $n = 0.89$, and super case-II transport

when $n > 0.89$. From the results of analysis of the apparent diffusion pattern, the value of n , has represented the diffusion pattern according to the Fickian diffusion ^[17].

Table 8.3: Dissolution rate constants and determination coefficients of HCS release from coated and uncoated tablets; n dissolution exponent.

Dissolution models		HCS/EC N10 Uncoated	HCS/EC P7 Uncoated	HCS/EC N10 Coated	HCS/EC P7 Coated
First order	K_1 (h^{-1})	0.29 ± 0.013	0.31 ± 0.027	0.4215 ± 0.057	0.456 ± 0.068
	R^2	0.9922	0.9709	0.9295	0.9153
Higuchi	K_2 ($\% hr^{-1/2}$)	29.29 ± 1.56	29.48 ± 2.07	34.41 ± 2.30	34.418 ± 2.303
	R^2	0.9498	0.9113	0.9040	0.9040
Hixson– Crowell	K_3 ($\% h^{-1/3}$)	0.08 ± 0.005	0.089 ± 0.008	0.1182 ± 0.176	0.126 ± 0.197
	R^2	0.9838	0.9622	0.8964	0.8829
Krosmer-Peppas	K_4 (hr^{-n})	31.32 ± 3.91	32.95 ± 5.14	40.48 ± 4.77	42.20 ± 6.11
	R^2	0.9532	0.9214	0.9375	0.8966
	n	0.46 ± 0.06	0.44 ± 0.08	0.40 ± 0.069	0.40 ± 0.069

4.0 Conclusions

In the current study HME was used as a robust technique to develop time delayed coated extruded tablet to provide sustained-release of HCS. The release patterns are governed by the polymer selection while performing the extrusion process and the coating respectively. The tablet was designed to release HCS in a pattern that imitates a healthy individual. The development of the HCS extruded tablet by HME is preferable since its preparation is quick, economical with fewer process steps which will make the future pilot scale formulation developments much easier. Furthermore, a full comparative analysis of drug release mechanism confirmed the release of HCS in extruded tablets according to first order kinetic model.

5.0 References

1. Breitenbach J. Melt extrusion: from process to drug delivery technology. *Eur J Pharm Biopharm* 2002; 54:107–117.
2. M.A. Repka, S.K. Battu, S.B. Upadhye, S. Thumma, M.M. Crowley, F. Zhang, C. Martin, J.W. McGinity, Pharmaceutical applications of hot-melt extrusion: Part II, *Drug Dev Ind Pharm* 2007; 33:1043–1057.
3. Cilurzo F, Cupone I, Minghetti P, Selmin F, Montanari L. Fast dissolving films made of maltodextrins, *Eur J Pharm Biopharm* 2008; 70: 895-900.
4. Zhang F, McGinity JW. Properties of sustained-release tablets prepared by hot-melt extrusion. *Pharm Dev Tech* 1999; 4(2), 241–250.
5. Maniruzzaman M, Boateng J, Douroumis D. Taste masking of bitter APIs by using hot melt extrusion (HME). *AAPS Journal* 2011; 13 (S2): T3273-T3273. ISSN 1550-7416.
6. Grunhagen HH, Muller O. Melt extrusion technology. *Pharm Manu Int.*1995 1, 167–170.
7. Breitzkreutz J, El-Saleh F, Kiera C, Kleinebudde P, Wiedey W. Pediatric drug formulations of sodium benzoate: II. Coated granules with a lipophilic binder. *Eur J Pharm Biopham* 2003; 56, 255-60.
8. De Brabander C, Vervaet C, Fiermans L, Remon JP. Matrix mini-tablets based on starch/microcrystalline wax mixtures. *Int J Pharm* 2000; 199: 195-203.
9. De Brabander C, Vervaet C, Remon JP. Development and evaluation of sustained release mini-matrices prepared via hot melt extrusion. *J Cont Rel* 2003; 89: 235–247.
10. Roblegg E, Jäger E, Hodzic A, Koscher G, Mohr S, Zimmer A, Khinast J. Development of sustained-release lipophilic calcium stearate pellets via hot melt extrusion. *Eur J Pharm Biopharm* 2011; 79:635–645.
11. Clark MR, Johnson TJ, McCabe RT, Clark JT, Tuitupou A, Elgendy H, Friend DR, Kiser PF. A hot-melt extruded intravaginal ring for the sustained delivery of the antiretroviral microbicide UC781. *J Pharm Sci* 2012; 101(2):576-87.
12. Vithani K, Maniruzzaman M, Mostafa S, Cuppok Y, Douroumis D. Compritol® 888 ATO Lipid Matrices for Sustained Release Processed by Hot-Melt Extrusion. 39th Annual meeting and Exposition of CRS 2012, Quebec, Canada.
13. Maniruzzaman M, Hossain MA, Douroumis D. Sustained release of hydrocortisone tablets processed by hot-melt extrusion (HME). *UKPharmSci* 2012a. UK

14. Lam PL, Lee KKH, Wong RSM, Cheng GYM, Cheng SY et al. Development of hydrocortisone succinic acid/and 5-fluorouracil/chitosan microcapsules for oral and topical drug deliveries. *Bio Med Chem Lett* 2012; 22:3213–3218.
15. Abrahamsson B, Alpsten M, Bake B, Jonsson UE, Eriksson- Lepkowska M, Larsson A. Drug absorption from nifedipine hydrophilic matrix extended-release (ER) tablet comparison with an osmotic pump tablet and effect of food. *J Contr Rel* 1998; 52: 301–310.
16. Li SP, Mehta GN, Grim WN, Buehler JD, Harwood RJ. A method of coating non-uniform granular particles. *Drug Dev Ind Pharm* 1988; 14: 573–585.
17. Hayashi T, Kanbea H, Okada M, Suzuki S, Ikeda Y, Onuki Y, Kaneko T, Sonobe T. Formulation study and drug release mechanism of a new theophylline sustained-release preparation. *International Journal of Pharm* 2005; 304:91–10.
18. Hixson AW, Crowell JH. Dependence of reaction velocity upon surface and agitation. *Ind Eng Chem* 1931; 23: 923– 931.
19. Higuchi T. Mechanism of sustained-action medication. Theoretical analysis of rate of release of solid drugs dispersed in solid matrices. *J Pharm Sci* 1963; 52: 1145–1149.
20. Gibaldi M, Feldman S. Establishment of sink conditions in dissolution rate determinations—theoretical considerations and application to non disintegrating dosage forms. *J Pharm Sci* 1967; 56: 1238–1242.
21. Korsmeyer RW, Gurny R, Doelker EM, Buri P, Peppas NA. Mechanism solute release from porous hydrophilic polymers. *Int J Pharm* 1983; 15: 25–35.
22. Costa P, Sousa Lobo JM. Modeling and comparison of dissolution profiles. *Eur J Pharm Sci* 2001; 13: 123–133.
23. DiNunzio JC, Brough C, Hughey JR, Miller DA, Williams III RO, McGinity JW. Fusion production of solid dispersions containing a heat-sensitive active ingredient by hot melt extrusion and Kinetisol-dispersing. *Eur J Pharm Biopharm* 2010; 74: 340–351.
24. Zheng X, Yang R, Tang X and Zheng L. Part I: Characterization of Solid Dispersions of Nimodipine Prepared by Hot-melt Extrusion. *Drug Dev Ind Pharm* 2007; 33:791–802.
25. Maniruzzaman M, Hossain MA, Abiodun A, Douroumis D. Chrono – Delivery of Hydrocortisone Tablets Processed by Hot-Melt Extrusion (HME). 39th CRS exposition 2012b; Canada.

CHAPTER 9: CONCLUSIONS AND FUTURE WORK

9.1 Overall conclusions

Hot-melt extrusion (HME) has proved to be a robust method of producing several drug delivery systems and therefore it has been found to be useful in the pharmaceutical industry enlarging the scope to include a range of polymers and APIs that can be processed with or without plasticizers. In this current study HME processing was employed as a means to increase the dissolution rates of three water insoluble drugs. INM and FMT were extruded with SOL, VA64 and S630 at different loadings up to 40% without the presence of traditional plasticizers while IBU was extruded and embedded within Eudragit EPO polymer matrix. The extrusion process was optimized to produce amorphous solid dispersions of the drug substances. Further physicochemical characterization studies confirmed the theoretical drug – polymer miscibility for all binary mixtures as predicted by the theoretical approaches of Greenhalgh and Bagley. Increased aqueous solubility was observed in both API mixtures with all polymers, and the extruded solid dispersions resulted in greater dissolution rates compared to the bulk drugs. The *in vivo* taste-masking evaluation of extruded IBU formulations showed that HME processing can be used to efficiently mask the taste of bitter active substances without compromising tablet palatability. The ODTs developed displayed disintegration times and crushing resistance similar to commercial Nurofen® tablets but improved tablet friability. Finally the increased IBU release rates of the developed ODTs were faster than the commercial Nurofen® tablets.

PMOL was found to exist in either the crystalline or amorphous state depending on the polymer used for extrusion. The optimized formulations were evaluated in terms of taste masking efficiency both by *in vivo* human panellists and an electronic tongue. The extruded formulations of VA64 demonstrated better taste masking compared to those of EPO while the e-tongue was found to be a valuable tool for taste masking assessments and formulation development. Similarly, DPD, PRP, CTZ and VRP were found to be in the amorphous state after extrusion due to the formation of solid dispersions. The optimized formulations evaluated by both *in vivo* and *in vitro* taste masking tests correlated with each other very well. The extruded formulations of L100 demonstrated better taste masking compared to those of EZE while the e-tongues were found to be a valuable tool for taste masking assessments and formulation development.

Furthermore, HME has successfully been employed as a robust technique to form solid dispersions of APIs into polymer matrices via intermolecular interactions. The existence of amorphous APIs in the polymer matrices has been confirmed by thermal analysis. Molecular modelling was used to predict/assess the possible presence and strength of intermolecular interactions between drug and polymer molecules. The foregoing was confirmed by FT-IR and NMR studies. XPS analysis was used to confirm the mechanism of the interaction via H-bonding between the carboxyl group of the anionic methacrylate co-polymer and the amide group of the active substances and estimate the bond strengths involved. The foregoing studies confirmed that the stronger the interaction between oppositely charged drug and the polymer, the better the taste masking in extruded solid dispersions.

The release patterns of HCS from tablets processed by HME were governed by the thermal characteristics of the polymer used as a carrier during the extrusion process and the enteric coatings of the polymer, respectively. The tablets were designed to release HCS in a pattern that imitates the cortisol level in healthy individuals. Furthermore, a full comparative analysis of the mechanism of drug release confirmed the release of HCS in extruded tablets according to a first order kinetic model.

9.2 Future work

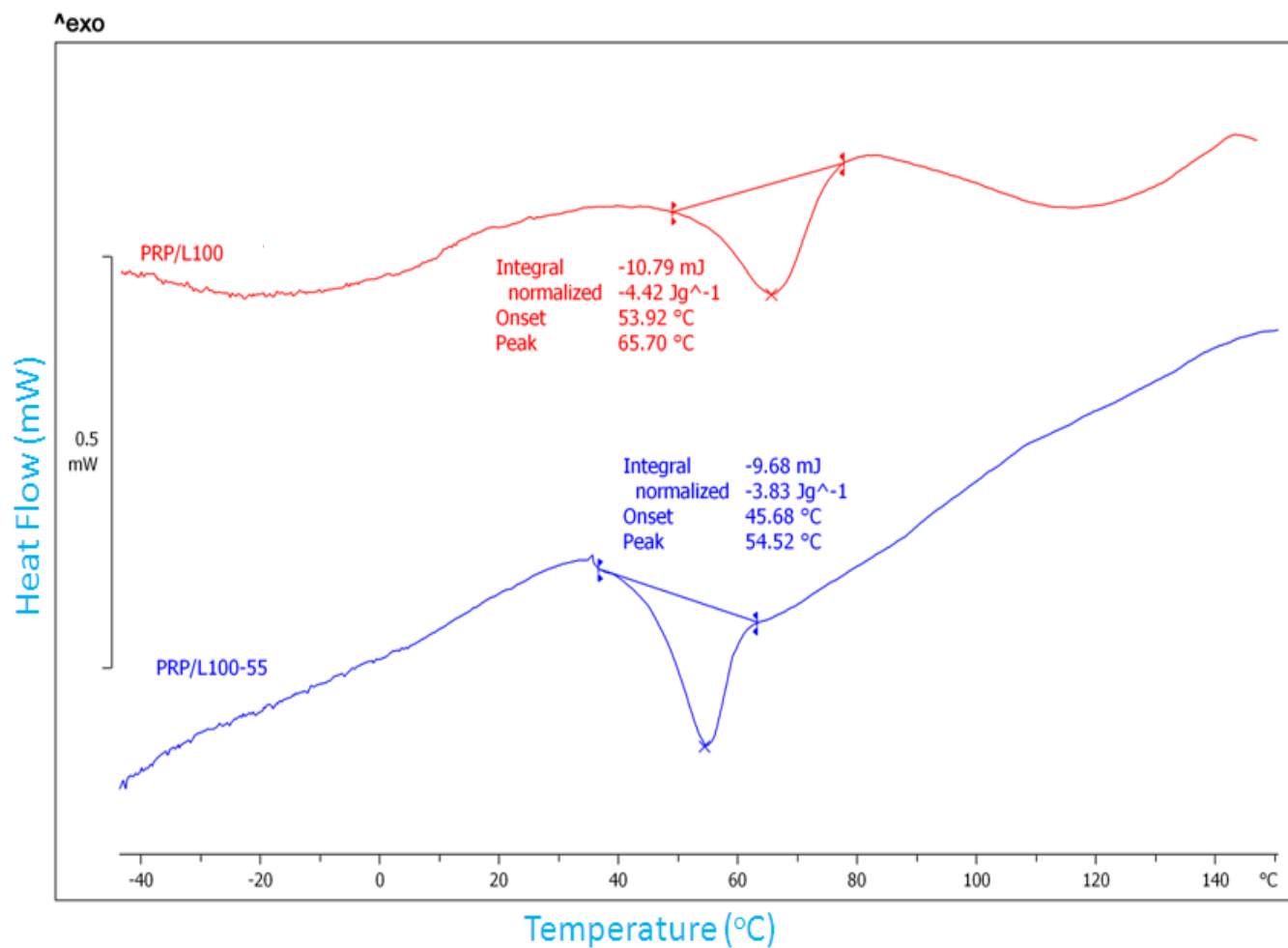
The scope of the HME technology has already broadened to include a range of polymers and APIs that can be processed through the application of supercritical fluids and plasticizer assisted HME.

Future work using HME could include the following.

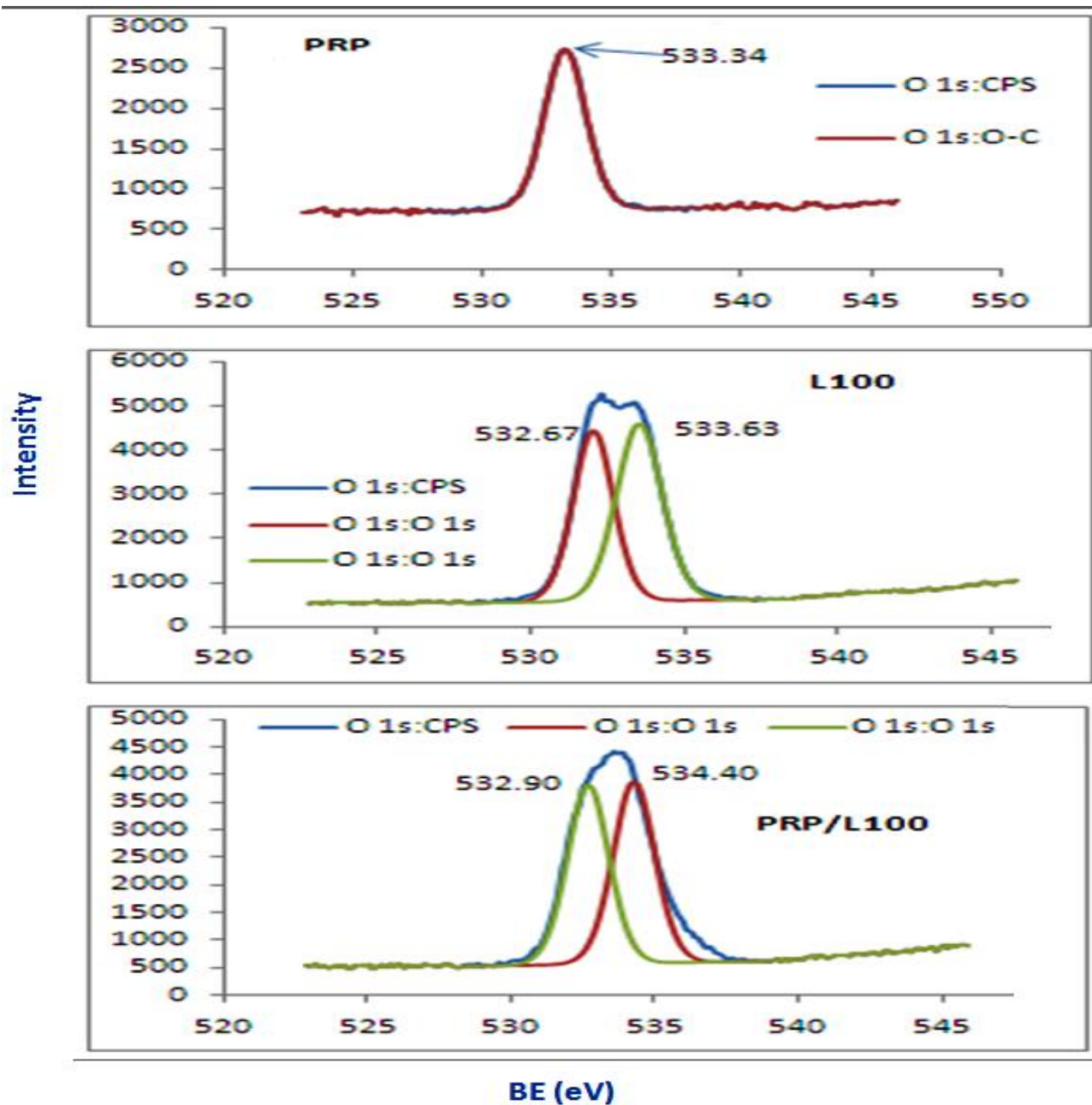
- Development, optimization and characterization of various orally dispersible/bioadhesive film formulations. Hot-melt extruded films would be able to deliver high amounts of taste masked drugs and, therefore, would increase patient compliance.
- Formulation of various APIs with lipids for sustained release of drugs, using HME also need to be explored in order to facilitate cold extrusion for heat sensitive APIs.
- The growing market in medical devices, including incorporating drugs such as biodegradable stents and drug-loaded catheters will undoubtedly require HME manufacturing processes. These are required to be commercialised and may lead to new areas of inter-disciplinary research in the areas of pharmaceuticals, medical devices and biotechnology.

CHAPTER 10: SUPPLEMENTARY DATA

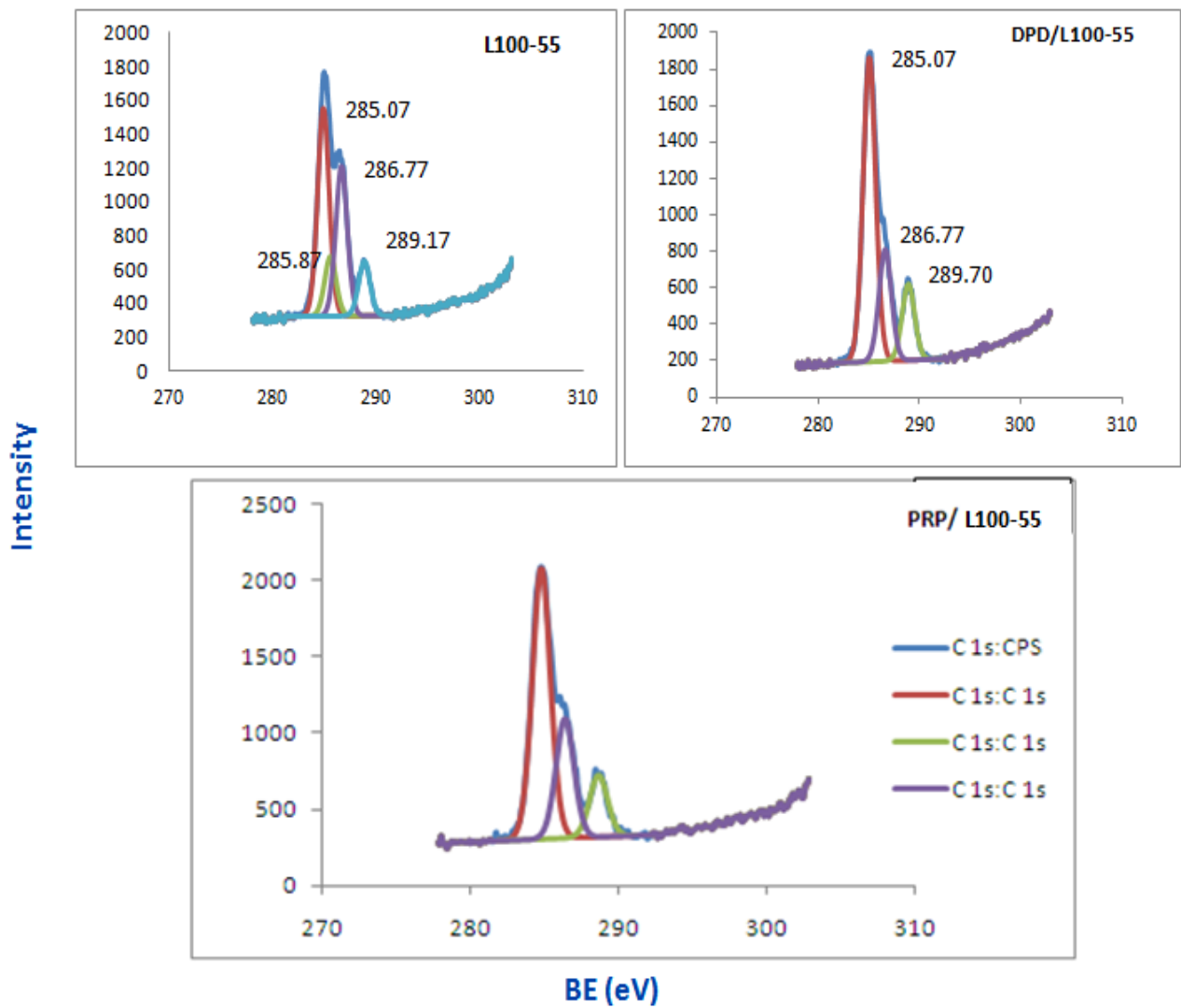
10.1 Supplementary figures



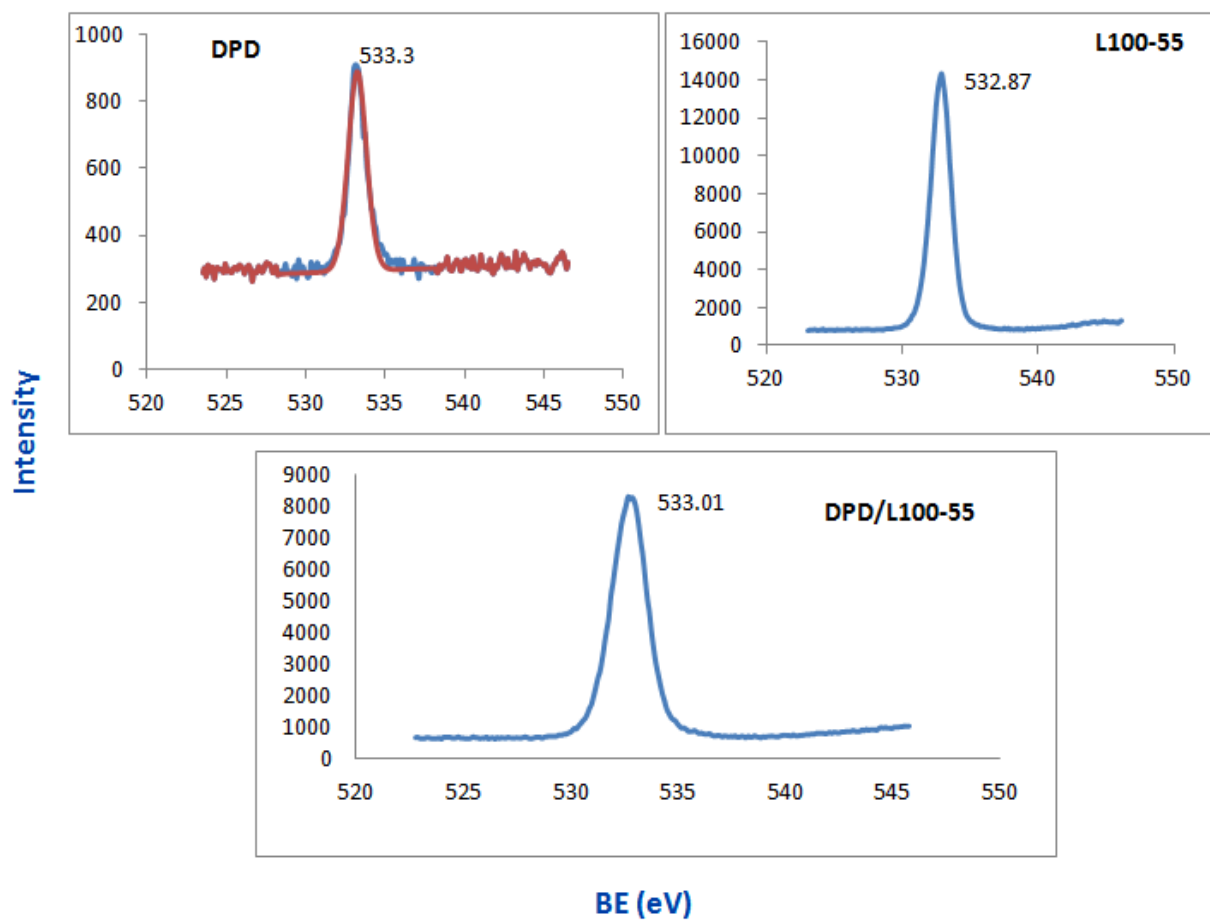
Supp. Fig. 1: N 1s BE peaks of DPD and DPD based extruded formulations.



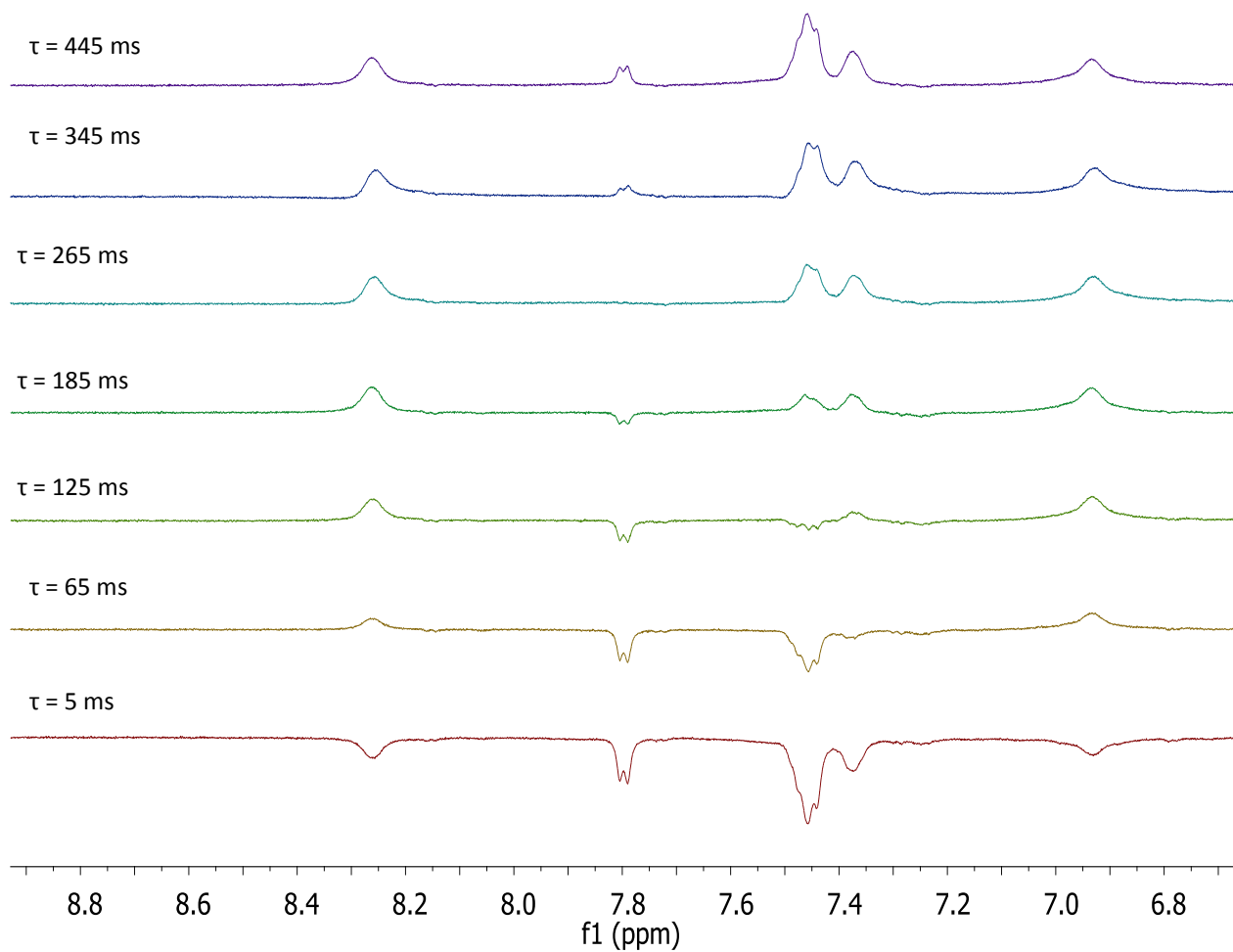
Supp. Fig. 2: XPS O 1s peaks for PRP, L100 and PRP/L100 formulations.



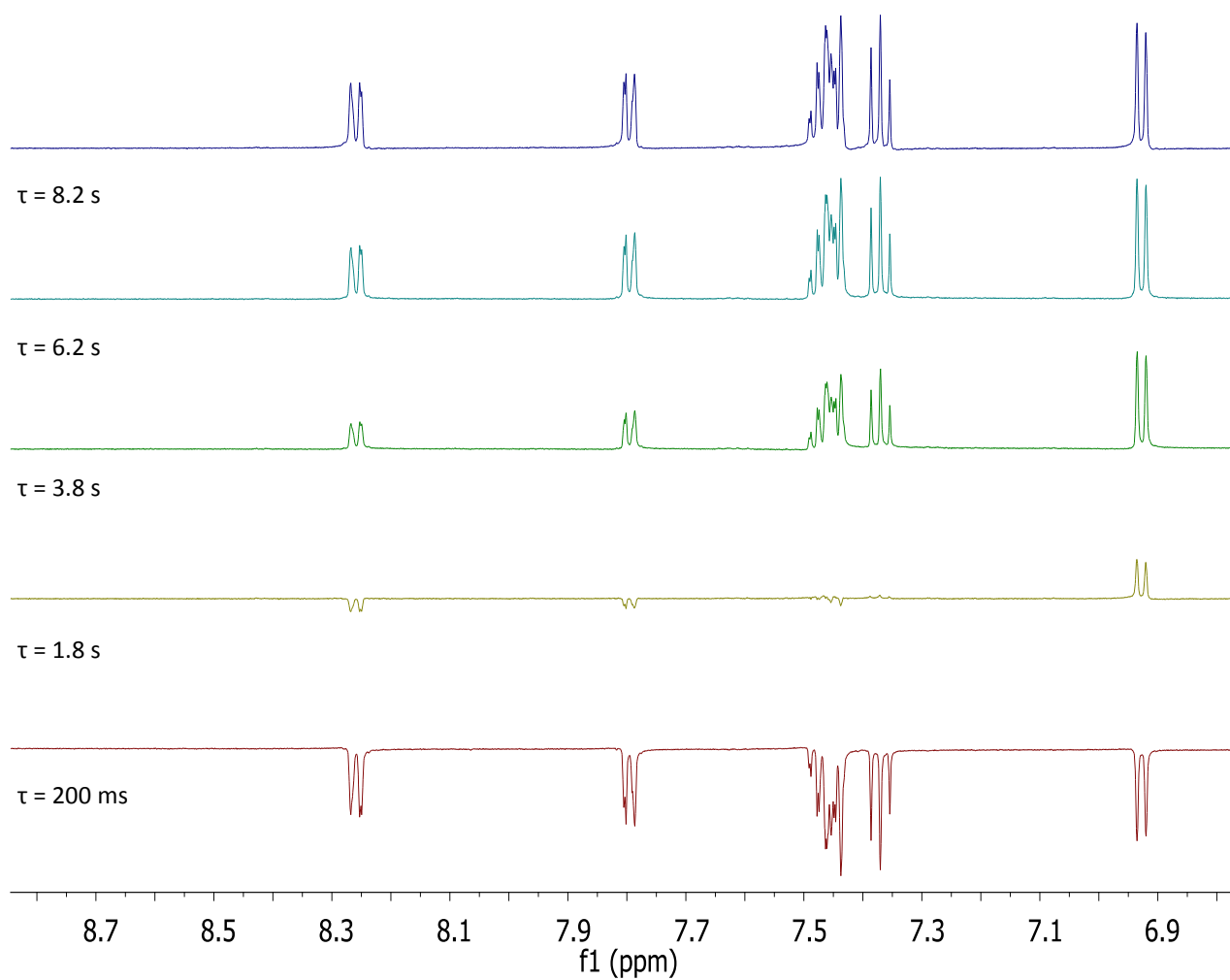
Supp. Fig. 3: C 1s BE peaks for L100-55, PRP/L100-55 and DPD/L100-55.



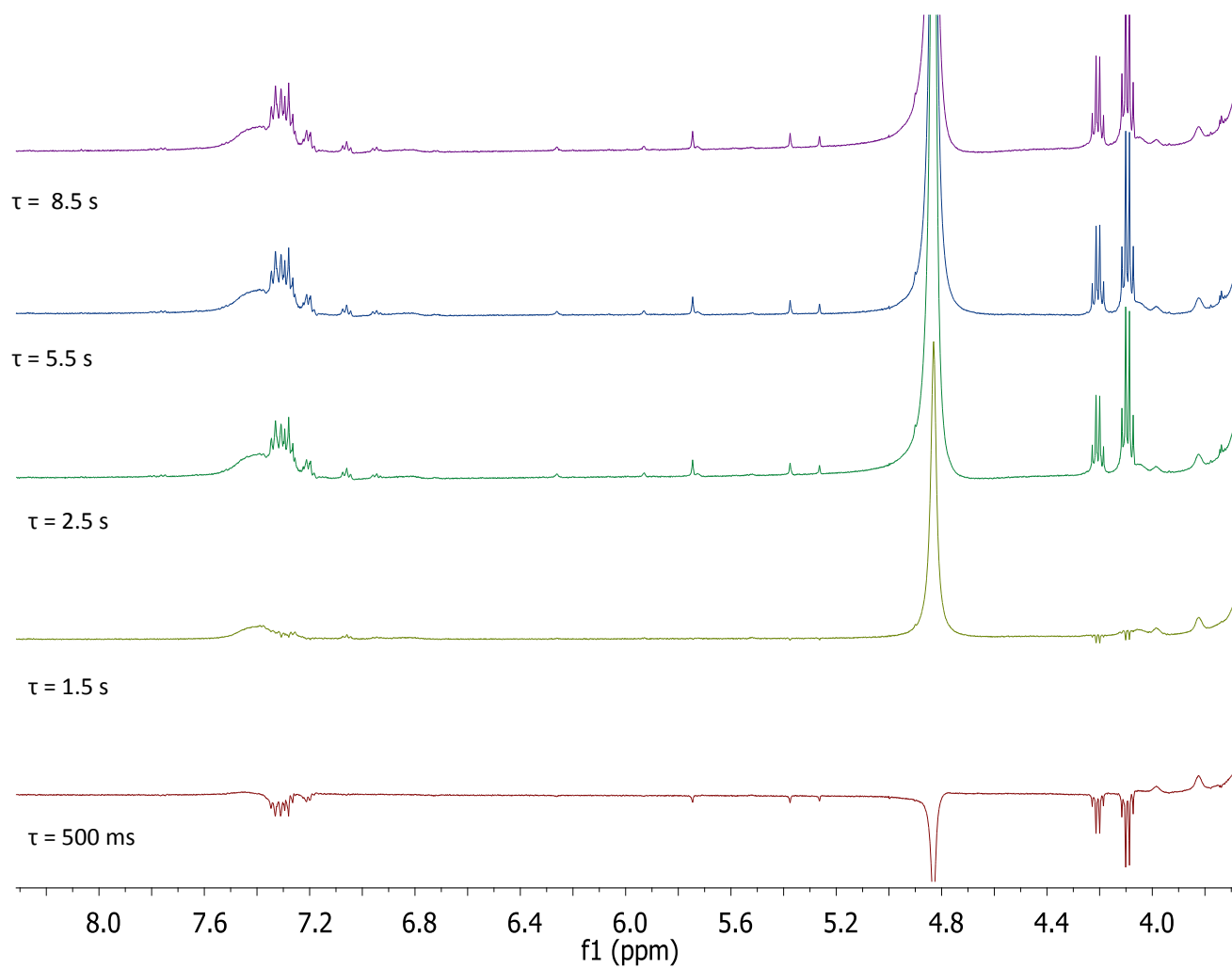
Supp. Fig. 4: O 1s BE peaks for L100-55, DPD and DPD/L100-55 formulations.



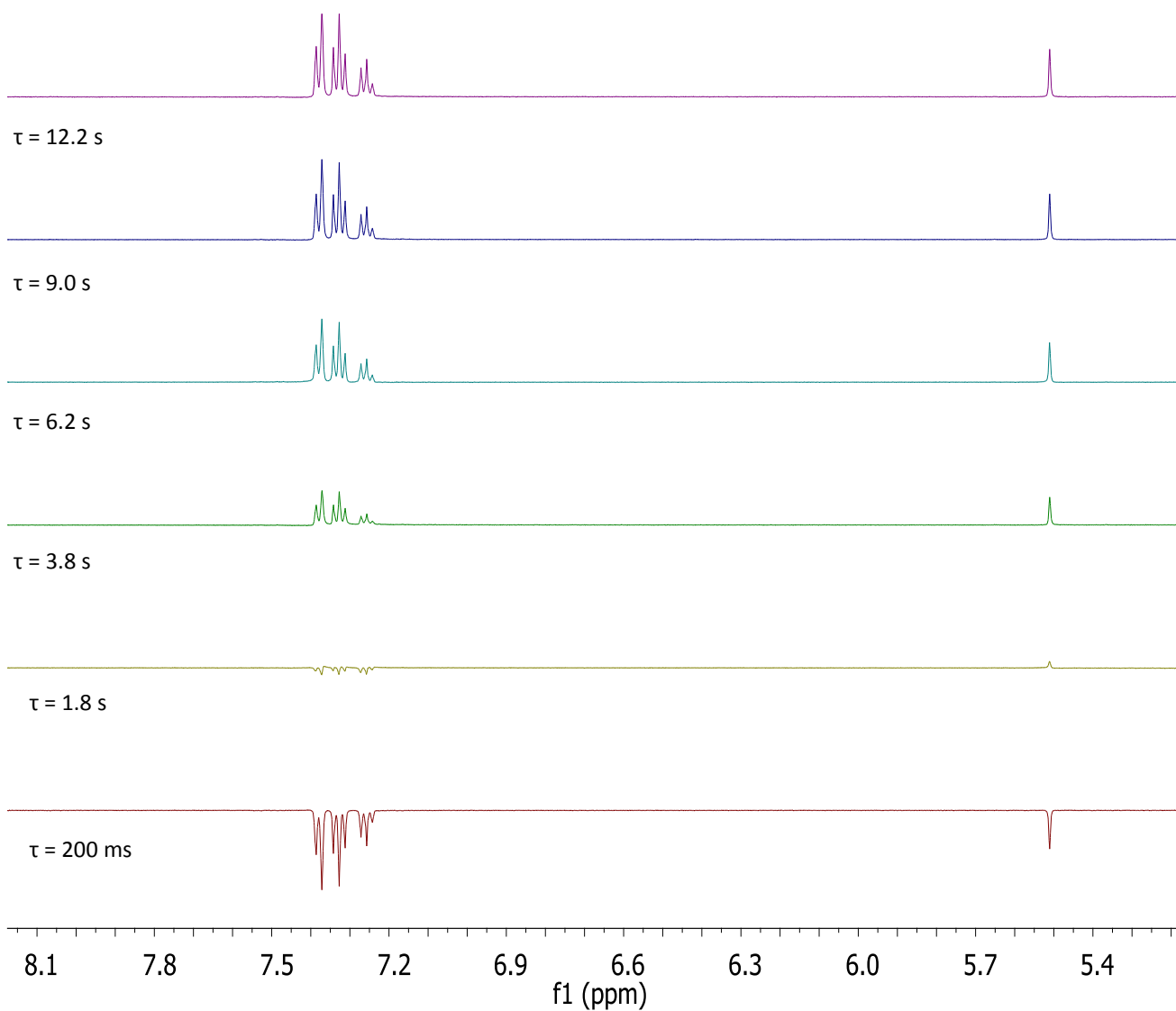
Supp. Fig. 5: Part, ^1H T_1 spectra (aromatic region) for the propanolol HCl/ Eudragit L-100 formulation.



Supp. Fig. 6: Part, ^1H T₁ spectra (aromatic region) for the propanolol HCl.



Supp.Fig.7: Part, ^1H T₁ spectra for the diphenhydramine HCl / Eudragit L-100 formulation.

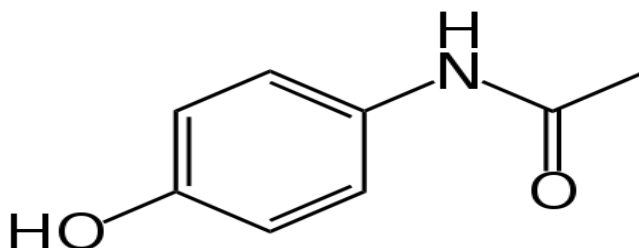


Supp. Fig.8: Part, ^1H T₁ spectra for the diphenhydramine HCl.

10.2 Supplementary calculations

Example of the calculations of Hansen solubility parameters of drug and polymer

(1) Paracetamol:



Molecular formula: C₈H₉NO₂

Molecular weight: 151

Density: 1.263 gm/cm³

Therefore, molecular Volume (V) = MM/density

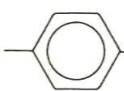
$$= 151/1.263$$

= 119.56 cm³ (equal to the sum of the functional groups contribution from respective structure)

Now, some known values for solubility parameter component group contribution (Table Suppl. 1)-

Structural groups	F _{di}	F _{pi}	F _{hi}
-CH ₃	420	0	0
-OH	210	500	20000
>C=O	290	770	200
>N-H	160	210	3100
	1270	110	0

Supplementary table 1: Solubility parameter component group contribution

Structural group	F_{di} ($J^{1/2} \cdot cm^{3/2} \cdot mol^{-1}$)	F_{pi} ($J^{1/2} \cdot cm^{3/2} \cdot mol^{-1}$)	E_{hi} (J/mol)
-CH ₃	420	0	0
-CH ₂ -	270	0	0
	80	0	0
	-70	0	0
=CH ₂	400	0	0
=CH-	200	0	0
	70	0	0
	1620	0	0
	1430	110	0
 (o, m, p)	1270	110	0
-F	(220)	-	-
-Cl	450	550	400
-Br	(550)	-	-
-CN	430	1100	2500
-OH	210	500	20000
-O-	100	400	3000
-COH	470	800	4500
-CO-	290	770	2000
-COOH	530	420	10000
-COO-	390	490	7000
HCOO-	530	-	-
-NH ₂	280	-	8400
-NH-	160	210	3100
	20	800	5000
-NO ₂	500	1070	1500
-S-	440	-	-
=PO ₄ -	740	1890	13000
ring	190	-	-
one plane of symmetry	-	0.50X	-
two planes of symmetry	-	0.25X	-
more planes of symmetry	-	0X	0X

$$\sum F_{di} = 2352, \sum F_{pi} = 899100, \sum F_{hi} = 23300$$

From Van krevelen Equation We know,

$$\delta = \sqrt{\delta_d^2 + \delta_p^2 + \delta_h^2} \quad (1)$$

Where,

$$\delta_d = \frac{\sum F_{di}}{V_i}, \delta_p = \frac{\sqrt{\sum F_{pi}^2}}{V_i}, \delta_h = \sqrt{(\sum E_{hi} / V_i)}$$

i = structural groups within the molecule

δ = the total solubility parameter.

F_{di} = molar attraction constant due to molar dispersion forces

F_{pi}^2 = molar attraction constant due to molar polarization forces

E_{hi} = hydrogen bonding energy.

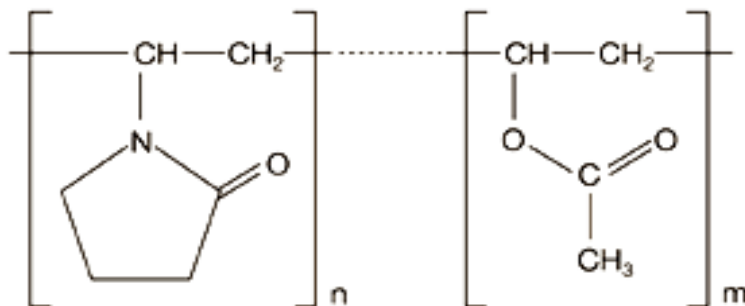
V_i = group contribution to molar volume

$$\text{Now, } \delta_d = \sum F_{di} / V = 2352 / 119.56 = 19.672$$

$$\text{And, } \delta_p = 948.21 / 119.56 = 7.93, \delta_h = \sqrt{(23300 / 119.56)} = 13.96$$

$$\text{So now, } \delta = \sqrt{\{(19.672)^2 + (7.93)^2 + (13.96)^2\}} = 20.25, 8.16, 14.16 \\ = 25.77 \text{ MPa}^{1/2}$$

(2) Kollidon VA64



MW = 219.2 (above structure)

$$N = 55000 / 219.2 = 250.912$$

$$\text{Density: } 1.29 \text{ g/cm}^3$$

Molar Volume (v) = $55000 / 1.39 = 39568.35 \text{ cm}^3$ (equal to the sum of the functional groups contribution from respective structure)

Structural groups	F_{di}	F_{pi}	F_{hi}
-CH ₃	420	0	0
-CH ₂ -	270	0	0
-O-	100	400	3000
>C=O	290	770	200
1.2 x >C=O	348	924	240
1.2 x >N-	24	960	6000
4.8 x -CH ₂ -	1296	0	0
1.2 x >CH-	96	0	0

$$\sum F_{di} = 713593.728, \sum F_{pi}^2 = 634374787.7, \sum F_{hi} = 2368609.28$$

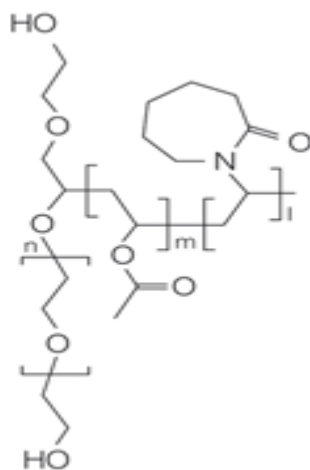
By using the same van krevelen calculation shown above for Temoporfin, we get

$$\delta_d = \sum F_{di} / V = 18$$

$$\text{And, } \delta_p = 0.64, \delta_h = 7.73$$

$$\begin{aligned} \text{So now, } \delta &= \sqrt{\{(18.0)^2 + (0.64)^2 + (7.73)^2\}} \\ &= \mathbf{19.60 \text{ MPa}^{1/2}} \end{aligned}$$

(3) Soluplus



$$= N (\text{mw} = 418 \text{ g/mol})$$

Molecular Weight = 90000 g/mol

$N = 215.3$; Density = 1.08 g/cm^3

Molar Volume (V) = 83333.33 cm^3 (equal to the sum of the functional groups contribution from respective structure)

Structural groups	F_{di}	F_{pi}	F_{hi}
-CH ₃	420	0	0
14 x -CH ₂ -	3780	0	0
2 x -OH	420	1000	40000
4 x -O-	400	1600	12000
2 x >C=O	580	1540	400
3 x >CH-	240	0	0
>N-	20	800	5000

$$\sum F_{di} = 1261658, \sum F_{pi}^2 = 1414865480, \sum F_{hi} = 12358220$$

By using the same van krevelen calculation shown above for Temoporfin, we get

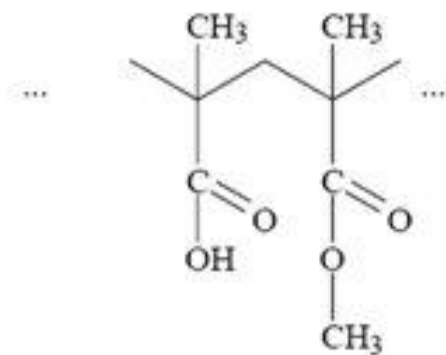
$$\delta_d = \sum F_{di} / V = 15.14$$

$$\text{And, } \delta_p = 0.45, \delta_h = 12.18$$

$$\text{So now, } \delta = \sqrt{\{(15.14)^2 + (0.45)^2 + (12.18)^2\}}$$

$$= 19.43 \text{ MPa}^{1/2}$$

(4) Eudragit L100



$$, N = (125000/202 = 618.81)$$

Molecular Weight: 125000 g/mol

Density: 1.25 g/cm³

Molar Volume (V) = 125000/1.25 = 100000 cm³ (equal to the sum of the functional groups contribution from respective structure)

Structural groups	F _{di}	F _{pi}	F _{hi}
5 x -CH ₃	2100	0	0
2 >C<	-140	0	0
2 >C=O	580	1540	400
-O-	100	400	3000
-OH	210	500	20000
-CH ₂ -	270	0	0
N= 618.81	∑ F_{di} = 1930687.2	∑ F_{pi}² = 1721281896	∑ F_{hi} = 14480154

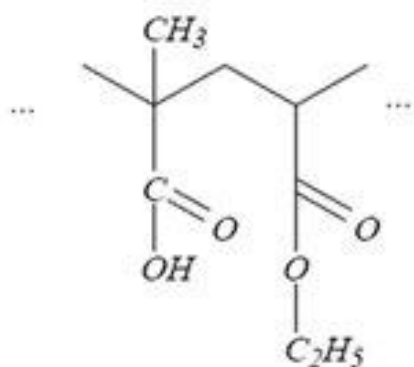
By using the same van krevelen calculation shown above, we get

$$\delta_d = \sum F_{di} / V = 19.31$$

And, $\delta_p = 0.41$ and, $\delta_h = 12.03$

So now, $\delta = 22.75 \text{ MPa}^{1/2}$

(5) Eudragit L100-55 (Acryl EZE)



$$N = (320000/202 = 1584.1584)$$

Molecular Weight = 320000 g/mol

Molecular Volume (V) = 320000/1.18 = 271186.4407 cm³ (equal to the sum of the functional groups contribution from respective structure)

Structural groups	F _{di}	F _{pi}	F _{hi}
4 x -CH ₃	1680	0	0
>C<	-70	0	0
2 >C=O	580	1540	400
-O-	100	400	3000
-OH	210	500	20000
2 x -CH ₂ -	540	0	0
>CH-	80	0	0
N= 1584.1584	∑ F_{di} = 4942574.208	∑ F_{pi}² = 4406495005	∑ F_{hi} = 37069306.56

By using the same van krevelen calculation shown above, we get

$$\delta_d = \sum F_{di} / V = 4942574.208 / 271186.4407 = 18.226$$

And, $\delta_p = 0.245$ and, $\delta_h = 11.692$

$$\begin{aligned} \text{So now, } \delta &= \sqrt{\{(18.226)^2 + (0.245)^2 + (11.692)\}} \\ &= 21.65 \text{ MPa}^{1/2} \end{aligned}$$